

UNIVERSITY OF BELGRADE
FACULTY OF MATHEMATICS

Georgios Tsirvoulis

SECULAR DYNAMICS OF SELECTED
ASTEROID FAMILIES

Doctoral Dissertation

Belgrade, 2019

UNIVERZITET U BEOGRADU
MATEMATIČKI FAKULTET

Georgios Tsirvoulis

SEKULARNA DINAMIKA IZABRANIH
FAMILIJA ASTEROIDA

Doktorska Disertacija

Beograd, 2019

Supervisor:

Dr. Bojan Novaković, Assistant Professor
Faculty of Mathematics
University of Belgrade

Committee members:

Dr. Bojan Novaković, Assistant Professor
Faculty of Mathematics
University of Belgrade

Dr. Zoran Knežević, Academic
Department of Mathematics, Physics and Geo Sciences
Serbian Academy of Sciences and Arts

Dr. Kleomenis Tsiganis, Associate Professor
Department of Physics
Aristotle University of Thessaloniki

Dr. Andjelka Kovačević, Associate Professor
Faculty of Mathematics
University of Belgrade

To Andrea

Acknowledgement

First and foremost I would like to thank Bojan Novaković for being not only my supervisor and collaborator, but also a true friend throughout all the years of my PhD studies.

I am forever grateful to Zoran Knežević and Andrea Milani, the giants who graciously lent me their shoulders to stand on. I also feel privileged to have Kleomenis Tsiganis as my mentor and friend since my undergraduate studies.

For making me feel like home I would like to thank all the people I had the chance to work with at the Department of Astronomy, Viktor Radović, Clara Maurel, Vladimir Djošović, Ana Todović and Adrien Brunel.

I would like to thank the coordinators of the Stardust ITN, for funding and supporting my research, and enabling me to meet and have fun with all the beautiful people of the Stardust ESR and ER team (Stardust Barbarians): Ioannis Gkolias, Nicolas Thiry, Stefano Maró, Davide Amato, Helene Ma, Clemens Rumpf, Natalia Ortiz, Marko Janković, Chiara Tardioli, Massimo Vetrivano, Kartik Kumar, Piyush Mehta and Aaron "Rodoklados" Rosengren.

For the two three-month internships I did during my PhD studies, I would like to thank Federica Spoto, Fabrizio Bernardi and all the people of SpaceDyS and the University of Pisa, and Alessandro Morbidelli and Marco Delbo of the Observatoire de la Côte d'Azur, Nice, for the time and knowledge they shared with me.

For all the good memories from living in Belgrade, I would like to thank Georgia Mentele, Christos Zervas and Dušica "Imitreli" Popović. For keeping me company I thank all the members of the KSFP club, and especially the founding fathers: Stefanos "DeneB" Goutsios, Filippos "SuitedAceZZ" Lazaridis, Ioannis "OjosDeBrujos" Gkolias, Nikos "eimaikoulouri" Konst and Gerasimos "nomercy4" Kalesis.

For being always there, I thank my Sissy.

For their constant love and support, I thank my family, Stratos, Giota and Christos.

SECULAR DYNAMICS OF SELECTED ASTEROID FAMILIES

Abstract

Asteroid families are populations of asteroids in the Main Belt that share a common origin, that is they are the fragments of energetic collisions between two asteroids. Their study over the years has produced a number of important results concerning the collisional and dynamical evolution of the Main Belt, the physical properties of the primordial bodies of the Solar System and the physics of energetic collisions, to name a few.

The contribution of the present thesis can be summarized into two main topics: The first is the discovery of a new mechanism that leads to significant perturbations on the orbits of asteroids, and consequently on the evolution of asteroid families affected by it, and the second is the discovery of a couple of new families, each with its own peculiarities.

The first part of this thesis was initially motivated by the irregular shape of the (1726) Hoffmeister asteroid family. In an effort to explain this peculiarity we carried out a thorough dynamical analysis of its past evolution and found out that none of the mechanisms known to affect the orbits of asteroids could explain it. Investigating further we discovered that the linear nodal secular resonance with the most massive asteroid (1) Ceres, is the mechanism responsible for the anisotropic inclination distribution of Hoffmeister family members.

Having established the importance of the nodal secular resonance with Ceres, we sought to expand on the subject with the study of all linear secular resonances, nodal and periapsidal, involving not only (1) Ceres, but (4) Vesta, the second most massive asteroid, as well. To do so we utilized numerical integrations of test particles across the whole Main Belt, and evaluated the impact of these resonances on their orbits. Furthermore we identified all asteroid families crossed by one or more of these resonances. Two of these cases, the families of (1251) Seinajoki and (1128) Astrid were then studied in more detail, confirming the importance of the previously ignored secular resonances with massive asteroids.

The second part details the discovery of two new asteroid families. The first one, that of (326) Tamara family, was motivated by the unexpectedly high number of

dark asteroids in the Phocaea region, a part of the inner Main Belt which is expected to consist mostly of bright ones. Using all available physical data we were able to show that most of the dark asteroids therein belong to a single dynamical family, which we then further analyzed finding that it is 264 ± 43 Myrs old and that it could have a significant contribution to the influx of small dark asteroids toward the Near Earth region. The second discovered family, that of (633) Zelima, is a small cluster, sub-family of the large (221) Eos family. After identifying its members, we derived the age of the Zelima family, which turned out to be only about 3.66 Myrs.

Keywords: asteroids, dynamics, families, resonances

Scientific area: Astronomy

Scientific field: Planetary astronomy

UDC Number: 523.44

SEKULARNA DINAMIKA IZABRANIH FAMILIJA ASTEROIDA

Sažetak

Asteroidne familije predstavljaju populacije asteroida u glavnom prstenu koji vode zajedničko poreklo, tj. predstavljaju fragmente nastale u sudaru dve asteroida. Njihovo proučavanje tokom godina dalo je brojne značajne rezultate koji se odnose na sudarnu i dinamičku evoluciju glavnog prstena, fizičke karakteristike primordijalnih tela u Sunčevom sistemu, fiziku sudara visokih energija i mnoge druge.

Doprinos ove teze može se sažeti u dve glavne teme, prva je otkriće novog mehanizma koji dovodi do značajnih poremećaja putanja asteroida, a time i evolucije familija asteroida, dok je druga otkriće par novih familija, svaka sa nekim svojim specifičnostima.

Prvi deo teze je prvobitno bio motivisan nepravilnim oblikom (1726) Hofmeister familije asteroida. U nastojanju da objasnimo ovu posebnost sproveli smo detaljnu dinamičku analizu njene evolucije i zaključili da nijedan od mehanizama poznatih da utiču na orbite asteroida ne može biti objašnjenje. Daljim istraživanjem otkrili smo da je linearna sekularna rezonanca čvora sa najmasivnijim asteroidom (1) Ceres, mehanizam odgovoran za nesimetričnu raspodelu nagiba članova Hofmeister familije.

Nakon što smo utvrdili važnost sekularne rezonance čvora sa Ceresom, proširili smo temu na proučavanje svih linearnih sekularnih rezonanci, i čvora i perihela, uključujući ne samo (1) Ceres, već takodje i (4) Vestu, drugi najmasivniji asteroid. U tu svrhu koristili smo numeričke integracije test čestica raspoređenih u svim relevantnim delovima glavnog prstena i procenili uticaj pomenutih rezonanci na njihove orbite. Osim toga, identifikovali smo sve familije asteroida koje preseca neka od proučavanih rezonanci. Dva takva slučaja, familije (1251) Seinajoki i (1128) Astrid zatim su detaljnije proučene, potvrđujući značaj prethodno ignorisanih sekularnih rezonanci sa masivnim asteroidima.

Drugi deo disertacije opisuje otkriće dve nove familije asteroida. Prvo od tih otkrića, familije (326) Tamara, bilo je motivisano neočekivano velikim brojem tamnih asteroida u Fočea regionu, unutrašnjem delu glavnog prstena za koji se očekuje da se sastoji uglavnom od svetlijih objekata. Koristeći sve dostupne fizičke podatke

pokazali smo da najveći deo tamnih asteroida pripadaju jednoj dinamičkoj porodici, koju smo zatim dalje analizirali procenivši da je stara 264 ± 43 miliona godina, kao i da može biti značajan izvor malih tamnih asteroida za populaciju objekata bliskih Zemlji. Druga otkrivena porodica, (633) Zelima, je mala grupa objekata, koja predstavlja subporodicu velike (221) Eos porodice. Nakon identifikacije njenih članova, daljom analizom starost Zelima porodice procenjena je na samo oko 3.66 Mgod.

Ključene reči: asteroidi, dinamika, porodice, rezonance

Naučna oblast: Astronomija

Uža naučna oblast: Planetarna astronomija

UDK Broj: 523.44

Contents

Preface	1
1 Introduction	5
1.1 Proper elements	6
1.1.1 Concept and history	6
1.1.2 Analytical theory of proper elements	8
1.1.3 Synthetic theory of proper elements	10
1.2 Identification of asteroid families	12
1.2.1 The Hierarchical Clustering Method	14
1.3 Dynamical evolution of asteroid families	18
1.3.1 Mean Motion Resonances	19
1.3.2 Secular Resonances	20
1.3.3 The Yarkovsky Effect	21
1.3.4 Numerical simulations and chaos	27
2 Dynamical evolution of asteroid families: Secular resonances with massive asteroids	28
2.1 The Hoffmeister asteroid family	28
2.1.1 Family membership	29
2.1.2 The dynamical environment	32
2.1.3 Numerical simulations	33
2.1.4 Age of the Hoffmeister family	46
2.2 Secular resonances with massive asteroids	50
2.2.1 Ceres and Vesta	51
2.2.2 Location of the secular resonances	52
2.2.3 Numerical simulations	58
2.2.4 Asteroid families	66
2.3 The Seinajoki and Astrid asteroid families	71
2.3.1 The (1521) Seinajoki asteroid family	72
2.3.2 The (1128) Astrid asteroid family	77
2.4 Summary	82

3	New asteroid families: Discoveries and dynamical properties	84
3.1	The (326)Tamara asteroid family	84
3.1.1	Dark Phocaea asteroids: identification and search for a family	85
3.1.2	Dynamical and physical properties	88
3.1.3	Dynamical evolution of the Tamara family	92
3.1.4	Summary	96
3.2	The (633) Zelima cluster	96
3.2.1	Introduction	96
3.2.2	Identification of the new family	97
3.2.3	Age of the cluster	100
3.2.4	Dynamical and physical properties	106
3.2.5	Summary	111
4	Conclusions	112
	Bibliography	115
A	Appendix	
	Reconstructing the size distribution of the primordial Main Belt	127
	List of Figures	151
	List of Tables	159
	Biography of the author	160

Preface

” ” *We're made of star stuff. We are a way for the cosmos to know itself.*

— Carl Sagan

This is a story about rocks. Not the kind of rocks we find in the countryside, that we played with as kids, but rocks floating in space! On a good clear night nobody can help but look upon the sky, to witness the universe in awe. Thousands of bright stars, planets, whole galaxies with their own stars, all of them composing one of the most humbling spectacles available. All these little dots made people ask questions, invent deities, fall in love, think. But that is not all the night sky has to offer. Occasionally, something brief but bright, something fast enters the stage. Falling stars was the name given to them initially, and the name is still used. In reality they are not falling stars of course, they are merely rocks. Rocks falling from the sky? Well, yes; now it got interesting.

Why are there rocks in the sky in the first place? Why can't we see them? Who put them up there in the first place? Who is throwing rocks at us? Humans are curious beings. Once you start asking questions yourself, no matter if they are reasonable or not, you have taken the first step into science. All the remaining steps are the strive to get the answers, but the question is the spark. One might ask: You see planets and stars and galaxies and galaxy clusters and the whole Universe in a glimpse of the sky, all of them with a gazillion of their own questions, and you got interested in ROCKS? Well, yes.

It is no coincidence we find rocks in the countryside. Essentially the whole planet's crust is a rock, so what is the connection? Some 4.6 billion years ago the Solar System was formed. A cloud of gas and dust collapsed under its own gravity to

form a disk, at the center of which the Sun was born. The remainder of the dust in the disk continued stirring around the new-born star, gathering into larger and larger clumps, called planetesimals. These clumps would keep colliding with each other, growing in mass and size, ultimately creating the planets of the Solar System together with the surrounding gas. But as with our child toys, not all building blocks go into our fearsome constructions. Some are left over on the floor. Similarly, planetesimals that did not manage to make it into the planet-forming pipeline got left aside, floating eternally in space. Some of them follow bizarre orbits, and when they come close to the Sun they emit gases in a long bright tail. The people of ancient times witnessed such events and they could not help but correlate them to the presence of their gods. These are the comets. Some others orbit the Sun peacefully, in almost circular orbits. Those are the asteroids.

Although asteroids can be found throughout the Solar System, there is one population of particular interest. Lying between the orbits of Mars and Jupiter is the Main Asteroid Belt. With almost a million discovered asteroids, its name is well justified. The reason for its existence goes back to the era of planetary formation. After Jupiter was formed, its sheer mass made it impossible for other planets to form in close proximity. Disproportionally many unused planetesimals were doomed to never fulfill their destiny and become planets.

But the asteroids in the Main Belt do not live boring lives. They are close to the planets, feeling their gravitational attraction. They are also close enough to the Sun, feeling its heat. And they are many in a tight space. All those effects combined, and we have changes in their orbits, ejections from the Solar System, collisions that shatter them. And when they break apart, new asteroids are born. The original parent asteroids give birth to generations of thousands of all new asteroids. These young generations of asteroids are called asteroid families, reminiscent of their common origin.

Outline

The present thesis is based on the research cases I have been involved with during my PhD studies at the Department of Astronomy, University of Belgrade, under the supervision of Dr. Bojan Novaković.

Chapter 1 provides an introduction to some topics relevant in asteroid family studies, including asteroid collisions, the computation of proper elements, the method used to identify asteroid families, perturbing mechanisms acting on the orbits of family members of gravitational and non-gravitational nature and the principal method for age estimation.

Chapter 2 details the discovery and analysis of the importance of secular resonances with massive asteroids on the evolution of the orbits of small asteroids. The first section presents the study of the (1726) Hoffmeister asteroid family. This work was carried out in collaboration with Bojan Novaković, Zoran Knežević and Clara Maurel, and the main results of it have been published in Novaković et al. (2015). The next section presents the analysis of all linear secular resonances with the two most massive asteroids, involving the precession frequencies of their nodes and perihelia. This work was carried out in collaboration with Bojan Novaković and its main results have been published in Tsirvoulis and Novaković (2016a). The third section presents the analyses of the families of (1251) Seinajoki and (1128) Astrid which were carried out in collaboration with Bojan Novaković, Stefano Maró, Vladimir Djošović and Clara Maurel, with the main results published in Novaković et al. (2016).

Chapter 3 discusses the discovery of two new asteroid families. The first section contains the discovery and analysis of a dark asteroid family, that of (326) Tamara, within the Phocaea region. This work was carried out in collaboration with Bojan Novaković, Mikael Granvik and Ana Todović and its main results have been published

in Novaković et al. (2017). The second section presents the case of a young cluster, sub-family of the (221) Eos family. The main results have been published in Tsirvoulis (2019).

Chapter 4 presents the conclusions and discusses the contributions to the topics of the thesis.

During the course of my PhD studies I worked as an intern at the Observatoire de la Côte d'Azur for three months, where I studied the size distribution of the primordial population of asteroids under the supervision of Alessandro Morbidelli and Marco Delbo, and in collaboration with Kleomenis Tsiganis of the Aristotle University of Thessaloniki. The work carried out there does not focus strictly on asteroid families, but rather on the opposite, that is the state of the population of asteroids before the collisional evolution became a major factor in their evolution. In this context we also extract interesting conclusions about the possible existence of ancient asteroid families which would be unidentifiable today. As such I decided to present the article we published based on these results (Tsirvoulis et al., 2018) in its entirety in the Appendix.

Introduction

Collisional disruption of asteroids is an important factor in the evolution of the Main Asteroid Belt over the age of the Solar System. With so many objects residing therein, and with a number of different gravitational and non-gravitational forces acting upon their orbits, collisions are inevitable given enough time, with the average collisional lifetimes of 1, 10 and 100 km asteroids found by Bottke et al. (2005a) to be 330, 4700 and 34,000 Myrs respectively¹.

The collision depending on the size and relative velocity of the colliding asteroids, usually results in their disruption, either partial or total. In either case a plethora of fragments, new asteroids that is, are created and are ejected into the surrounding space. Immediately after the impact, the fragments act as a closed system which is expanding, with the fragments having ejection velocities (V_{ej}) which depend on the conditions of the impact and follow a Gaussian distribution², fighting against the gravitational pull of the cluster. The latter depends on the size of the parent body, and its strength is correlated to the escape velocity from it (V_{esc}). The expansion practically ends when the fragments have reached the velocity at infinity (V_{∞}) which is equal to:

$$V_{\infty} = \sqrt{V_{ej}^2 - V_{esc}^2} \quad (1.1)$$

The velocity field obtained this way represents the relative velocities of the fragments after the energy of the impact has been dissipated. These relative velocities are usually of the order of tens of meters per second. Since these values are much smaller than the typical orbital velocities in the Main Belt, which are of the order of a few tens of kilometers per second, we reach an important conclusion: The fragments will follow very similar orbits after their initial dispersion, at least in the absence of strong perturbative effects. But the collisions and the creation of the families of fragments we study do not happen in isolation, we need to be able to study them in their physical environment, which requires overcoming some challenges.

¹For a further discussion on the collisional evolution with respect to the diameters of asteroids see section A.5 of the appendix.

²This is strictly true in the case of the complete fragmentation of the parent body, where the ejection field is considered isotopic.

1.1 Proper elements

From observations of the night sky over the past two centuries, we have discovered nearly a million asteroids in the Main Belt, and for the majority of them we have reasonably good orbits.

Suppose we know of the existence of an asteroid family therein, outcome of a collision that happened at some point in the past, as we described above. The main challenge arising is to find the means to identify which asteroids from the whole population belong to the family in question.

Had the collision happened recently in the past, say yesterday for arguments sake, we would witness a dense clustering of the orbits of the family members within the total population of asteroids. But if it happened millions of years ago their osculating elements, derived from their present day positions and velocities, would not reveal any concentrations. In this case, which is the realistic one, we need to seek for clusterings of the orbits as we trace their evolution back in time, i.e. taking into account all the relevant perturbations.

1.1.1 Concept and history

The first step is therefore to find a way to eliminate from the orbits of the asteroids the effects of the periodic planetary perturbations, in order to be left with the unperturbed orbits which should reveal the presence of the family.

This was first done 100 years ago by Kiyotsugu Hirayama in his celebrated work (Hirayama, 1918), where he witnessed that asteroids formed clusters if their osculating elements were projected onto the $(e \cos \varpi, e \sin \varpi)$ plane. Later (Hirayama, 1922, 1927), using the perturbing potential in the linear theory of secular perturbations of Lagrange and Laplace, he was able to derive the first proper elements of the motion of asteroids. Neglecting the terms of the perturbing function that contain the anomalies in the arguments, the short periodic perturbations from the planets are eliminated. The secular part in the eccentricity and inclination is then approximated by a system of linear differential equations. The elimination of the short periodic perturbations results in a constant semi-major axis, which is an integral of the motion, therefore it is the *proper* semi-major axis (a_p).

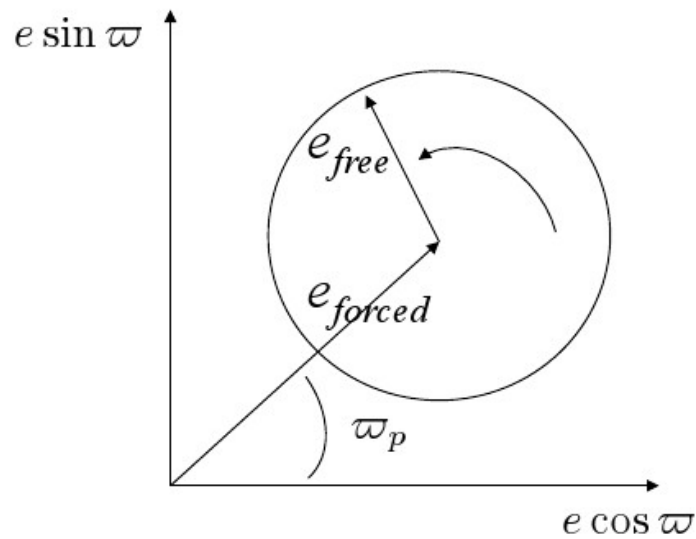


Fig. 1.1.: The geometrical relationship among the osculating, free and forced eccentricities and longitudes of pericenter (From Murray and Dermott (1999))

The solutions of the linearized secular system can be represented in the planes $(h, k) = (e \sin \varpi, e \cos \varpi)$ and $(p, q) = (\sin i \sin \Omega, \sin i \cos \Omega)$ as the sum of proper modes, one for each planet, plus one for the asteroid. This results in an epicyclic motion, with the contributions of all the planets represented by the forced term, and with the free oscillation of the asteroid being the additional circular motion. An illustration of this is shown in ???. The amplitudes of the latter are also integrals of the motion and correspond to the *proper* eccentricity (e_p) and the sine of the *proper* inclination ($\sin i_p$). This set of proper elements allowed Hirayama to identify the first asteroid families, namely Koronis, Eos, Themis, Flora and Maria.

The proper elements are therefore exact integrals of the approximated equations of the motion of an asteroid. For the complete equations of motion they can only be treated as approximate, or quasi-integrals of the motion.

The struggle over many years has been to derive more accurate approximations, leading to more accurate proper elements, that should be stable over longer time spans. The linear theory of Laplace and Lagrange is truncated to order one in the ratio μ of the masses of the perturbing planet to that of the Sun, and to degree two in the eccentricities and inclinations.

The first improvement was introduced by Brouwer (1951), who included also a couple of resonant terms of second order in the masses and used an improved model for the motion of the planets.

Bretagnon (1974) developed the first theory of secular perturbations for the planets up to order two in the masses and degree four in the eccentricities and inclinations. A similar theory of secular perturbations, of order two and degree four, but for the motion of an asteroid of negligible mass under the influence of the major planets was developed by Yuasa (1973), but was not used to compute the proper elements of asteroids.

Kozai (1979) used a similar theory to that of Yuasa for high inclination asteroids to define a set of proper parameters and identify asteroid families, but Knežević (1988, 1989) was the first to correct and complete the theory of Yuasa with the necessary indirect part, and use it to derive more accurate proper elements.

1.1.2 Analytical theory of proper elements

The analytical computation of the proper elements of the motion of an asteroid starts with a hamiltonian of the form:

$$H = H_0 - \epsilon \mathcal{R} \tag{1.2}$$

where H_0 is the Hamiltonian of the unperturbed two body problem, and the effects of the planets are considered as perturbations of the Keplerian motion represented by \mathcal{R} multiplied by the small parameter ϵ corresponding to the ratio of the masses of the perturbing planets to that of the Sun. In Delaunay canonical variables³ the Keplerian part is completely degenerate, being a function only of the variable L . Since in the two body problem the perihelion and the node do not precess at all, the corresponding frequencies are zero. The problem that arises is that the perturbed problem, with hamiltonian:

$$H = H_0(L) - \epsilon \mathcal{R}(L, G, J, \ell, g, j, \ell') \tag{1.3}$$

³ $L = \sqrt{Gm_{\odot}a}$, $G = L \cdot \sqrt{1 - e^2}$, $J = G \cdot \cos I$, $\ell = M$, $g = \omega$, $j = \Omega$

usually requires the substitution of a solution of H_0 into the perturbing function \mathcal{R} , and therefore the mean anomaly conjugate to L can be eliminated, but the other angles (g, j) , conjugate to the other action variables (G, J) cannot be removed by averaging.

To overcome this problem the procedure to compute the proper elements is comprised by two steps. First the short periodic perturbations are eliminated by a transformation that averages over the fast variables l, l' . After this step the mean elements are obtained. Another transformation is then performed, in order to eliminate the long periodic perturbations, represented by the terms of the perturbing function containing the variables g, j , providing the proper elements.

The computation of proper elements is therefore reduced to the choice of an appropriate expansion of the disturbing function, and the techniques required to perform the transformations.

The expansion used by the currently most acclaimed theory, that of Milani and Knežević (1994) is essentially the expansion computed by Yuasa (1973), corrected and completed by Knežević (1989, 1993). The expansion is complete to degree four terms in eccentricities and inclination in the first order with respect to perturbing mass, and to degree two in the second order. Milani and Knežević (1990) found that at orders in the masses beyond the first, explained that the canonical map provided explicitly by the formulas of the perturbation theory based on the Lie series transformations are from the proper to mean elements, i.e. in the opposite direction from the desired one. Therefore the computation of the proper elements from the mean ones requires the solution of an inverse function problem, which is achievable only by the use of an iterative procedure.

This expansion, of order two and degree four, is then handled by a perturbation technique based on the use of algebraic manipulation, which allows the perturbing function to be approximated by a finite sum of terms, each with a simple expression of the form:

$$\mu b(L) e^h e'^k I^j I'^m \cos(p\ell + q\ell' + \delta) \quad (1.4)$$

where h, k, j, m, p, q are integers, the primed elements refer to a perturbing planet, b is a known function and δ is a combination of the angles including g, g' , the

perihelia, and j, j' , the nodes of the asteroid and the planet. The simple form of these terms allows the analytical computation of both derivatives and integrals, meaning that the series can be handled term by term. The problem is thus reduced to the evaluation of a finite number of elementary operations.

The main limitation of the analytical method arises from the fact that the series is truncated to a certain order in the masses and degree in the eccentricities and inclinations, leading to a deteriorating accuracy for high values of these variables.

It is noteworthy that the expansion of the perturbing function and the perturbative method used to manipulate it is entirely a matter of choice, which is instructed by the target accuracy of the proper elements for the specific problem at hand each time. Nevertheless, the procedure followed is quite standard and can be broken down to a number of basic steps, as pointed out also by Lemaitre (1993):

1. modeling of the asteroid motion in a convenient way according to the scope of the problem, and separating the perturbations depending on the mean longitudes from the rest. This enables the distinction between the short and long periodic perturbations.
2. computation of the mean orbital elements by removing the short periodic perturbations. The first proper element, the proper semi-major axis is obtained at this point.
3. splitting of the resulting hamiltonian into the integrable, secular part, and the perturbation, the part depending on the slow secular angles.
4. removal of the long periodic terms and computation of the remaining proper elements and secular frequencies.

The realization that the proper elements are the outcome of this simple sequence of steps, no matter the method used to perform each one of them, led to the development of a new theory that performs these steps in a purely numerical way.

1.1.3 Synthetic theory of proper elements

Knežević and Milani (2000) developed a synthetic theory for the computation of proper elements. They devised a method that uses numerical procedures to

execute the steps enlisted above, deriving the same classical set of proper elements $(a_p, e_p, \sin i_p)$ and fundamental frequencies $(\dot{\varpi}_p = g, \dot{\Omega}_p = s)$. The theory is an adaptation of the approach used by Carpino et al. (1987) to numerically derive the motion of the outer planets, with the necessary alterations for the asteroid case.

The first step is the numerical integration of the orbit of the asteroid together with the orbits of the perturbing planets. The time span of the integration has to be long enough, optimally at least twice as long as the period of the slowest secular perturbation. The choice of Knežević and Milani (2000) was initially 2 Myrs, in an effort to maintain balance between accuracy and computational cost, but longer time spans were used for cases where the required accuracy was not met. The integrator used was the ORBIT9 propagator-interpolator, which uses a symplectic single-step method (implicit Runge-Kutta Gauss) as starter, and a multistep predictor-corrector to perform the rest of the integration (Milani and Nobili, 1988). The indirect effects of the planets that are not included in the integration explicitly, are taken into account by adding their mass to that of the Sun, and applying a barycentric correction to the initial conditions.

The fact that the N-body problem is strongly degenerate, that is the spectrum of the orbital elements is divided into high and low frequencies quite distinctively, allows the removal of the short-periodic perturbations "on-line": A specially adapted digital low-pass filter, with a frequency response as the one shown in the example in Figure 1.2 (for more details see: Carpino et al., 1987), is applied to the immediate output of the integrator, removing the short periodic oscillations and outputting directly the mean elements at each time-step during the numerical integration.

The equivalent of the next steps, that is the splitting of the integrable secular part from the perturbation, and the removal of the long periodic perturbations, were achieved by performing Fourier analysis on the time series of the mean elements once the integration was completed.

The time series of the mean equinoctial elements $(h, k) = (e \sin \varpi, e \cos \varpi)$ and $(p, q) = (\sin i \sin \Omega, \sin i \cos \Omega)$ are decomposed into Fourier components. The forced secular perturbations generated by the precession of the perihelia of Jupiter, Saturn and Uranus, which have known frequencies g_5, g_6, g_7 are removed by eliminating the components with these frequencies from (h, k) . The same is done with the components of (p, q) with frequencies corresponding to the precession rates of the nodes of Saturn, Uranus and Neptune (s_6, s_7, s_8) . Next the time series of the free arguments ϖ_f, Ω_f of the oscillations in the planes $(h, k), (p, q)$ is computed, by ex-

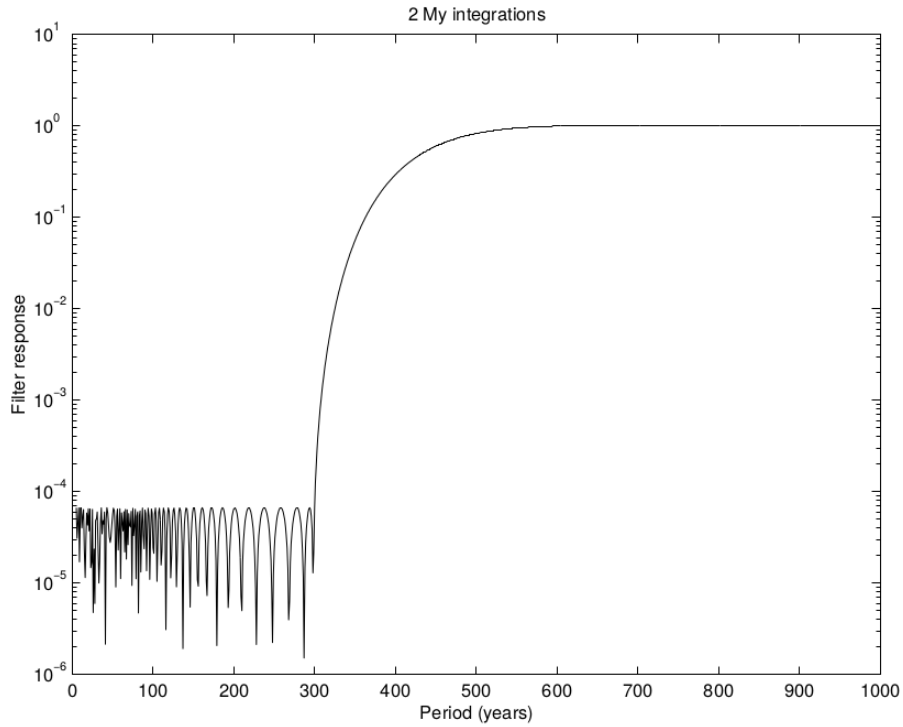


Fig. 1.2.: The frequency response of the digital filter used in the 2 Myrs integrations.

tracting the polar angles and adding multiples of 2π in order to obtain a continuous function. A least squares fit allows the estimation of the proper frequency g as the slope of the time series of ϖ_f , and of s as the slope of the time series of Ω_f . Finally the time series of $(h(t), k(t))$ and $(p(t), q(t))$ are converted into functions of ϖ_f and Ω_f respectively $[(h(\varpi_f), k(\varpi_f))$ and $(p(\Omega_f), q(\Omega_f))]$, and the proper modes are extracted as the components with periods 2π . The amplitudes of these proper modes are the proper elements e_p and $\tan I_p/2$.

1.2 Identification of asteroid families

Having obtained a suitable set of proper elements of the motion of all the asteroids we are concerned about, that is asteroids generated in collisions and ones that form the so-called "background" population, with satisfactory accuracy, we can demonstrate their importance in the identification of asteroid families.

Figure 1.3 shows the population of all asteroids in the Main Belt with absolute magnitudes $H < 15$. In the left panel the points represent the osculating orbital elements of the asteroids, while in the right panels their proper elements, derived by

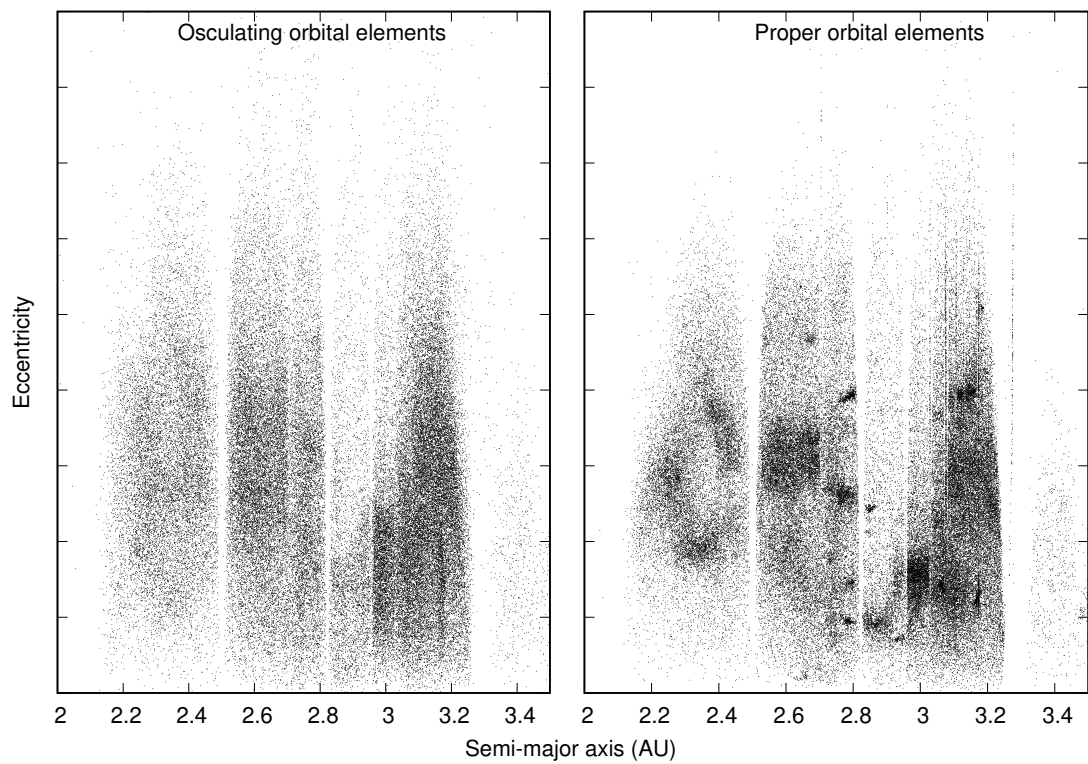


Fig. 1.3.: Comparison of osculating versus proper elements of the population of asteroids with $H < 15$ in the Main Belt.

the synthetic method, are shown. The difference is striking; many asteroids seem to form clumps in the proper elements phase space whereas in the osculating elements they seem to have a rather uniform distribution. The clumps of course correspond to asteroid families, groups of asteroids that were generated through collisional events as described above. By the computation of the proper elements we have successfully revealed the similarities in the orbits of family member asteroids, which were previously hidden due to the periodic perturbations from the planets.

Even though in the phase space of proper elements, some asteroid families are easily distinguishable by the contrast in the local number density of asteroids they produce, it could be argued that finding the boundary between an asteroid family and the local background is not a trivial task.

Asteroid families do have a higher number density than the background, but that density cannot be expected to be constant. On the contrary, it is often the case that the core of the family will have a high density, that drops toward its outskirts matching the local background population value. This means that separating the family is not as easy as drawing a surface around it ad-hoc.

Indeed after the discovery of the Hirayama families, many efforts were made to improve the classification of asteroids into families along with improved computations of proper elements (Arnold, 1969; Brouwer, 1951; Carusi and Massaro, 1978; Kozai, 1979; Lindblad and Southworth, 1971; Williams, 1979, 1989), but apart from the very prominent classical families, no agreement was ever established about the other proposed asteroid families. The major reason for this was that most of their analyses were based exactly on visual inspection and interpretation of the clusterings, only in some cases followed by statistical tests to evaluate the level of significance of the groups.

1.2.1 The Hierarchical Clustering Method

The need for a mathematically robust method to identify the members of families was met in 1990 with the introduction of the Hierarchical Clustering Method (HCM) by Zappalà et al. (1990), which is outlined below.

The first task is to establish a way to quantify the similarity between orbits in the proper elements phase space. This was done by defining a suitable metric

function with which distances in the proper elements three-dimensional space are measured.

Starting from the fact that families are generated by the explosive breakup of a parent body, following a collision with a "projectile" asteroid, for any pair of the fragments the differences in their osculating elements are linked to the components of the post-breakup ejection velocities through Gauss' equations:

$$\begin{aligned}\delta a/a &= 2\delta v_1/na \\ \delta e &= \delta v_2 \sin(f)/na + 2\delta v_1 \cos(f)/na \\ \delta i &= \delta v_3 \cos(\omega + f)/na\end{aligned}\tag{1.5}$$

where a, e, i, ω and f are the osculating semi-major axis, eccentricity inclination, argument of perihelion and true anomaly respectively, n is the mean motion, and na is the circular velocity of the parent body at the instant of breakup, while $\delta v_1, \delta v_2, \delta v_3$ are the along-track, radial and out of plane components of the ejection velocity. Were the angles f and $(\omega + f)$ known for any given family at the time of the impact, we could use the differences in the proper elements instead of the osculating ones. But even with f and $(\omega + f)$ unknown, Equation 1.5 show that if the chosen distance function in the proper elements space is of the form:

$$\delta v = na\sqrt{k_1(\delta a'/a')^2 + k_2(\delta e')^2 + k_3(\delta i')^2}\tag{1.6}$$

with coefficients k_1, k_2, k_3 of order unity, the metric will give an order of magnitude estimate of the velocity increment causing separation of the two orbits. By squaring Equation 1.5, averaging over f and $(\omega + f)$ and then substituting $\delta a'/a', \delta e', \delta i'$ into Equation 1.6 we get:

$$\delta v = \sqrt{x \langle \delta v_1^2 \rangle + y \langle \delta v_2^2 \rangle + z \langle \delta v_3^2 \rangle}\tag{1.7}$$

with

$$\begin{aligned}
x &= 4k_1 + 2k_2 \\
y &= k_2/2 \\
z &= k_3/2
\end{aligned}
\tag{1.8}$$

Since it is obvious that with this averaging method one cannot obtain $x = y = z = 1$ with $k_1, k_2, k_3 > 0$, the values $k_1 = 5/4$, $k_2 = 2$ and $k_3 = 2$ were chosen as standard metric coefficients, yielding the metric:

$$\delta v = na\sqrt{5/4(\delta a'/a')^2 + 2(\delta e')^2 + 2(\delta i')^2}
\tag{1.9}$$

Using this metric, all the distances between all asteroids to their nearby neighbors are determined. Then the two closest objects, labeled for example j and k , are identified, and are agglomerated into a new object $j + k$. Then all the distances are recomputed, defining the distance of any asteroid i to the agglomeration as $\delta(i, j + k) = \min[\delta(i, j), \delta(i, k)]$, i.e. to the closest member of the clustering. The whole process is then iterated until all asteroids have been agglomerated. The outcome of the algorithm is a dendrogram connecting all the objects, and for any selected threshold value $\delta v'$ of the distance, all clusterings are easily identified.

Often times, when the membership of specific asteroid family needs to be determined, a more practical implementation is used: instead of looking for all the clusterings and their growth with increasing distance δv , it is more convenient to look at the growth of only the cluster that likely corresponds to the core of the family.

Having a rough idea about the presence of an asteroid family is enough to identify the largest asteroid close to its center and assume that it is the largest remnant of the breakup. Even if this is not true, it is sufficient that the selected object is within the densest part of the family. Then a relatively small threshold value $\delta v'$ is selected, and the clustering method is applied until all objects with mutual distances smaller than $\delta v'$ are clustered together. The number of these objects is logged. Then the threshold distance is increased by a chosen increment and the process is iterated until all the objects are clustered together. This way the number of clustered asteroids as a function of distance threshold is obtained ($N(\delta v)$), and this enables the evaluation of the growth of the core cluster of the family. An example of this procedure is seen in Figure 1.4.

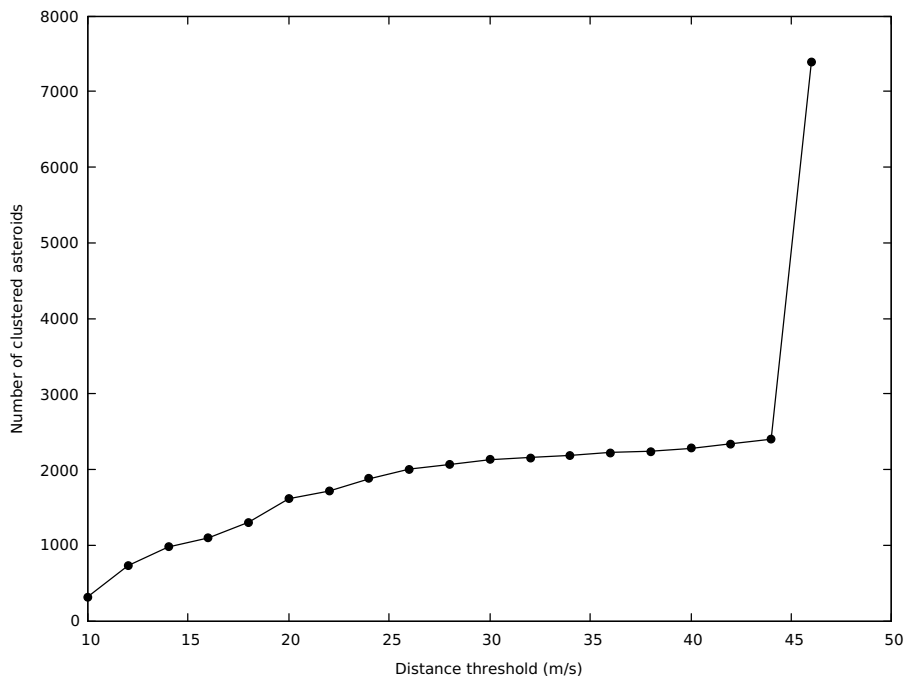


Fig. 1.4.: The number of clustered asteroids as a function of the distance threshold for an example case.

Even though the procedure up to this point has been instructed solely by the physical process of the breakup and the mathematical relations, the final step, that of the definition of the membership of the family, still includes the human factor. A specific value of the threshold distance is selected and the asteroids comprising the cluster at that value are deemed members of the family. Still the HCM is invaluable because it provides all the necessary information for that decision to be as justified as possible.

In the ideal case where a family is formed in relative isolation, or at least at a point in the phase space where the number density of the background population is low, the density contrast it will produce will be very sharp. This will translate to the number of objects as a function of the distance threshold to feature an initial steady growth, where the members of the family are being included in the cluster since the number density is not constant, followed by a flat part after all the members have been included, and then followed by (at much larger values of $\delta v'$) a sharp increase to the entire population. In this case the choice of the membership is obvious, corresponding to the steady state population. If, on the other hand a breakup happens at a location where the number density of the background population is comparable to that of the new cluster, perhaps as an outcome of other families also having formed in the region, the number of clustered objects with increasing $\delta v'$

may even never reach a steady state. In practice most of the families that have been studied are somewhere in the middle of these extreme cases, and an educated decision has to be made to define their membership.

To verify the results of the identification, statistical tests are usually required. They are usually based on the following idea: A quasi-random population, with the same number of asteroids, is randomly distributed within the same volume in the proper elements phase space as the real population. Then the HCM is run on this population, and the $\delta v'$ level at which random clusterings appear is logged. If the clusterings of the real population are denser and/or deeper⁴ than those of the random one, then they should correspond to real breakup events and they are not random artifacts.

Another implication that has to be noted is that, even in the ideal case described above, the number density of the background population may be small but not zero. This means that the family population will always be superimposed to the background population, and some asteroids from the latter will always end up in the membership list. These asteroids are dynamically equivalent to those that originated from the breakup, and they cannot be distinguished by methods such as HCM which are based solely on the dynamical characteristics of the asteroids in the population. This means that the HCM can only identify "dynamical families", which share asteroids but are not in a one-to-one correspondence to the "real families".

1.3 Dynamical evolution of asteroid families

The successful identification of the members of asteroid families, despite being a lengthy process as demonstrated, usually is nothing but the first stage of our studies. What we actually care about most of the time is reconstructing the whole evolution of the family population since its birth, and understanding the various phenomena, of gravitational and non-gravitational nature, that contributed bigger or smaller parts, to reach the presently observed situation.

We have already examined, in the computation of the proper elements, the effects of short and long periodic perturbations acting upon the asteroids from the planets. Viewing the procedure in reverse, we understand how these perturbations can cause apparent separations to initially similar orbits.

⁴by deeper we mean with a larger density gradient.

To eliminate the short and long periodic effects from the orbits of the asteroids, in order to derive the proper elements, we have essentially averaged over the fast and slow frequencies of the asteroidal motion. However there are cases where the averaging methods hide the complete dynamics of the motion, and special attention is needed. Such occasions are usually met at parts of the phase space where resonant effects arise.

1.3.1 Mean Motion Resonances

When the semi-major axes of an asteroid and a perturbing planet are such that the ratio of their mean motions is equal to a ratio of integers, a Mean Motion Resonance (MMR) occurs. This is usually denoted as:

$$\frac{n'}{n} = \frac{p}{p+q} \quad (1.10)$$

where n and n' are the mean motions of the asteroid and the perturbing planet respectively, and p, q are integers.

When this condition is met, the asteroid and the planet are guaranteed to have repeated occurrences of the exact same configuration in the physical space. Most important is the moment, and the repeating instances of it, when they are at a conjunction, i.e. at their closest distance. Immediately before these conjunctions, the tangential component of the force exerted from the planet to the asteroid is different from the one exerted immediately after, therefore there is a non-zero net tangential force over the course of the conjunction⁵ This net tangential force leads to exchange of angular momentum, which in the case of a planet perturbing an asteroid with negligible mass leads to a repeated gain or loss (depending on the geometry) of angular momentum of the asteroid.

In the Hamiltonian formulation, the series expansion of the perturbing function contains cosines with arguments of the form:

$$\sigma = k_j \lambda_j + k \lambda + l_j \varpi_j + l \varpi + m_j \Omega_j + m \Omega, \quad j = 1, N \quad (1.11)$$

⁵Apart from the extremely unlikely case where the two orbits are in perfect alignment ($\Omega = \Omega', \omega = \omega'$) and the conjunction happens exactly at the perihelion or the aphelion.

The MMR in the general case occurs when the mean motions of the asteroid and one or more perturbing bodies are such that the time derivative of a certain argument ($\dot{\sigma}$) becomes almost zero. When trying to integrate the terms of the hamiltonian, the vanishing time derivative of the resonant terms will appear at the denominator, and the problem of small divisors arises. The resonant terms become significantly larger than the non-resonant ones, and thus they cannot be averaged out, but they need to be retained and treated separately.

For the asteroid case, where the secular frequencies $\dot{\omega}$ and $\dot{\Omega}$ are much smaller than the orbital frequency $\dot{\lambda}$ the resonant relation becomes:

$$\dot{\sigma}_{MMR} \approx k_j \dot{\lambda}_j + k \dot{\lambda} \approx 0, \quad j = 1, N \quad (1.12)$$

from which the resonant semi-major axis (a_{res}) of the Keplerian approximation can be found. In higher order approximations, all arguments such as the one in Equation 1.11 with the same ratio of k and k_j but different l, l_j, m, m_j , provided that they obey the D'Alembert rules, correspond to the same MMR and to approximately the same a_{res} . Therefore each MMR with specific combination of k and k_j is composed of various resonant terms, which form the so-called resonant multiplet.

1.3.2 Secular Resonances

Another type of resonances that manifests over longer time scales, are the secular resonances. As the name suggests, in these cases the relevant frequencies are the slow ones, i.e. the precession frequencies of the ascending nodes and of the perihelia.

Considering that the asteroid is far from MMRs, and that its, and the perturbing planets' mean motions can be effectively averaged, we can study the motion of the whole orbits with respect to one another. Since the longitudes of the ascending nodes and of the perihelia represent the orientation of the orbits, their respective precession frequencies will determine whether there will be repeating occurrences of the same mutual configuration. So the secular resonances correspond to conjunctions of the whole orbits of the asteroid and the relevant perturbing planet in each case.

Returning to the expansion of the perturbing function and the general form of the arguments shown in Equation 1.11, we focus on the terms with $k, k_j = 0$. The secular resonant terms are then the ones for which:

$$\dot{\sigma}_{sec} \approx l_j \dot{\varpi}_j + l \dot{\varpi} + m_j \dot{\Omega}_j + m \dot{\Omega} \approx 0, j = 1, N \quad (1.13)$$

with l, l_j, m, m_j such that they follow the D'Alembert rules. The idea is similar to the case of the MMRs in that the arguments of the resonant terms appear as small divisors in the solution obtain after integration, and therefore the solution is not converging since it is sensitive to small variations in the frequencies.

The importance of secular resonances has been pointed out already in the 19th century by Le Verrier (1856) and Tisserand (1882) and Charlier (1900, 1902), who noticed a match between the location of the secular resonance concerning the precession of the perihelion of Saturn (ν_6) and the inner end of the Main Belt. A century later, thanks to the works of Froeschle and Scholl (1989), Knežević et al. (1991), Michel (1997), Milani and Knežević (1992), and Morbidelli and Henrard (1991) amongst others, we have a map of the locations of the most important secular resonances throughout the solar system, which are represented as surfaces in the three dimensional proper elements space. An example of a projection of such a map on the $(a_p, \sin i_p)$ plane is shown in Figure 1.5.

Secular resonances involving the precession frequencies of the nodes of the perturbing planets and the asteroid cause librations in the inclination of the latter, while those involving the precession frequencies of the perihelia affect its eccentricity. The magnitude of the effects depends primarily on the mass of the perturbing planet(s) and the proximity of the asteroid to them and the degree of the resonance, defined by the degree in the eccentricity or inclination of the resonant term in the perturbing function. The lowest degree resonances are therefore generally the strongest.

1.3.3 The Yarkovsky Effect

Another important perturbation on the orbits of asteroids, and certainly the most important non-gravitational one, is the one arising from the so-called "Yarkovsky effect". It was initially proposed by Russian civil engineer Ivan O. Yarkovsky, who noted in a privately published pamphlet (Yarkovsky, 1901) that heating a prograde-

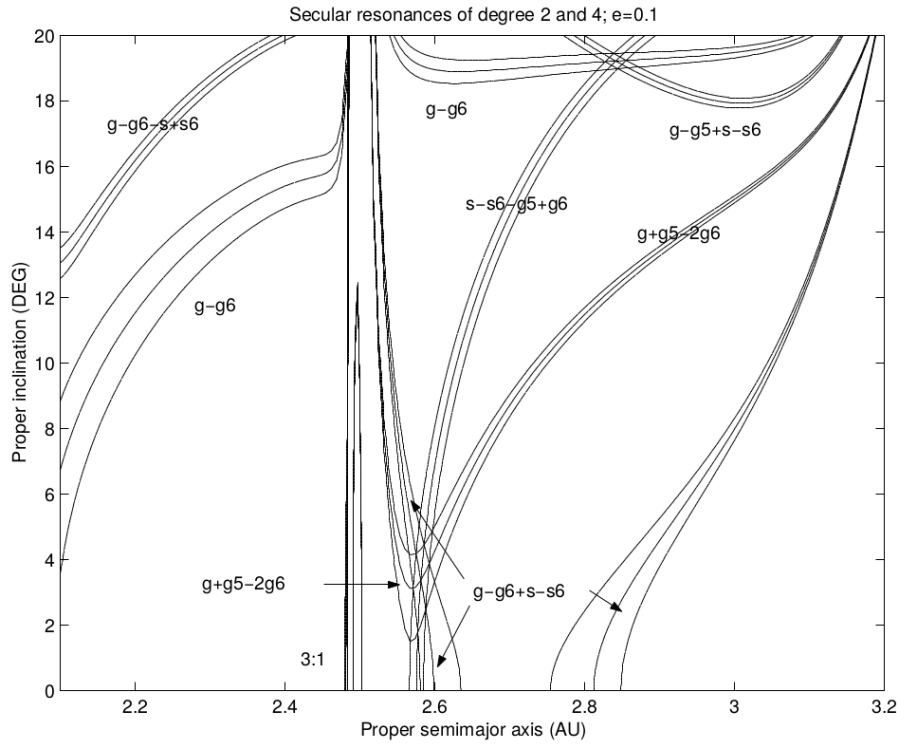


Fig. 1.5.: The locations of secular resonances of degree 2 and 4 for eccentricity $e = 0.1$ in the Main Belt, from Milani and Knežević (1990)

rotating planet should produce a transverse acceleration in its motion. Even though the context he put his work in was trying to find a way to counter-balance the assumed drag of the ether, a popular hypothesis at the time, the proposition was correct.

Ernst Öpik and Vladimir Radzievskii revisited the subject half a century later (Opik, 1951; Radzievskii, 1952), with the latter being the first to consider the effects of systematic photon thrust on a body's rotation despite his concept being based on a variable albedo coefficient across the surface, an assumption not supported by evidence for asteroids or meteors. Stephen Paddack and John O'Keefe (Paddack, 1969) realized that the irregular shape of the body along with the thermal radiation, rather than reflected sunlight, were the most important factors for the change of the spin rate, setting the strong foundation for what is now known as the Yarkovsky-O'Keefe-Radzievskii-Paddack effect, or YORP for short.

The next breakthrough came in the late 1990's through the works of David Rubincam and Paolo Farinella. While studying thermal perturbations on artificial satellites, they realized a direct link between the orbital effects acting on the geodynamics

satellites such as LAGEOS and those acting on small meteoroids (Farinella et al., 1998; Rubincam, 1995, 1998). This led to a number of new studies regarding the dynamical evolution of small asteroids and their populations' orbits due to the Yarkovsky effect (Bottke et al., 2001; Bottke et al., 2006; Vokrouhlický et al., 2006b), setting the Yarkovsky and YORP effect on the forefront of small body research ever since.

Classical model of the Yarkovsky effect

The Yarkovsky effect depends on the anisotropic emission of thermal radiation from a rotating asteroid, illuminated by the Sun. The directly reflected sunlight does not have any contribution on long-term dynamical effects on the orbital motion, as shown by Vokrouhlický et al. (2000). In order for the thermal re-emission of the absorbed radiation to be anisotropic, it is necessary that the thermal inertia of the asteroid is not zero. Under this reasonable assumption the shape of the body itself does not play an important role; even a spherical model is enough to provide a good approximation of the perturbation on the orbit.

The most prominent contribution of the Yarkovsky effect is the secular modification of the semi-major axis, despite small variations being induced in the other orbital elements as well. Under three basic assumptions, namely the linearization of the surface boundary condition, a rotation about a spin axis fixed in the inertial space and a circular orbit around the Sun, the orbit-averaged change in the semi-major axis a is composed of two contributions the diurnal and the seasonal:

$$\left(\frac{da}{dt}\right)_{diurnal} = -\frac{8}{9} \frac{\alpha\Phi}{n} W(R_\omega, \Theta_\omega) \cos \gamma \quad (1.14)$$

$$\left(\frac{da}{dt}\right)_{seasonal} = \frac{4}{9} \frac{\alpha\Phi}{n} W(R_n, \Theta_n) \sin^2 \gamma \quad (1.15)$$

where $\Phi = \pi R^2 F / (mc)$ (with R being the radius of the body, F the solar radiation flux at distance a from the Sun, m the mass of the body and c the speed of light), n is the orbital mean motion, $\alpha = 1 - A$ (with A being the Bond albedo) and γ is the obliquity of the spin axis. The factor Φ is a factor characteristic to any physical effect related to sunlight being absorbed or scattered by the surface of the body, and

since the mass is proportional to the cube of the radius, we obtain that Φ is inversely proportional to the radius. The function:

$$W(R_\nu, \Theta_\nu) = -\frac{\kappa_1(R_\nu)\Theta_\nu}{1 + 2\kappa_2(R_\nu)\Theta_\nu + \kappa_3(R_\nu)\Theta_\nu^2} \quad (1.16)$$

scales the magnitude of the effects depending on a set of thermal parameters of the body plus a relevant frequency ν . The relevant frequencies are the rotational frequency about the spin axis ω for the diurnal and the orbital mean motion n for the seasonal components respectively. The relevant physical parameters are the surface thermal conductivity K , the surface heat capacity C and the surface density ρ . W depends on those parameters through R_ν and Θ_ν . The characteristic penetration depth of temperature changes, assuming a periodic surface irradiation with frequency ν , is linked to the scale length $l_\nu = \sqrt{K/\rho C\nu}$. The non-dimensional radius of the body is subsequently defined as $R_\nu = R/l_\nu$. Θ_ν is a thermal parameter that depends on the surface thermal inertia $\Gamma = \sqrt{K\rho C}$ through the relation $\Theta_\nu = \Gamma\sqrt{\nu}/\epsilon\sigma T_\star^3$, with ϵ being the thermal emissivity of the surface, σ the Stefan-Boltzman constant and T_\star the sub-solar temperature. For bodies with size much larger than the characteristic scale length l_ν it was shown (Rubincam, 1995; Vokrouhlický, 1998) that the Function W does not depend on the size R , therefore the net effect is simply inversely proportional to R . Since the rotational frequency ω is usually much larger than the mean motion n , the thermal parameter Θ_ω is much larger than Θ_n , which implies that the diurnal effect usually dominates the seasonal effect.

The diurnal effect is based on the fact that for a rotating body with non zero thermal inertia, in the course of each rotation the point of maximum temperature, therefore of maximum emission, is lagging behind the point of maximum illumination. This results in a non-zero net emission of photons in the along-track direction, which carry away momentum. The law of conservation of momentum demands that the rotating body suffers a change in its along track speed, and consequently on its semi-major axis. As seen in Equation 1.14 the net effect is proportional to the cosine of the obliquity yielding a maximum increase rate of the semi-major axis for a purely prograde rotation ($\gamma = 0^\circ$) and a maximum decrease rate for a purely retrograde rotation ($\gamma = 180^\circ$).

The seasonal effect on the other hand is based on the fact that in the course of each revolution about the Sun there is a net emission of photons from the leading face of the body, therefore the conservation of momentum demands that the along-track

speed decreases and consequently the semi-major axis decreases as well. Indeed as seen in Equation 1.15 the drift rate is proportional to the square of the sine of the obliquity, meaning that, due to Equation 1.16, it is always negative, attaining its maximal value for $\gamma = 90^\circ$ and vanishing for $\gamma = 0^\circ$ or $\gamma = 180^\circ$, where the rotation of the body about its spin axis negates the effect completely.

The V-shape method

The most important application of the Yarkovsky effect is the determination of the ages of asteroid families, i.e. the time elapsed from the breakup of the parent asteroid to the present. The method (see e.g. Vokrouhlický et al., 2006b) is based on the diurnal component of the Yarkovsky effect, and on the very fact that the magnitude of the drift in semi-major axis induced by the effect is inversely proportional to the radius of each asteroid.

The fragments produced in a collision between asteroids, i.e. the family members, have sizes that cover a certain range. The upper boundary of the range is the size of the parent body itself, for the obvious reason that no matter how small fraction of it is expelled into fragments, it can only become smaller. The lower boundary of the range is limited by the ability of the telescopes to detect small objects; We can always expect pebbles or dust particles to originate from a collision, but we can never hope to see them and determine their orbits.

On the other hand, the spin axis orientation attained by each fragment after the breakup depends on the local conditions at the time of the collision, and in principle we can safely assume that there should be no correlations, resulting in a random distribution, independent of the sizes. ⁶

These facts together with the proportionality relations between the drift rate $(da/dt)_{diurnal}$ and the radius R and obliquity γ produce an interesting outcome, that is the distribution of the asteroids members of a family in a plane with coordinates the proper semi-major axis and the inverse of the radius (or as more frequently used the diameter), i.e. $(a_p, 1/D)$, will attain the shape of an inverted triangle, or as it is called a "V-shape" (see an example in Figure 1.6).

⁶The subsequent evolution of the rotational states of the fragments due to the YORP effect primarily, may alter the distribution (see e.g. Hanuš et al., 2013; Milani et al., 2018), but not to an extent of affecting the reliability of the V-shape method.

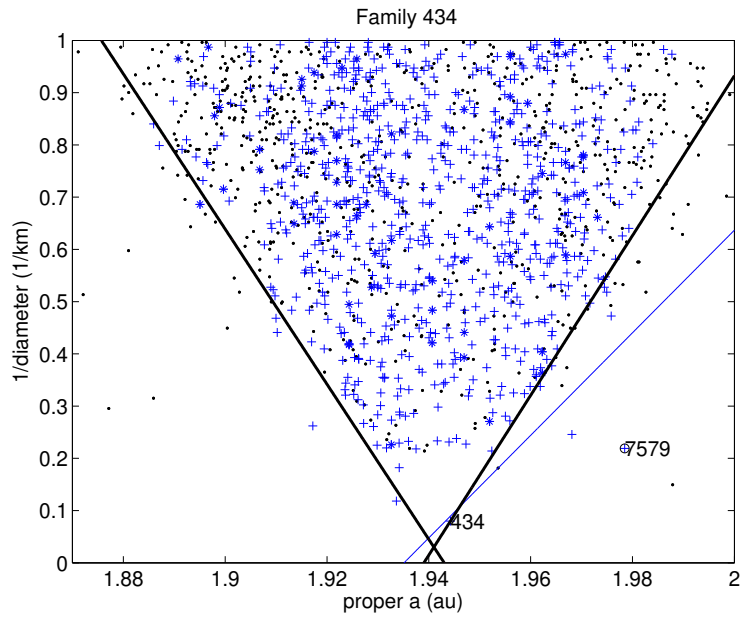


Fig. 1.6.: Distribution of the members of the (434) Hungaria asteroid family in the $(a_p, 1/D)$ plane, from Spoto et al. (2015).

The lines enveloping the distribution of asteroids in this plane, i.e. the lines forming the "V" correspond to the distance that the "fastest" asteroids could reach since the family formed as a function of their diameter; the IN side, toward lower semi-major axes, corresponds to the pure retrograde rotators while the OUT side, toward larger semi-major axes corresponds, to purely prograde rotators of a given diameter. Therefore the slopes of these lines correspond to the total drift in semi-major axis, suffered by a theoretical family member of 1 km in diameter since the formation of the family.

In the ideal case the determination of these slopes would be a simple task. However, in reality many factors that have to do with the dynamical interactions between the Yarkovsky drift and various resonances, chaotic diffusion of the orbits and errors in the observational data, only to name a few, render this a demanding effort. Various methods have been used to accurately determine these slopes, the most mathematically robust one which is also providing an estimate of the errors being the one developed by Spoto et al. (2015). It is based on the idea of dividing the asteroids in bins according to $1/D$, separating the IN from the OUT side, selecting the furthestmost points of each bin on each side and performing a least squares fit through these points, finally obtaining two values of the slopes, one for each side.

Assuming that all the family members have similar thermophysical characteristics, a reasonable assumption since they originated from the same parent body⁷, and that we can derive them somehow, we can use Equation 1.14 to obtain a reference value of the drift rate, that is the maximal ($\cos \gamma = 1 \iff \gamma = 0^\circ$) drift rate for an object with a diameter of 1km: $(da/dt)_{max}(1km)$.

Another approach to determine the reference value, as used in Spoto et al. (2015), is to use the Yarkovsky drift rate measured from observations of an actual asteroid, and then scale it appropriately to the parameters of each family.

It is then straightforward to use this value together with the measured slope of the bounding lines of the V-shape to derive the age of the family.

1.3.4 Numerical simulations and chaos

Due to the chaotic nature of the dynamics of the Solar System in general, and of the Main Belt in particular, asteroids move in inherently chaotic orbits. If this was not the case we would only need to start from their current osculating orbital elements and integrate their orbits backwards in time for as long as we wanted, and follow their complete dynamical path through history. However the chaotic nature of the orbits prohibits us from doing so for time spans longer than a few tens of million years. For asteroid families, with some exceptions, we usually have to deal with ages of hundreds of million years to few billion years. This means we can never replicate exactly the dynamical evolution of the very asteroids that make up a given family. Luckily enough, when studying asteroid families no specific asteroid is of particular interest, except maybe the parent body. What we are interested in is the dynamical evolution of the family as a population, and its statistical properties. Therefore instead of trying to follow the history of the actual family, which we cannot do, we rather follow the evolution of a statistically equivalent fictitious family, which we can do indeed. We can then iterate the process of choosing the parameters of the fictitious population and running the simulation until the final result matches the observed properties of the actual family, which means our initial conditions match the real family at the starting epoch.

⁷In the case the parent body was differentiated, and completely fragmented this assumption does not hold, but this is the case only for very large asteroids and the assumption here serves for demonstrating the method only.

Dynamical evolution of asteroid families: Secular resonances with massive asteroids

” *The very nature of science is discoveries, and the best of those discoveries are the ones you don't expect*

— Neil deGrasse Tyson

In this chapter we will describe the work performed and the results obtained concerning the study of several asteroid families which evolve under the gravitational influence of massive asteroids via secular resonances. We first present our study on the dynamical properties of the Hoffmeister asteroid family, during which we discovered the importance of said secular resonances on small asteroids. Next we will detail our work on finding the locations and relative strength of linear secular resonances with the two most massive asteroids, (1)Ceres and (4)Vesta. Finally we will present two more examples of asteroid families where the strong influence of Ceres on their dynamical evolution is evidently observed.

2.1 The Hoffmeister asteroid family

The (1726) Hoffmeister asteroid family is located in the middle part of the Main Belt, at relatively low eccentricities and inclinations, and more specifically within the ranges in proper elements:

$$\begin{aligned} 2.754 < a_p < 2.82 \text{ AU}, \\ 0.041 < e_p < 0.053, \\ 0.066 < \sin i_p < 0.088 \end{aligned} \tag{2.1}$$

The most intriguing feature of this otherwise indifferent asteroid family is the distribution of its member in the proper semi-major axis (a_p) versus sine of proper inclination ($\sin i_p$) plane, as seen in Figure 2.1. Indeed we witness that the family

appears to have a highly asymmetrical shape in this projection. Asteroids belonging to its inner half ($a_p \in (2.754, 2.78)$ AU) have a large dispersion in the sine of proper inclination, whereas the outer half ($a_p \in (2.78, 2.82)$ AU) is much more compact. In addition we see that in the proper semi-major axis versus proper eccentricity projection appears regular throughout the semi-major axis range covered by the family. Therefore it is evident that some dynamical mechanism has led to the excitation of the inclinations of the family members of the inner half, while leaving their eccentricities unaltered. The underlying cause of this irregularity was our motivation to further study this family and try to understand its dynamical history.

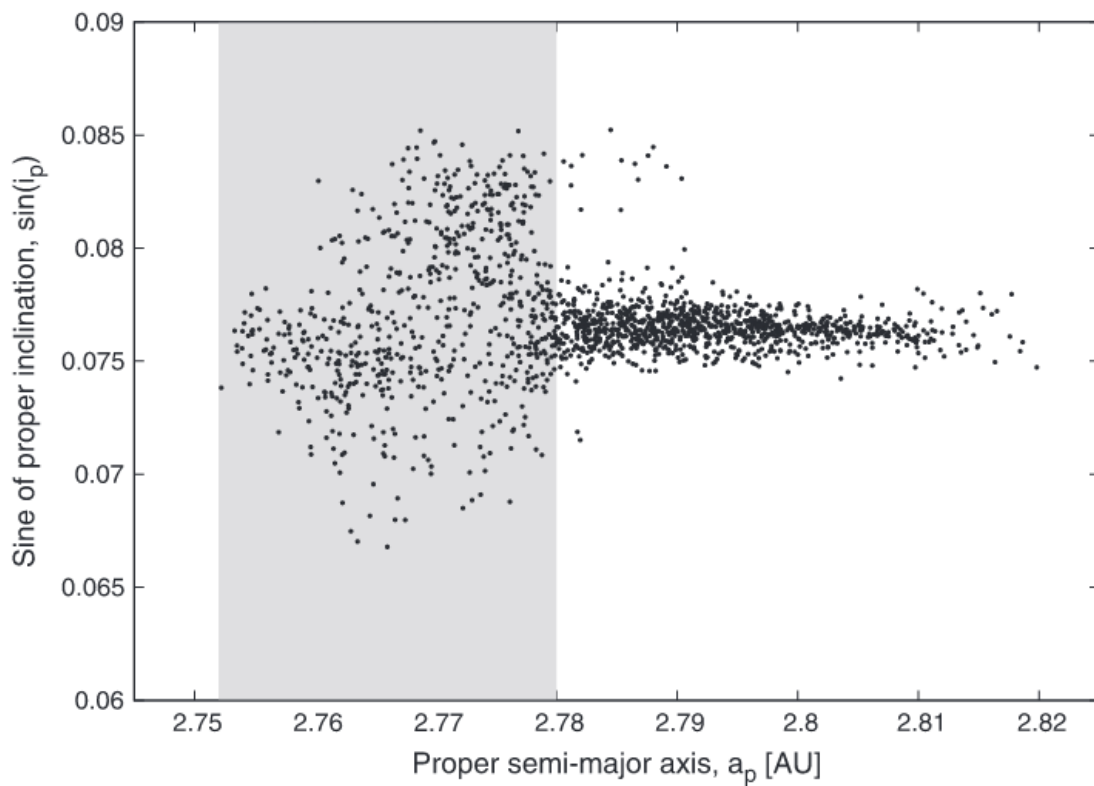


Fig. 2.1.: Distribution of the Hoffmeister family members in the proper semi-major axis versus sine of proper inclination plane ($a_p, \sin i_p$). The shaded part highlights the excited in inclination inner part of the family.

2.1.1 Family membership

The first step of our study was to accurately establish the membership of the family. To do so we applied the Hierarchical Clustering Method to the catalog of synthetic

proper elements (Knežević et al., 2002).¹ We chose the asteroid (1726) Hoffmeister as the starting object, and a starting distance threshold $d_c = 10$ m/s. We then increase the distance threshold in increments of 5 m/s, and monitor the clustering of asteroids until merging with the background population occurs, in this case at 60 m/s. We then plot the number of clustered asteroids as a function of distance threshold, as shown in Figure 2.2.

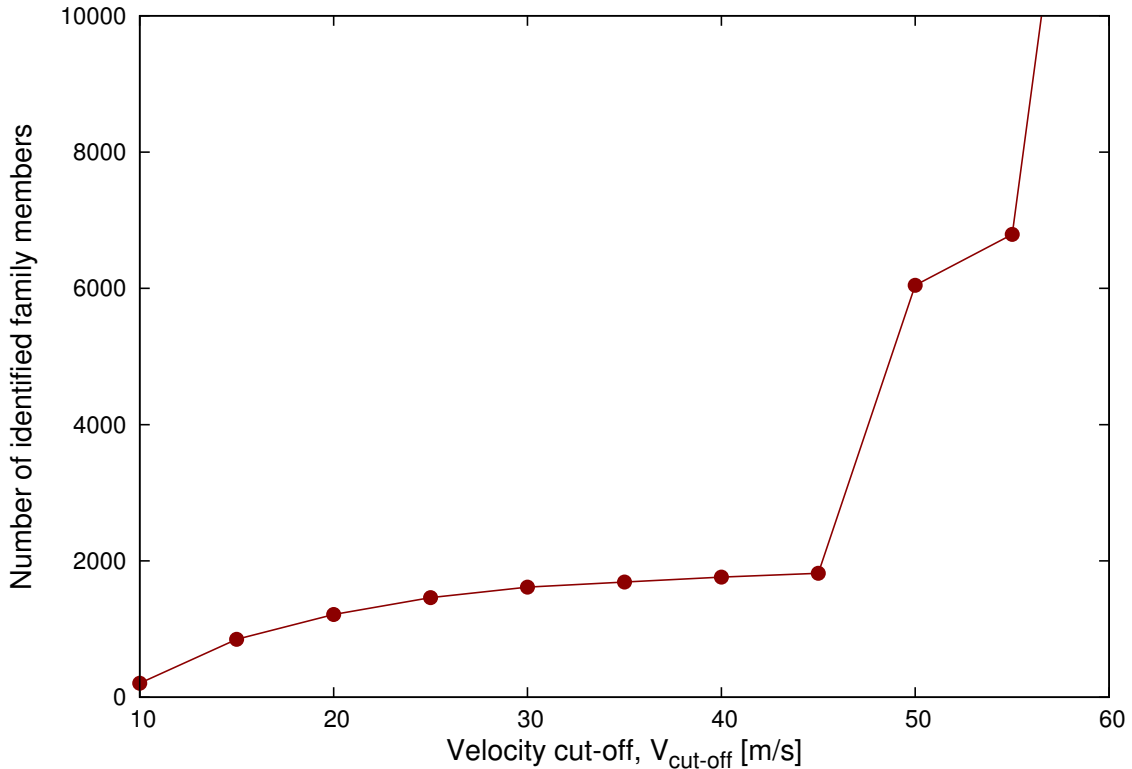


Fig. 2.2.: Number of associated asteroids versus distance threshold(d_c) for the Hoffmeister asteroid family.

We observe that the number of associated asteroids with the central body increases gradually from 10 m/s to 30 m/s, then remains almost constant until 45 m/s, at which point it rapidly increases again, finally merging with the background at 60 m/s. The usual practice (Nesvorný et al., 2005; Novaković et al., 2011) is to adopt the nominal membership at the middle of the aforementioned plateau. We thus chose the value of 35 m/s to establish the nominal membership of the Hoffmeister family, which returns 1687 member asteroids.

Usually dynamical studies of celestial objects focus solely on their orbits and the dynamical mechanisms that affect their evolution, with little to no respect paid to their physical subsistence. However as asteroid families are the outcomes of

¹available at the AstDyS database at: <http://hamilton.dm.unipi.it/astdys/>

collisional encounters, leading to populations of asteroids with common history, the physical properties of their members can prove essential for understanding their evolution in depth. In our case the physical properties of the Hoffmeister family members will help exclude potential interlopers from the membership at this stage of our study. As we will see later on, they will also enable us to develop the appropriate model for the Yarkovsky thermal force, essential for the reliability of our numerical simulations.

The spectral properties of the asteroid (1726) Hoffmeister have first been studied by Migliorini et al. (1996). Based on spectroscopic observations they found a featureless spectrum of this asteroid, characteristic of the taxonomic types C- or F. That is in agreement with the albedos of three family members, including (1726) Hoffmeister, derived by the Infrared Astronomical Satellite (IRAS) (Tedesco et al., 2002), with an average value of 0.049.

Further analysis performed by Monté-Diniz et al. (2005) concluded that the members of the Hoffmeister family are C-type asteroids.

The amount of information about the colors and albedos of the Hoffmeister family has changed drastically over the last decade, thanks to the Sloan Digital Sky Survey (SDSS) (Ivezić et al., 2001) and Wide-field Infrared Survey Explorer (WISE) (Masiero et al., 2011).

Among the 1961 members of the Hoffmeister family, we found 490 objects present in the the fourth release of the SDSS Moving Objects Catalog (Ivezić et al., 2001). These data confirm that the Hoffmeister family is dominated by asteroids of C-type. Similarly, in the WISE data (Masiero et al., 2011), albedos are available for 663 family members, giving an average albedo of 0.047, once again in agreement with C-type.

To identify interlopers we adopted the approach proposed by Radović et al. (2017). This method combines all the data about spectra, colors and albedos available for the identified family members. Asteroids that fall out of a range of specified criteria are considered as interlopers.

In this way, we identify 6 interlopers based on their SDSS colors, and 2 according to their WISE albedos. This means that only about 1% of the family members with available SDSS data, and only about 0.3% based on the available WISE data are considered as interlopers. The obtained fraction of interlopers is way below typical

values for the ratio interlopers/real-members in asteroid families. In fact, according to Migliorini et al. (1995), this ratio usually varies between 6 and 12%, except for the very well defined families, for which it is somewhat lower. Thus, the Hoffmeister family seems to be very well separated from the background population, and the probability to find interlopers is low, meaning that the obtained membership of the family is of high reliability.

In addition to the interlopers identified based on the SDSS and WISE data, we found one more interloper based on its albedo provided by IRAS, rising the total number of identified interlopers to 9.

2.1.2 The dynamical environment

In order to better understand the dynamical history of the Hoffmeister asteroid family, it is helpful to first study its dynamical environment. The Main Belt features a multitude of mean-motion and secular resonances as well as a considerable number of very massive asteroids. The localized nature of these mechanisms renders each specific region of the Main Belt unique in the way the orbits of small asteroids evolve therein. Therefore identifying such mechanisms in the region occupied by the members of the Hoffmeister family helps develop a clearer picture of its post-impact evolution.

As we noted above, the innermost edge of the family reaches values of proper semi-major axes of approximately 2.754 AU. Close to that value, and specifically at 2.752 AU there is the three-body MMR 3-1-1 with Jupiter and Saturn. Although the family seems to only just reach this resonance, therefore practically its members haven't been able to interact it, is worth keeping it in mind going forward as it might be useful when analyzing the numerical integrations later on. At the outermost edge of the family, at proper semi-major axes of 2.82 AU, we encounter a similar situation. There we find the 5/2 MMR with Jupiter, which although more powerful than the 3-1-1 in its ability to affect the orbits of small asteroids, has also only just been reached by Hoffmeister family members. Therefore it seems safe to conclude that the range in semi-major axis spanned by the family members as observed, reflects their unhindered evolution due to the Yarkovsky effect, which has not been abruptly delimited by MMRs.

Close to the family we also find a well known secular resonance, namely the:

$$z_1 = g + s - g_6 - s_6 \quad (2.2)$$

which crosses the inner half of the region occupied by the family members, at high eccentricities and inclinations. Indeed it is evident that only family members of the inner, disperse in proper inclination part of the family have reached this resonance and have potentially interacted with it. Let us note that since the z_1 contains both the g and s proper frequencies of the perturbed body, such interaction is expected to affect both the proper eccentricity and proper inclination of the latter.

Another important aspect, which directly impacts the dynamical structure of the region is the fact that the most massive asteroid, (1) Ceres has a proper semi-major axis of 2.767, placing it right in the region covered by the family members. This can lead to strong perturbations on the orbits of small asteroids through both the 1/1 MMR and close encounters with Ceres (see eg. Carruba et al. (2003)).

2.1.3 Numerical simulations

The main part of the study involved numerical integrations of test particles, simulating the dynamical evolution of family members since their initial, post-impact era. Although the present day distribution of asteroid family members in the proper elements space can give hints of the action of the different dynamical mechanisms present in the region, we cannot constrain in detail when and exactly how they have altered each orbit. By implementing numerical simulations we are enabled to fill exactly this piece of the puzzle: we are able follow closely the evolution of the orbit of each asteroid and witness the effect of all mechanisms at the exact moment they act. And this means we can recreate the full history of the family, and reveal all its nuances.

To carry out the numerical simulations and expect the results to accurately reproduce the evolution of the Hoffmeister family, we first need to establish all the relevant parameters, that include: the initial distribution of the test particles in the orbital elements space, their total number and sizes, their physical properties relevant to the modeling of the Yarkovsky effect, the dynamical model of the Solar System within which the integrations will be run, and the duration of the integrations.

Initial conditions of test particles

The initial distribution of the test particles in the orbital elements space must correspond to the distribution of the fragments of the real family immediately after the impact that formed it. As distances in the orbital elements space translate to differences in velocities, the size of the initial distribution that we need to constrain is the size of initial ejection velocity field. This size is known to be related to the size of the parent body, or more precisely to its escape velocity, v_{esc} . Recently Carruba and Nesvorný (2016) found that for most of the known asteroid families, initial velocity dispersion in the space of proper elements (i.e. *terminal velocity*, v_t) is in the range $0.5 - 1.5 \cdot v_{esc}$. Therefore, in order to derive the initial velocity field we must first have an estimation of the size of the parent body.

There have been several efforts in the past to estimate the size of the parent body of the Hoffmeister. Migliorini et al. (1996) found that its diameter should be between 50 and 100 km, whereas Durda et al. (2007) later suggested a somewhat larger size of 134 km. The most recent estimation of the Hoffmeister family parent body has been by Brož et al. (2013), at about 93 km.

Using the derived list of the family members (free of potential interlopers), and summing-up their masses into a single object, we found its diameter to be 62 km. Assuming there is no large interloper still present in our membership list, this value should be considered as the lower limit. The fact that most of the km-sized asteroids have been already discovered at the location of the Hoffmeister family, suggests that the upper limit is not significantly larger. In this respect we believe the value found by Brož et al. (2013) should be considered as the upper limit. Thus the size of the parent body should be 60 – 90 km.

To estimate the escape velocity from the parent body, we assume its density to be 1300 kgm^{-3} , an appropriate value for C-type asteroids. The range of plausible diameters of the parent body along with the assumption about its density give an escape velocity in the range $26 - 38 \text{ ms}^{-1}$, which translates to $13 - 58 \text{ ms}^{-1}$ in the range of terminal velocities. We selected a value roughly in the middle of the range, i.e. $v_{tv} = 40 \text{ ms}^{-1}$, to calculate the initial velocity field for the Hoffmeister family.

The largest fragment in the family is asteroid (1726) Hofmeister with only about 26 km in diameter; thus, the largest fragment to parent body mass ration is $M_{LF}/M_{PB} < 0.1$, implying that the family is likely of the super-catastrophic type

(Michel et al., 2015). In this disruption regime the initial velocity field is usually isotropic,² thus, the initial distribution in the proper elements space is contained within an ellipsoid. This equivelocity ellipsoid is computed from the Gaussian equations, as explained in Morbidelli et al. (1995). Figure 2.3 presents, in both the (a_p, e_p) and $(a_p, \sin(i_p))$ planes, the equivelocity ellipses, which are used in the following steps.

With the borders of the initial distribution defined, the next step is to distribute randomly therein the test particles. For asteroid family studies it is essential for the population of test particles to follow the same size-frequency distribution as the real family. If this condition is met, we can always create an arbitrary number of test particles, extending down to the smallest sizes we want, and we can rest assured that the fictitious population represents the actual family correctly. For this study though, since we are interested in matching the distribution of the real family in the proper elements space, we do not care about asteroids of smaller size than the identified members. We chose to generate test particles with a one-to-one correspondence to the identified family members, in terms of their total number and individual sizes. Therefore we generated 1678 test particles, with initial osculating elements such that their proper elements are randomly distributed inside the equivelocity ellipsoid³. We then assign each test particle with a diameter equal to that of an actual family member. To calculate the diameters of the latter we use their respective absolute magnitudes, as provided by the AstDyS service, and using the relation:

$$D = \frac{1329}{\sqrt{p_v}} 10^{-0.2H} \quad (2.3)$$

where we used the average geometric albedo of the family members $p_v = 0.047$, as discussed in Section 2.1.1.

Implementation of the Yarkovsky effect

The Yarkovsky effect which affects the semi-major axes of small asteroids is of paramount importance in the study of asteroid families, and it is essential to model

²Contrary to the catastrophic regime, cratering events often produce anisotropic ejection velocity fields (see e.g. Novaković et al., 2012b).

³For simplicity we did not assume any dependence of the ejection velocity on the size of the objects. Although this should not affect our analysis we caution that such dependence exists, as reported by Cellino et al. (1999) and more recently Carruba et al. (2016a).

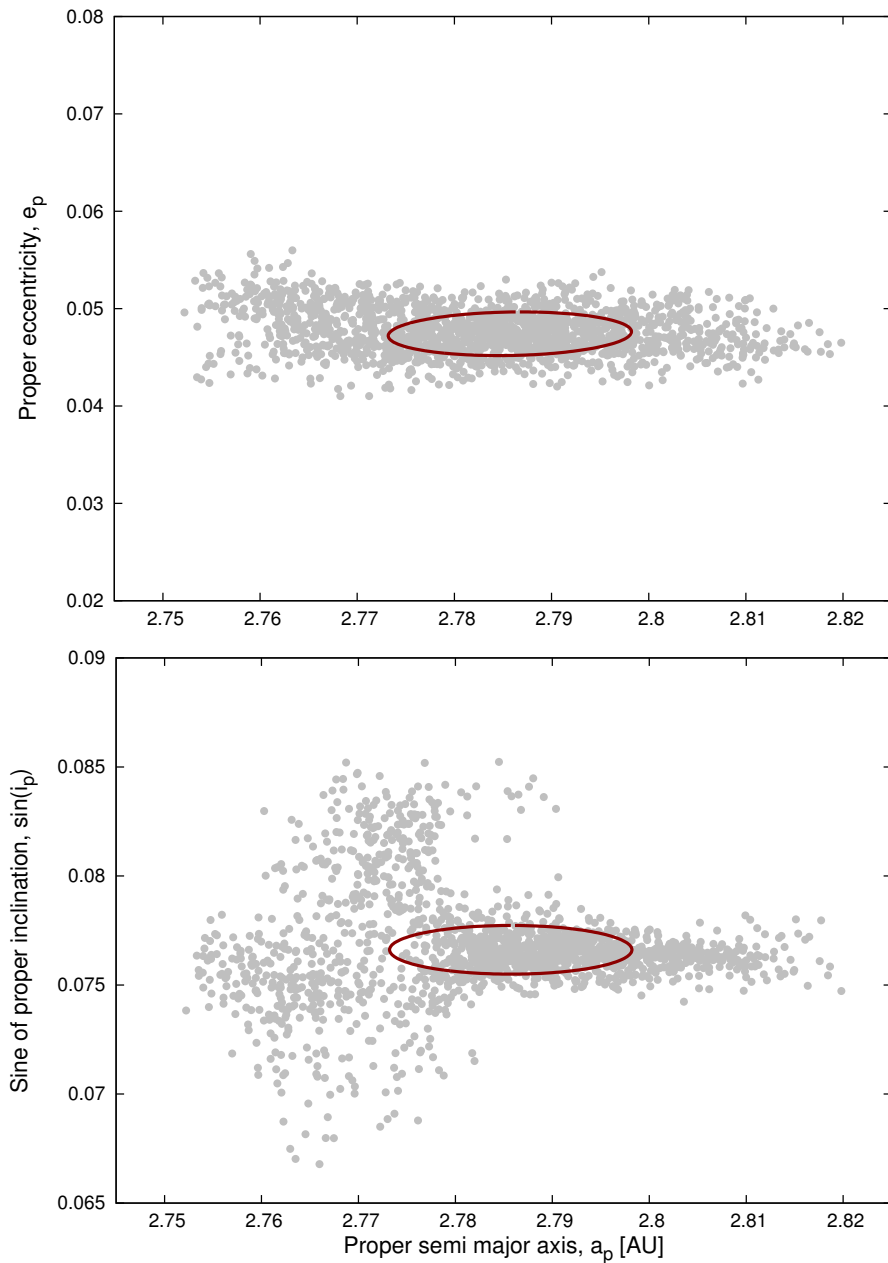


Fig. 2.3.: Initial equivelocity ellipse (dark red line) plotted in the (a_p, e_p) and $(a_p, \sin(i_p))$ planes. Background grey dots represent the family identified using the HCM for a distance threshold of 35 m/s. The ellipse is obtained assuming an initial ejection velocity of 40 m/s, a mean anomaly of 90° , and an argument of pericenter of 330° .

it as accurately as possible in order to obtain reliable results. In principle the Yarkovsky effect does not act alone in nature; asteroids do not move through space under its influence unimpeded. Weak collisions with small bodies, and torques resulting from the YORP effect result to continuous changes of their spin axes

orientations and spin rates, both directly impacting the net force exerted by the Yarkovsky effect. One way to tackle this is to try and model the actions of all these factors separately, and incorporate them in the final model. A simpler approach, which we followed in this study, is to average out the “microscopic” modifications of the Yarkovsky effect originating from these mechanisms, and use a constant along-track acceleration for each asteroid resulting in the same “macroscopic” average drift rate.

To assign each test particle the appropriate drift rate, we must first calculate a reference value, that is the maximum possible drift rate for an asteroid of 1 km in diameter. This reference value is determined using the model developed by Vokrouhlický (1998, 1999), assuming thermal parameters commonly adopted for regolith-covered C-type objects: surface and bulk densities $\rho_s = \rho_b = 1300 \text{ kg m}^{-3}$, surface thermal inertia $\Gamma = 250 \text{ J m}^{-2} \text{ s}^{-1/2} \text{ K}^{-1}$ (Delbó and Tanga, 2009), and thermal emissivity parameter $\epsilon = 0.95$. The resulting reference value obtained in this way is approximately equal to $\left(\frac{da}{dt}\right)_{ref} \approx 4.5 \times 10^{-4} \text{ AU/Myr}$.

The final drift rate for each test particle now depends on two parameters: its diameter and the orientation of its spin axis. Since the force exerted by the Yarkovsky effect on an asteroid is inversely proportional to its diameter, we can easily scale the reference value accordingly. As for the orientations of the spin axes, we assumed a uniform distribution immediately after the breakup event, resulting to a uniformly random distribution of obliquities in the range $0^\circ < \beta < 180^\circ$. Therefore the final drift rate for the i_{th} asteroid was obtained using the formula:

$$\left(\frac{da}{dt}\right)_i = \left(\frac{da}{dt}\right)_{ref} \cdot D_i^{-1} \cdot \cos \beta_i \quad (2.4)$$

The dynamical model

As the Hoffmeister asteroid family is located in the middle part of the Main Belt, where the perturbations of the inner planets are generally insignificant, we chose to use a dynamical model that includes only the four giant planets, from Jupiter to Neptune, as perturbing bodies. The indirect effect of the inner planets is accounted for by adding their masses to that of the Sun, and by applying a barycentric correction. We chose to integrate the orbits of the test particles for a total of 300Myrs, based on the age estimation performed by Nesvorný et al. (2005), and more recently

by Spoto et al. (2015), who found the Hoffmeister family to be about 300 and 330 Myr old, respectively. The integrations were performed using the Orbit9 integrator embedded in the multipurpose OrbFit package⁴.

Results of the first run

Once the numerical integration of the orbits of the test particles is finished we proceed to analyze the results and assess the outcome. The output of the Orbit9 integrator is the evolution of the osculating orbital elements of each test particle in time. A benefit of using this integrator is the fact that it is also capable of outputting the mean elements, i.e. orbital elements free of short periodic perturbations. This is achieved by applying on-line a digital filtering algorithm to the osculating elements. We then split the time-series of the mean elements into windows of 10 Myrs, and for each such window we calculate the corresponding synthetic proper elements, by means of removing the long periodic perturbations using Fourier filtering. Utterly for each test particle we end up with the time evolution of its proper orbital elements with a resolution of 30 points (300Myr in 10Myr steps). This was the first part of the analysis of the data coming out of the Orbit9 integrator also for all subsequent simulations.

We can now plot the distribution of test particles and compare it to the observed distribution of the real family. This is shown in Figure 2.4. We directly witness that the sought after reproduction of the asymmetrical distribution of family members in the $(a_p, \sin i_p)$ plane is not achieved to any extent no matter how deep into the simulation we look. Even though the family members did spread along the semi-major axis direction due to the Yarkovsky effect as expected, no lateral movement in the inclination direction happened at all. This raised a serious concern, as a nonetheless unexpected result.

Improvements in the model

To address this we looked back at the parameters chosen during the simulation setup, and tried to judge which would be meaningful to be adjusted in order to lead to the desired result. As the generation of the test particles, in terms of their initial conditions and Yarkovsky drift rates depend solely on physical parameters, in

⁴Available from <http://adams.dm.unipi.it/orbfit/>

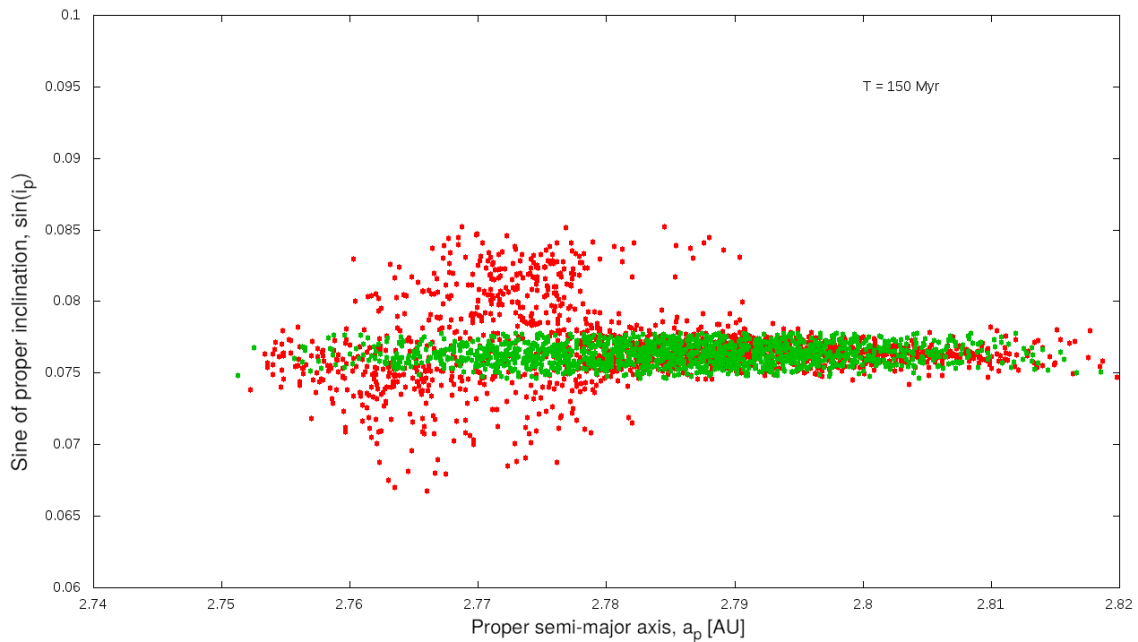


Fig. 2.4.: Comparison between the distribution of the real family members (red), and the test particles after 150 Myrs of the simulation (green).

which we held our trust to be correct, the only remaining simulation parameter to be altered was the dynamical model of the Solar System used. It may be generally true that the four giant planets dominate the perturbation spectrum for middle-to outer-belt asteroids, but that does not exclude the possibility that some other massive body can also exert meaningful perturbations locally at some region. Having in mind the previous study of the dynamical environment around the Hoffmeister family, it comes only naturally to mind that the most massive asteroid, (1)Ceres should be the first candidate for localized action here. We immediately included Ceres in the dynamical model, and keeping all other parameters the same we run the numerical integrations again.

New results

Producing the same plot again, seen in Figure 2.5, it is immediately evident that this simulation tells a completely different story, one that reproduces the anisotropic distribution of thereal family.

To further illustrate the difference we show in Figure 2.6 a comparison between the two models, and of the second model to the real family at two points in time,

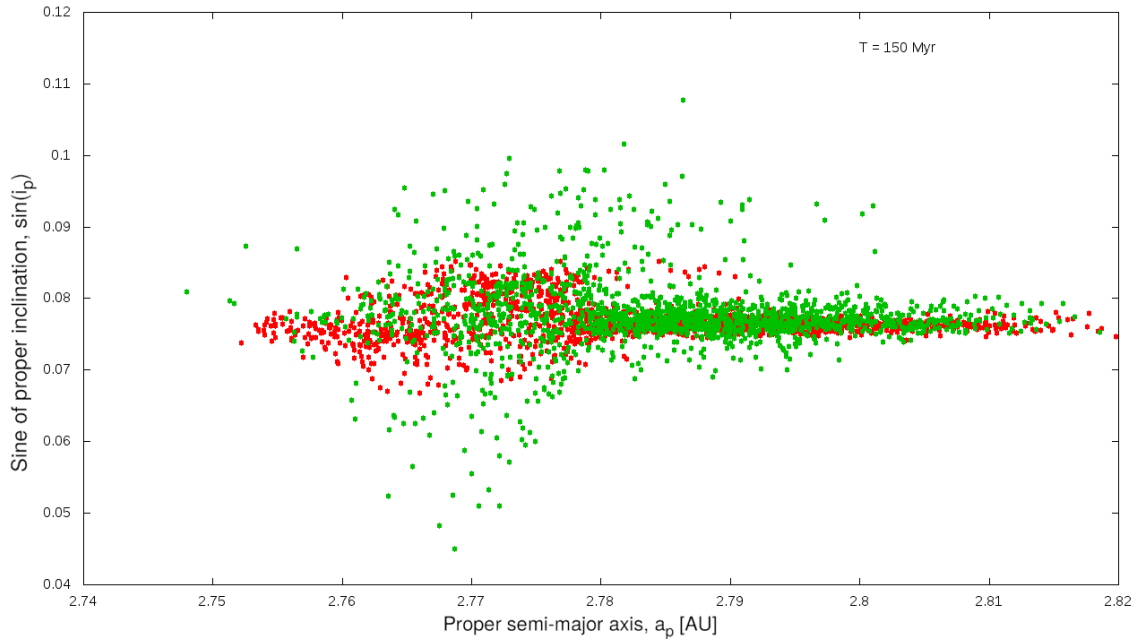


Fig. 2.5.: Comparison between the distribution of the real family members (red), and the test particles after 150 Myrs of the simulation (green), with Ceres included in the model.

one near the beginning and one near the end of the simulation. We see that even at a short time into the integration at 15 Myr, some asteroids begin to deviate from their initial distribution toward both higher and lower inclinations all the while being spread in semi-major axis due to the Yarkovsky effect. Ultimately after about 145 Myr we see that the shape of the real family in the $(a_p, \sin i_p)$ plane is qualitatively reproduced. Compared to the result of the first simulation we can safely conclude that in the case of the Hoffmeister family, the perturbations of Ceres on the family members are of the utmost importance, and Ceres should be considered the principal driver of their evolution.

Having established that, it is both intriguing and necessary to pursue the study further and identify the exact mechanism by which Ceres is able to affect the orbits of the Hoffmeister family members to this extent. As already mentioned, previous studies (see e.g. Carruba et al. (2003) and Christou and Wiegert (2012)) have signified that Ceres can affect the orbits of small asteroids through both its 1/1 MMR and close encounters. Having a semi-major axis value within the region covered by the Hoffmeister family, the 1/1 MMR is definitely able to interact with family members, and the probability of a close encounter is increased.

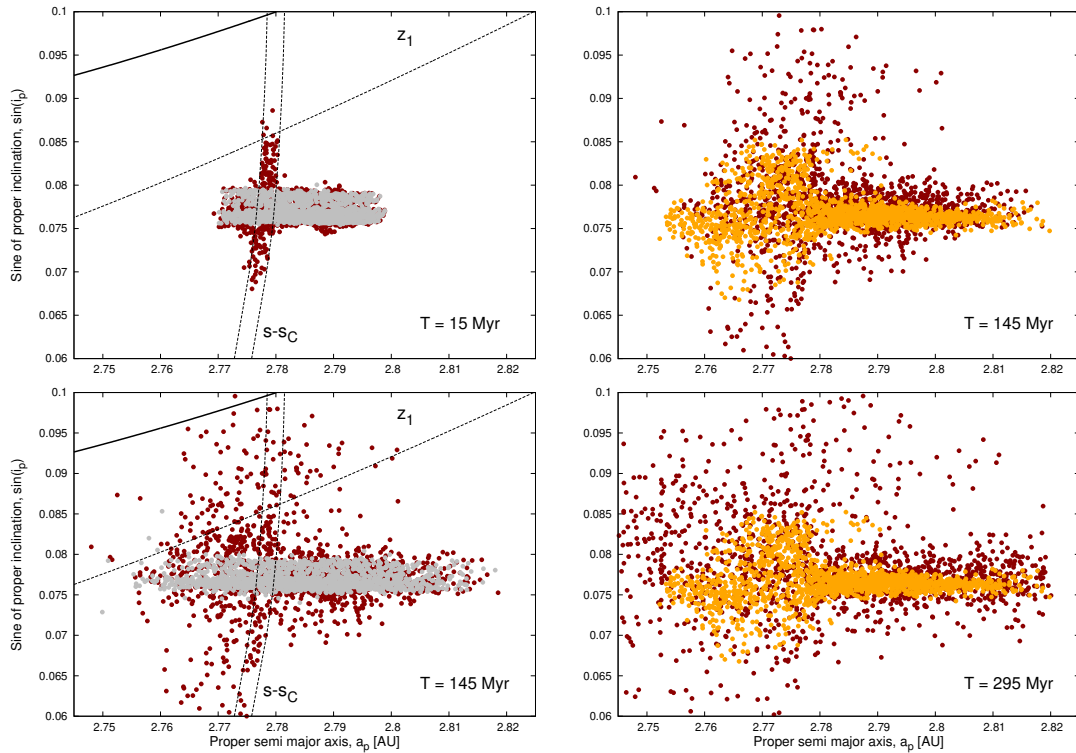


Fig. 2.6.: In the left panels a comparison between the distributions of the test particles in the two models (red points correspond to the model containing Ceres while gray points to the one without it) is shown for two times, 15 Myrs (top) and 145 Myrs (bottom). In the right panels the test particles of the simulation that includes Ceres are compared to the real family members at the same times.

To assess the action of the 1/1 MMR we followed a few particular asteroids with initial conditions and Yarkovsky drift rates that happened to be ideal to guarantee a crossing of the resonance. One such example is shown in Figure 2.7.

We see that this particular test particle reaches the 1/1 MMR with Ceres at a time of about 130 Myr, and exits it at about 145 Myrs. We notice however that during that time, no net change in the mean inclination is observed. On the contrary, one significant increase in the mean inclination happens at about 65-75 Myr, a time at which the MMR is completely out of the picture. Moreover, if MMRs were the responsible mechanisms for the excitation of the inclinations, we should also expect to see a similar effect on the eccentricities of the family members, which we do not. Therefore it is safe to conclude that the perturbations in inclination do not originate from the action of the MMR.

In the same spirit we turned our attention to the close encounters as a possible mechanism by which Ceres might be able to perturb the orbits of the test particles.

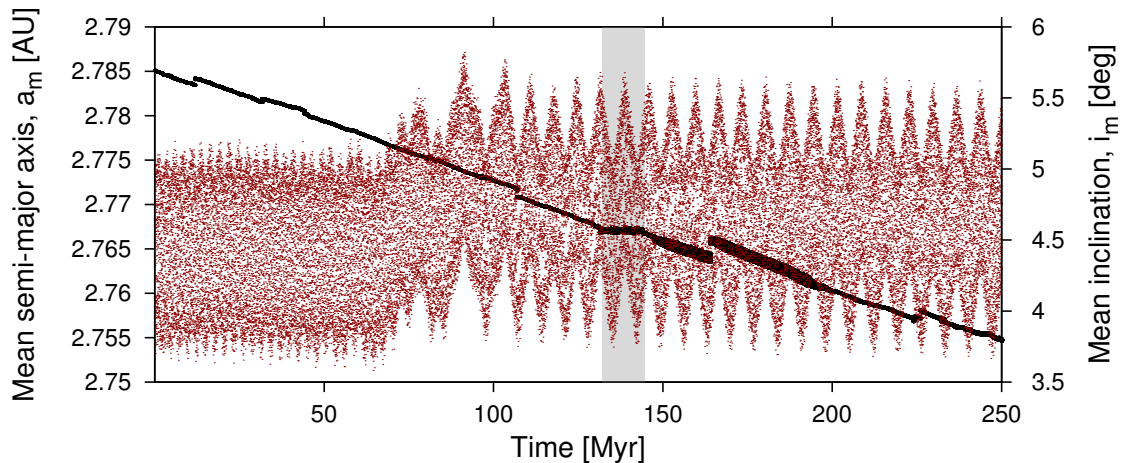


Fig. 2.7.: Example of a test particle crossing the 1/1 MMR with Ceres. The black line mapped on the left y-axis shows its semi-major axis drifting due to the Yarkovsky effect, whereas the red points mapped on the right y-axis show its mean inclination.

We used a simple algorithm to select test particles that had, at some point during their evolution, come close to Ceres in the physical space. We analyzed all such cases and reached another negative conclusion. As seen in the representative example presented in Figure 2.8, the timing of the close encounter does not match any significant alteration of the mean inclination. A theoretical questioning of the mechanism reaches the same result as in the case of the 1/1 MMR: there is no reason that close encounters would preferentially affect only the inclinations of asteroids without any statistically significant effect on their eccentricities.

The last mechanism we had remaining to study was the action of the z_1 secular resonance, which is located close to the family. It is true that this resonance was already present in the simulation that did not include Ceres as a perturbing body, with no effect at all, but we could not exclude the possibility that the interplay between it and the other two mechanisms involving Ceres, 1/1 MMR and close encounters, could be in some way responsible for the peculiar evolution of the orbits. Although not a very promising attempt, due to the position of the z_1 secular resonance, which does not correspond sufficiently to the “inflated” part, as well as the fact that it also should, in principle, affect eccentricities as well, we decided to examine it in detail. To do so, we plotted the secular frequencies of the test particles against each other ((g, s) plane); test particles interacting with the z_1 secular resonance should appear aligned along its path on this plane. Indeed on this plane we see such an alignment as seen in Figure 2.9, meaning that some asteroids do interact with it. However, more interesting was the existence of another such

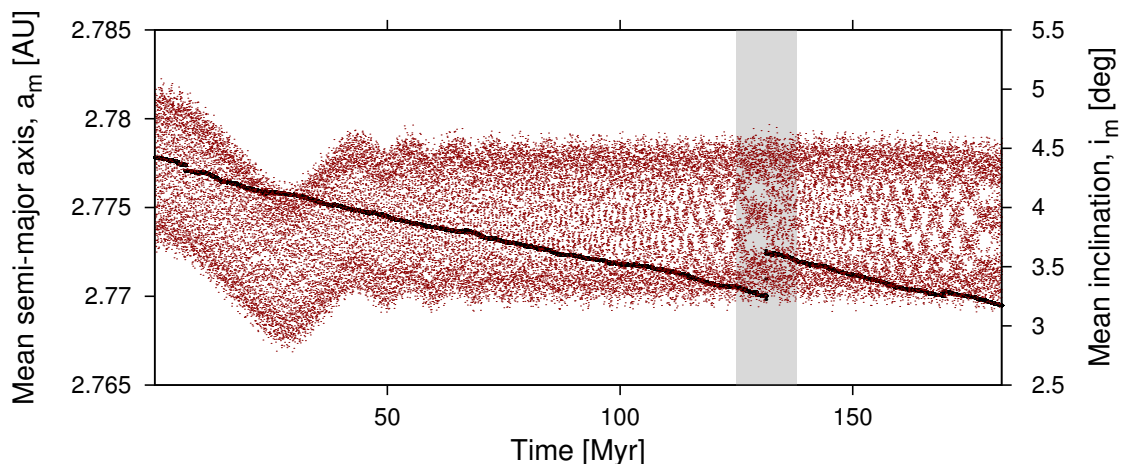


Fig. 2.8.: Example of a test particle suffering a close encounter with Ceres. The black line mapped on the left y-axis shows its semi-major axis drifting due to the Yarkovsky effect, whereas the red points mapped on the right y-axis show its mean inclination. The highlighted region and the sudden increase of the semi-major axis therein correspond to a close encounter with Ceres.

alignment of test particles on this plane, namely parallel to the g -axis at an s value of $-59.2''/yr$. What made things really interesting is the fact that this is the exact value of the precession frequency of the ascending node of Ceres, s_c ⁵. Leaving the not-so-promising z_1 aside for the moment, we turned our attention to this new observation, and followed by another hypothesis: Could Ceres affect the orbits of small asteroids through a secular resonance? Such an interaction had never been examined in past endeavors by anyone.

The $s - s_c$ secular resonance with Ceres

To test the hypothesis we used the same trusted method as before. We identified test particles that suffered a significant modification of their proper inclination at some point in the integration and then constructed the critical angle for the secular resonance:

$$\sigma_{s-s_c} = \Omega - \Omega_c \quad (2.5)$$

⁵Hereafter the subscript "c" will be used to denote parameters of Ceres.

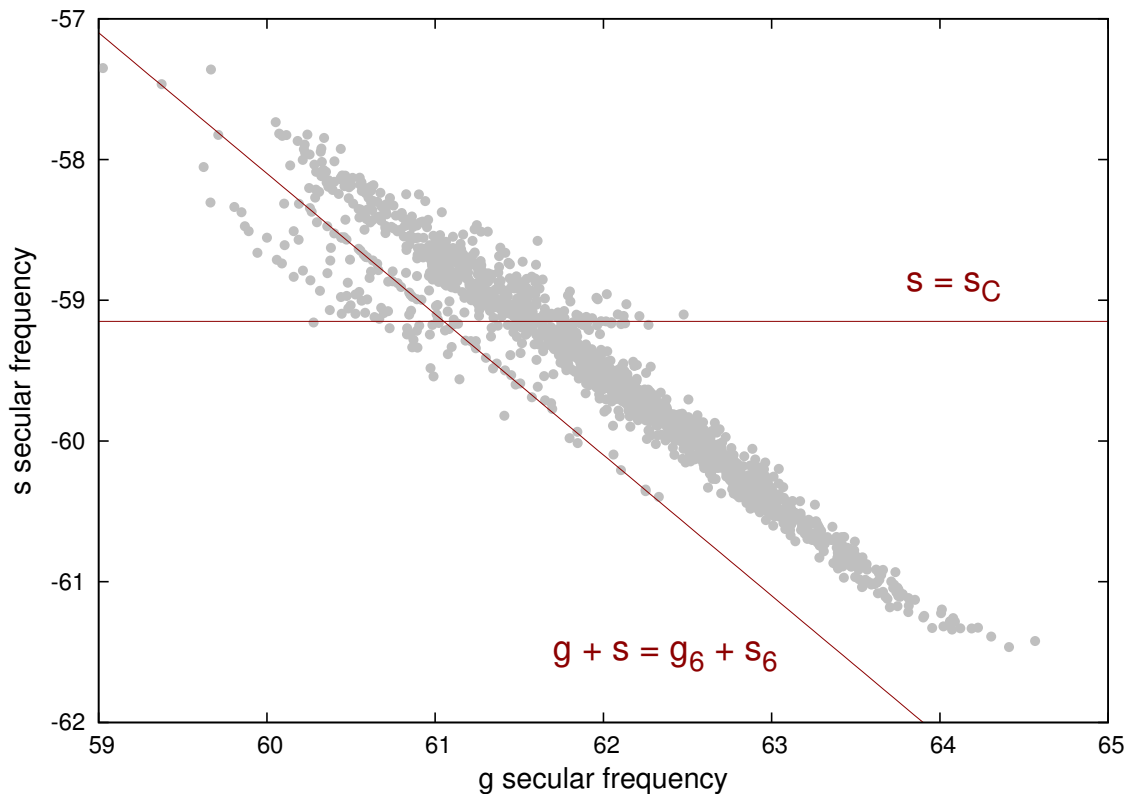


Fig. 2.9.: The proper frequencies of the test particles representing the Hoffmeister family. The lines denote the solutions for which alignment of the test particles implies interaction with the z_1 and $s - s_c$.

and plotted its evolution in time against the evolution of the mean inclination, as shown in Figure 2.10

The result is stunning: we see an exact match between the time at which the test particle crosses the secular resonance and the time at which it suffers a significant increase of its mean inclination. Other test particles showcase the same behavior, where the crossing of the $s - s_c$ secular resonance corresponds to increases or decreases of their mean inclinations. In order to understand why some asteroids get an increase in their inclination while others get a decrease, it is key to study the circumstances under which the interaction occurs. Consider a small asteroid that starts outside the resonance and it is pushed by the Yarkovsky effect towards it. When it enters the resonance it undergoes periodic oscillations in its inclination. But since the Yarkovsky effect continues its action independently, it will at some point push the asteroid out of the resonance. Exiting the resonance the asteroid will adopt the last value of inclination it had while oscillating inside the resonance. The exact time of exiting the resonance, and in consequence the point in the inclination

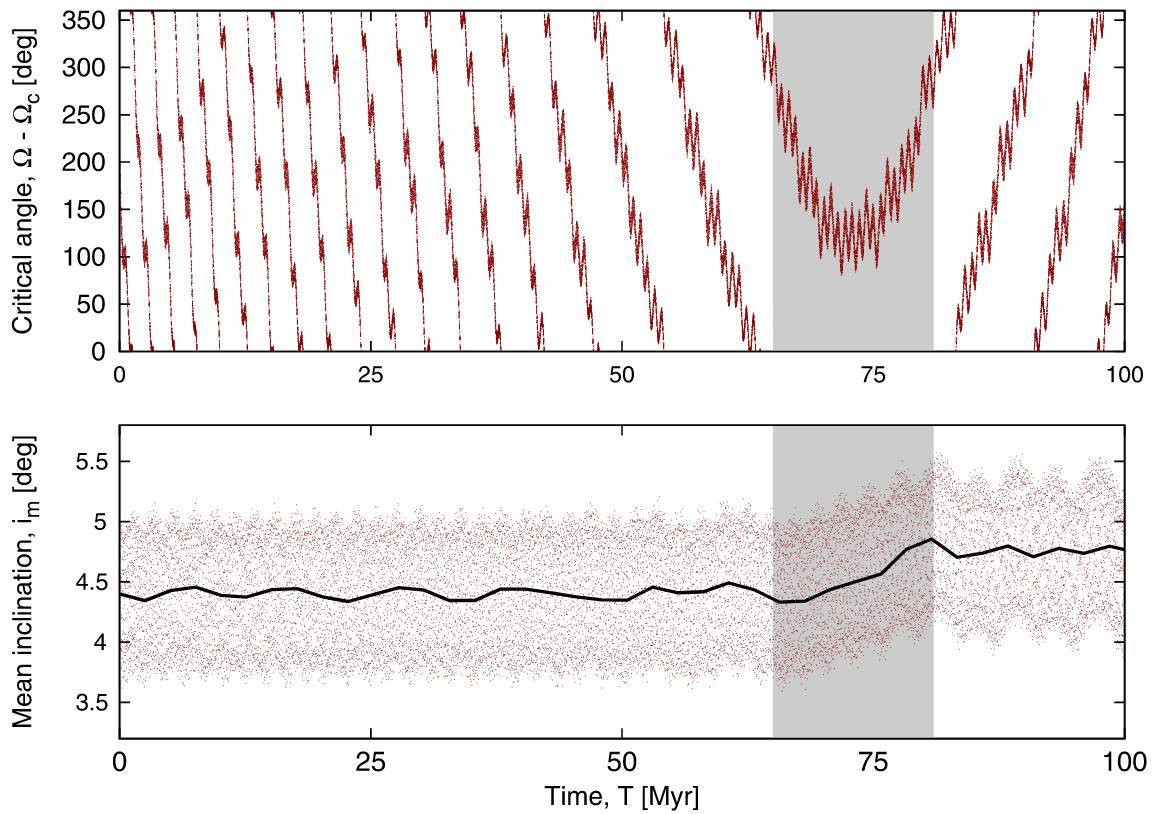


Fig. 2.10.: Example of a test particle crossing the $s - s_c$ secular resonance. In the top panel we show the evolution of the critical angle $\sigma = \Omega - \Omega_c$. In the bottom panel we show the evolution of the mean inclination in red dots. The black line shows an average of the mean inclination for clarity. The shaded regions correspond to the time of libration of the critical angle.

oscillation is in principle random, so we witness asteroids both gaining and losing inclination.

As expected from the fact that this resonance contains only the s secular frequency, the eccentricities of these test particles remain unaltered. This one more piece of evidence strengthening the case in favor of this secular resonance as responsible for the shape of the Hoffmeister family in the proper elements space, as it explains its appearance in both the $(a_p, \sin i_p)$ and (a_p, e_p) planes.

Let us now present some more examples capturing all the relevant dynamical interactions for Hoffmeister family members. in Figure 2.11, we show the evolutionary tracks of three sample test particles on the proper semi-major axis versus the sine of proper inclination plane $(a_p, \sin i_p)$ on the left, and versus the proper eccentricity plane (a_p, e_p) on the right. We have over-plotted the locations of the $s - s_c$ and z_1

secular resonances with red and blue lines respectively, the width of which denotes a range of $\pm 0.5''/yr$. At first all three test particles drift inwards, toward smaller semi-major axes, due to the action of the Yarkovsky effect with their eccentricities and inclinations practically unaltered (yellow points). When they reach the $s - s_c$ secular resonance, and while they are within it, they gain or lose inclination due to the interaction with Ceres (red points). After they exit the resonance they continue drifting inwards due to the Yarkovsky effect, only this time with their proper inclination having attained its new, almost stable value (yellow points). We also see that after a while the test particle on the top panels, the one that has gained a significant increase in inclination is able to also enter the z_1 secular resonance, which affects both its inclination and eccentricity, as expected. This also confirms our conclusion that z_1 played only a minor role in the evolution of the Hoffmeister family, as in order for asteroids to reach its path and interact with it, the action of the protagonist, the $s - s_c$ secular resonance, is absolutely necessary.

2.1.4 Age of the Hoffmeister family

The age of the Hoffmeister family has previously been computed by Spoto et al. (2015) and was found to be $\sim 330 \pm 90 Myrs$. Because the goal of that work was to produce a mathematically rigorous method for computing family ages in a uniform way, the specific characteristics of each family were not taken into account. Judging by the rather high standard deviation of the age they derive, we decided to take a different approach and try to obtain an estimate of the age ourselves.

The idea behind our approach is based on the unusual shape of the distribution of the family members when projected onto the proper semi-major axis versus sine of proper inclination plane. Having a satisfactory calibration of the Yarkovsky-induced drift in semi-major axis and the initial distribution of fragments immediately after the breakup event as discussed above, we can estimate the age judging upon the best fit on the $(a_p, \sin(i_p))$ plane, among a snapshot of our numerical simulations compared to the distribution of the actual family members.

To this purpose we use the following method: We first divide the area of the $(a_p, \sin(i_p))$ plane covered by the real family members into square bins, the number of bins in each dimension, given by Doane's formula (Doane, 1976), being 13 and 15 in a_p and $\sin(i_p)$ respectively (see 2.12). Then we calculate the fraction of real family members $n_{real}(j, k)$ that belong to each bin, and do the same for the simulated particles at each time-step t , obtaining $n_{sim}(j, k, t)$. Finally we measure how well

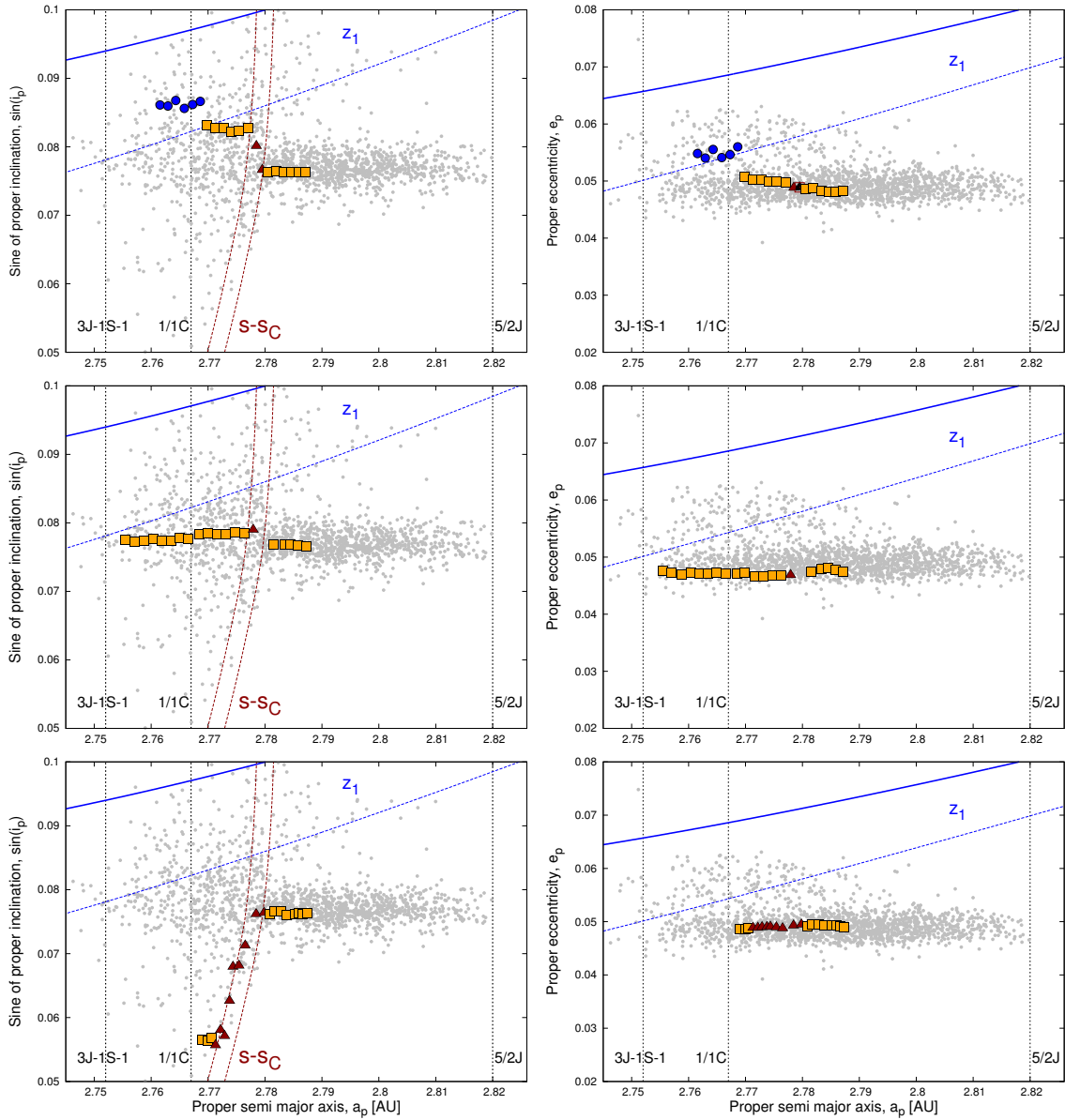


Fig. 2.11.: Evolution of the orbital elements of three example particles on the $(a_p, \sin i_p)$ plane on the left, and on the (a_p, e_p) plane on the right. Yellow points denote evolution under the influence of the Yarkovsky effect only, red points denote interaction with the $s - s_c$ secular resonance (red lines), blue points denote interaction with the z_1 secular resonance (blue lines), while gray points show the final snapshot of the evolution of the entire population. Black dashed lines show the locations of MMRs.

each distribution of the simulated particles at time t matches that of the real family using a χ^2 like function defined as:

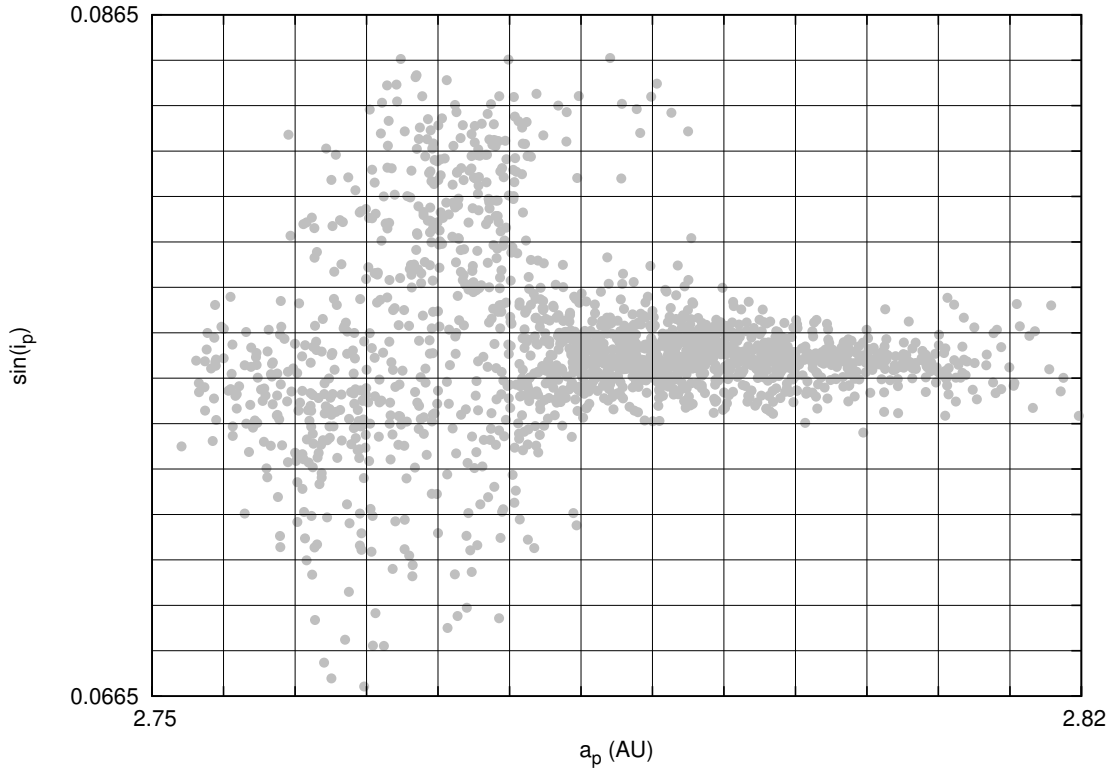


Fig. 2.12.: The division of the $(a_p, \sin(i_p))$ into bins for the estimation of the family age.

$$\psi(t) = \sum_{j=1}^{13} \sum_{k=1}^{15} \frac{[n_{sim}(j, k, t) - n_{real}(j, k)]^2}{n_{real}(j, k)}. \quad (2.6)$$

Note here that we take into account only bins that include real family members, despite the fact that at each time-step of our simulation particles may be found in other bins too. This should not affect the age estimation itself for two reasons. First we use the fractions of particles in each bin and not the absolute numbers, so the comparison with the real family is valid. Second, the fact that some test particles' orbits evolve out of the bins occupied by real family members or even out of the boundaries of the binned area which we evaluate, is an expected result of the random way in which we generated our initial conditions and Yarkovsky drifts. Therefore we seek the point in time where the relative shape of the family is reproduced, and not for a one-to-one match of asteroids to test particles. While no single test particle can simulate the evolution of an actual family member, the statistical properties of the population, and the estimated age as such, should be correct.

We can now plot the value of ψ at each time-step t , shown in 2.13 with black crosses, and estimate the age of the family by the global minimum. To better evaluate the

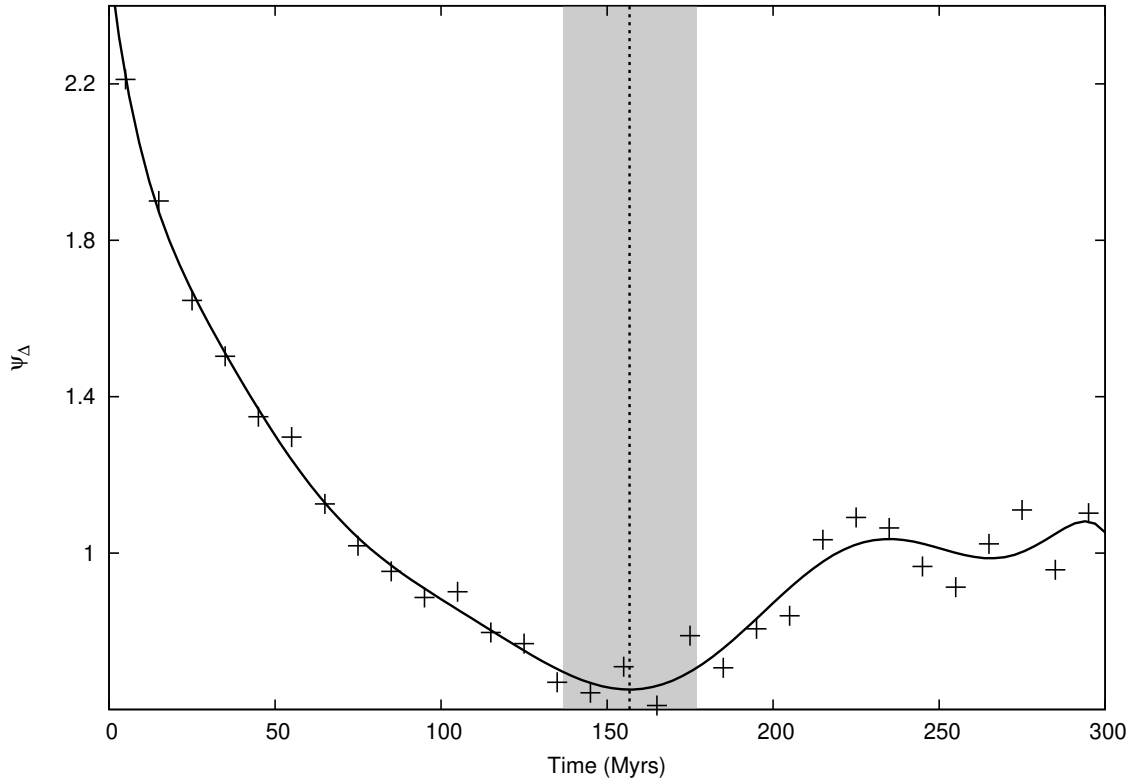


Fig. 2.13.: Estimation of the age of the Hoffmeister asteroid family. The black crosses show the calculated values of ψ as a function of time and the solid black line the fitted 10th degree polynomial. The vertical dashed line denotes the location of the global minimum of the polynomial at ~ 156 Myrs and the gray shaded region the standard deviation of ± 20 Myrs

position of the global minimum, we fit a tenth degree polynomial⁶ to the data points and find its minimum at $t \sim 156$ Myrs. The error of the fit is then translated to the standard deviation of our age estimation, so our final result for the age of the Hoffmeister family is $\tau = 156 \pm 20$ Myrs.

The obtained age is by a factor ~ 2 younger than in Spoto et al. (2015). Although we must clearly stress that our approach used here is generally less accurate than the one used by Spoto et al., there is however reason to believe that our results may be more accurate in this specific case, since we take into account also the spreading of the inclinations caused by the secular resonance, and not only of the semi-major axes.

⁶The degree of the polynomial we decided to fit our data with was selected such that the minimum we obtain is not influenced much by the local variations of the values of ψ which may be resulting from the discretization of the spatial and time coordinates.

Looking at the V-shape of the Hoffmeister family used by Spoto et al. to estimate the age⁷ it could be noted that the inner age in terms of the semi-major axis should be truncated at about 2.752-AU. Actually, all asteroids beyond this border, smaller than about 4 km, seem to be removed. At this value of the semi-major axis the most powerful 3-body MMR, namely $3J - 1S - 1A$, is located, suggesting that it might be the reason for this situation. However, neither our numerical simulations nor the situation with some other nearby families (e.g. (363) Padua or (93) Minerva) support the idea that the $3J - 1S - 1A$ resonance is powerful enough to make a sharp boundary. Moreover, this conclusion is also in agreement with a recent result obtained by Milić Žitnik and Novaković (2016), who found that many objects, subject to semi-major axis mobility, could successfully cross MMRs.⁸

It is also important to note that Yarkovsky calibration is not responsible for the discrepancy in the age estimation obtained here and in Spoto et al. (2015). In this respect, we even assumed about 30% slower Yarkovsky-induced drift of 4.5×10^{-4} AU/Myr, compared to 5.9×10^{-4} AU/Myr used by Spoto et al. (2015). Yet, as we did not use only the semi-major axis to estimate the age, this ratio does not imply that there is an additional difference of about 30% between two age estimations, but rather suggests that the real difference is somewhat larger than the nominal results indicate.

2.2 Secular resonances with massive asteroids

Having established that secular resonances with Ceres can be really important in the dynamical evolution of asteroid families, as the case of the Hoffmeister family has shown, we now set to examine the whole Main Belt for the effect of such resonances. Our study consists of four steps: First, to decide which secular resonances are the most promising candidates to induce significant perturbations on the orbits of small asteroids they affect. Doing so we will be able to determine which asteroids have sufficient masses to give rise to important secular resonances, and also which orbital elements we expect each resonance to affect. Second, to locate these resonances across the Main Belt. This will enable us to obtain a clear picture of the parts of the Main Belt where we expect asteroids to have their orbits significantly perturbed. Third, to assess the strength of the perturbations each secular resonance induces,

⁷Available at http://hamilton.dm.unipi.it/astdys2/fam_ages/index.html

⁸Strictly speaking Milić Žitnik and Novaković (2016) analyzed the mobility of asteroids over 2-body MMRs, but likely this conclusion is valid also for 3-body resonances.

in the different parts of the Main Belt. This will give us a better understanding on the role that the mass of the perturbing body and its proximity to the perturbed asteroids plays in the magnitude of the modification of the orbital elements of the latter. Finally, we examine each of the resonances under study, to catalog any asteroid families that they appear to interact with. Thus, we will obtain a clear view on the effect of each resonance on the dynamical evolution of asteroid families.

2.2.1 Ceres and Vesta

Naturally, the first candidate for a perturbing body is (1) Ceres, being the most massive asteroid, and having been proven to have a significant effect on the evolution of the orbits of the Hoffmeister asteroid family members through its linear nodal secular resonance (Novaković et al., 2015):

$$\nu_{1c} = s - s_c \quad (2.7)$$

Since we know that this resonance is strong enough to have an observable effect, it is suggestive that the other linear secular resonance with Ceres, the one involving the longitude of perihelion:

$$\nu_c = g - g_c \quad (2.8)$$

should be of particular interest for further investigation. We expect this secular resonance to have an influence on the eccentricities of perturbed asteroids, since it contains only the secular frequency g .

Apart from Ceres, we choose to also study secular resonances with the second most massive asteroid in the Main Belt, (4) Vesta. Despite its mass being only about 28% of that of Ceres, it is a good candidate for our study, as it resides in a different region than Ceres, the inner Main Belt, therefore we will get an insight of the effect of these resonances there too. Moreover, we will be able to probe the importance of the mass on the potential of these large bodies to give strong perturbations. Therefore we will also study the two linear secular resonances of asteroids with (4) Vesta:

$$\begin{aligned} \nu_{1v} &= s - s_v \\ \nu_v &= g - g_v \end{aligned} \quad (2.9)$$

in the same manner as those of (1) Ceres.

2.2.2 Location of the secular resonances

The next step of our study is to locate the path of each of the four secular resonances mentioned above, across the Main Belt. The most straightforward and easy to implement way to determine these locations is by analytical methods, as performed in Knežević et al. (1991). Essentially this method comprises of computing the analytical proper elements over a dense grid of initial conditions in the region under study. Then at each of the grid points we evaluate the critical argument of each secular resonance using the obtained proper frequencies. Then the exact location of each resonance is determined by the place where the critical argument changes sign between adjacent points of the grid. While this method is good to obtain quickly a clear overall idea of the location of each resonance we have found that the error of this approach for high eccentricities and inclinations is too high for the needs of our study. It is known that the accuracy of the analytical proper elements deteriorates as the eccentricity and inclination increase, as a consequence of the finite number of terms that are used in the expansion of the perturbing function. Therefore if we need to accurately find the location of each secular resonance we need to resort to another idea.

To overcome the shortcomings of the analytical proper elements as described above, the first natural idea is to use the synthetic proper elements (Knežević and Milani, 2000) instead. However since the computational time required to obtain those is much greater than in the case of the analytical ones, it would be very inefficient to compute them in every point of a fine grid as described above. We have chosen thus to proceed with a different approach, based on the synthetic proper elements, and more specifically the proper frequencies, of the actual main belt asteroids, as released by the AstDyS service⁹. From the catalog of proper elements we extract the proper frequencies of (1) Ceres:

$$\begin{aligned}g_c &= 54.07''/yr, \\s_c &= -59.17''/yr\end{aligned}\tag{2.10}$$

and (4) Vesta:

⁹available at: <http://hamilton.dm.unipi.it/astdys2/>

$$\begin{aligned} g_v &= 36.87''/yr, \\ s_v &= -39.59''/yr \end{aligned} \tag{2.11}$$

Then, for a given secular resonance that we want to visualize, we select from the catalog those asteroids with proper frequencies that satisfy the corresponding resonant equation, within some margin corresponding to the strength of each resonance. To decide on the value of this margin we benefited from the analytical work of Knežević et al. (1991), where they use $2''/yr$ for the most powerful secular resonance ν_6 , and $0.5''/yr$ for weaker, fourth-degree resonances such as the $g + s - g_6 - s_6$. Expecting that the secular resonances with massive asteroids should be relatively weak, we used $0.2''/yr$. The asteroids with proper frequencies within these margins should lie along the path of the secular resonance in question. Figure 2.14 shows an example of this approach for the secular resonance ν_{1c} , where the analytical solution is also plotted for comparison. Note the difference for high eccentricity and inclination between the two methods.

The ν_{1c} resonance

The first secular resonance we studied is the linear nodal secular resonance ν_{1c} . Figure 2.15 shows the proper semi-major axis versus the sine of proper inclination and the proper eccentricity projections of the main asteroid belt. The resonant asteroids, the ones that satisfy the relation $s - s_c = \pm 0.2''/yr$, are highlighted, revealing the location of the resonance. Since the secular resonances are represented as surfaces in the three dimensional proper element space, we use a color code to grasp the third dimension when projecting on the plane.

We notice that the secular resonance crosses the middle ($2.5 < a_p < 2.82 AU$) and outer ($2.82 < a_p < 3.26 AU$) parts of the Main Belt. In the top panel of Figure 2.15, we see that this resonance's projection on the (a_p, e_p) plane appears as a wide strip that crosses the middle belt at an angle. This strip has a well defined lower boundary which corresponds to zero inclination, with the upper boundary being due to the gap in the distribution of asteroids at $\sin i_p \sim 0.3$. In the outer belt the resonant asteroids are less and more localized: two concentrations are found in the region $2.82 < a_p < 2.9$ and another two at high inclinations past $3AU$, corresponding to asteroid families as will be discussed in the next section.

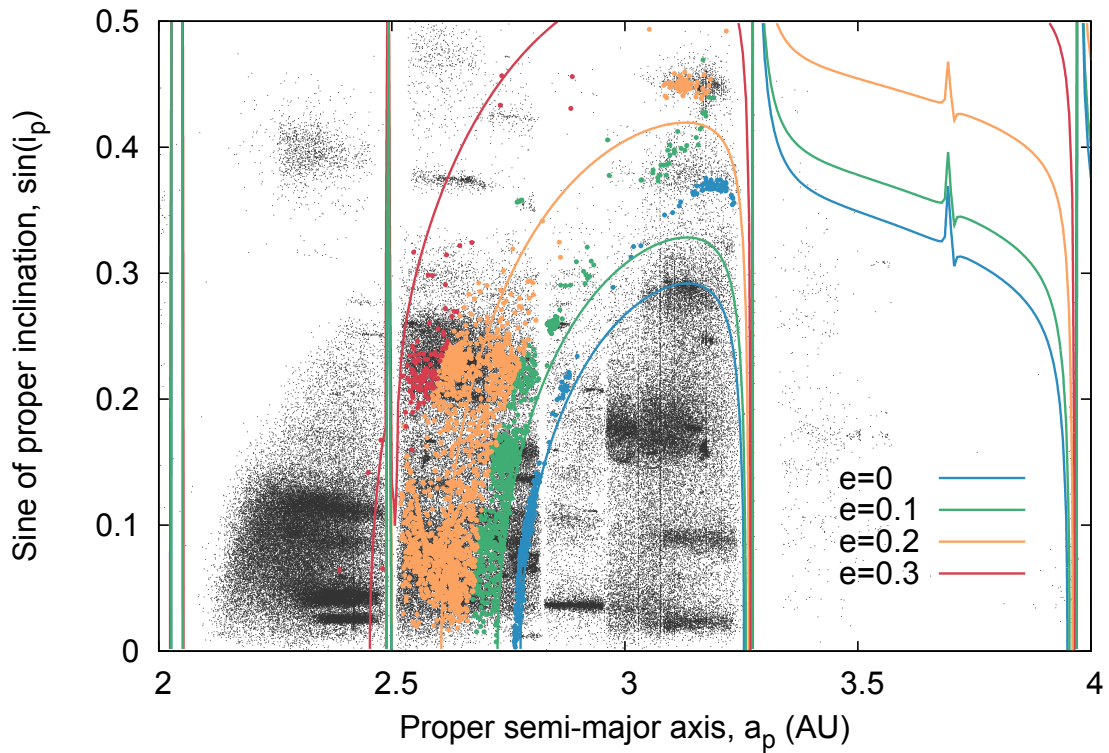


Fig. 2.14.: The location of the ν_{1c} secular resonance on the $(a_p, \sin i_p)$ plane. Solid lines represent the analytical solution for different values of the eccentricity (see legend). The colored dots show the resonant asteroids within $0.2''/yr$, while the different colors correspond to values of eccentricity centered to those of the analytical solutions and spanning 0.05 in each direction

The ν_c resonance

Following the same procedure we find the location of the ν_c secular resonance, by plotting the asteroids that satisfy the resonant relation $g - g_c = \pm 0.2''/yr$. The result is shown in Figure 2.16, showing the proper semi-major axis versus the sine of proper inclination of the main belt $(a_p, \sin i_p)$, with the resonant asteroids highlighted in color for different proper eccentricities. This secular resonance also crosses mostly the middle part of the main belt, as well as the high inclination part of the outer belt.

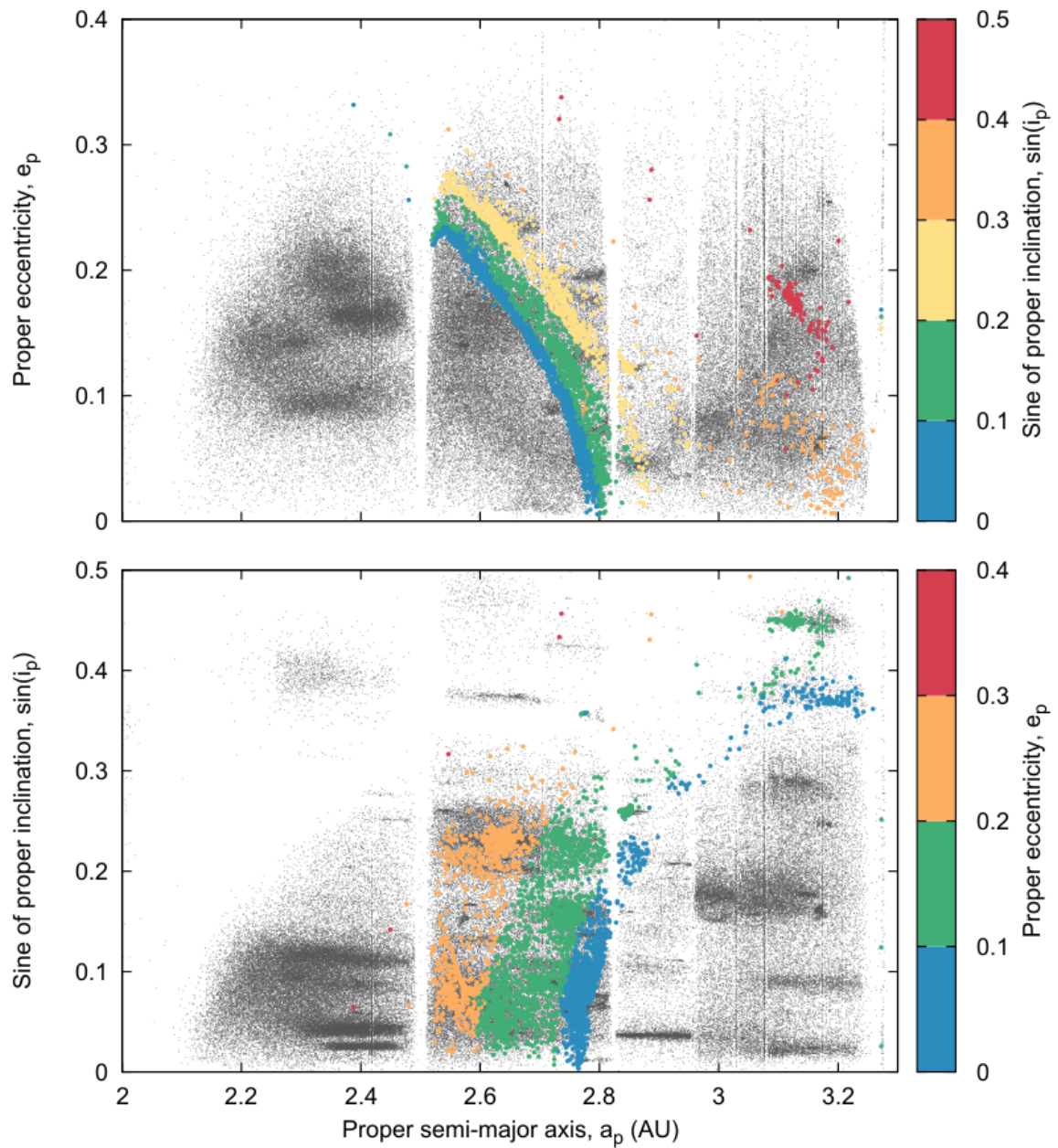


Fig. 2.15.: The location of the ν_{1c} secular resonance on the (a_p, e_p) plane (top), and on the $(a_p, \sin i_p)$ plane (bottom). The gray dots represent all main belt asteroids, and the colored points the resonant ones for different inclinations (top panel) and eccentricities (bottom panel) according to the respective color codes given in the legend.

The ν_{1v} resonance

As the asteroid (4) Vesta is located in the inner ($2 < a_p < 2.5 \text{ AU}$) main belt, we expect the secular resonances involving it to predominantly affect this region.

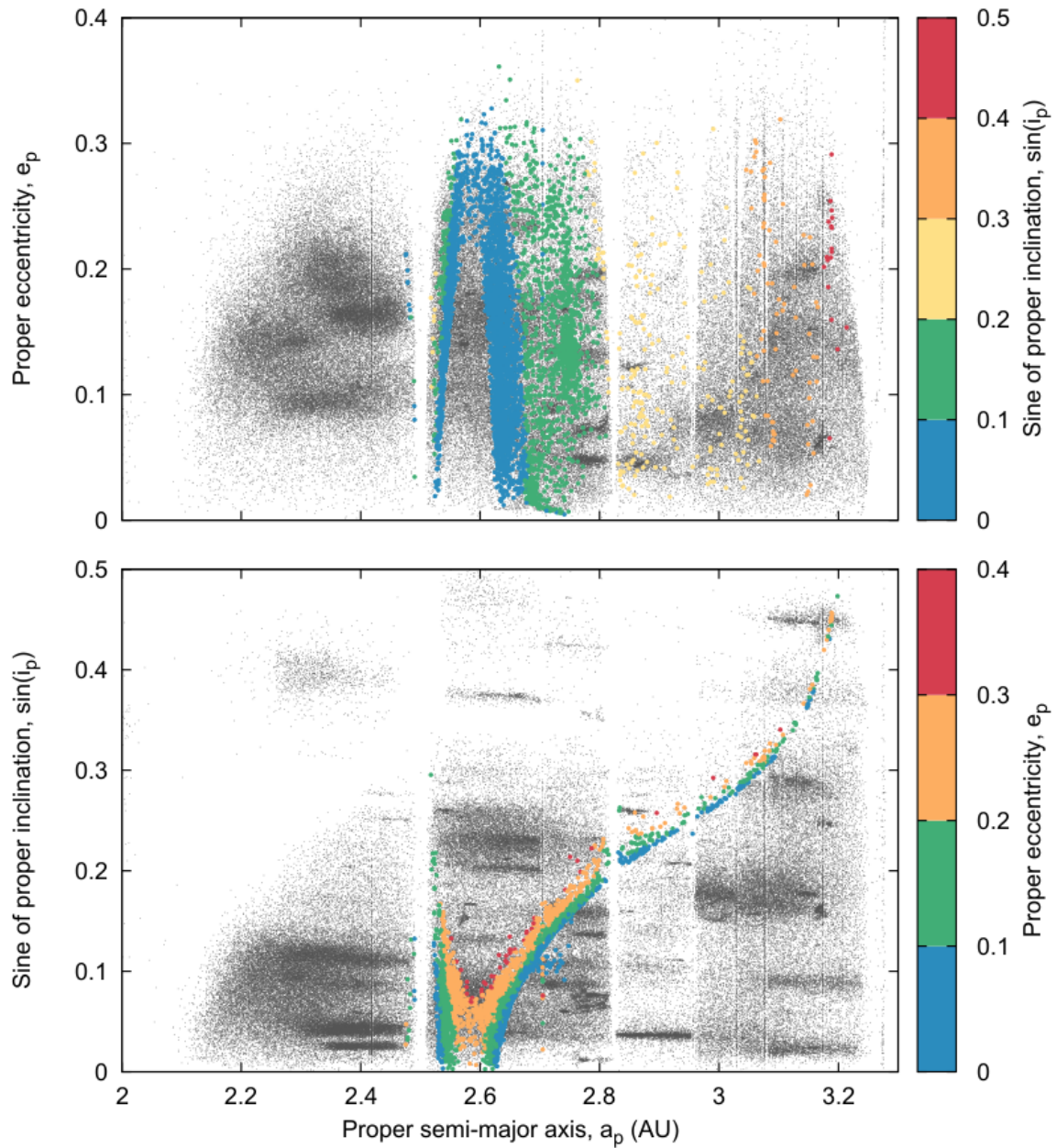


Fig. 2.16.: The location of the ν_c secular resonance on the (a_p, e_p) plane (top), and on the $(a_p, \sin i_p)$ plane (bottom). The gray dots represent all main belt asteroids, and the colored points the resonant ones for different inclinations (top panel) and eccentricities (bottom panel) according to the respective color codes given in the legend.

Indeed in Figure 2.17 we see the location of the ν_{1v} secular resonance, as before by highlighting the asteroids with proper frequencies that satisfy the relation $s - s_v = \pm 0.2''/yr$, where we see that the inner belt is crossed by the resonance in a wide range of eccentricities and inclinations, while there are also some resonant asteroids with high inclinations in the middle belt.

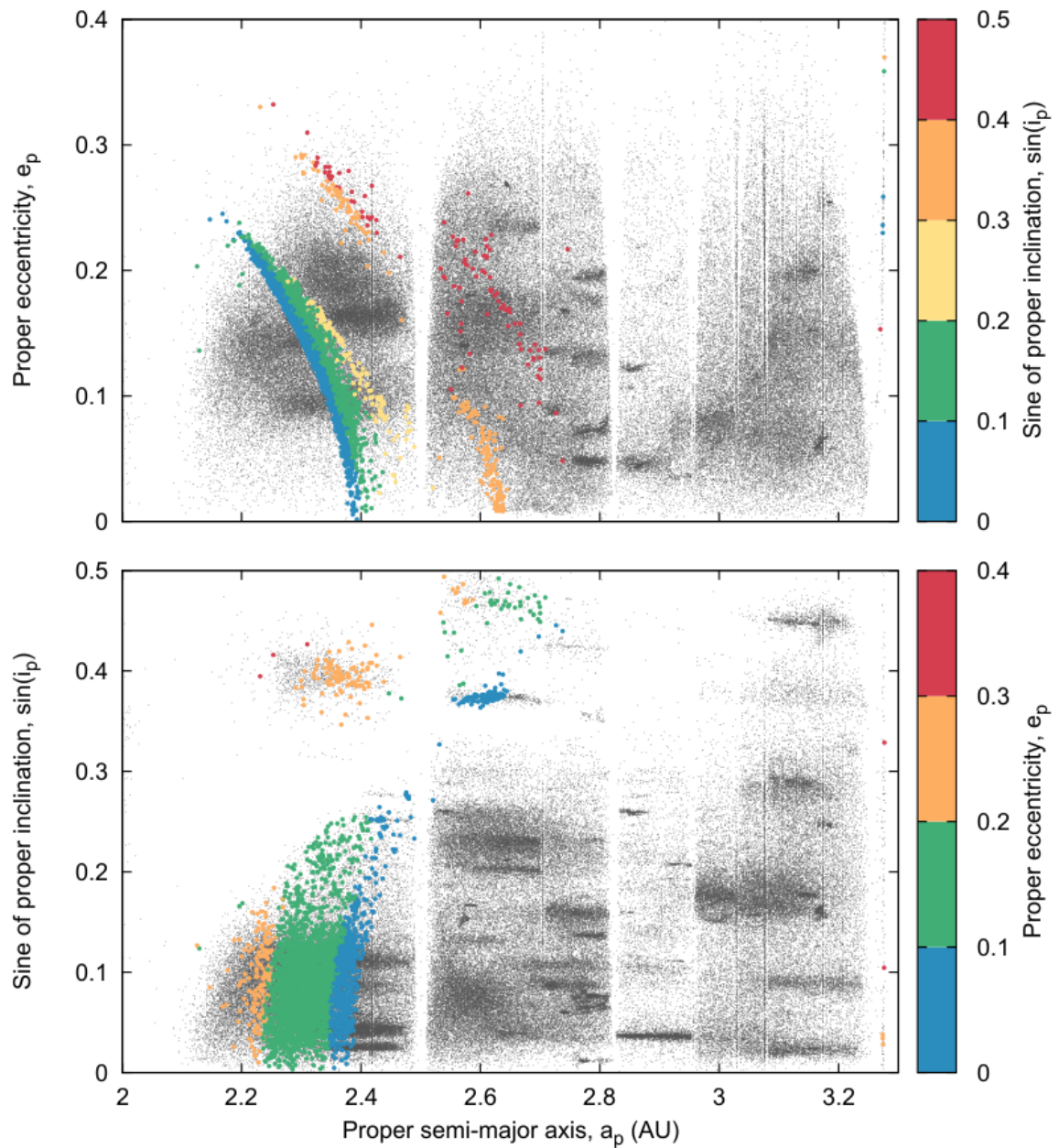


Fig. 2.17.: The location of the $\nu_{1\nu}$ secular resonance on the (a_p, e_p) plane (top) and on the $(a_p, \sin i_p)$ plane (bottom). The gray dots represent all main belt asteroids, and the colored points the resonant ones for different inclinations (top panel) and eccentricities (bottom panel) according to the respective color codes given in the legend.

The ν_ν resonance

The last secular resonance we studied is the one involving the precession frequency of the perihelion of (4) Vesta, namely ν_ν . Figure 2.18 shows the location of the

asteroids whose proper frequencies g satisfy the relation $g - g_v = \pm 0.2''/yr$, revealing the location of the secular resonance across the main belt as in the previous cases. In the $(a_p, \sin i_p)$ plane we notice the pretty clear path of the resonance, crossing the inner belt from low to moderate inclinations, continuing to the high inclination part of the middle belt and on to a very high inclination range of the outer main belt, always covering a very wide range of eccentricities as can be seen in the (a_p, e_p) plane.

2.2.3 Numerical simulations

Having obtained the location of each secular resonance, we proceed to study them individually using numerical integrations of the orbits of test particles. As we highlighted above the parts of the Main Belt that each resonance crosses, we proceed to choose the initial conditions of our test particles focused in these regions. There is no strict rule for selecting initial conditions other than the proximity to the location of the secular resonance we examine in each case. We thus chose initial conditions in such a way, so a wide range of the proper elements of the main belt asteroids is sampled sufficiently for each case, as we will describe individually below.

After selecting which parts we want to study, we proceed in the following way: We created tight groups of 20 fictitious particles with similar initial conditions and integrated their orbits for $50 Myrs$, using the Orbit9 propagator, within two dynamical models: one including the four giant planets, from Jupiter to Neptune, and the massive asteroid relevant for each resonance as main perturbers¹⁰, and another one only with the four planets, which serves as a reference. Both dynamical models also incorporated the Yarkovsky effect as a secular drift in semi-major axis. This drift is expected to force the test particles to cross the resonance, causing the simulation that includes the massive asteroid as a perturber in the dynamical model to reveal the effect of the secular perturbations. We selected a value of $\frac{da}{dt} = 4 \cdot 10^{-4} AU \cdot Myr^{-1}$ for the strength of the Yarkovsky induced drift, that may be considered as a typical reference value for asteroids of 1 km in diameter Vokrouhlický et al. (2015). This value allows for reasonably short integration times ($50 Myrs$) while allowing enough time for the test particles inside the resonance to manifest their effect. From the numerical integrations we obtained the time evolution of the asteroids' mean orbital elements. We then partitioned these in

¹⁰In these simulations we used values of 4.76×10^{-10} and $1.3 \times 10^{-10} M_\odot$ for the masses of Ceres and Vesta, respectively Baer et al., 2011; Kuzmanoski et al., 2010.

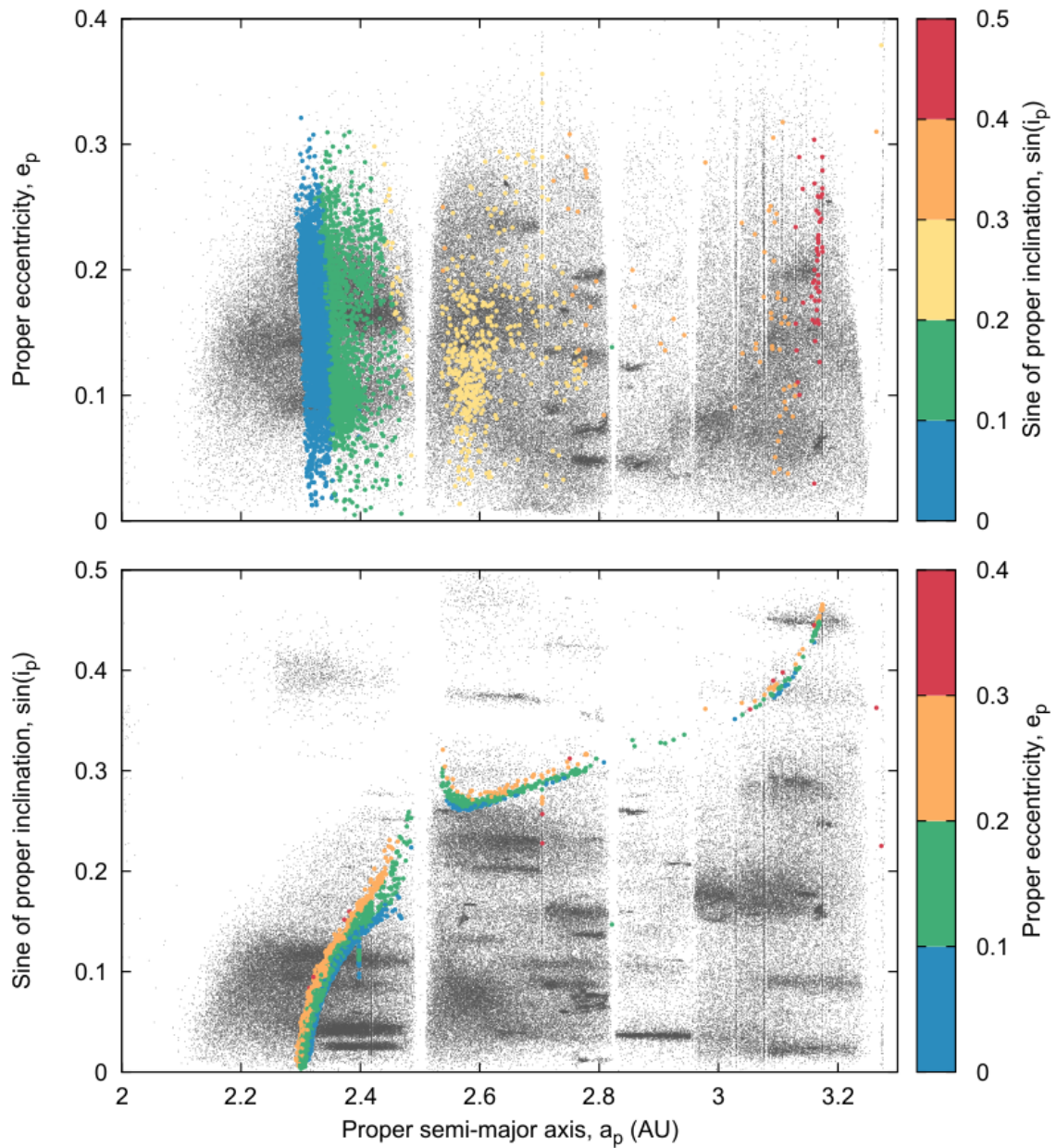


Fig. 2.18.: The location of the v_v secular resonance on the (a_p, e_p) plane (top), and on the $(a_p, \sin i_p)$ plane (bottom). The gray dots represent all main belt asteroids, and the colored points the resonant ones for different inclinations (top panel) and eccentricities (bottom panel) according to the respective color codes given in the legend.

a running window manner with a window width of $10M_{yr}$ and shifting them by $2M_{yr}$. Thus we have obtained the time series of the synthetic proper elements for each asteroid. The comparison of the evolution of the test particles' proper orbital elements between the two dynamical models reveals the role of the secular resonances with the massive asteroids.

The ν_{1c} resonance

In order to study the effect of the resonance, we considered three regions that are crossed by it. Since, as discussed above this secular resonance forms a strip-like shape in the middle belt on the (a_p, e_p) plane, it is intuitive to choose the initial conditions for our test particles just outside this strip, so they are forced to cross the resonance by drifting in semi-major axis due to the Yarkovsky effect. This idea will guide the selection of the initial conditions for the other secular resonances analyzed in the following. Therefore, we can distinguish the relevant regions into the very low and moderate inclination parts of the middle belt, and the high inclination part of the outer belt.

We created a number of groups of 20 test particles as shown in Figure 2.19 for each region, and integrated numerically their orbits within the two dynamical models we explained above. As this secular resonance is a linear one involving only the proper frequency of the precession of the ascending node (s) of the test particles, it only produces perturbations in the proper inclination of the latter, and not in their eccentricity. Therefore we are only interested in the evolution of the proper inclination of the affected asteroids. The situation is the opposite for the secular resonances where the proper frequency of the precession of the longitude of perihelion (g) is involved, perturbing only the eccentricities and not the inclinations of the asteroids.

A representative example of the results for each region is shown in Figure 2.20. The left panels show the evolution in time of the proper inclination of a single particle belonging to a group of initial conditions, plotted over the time evolution of the resonant critical angle:

$$\sigma = \Omega - \Omega_c \quad (2.12)$$

We see that the crossing of the resonance, corresponding to the libration of the critical angle, results in excitation of the proper inclination when Ceres is included in the model as a perturber, whereas for the same initial condition the inclination of the orbit remains stable if we do not include Ceres. The right panels show the evolution in the proper semi-major axis versus sine of proper inclination plane $(a_p, \sin i_p)$ of the 20 particles of each group, in the two dynamical models.

Asteroids entering the resonance experience oscillations in their inclination for as long as their critical angle librates, as seen in the left panel of Figure 2.20. In order to quantify the effect of the perturbation induced by Ceres through the secular

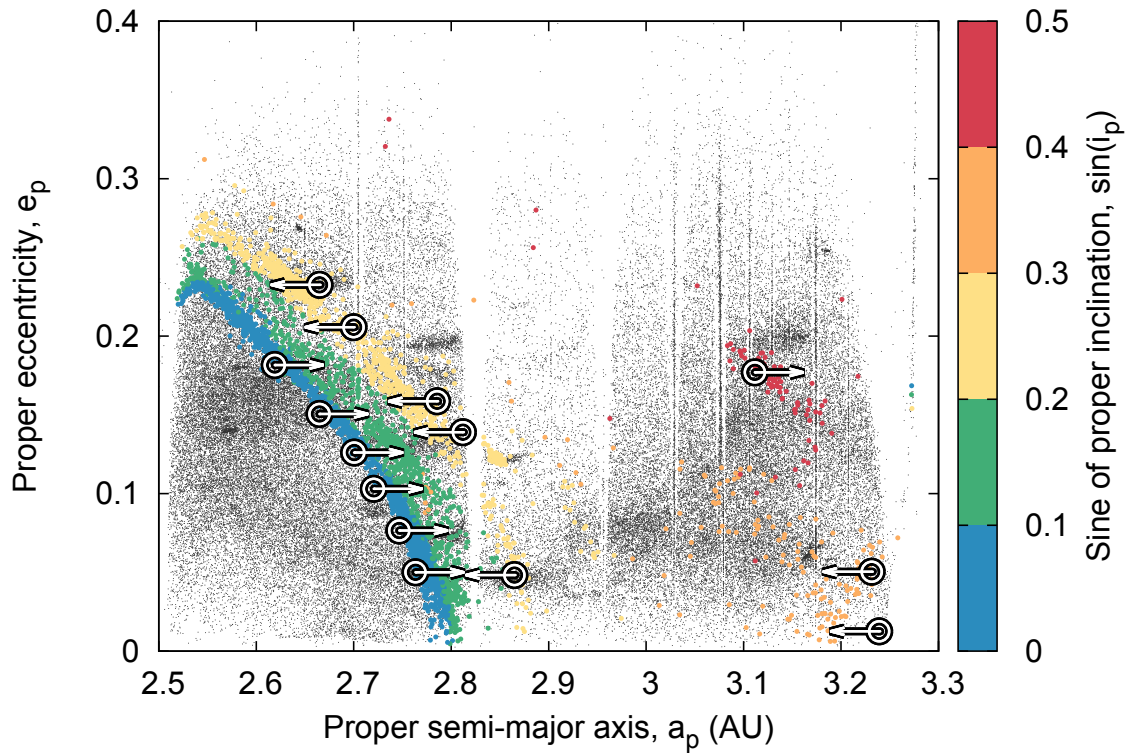


Fig. 2.19.: The location of the groups of initial conditions for the simulations about the v_{1c} secular resonance on the (a_p, e_p) plane. The gray dots represent all main belt asteroids, and the colored points the resonant ones for different inclinations according to the color code. Black circles denote the location and black arrows the Yarkovsky drift direction of each group of initial conditions.

resonance, we measure the maximal change in the proper inclination of the test particles, as they cross the resonance. For the low inclination middle belt we have measured an average amplitude of variations of the order of: $\Delta \sin i_p = 7 \cdot 10^{-4}$ for the groups of test particles with semi-major axes close to that of Ceres ($a_{pCeres} = 2.767AU$), decreasing to $4 \cdot 10^{-4}$ as we move to lower semi-major axes towards $2.6AU$ for our innermost group. For the high inclination middle belt we found an average amplitude of $3 \cdot 10^{-4}$. In the farther part of the outer belt ($a_p > 3AU$), the amplitude of the oscillations is substantially smaller, around $1 - 2 \cdot 10^{-4}$, making it more difficult to separate the effect of the secular resonance from the other perturbing mechanisms that act on the region.

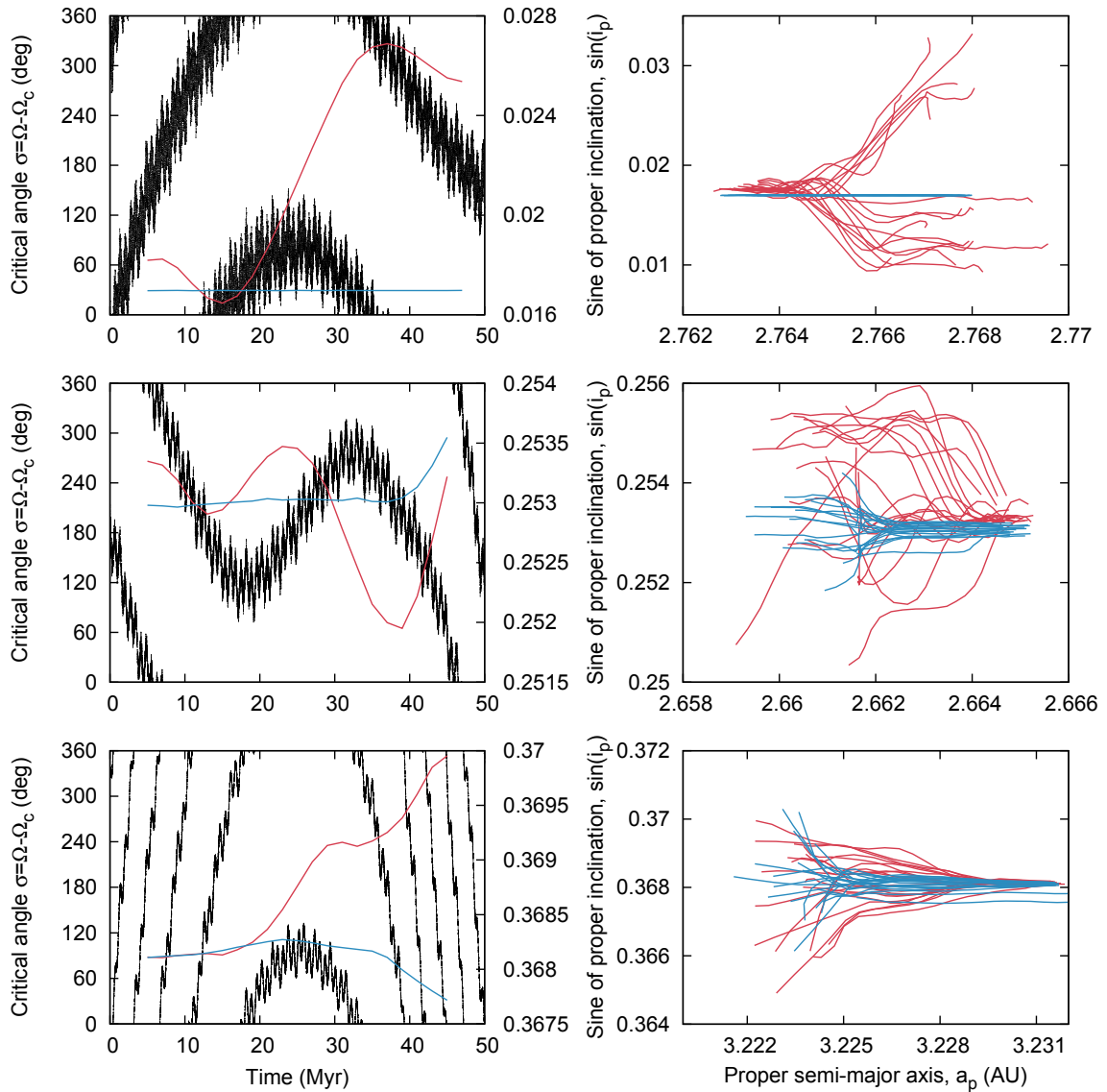


Fig. 2.20.: Orbital evolution due to the secular resonance ν_{1c} for the three representative regions. Top: low inclination middle belt, Mid: high inclination middle belt, Bottom: high inclination outer belt. Left panels: In black the evolution of the critical angle $\sigma = \Omega - \Omega_c$ of a test particle. The red line shows the evolution of the sine of proper inclination of the same test particle with Ceres included in the model. The blue line shows the evolution of the proper inclination of the same test particle without Ceres in the model. Right panels: The evolution of the 20 test particles of the whole group in the two dynamical models, red with Ceres and blue without.

The ν_c resonance

Continuing our previous approach, we distinguish three regions to focus our study on: The low eccentricity ($e_p < 0.05$) and high eccentricity ($e_p > 0.2$) parts of the

middle belt, and the outer belt. Representative examples of the behavior of asteroid orbits in these three regions, resulting from our numerical integrations of test particles are shown in Figure 2.21. Following the same method as for the ν_{1c} secular resonance, we determine the strength of this resonance by the amplitude of the induced oscillations in proper eccentricity, as shown in the example of Figure 2.21. For the low eccentricity middle belt we found a maximum amplitude of 0.01, for test particles close to Ceres (in terms of semi-major axis), decreasing to 0.003 as we move further away. For the high eccentricity middle belt and inner part of the outer belt, the measured amplitude was of the order of 0.003, while the relative strength of the perturbations from other causes increased significantly. For the farther part of the outer belt ($a_p > 3 AU$), although we have clear signature from the critical angle that the test particles cross the secular resonance, its impact on the eccentricities of the orbits is effectively zero, as the two models give statistically indistinguishable results, as can be seen in the bottom part of Figure 2.21. Indeed even though Ceres is included in the model and the resonance is crossed, the evolution of the orbits appears the same as in the model without Ceres.

The ν_{1v} resonance

The situation with this resonance is slightly different than with the ones involving Ceres. When we examine the path of the resonance in Figure 2.17, we see that the high inclination region of the inner belt is also highly eccentric, while the high inclination resonant region of the middle belt has also a low eccentricity part. This led to the result we present in Figure 2.22, that is the high inclination part of the inner belt, despite being close in semi-major axis to Vesta, shows no distinctive evolution caused by the resonance, whereas the resonant region in the middle belt, has a very small ($\delta \sin i \sim 0.0002$), but identifiable signature of inclination excitation due to the resonance. The low inclination part of the inner belt is showing as expected the largest amplitudes of oscillations in the sine of inclination, of the order of 0.004.

The ν_v secular resonance

For this resonance we focused our numerical simulations on the inner belt only. The method we used for revealing the effect of each resonance depends on the action of the Yarkovsky effect in order to force the test particles through the secular

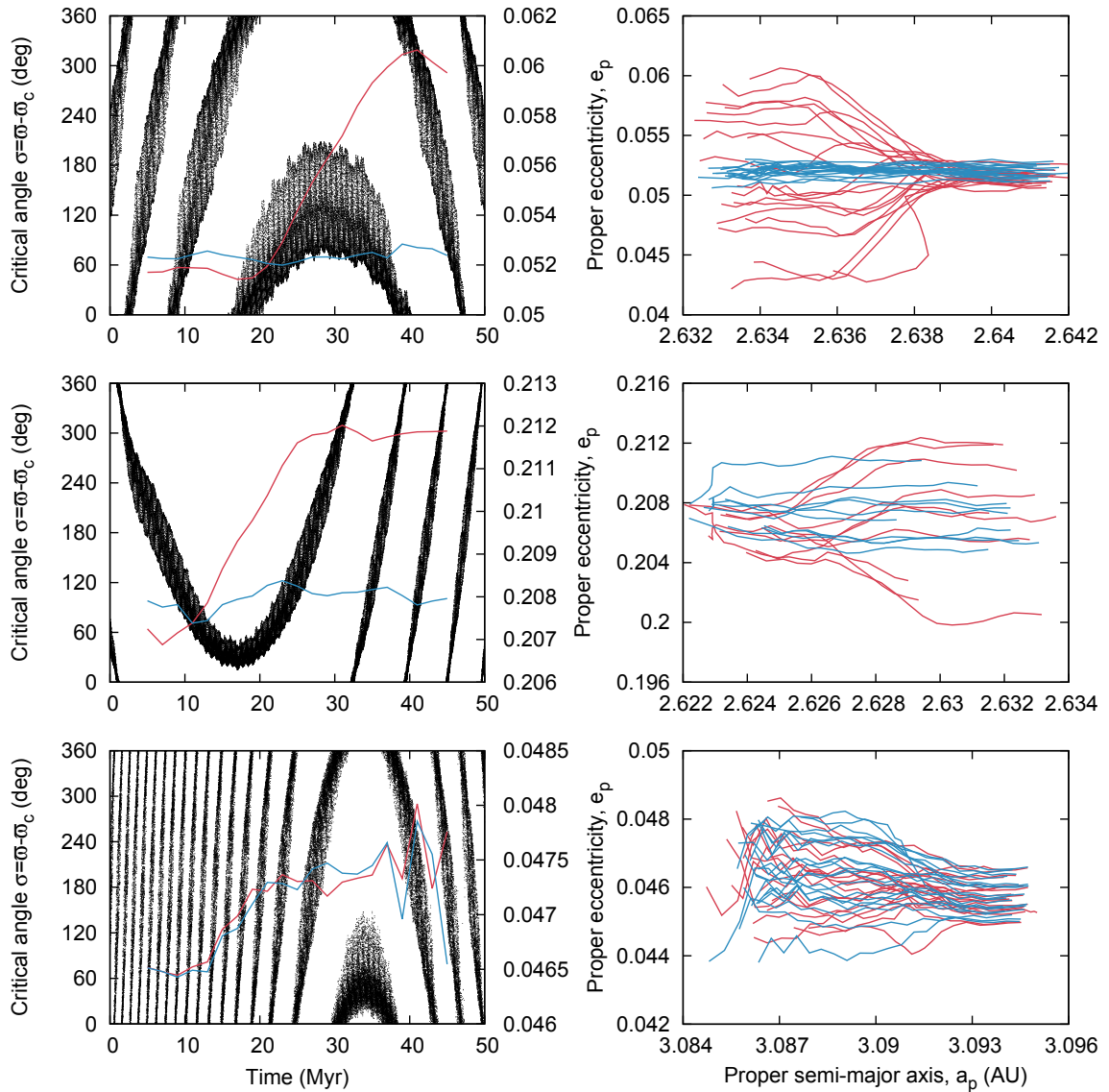


Fig. 2.21.: Orbital evolution due to the secular resonance ν_c for the three representative regions. Top: low eccentricity middle belt, Mid: high eccentricity middle belt, Bottom: outer belt. Left panels: In black the evolution of the critical angle $\sigma = \varpi - \varpi_c$ of a test particle. The red lines show the evolution of the proper eccentricity of the same test particle with Ceres included in the model. The blue lines show the evolution of the proper eccentricity of the same test particle without Ceres in the model. Right panels: The evolution of the 20 test particles of the whole group in the two dynamical models, red with Ceres and blue without.

resonances. This means that it is difficult to apply this scheme if a secular resonance's path is parallel, or almost parallel, to the a_p axis, as is the case for the ν_v secular resonance in the middle belt, and for this reason we did not manage to

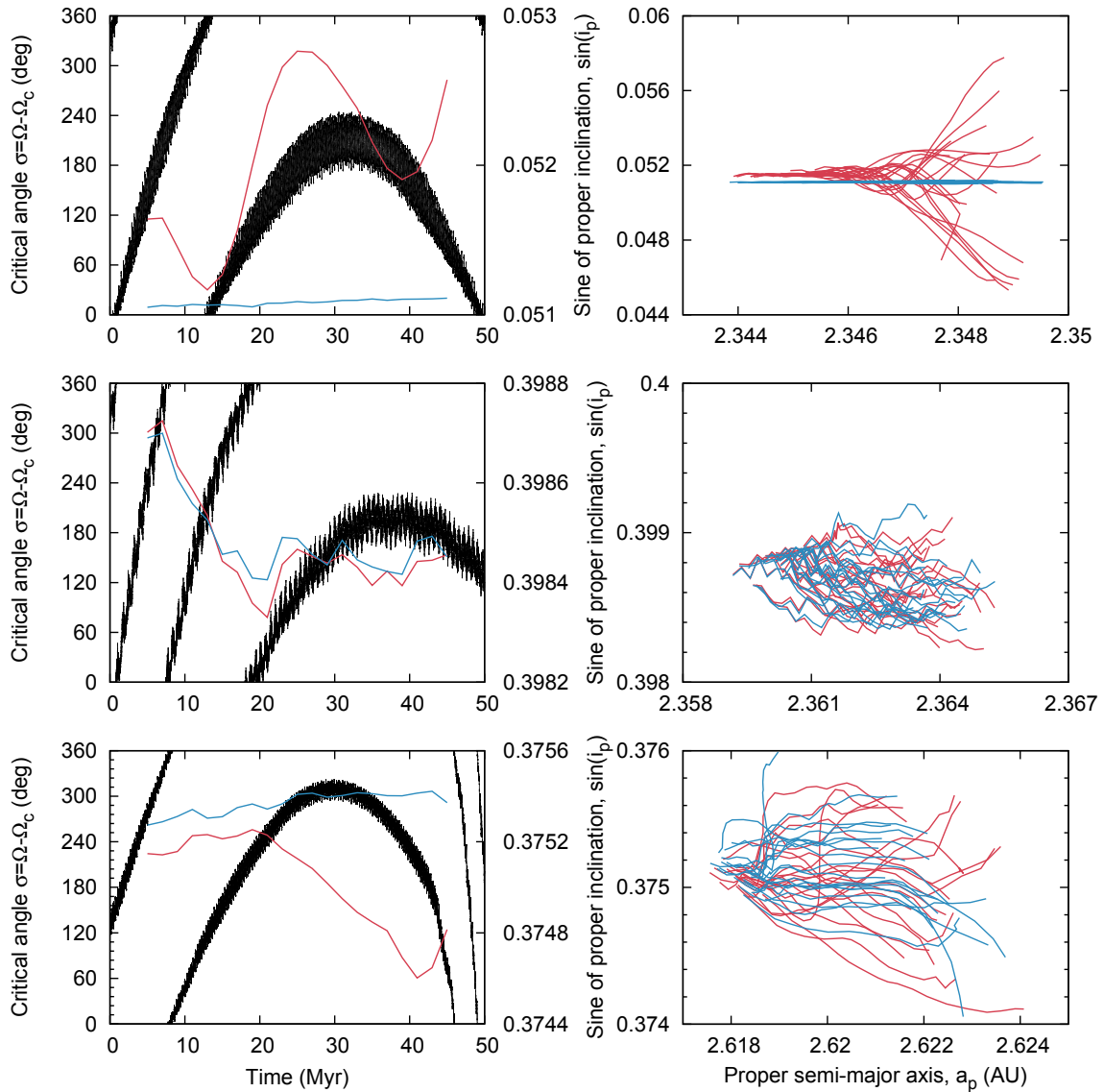


Fig. 2.22.: Orbital evolution due to the secular resonance ν_{1v} for the three representative regions. Top: low inclination inner belt, Mid: high inclination inner belt, Bottom: high inclination middle belt. Left panels: In black the evolution of the critical angle $\sigma = \Omega - \Omega_v$ of a test particle. The red line shows the evolution of the sine of proper inclination of the same test particle with Vesta included in the model. The blue line shows the evolution of the proper inclination of the same test particle without Vesta in the model. Right panels: The evolution of the 20 test particles of the whole group in the two dynamical models, red with Vesta and blue without.

investigate this part. In the inner belt we found oscillations in proper eccentricity with amplitudes of the order of 0.004 as shown in Figure 2.23.

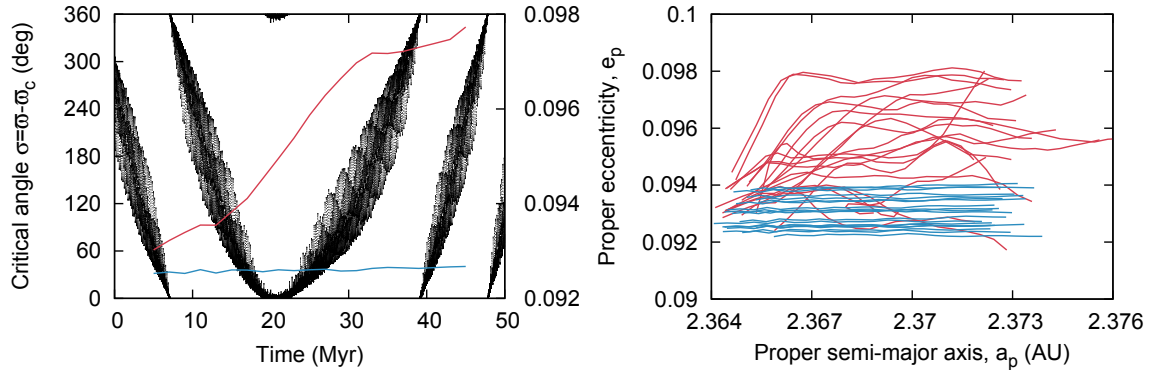


Fig. 2.23.: Orbital evolution due to the secular resonance ν_v for the inner belt. Left panel: In black the evolution of the critical angle $\sigma = \Omega - \Omega_v$ of a test particle. The red line shows the evolution of the proper eccentricity of the same test particle with Vesta included in the model. The blue line shows the evolution of the proper eccentricity of the same test particle without Vesta in the model. Right panel: The evolution of the 20 test particles of the whole group in the two dynamical models, red with Vesta and blue without.

Tab. 2.1.: Summary table of the maximal changes in the proper elements of the main belt asteroids caused by the secular resonances with Ceres and Vesta.

Secular resonance	Measured quantity	Range in a_p (AU)		
		$2 < a_p < 2.5$	$2.5 < a_p < 3$	$a_p > 3$
ν_{1c}	$\Delta \sin(i_p)$	-	$4 - 7 \cdot 10^{-4}$	$2 \cdot 10^{-4}$
ν_c	Δe_p	-	$3 \cdot 10^{-3} - 1 \cdot 10^{-2}$	$3 \cdot 10^{-3}$
ν_{1v}	$\Delta \sin(i_p)$	$4 \cdot 10^{-4}$	$2 \cdot 10^{-4}$	-
ν_v	Δe_p	$4 \cdot 10^{-3}$	-	-

The results for all the cases we investigated are summarized in Table 2.1. Where ranges are given, the largest value corresponds to asteroids with proper semi-major axes close to those of the respective perturbing body (Ceres or Vesta). We notice that the maximal values of the changes in proper inclination and eccentricity caused by Ceres are almost two times bigger compared to the ones caused by Vesta, a consequence of the fact that Ceres is approximately 3.5 times more massive than Vesta, thus exerting stronger perturbations as expected.

2.2.4 Asteroid families

One important aspect of the action of the secular resonances with massive asteroids we have presented, is the effect they may have on the orbital evolution of asteroid family members. Since the asteroid families are more or less compact in the space of proper elements, the action of the secular resonances should give a distinct

signature, identifiable merely by the shape of the family member distributions in the different projections of the proper elements. Indeed we have previously shown in section 2 that the asymmetric shape in the proper semi-major axis versus proper inclination plane $(a_p, \sin i_p)$ of the Hoffmeister family is caused by the ν_{1c} secular resonance with Ceres.

Thus we proceeded to identify all asteroid families that can potentially be affected by the four secular resonances we studied. This is done in a similar way as our numerical method of finding the location of the resonances. Instead of looking at the whole catalog of proper elements for resonant asteroids, we are instead looking in the catalog of only those asteroids that belong to asteroid families. For this we use the classification of Milani et al. (2014). In this way we can find which families are crossed by the secular resonances we present here and which, if any, show signs of interaction with them.

Asteroid families interacting with the ν_{1c} secular resonance

Using the method described above, we find that ten asteroid families have a significant number of their members currently in resonance¹¹ as shown in Figure 2.24. These families are: (3) Juno, (5) Astraea, (31) Euphrosyne, (93) Minerva, (569) Misa, (847) Agnia, (1128) Astrid, (1521) Seinajoki, (1726) Hoffmeister and (3827) Zdenekhovsky.

Apart from the families of (1128) Astrid, (1521) Seinajoki and (1726) Hoffmeister which we have already studied separately, as mentioned above, the ν_{1c} secular resonance may be of some importance for the families of (569) Misa (847) Agnia and (3827) Zdenekovsky as these are close to (1) Ceres in terms of semi-major axis, and cover ranges in the sine of proper inclination comparable to the magnitude of the induced perturbations as we measured them.

The case of (847) Agnia may be of particular interest, as this family is also crossed by the $z_1 = g + s - g_6 - s_6$ secular resonance. Indeed in the $(a_p, \sin i_p)$ plane the two resonances cross the family in a perpendicular way with respect to each other, and because of that we discovered some hints that the secular resonance with

¹¹By significant we mean a number of the order of at least ten asteroids in regular, non-chaotic orbits. We make this discrimination as there may be asteroids with proper frequencies that satisfy the resonant relation, but the error in their frequency is large, resulting from other effects such as a mean motion resonance.

Ceres might be able to drive asteroids out of the z_1 . Of course, this requires further investigation to be proven, that is out of the scope of this work.

The family of (31) Euphrosyne is another example of potential interaction between resonances, as it is crossed by a multitude of them. The secular resonances with the giant planets are more powerful than ν_{1c} in this region, and play an important role in the evolution of the family (Carruba et al., 2014). Still it is possible that even a weak perturbation by ν_{1c} could have an amplified effect due to the interaction with them. Finally the family of (93) Minerva is crossed by the $3 - 1 - 1$ three body resonance with Jupiter and Saturn (Nesvorný and Morbidelli, 1998) at the same location where the ν_{1c} crosses it, making the effect of the latter practically indistinguishable.

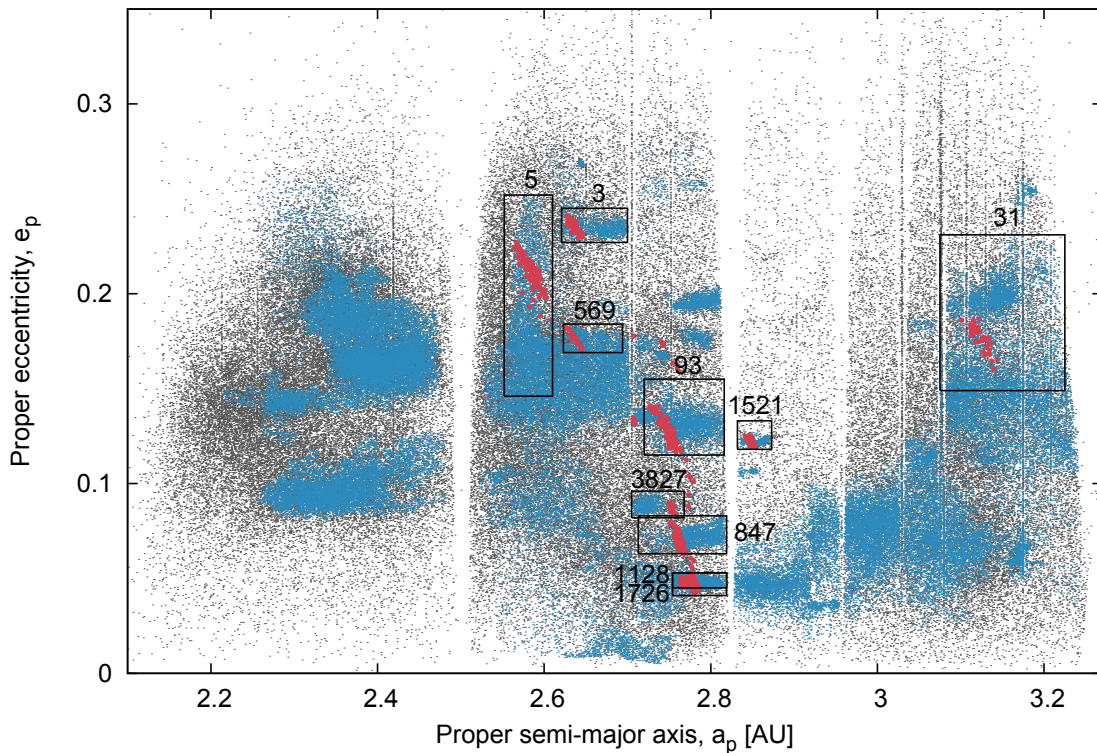


Fig. 2.24.: Asteroid families crossed by the secular resonance ν_{1c} with Ceres. Gray dots represent all main belt asteroids, and blue dots those who belong to asteroid families. The red points represent resonant asteroids belonging to asteroid families (highlighted in black boxes).

Asteroid families interacting with the ν_c secular resonance

In the same manner we identify the asteroid families that are crossed by the ν_c secular resonance, shown in Figure 2.25. The families crossed by this resonance are: (93) Minerva, (410) Chloris, (7744) 1986QA₁ and (10955) Harig. Of these families (410) Chloris and (7744) 1986QA₁ are narrow enough in proper eccentricity so that the secular resonance could be of some importance in their evolution whereas (93) Minerva and (10955) Harig might also seem to be good candidates for further study, as they are large families and their shapes suggest possible influence by the secular resonance. However such a study is not trivial as for the case of (93) Minerva the ν_c secular resonance and the 3 – 1 – 1 overlap, as in the previous case, and the latter dominates the perturbations in eccentricity, whereas Harig is in a place where many secular resonances with the giant planets converge, making it impossible to distinguish the effect of Ceres.

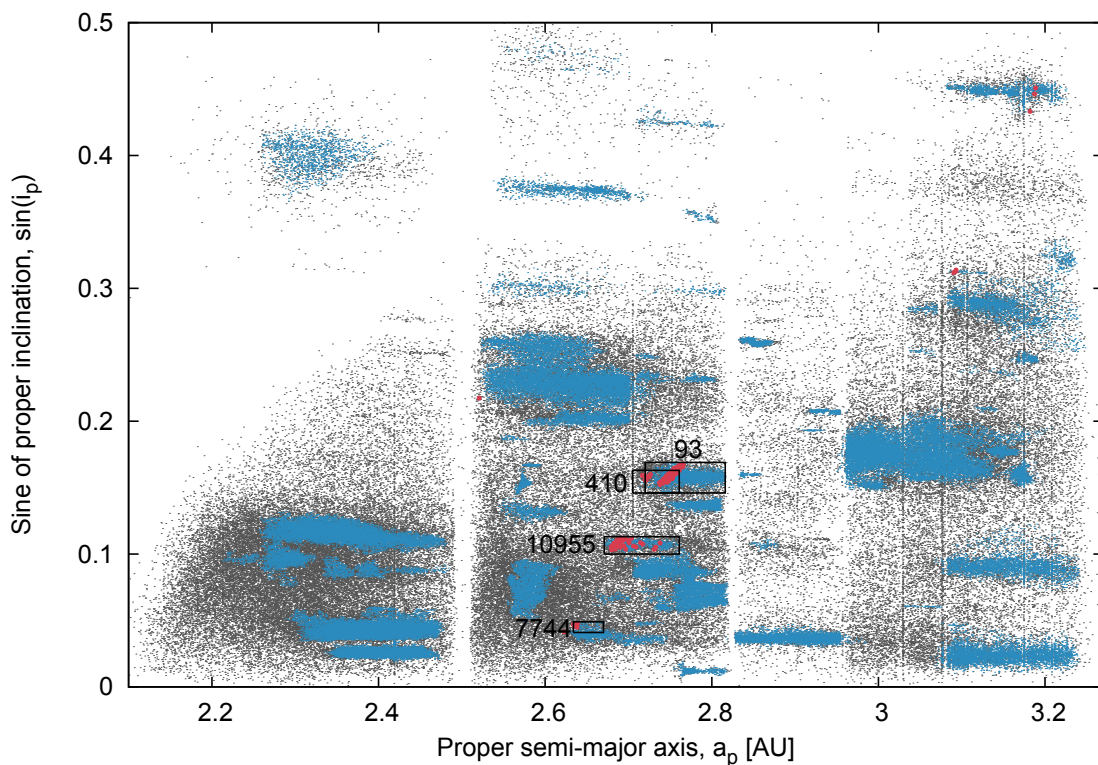


Fig. 2.25.: Asteroid families crossed by the secular resonance ν_c with Ceres. Gray dots represent all main belt asteroids, and blue dots those who belong to asteroid families. The red points represent resonant asteroids belonging to asteroid families (highlighted in black boxes).

Asteroid families interacting with the ν_{1v} secular resonance

In Figure 2.26 we present the results for the case of the ν_{1v} secular resonance with Vesta. We found five families that are crossed by the resonance, which are: (4) Vesta, (135) Hertha, (480) Hansa, (945) Barcelona and (2076) Levin. Our interest for this case is drawn not in the big families, where nothing special seems to happen, but at the very high inclination family of (945) Barcelona. The size of this family in the proper elements space is comparable to the magnitude of the perturbations given by the ν_{1v} secular resonance, and it shows some hints of irregular at the location interacting with it. Even the possibility that a secular resonance with Vesta might be important at such a high inclination in the middle belt is intriguing, and deserves further study.

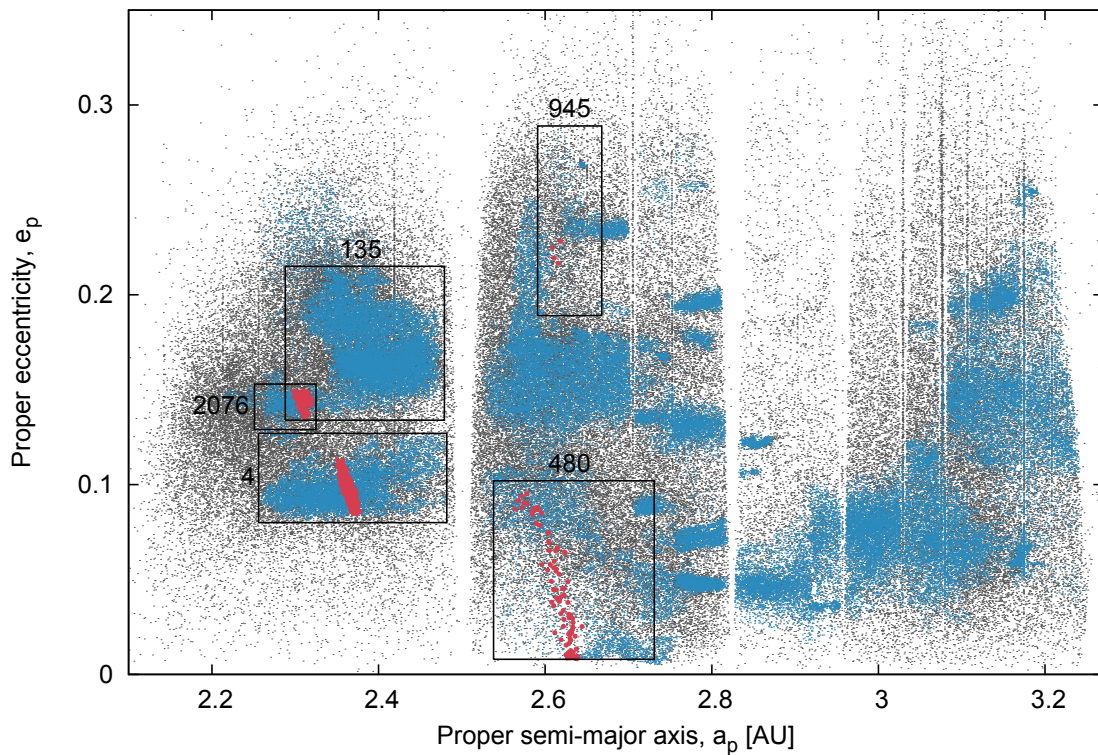


Fig. 2.26.: Asteroid families crossed by the secular resonance ν_{1v} with Vesta. Gray dots represent all main belt asteroids, and blue dots those who belong to asteroid families. The red points represent resonant asteroids belonging to asteroid families (highlighted in black boxes).

Asteroid families interacting with the ν_v secular resonance

In Figure 2.27 we present the asteroid families which we found to be crossed by the last secular resonance we consider here, the ν_v secular resonance with Vesta. We found six such families, namely: (4) Vesta, (31) Euphrosyne, (135) Hertha, (163) Erigone, (170) Maria and (729) Watsonia. However, we were unable to relate any specific property of these families to the existence of the resonance, as these families are either too large, in which case the perturbations can not lead to significant alteration of their shape, or too far away from Vesta, where the perturbations are not strong enough.

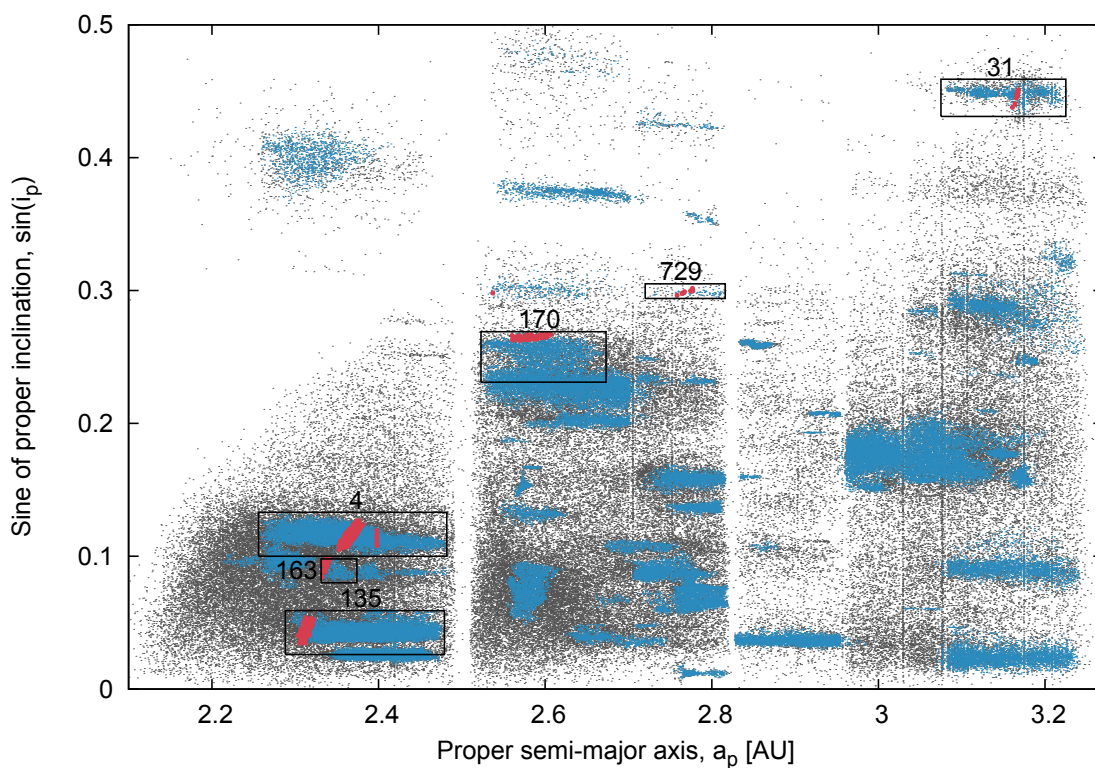


Fig. 2.27.: Asteroid families crossed by the secular resonance ν_v with Vesta. Gray dots represent all main belt asteroids, and blue dots those who belong to asteroid families. The red points represent resonant asteroids belonging to asteroid families (highlighted in black boxes).

2.3 The Seinajoki and Astrid asteroid families

With the locations of the linear secular resonances with Ceres and Vesta determined, and with the list of potentially affected asteroid families for each resonance at hand,

it is now possible to extend our study to other families as well. We chose to analyze two more asteroid families, in an effort to verify the importance of the studied resonances on the long-term evolution of asteroid families. To this purpose we chose to study two more families, namely (1521) Seinajoki and (1128) Astrid. For both of these families the secular resonance in question is the $s - s_c$, and they both have orbital distributions of their members in the proper elements space suggestive of significant and measurable contribution by the secular resonance.

2.3.1 The (1521) Seinajoki asteroid family

The (1521) Seinajoki asteroid family ¹² is located in the outer part of the Main Belt, at a relatively high inclination, and moderate eccentricity. More specifically its members are confined in the proper elements space in a box, approximately covering the ranges:

$$\begin{aligned} 2.825 < a_p < 2.89 \text{ AU}, \\ 0.254 < \sin i_p < 0.265, \\ 0.118 < e_p < 0.135 \end{aligned} \tag{2.13}$$

We have carried out a thorough analysis of the family from a dynamical point of view, in order to verify the importance of the $s - s_c$ secular resonance, which we found to be crossing the family as previously mentioned, in its evolution.

Identification of family members and physical properties

Once again, the first step of our analysis was to establish the membership of the family. The fact that the family is actually situated at the innermost part of the outer belt, which is commonly referred to as the pristine zone, renders the identification procedure rather trouble-free. This is because the pristine zone has a much lower number density of background asteroids compared to any other part of the Main Belt, even less so at high inclinations, so the families are well isolated from one another, and the density contrast to the background is sharp. Starting from the

¹²This family is often referred to as (293) Brasilia, but since the asteroid Brasilia itself is an interloper as we will demonstrate shortly, asteroid (1521) Seinajoki bears the namesake as the next lowest numbered asteroid.

largest asteroid in the region, (293) Brasilia, we applied the HCM with distance thresholds ranging from 10 to 150 m/s in increments of 10 m/s, and monitoring the number of asteroids clustered at each step. The resulting dependence of the number of associated asteroids on the increasing distance threshold is shown in Figure 2.28. We verify that the family is well isolated from other families and the background population as the membership remains practically constant for distance threshold values in the range 30 to 140 m/s, and we adopt as nominal the membership corresponding to the middle of this plateau, 70 m/s. This yields 914 family members. To refine the membership of the family, but also to extract important information about its physical properties, we once again turn to available physical data.

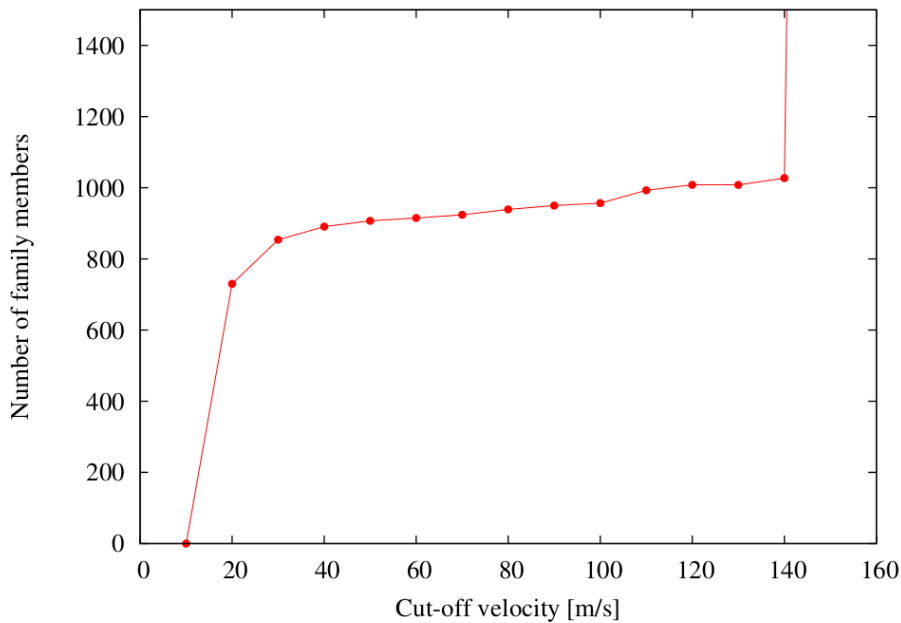


Fig. 2.28.: Number of associated asteroids versus distance threshold(d_c) for the Seinajoki asteroid family.

The Wide-field Infrared Survey Explorer (WISE) provides albedos for 136 (about 14%) family members (Masiero et al. 2011). We calculated the mean geometric albedo of the family and found it to be $p_v = 0.171 \pm 0.061$, while in Figure 2.29 we present the distribution of the albedos of the family. Both the mean albedo and the histogram reveal a rather bright family, corresponding most probably to S and X taxonomic types. With that in mind, we can safely deduce that any potential dark asteroids found in the membership should actually be interlopers and thus discarded. In this work, for an asteroid to be considered dark and be removed from the membership, we required that its albedo plus three times the standard deviation of its measurement, amount to less than 0.09. This led to the identification

and removal of only two asteroids from the family, most importantly of asteroid (293) Brasilia with an albedo of 0.0327, which is the largest asteroid of the family if defined using only dynamical criteria. To better assess whether the Seinajoki family

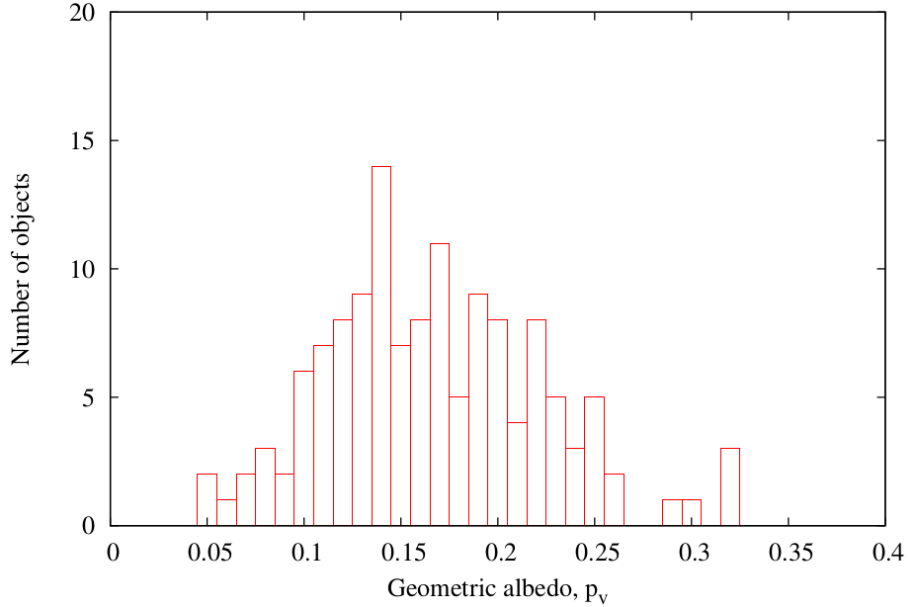


Fig. 2.29.: Distribution of geometric albedos of the members of the Seinajoki asteroid family.

consists of S- or X-type asteroids we used Sloan Digital Sky Survey (SDSS) color data. It was shown by Ivezić et al. (2002) that SDSS photometry is consistent with available spectra of asteroids, meaning that the colors provided by the SDSS could be used to separate at least broad taxonomic classes, such as C/X and S. For this study we adopted the approach of Parker et al. (2008a), excluding the u-band from our analysis, and using the a^* color defined as:

$$a^* = 0.89 \cdot (g - r) + 0.45 \cdot (r - i) - 0.57 \quad (2.14)$$

It is known that asteroids show a bimodal distribution in a^* , where C/X-type objects are characterized with $a^* < 0$, while S-type objects typically have $a^* > 0$. In the fourth release of the SDSS Moving Object Catalog we found data for 69 family members, yielding a mean value of the a^* color of -0.0395 ± 0.0334 . This value of the a^* color is consistent with C- and X-type, which combined with the WISE data led us to the conclusion that the Seinajoki family belongs to the X-type. To further confirm this conclusion we also used results by Carvano et al. (2010) who defined a new classification algorithm based on the SDSS colors. This scheme allows for a finer distinction between taxonomic classes. The available data is shown in Figure 2.30.

Despite the low reliability of spectral type associations for some asteroids, this data undoubtedly confirms that family is composed of X-type objects.

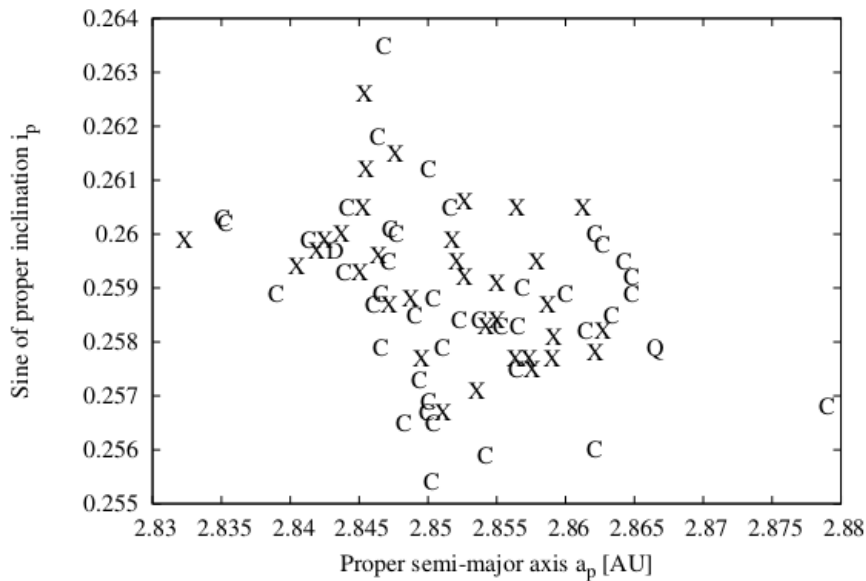


Fig. 2.30.: Distribution of the members of the Seinajoki asteroid family with available SDSS color data, in the proper elements space. Each asteroid is represented by its taxonomic type letter.

Numerical simulations

The main part of this study was to assess the importance of Ceres on the dynamical evolution of the Seinajoki family through the $s - s_c$ secular resonance, which as mentioned appears to cross the family.

As in the case of the Hoffmeister family, the main tool we utilized was numerical integrations of the orbits of test particles, simulating the evolution of the actual family members since the era of the formation of the family, within different dynamical models. The usual practice for studies of families in the outer Main Belt, is to consider the dynamical model consisting of the Sun and the four giant planets the benchmark of all simulations. To that baseline model we add the dwarf planet Ceres, as done previously, to grasp its effect through the secular resonance. Another possibly important aspect arises from the fact that the Seinajoki family features moderate average eccentricity and rather high average inclination of its members. This suggests that apart from the giant planets and Ceres, the inner planets should also play a non negligible role in the dynamical evolution of the orbits of the family members. Thus we also examined a dynamical model including seven planets and

Ceres. Mercury was not included in this model as it indeed should have a negligible effect on the orbits of the test particles, so small that did not justify the increased demand in computational time it would require. We note that in any model that does not include one or more planets, their indirect effect was taken into account by adding their mass to that of the Sun and applying a relevant barycentric correction on the initial conditions.

The test particles were once again generated in a one to one correspondence to the actual family members, with respect to both their total number and individual sizes. Their initial positions in the orbital elements space was once again determined by the equivelocity ellipsoid derived from the Gauss equations, the size of which in turn depends on the size of the parent body. To determine that, we summed up the masses of all the identified family members, assuming the same density of 2500 kg/m_3 and geometric albedo of $p_v = 0.172$, as resulting from the physical data presented above. This way we compute the parent body to be 34.3 km in diameter, with an escape velocity of 20 m/s. The test particles are finally randomly distributed within the equivelocity ellipsoid, yielding the initial conditions for our simulations.

All three models also incorporate the action of the Yarkovsky effect, which is the main driver of the semi-major axis mobility of small asteroids. The reference value of the maximum drift for a 1 km asteroid with the physical characteristics we have presented above, turned out to be $3 \cdot 10^{-4} \text{ AU/Myr}$. Each test particle was then assigned a drift rate, scaled from this reference value with respect to its size, and factored with a random number to account for the different possible spin axes obliquities.

The orbits of the test particles were numerically integrated for 200 Myr using the Orbit9 integrator, which outputs the evolution of the mean orbital elements by applying an on-line filtering algorithm to remove the short periodic oscillations of the osculating orbital elements. The output was then split in running windows of 10 Myr, in order to obtain the time-series of the proper orbital elements, as was done in the Hoffmeister case.

Results of the simulations

The result of the first model, the one containing only the four giant planets, is not in agreement with the distribution of the real family. With our experience from the Hoffmeister case, we could argue that this was more or less expected. Indeed we see in the bottom panel of Figure 2.31 in black, that the test particles show practically no evolution in their proper inclinations. This model obviously cannot explain the shape of the Seinajoki asteroid family.

Moving on to the model containing the four giant planets and the dwarf planet Ceres, we witness that we are able to reproduce the main features of the actual family. In the bottom panel of Figure 2.31 in gray we see that the test particles crossing the $s - s_c$ secular resonance (highlighted by the black lines) get dispersed in their proper inclinations, matching the main features of the actual family.

Still we see that the simulations do not reproduce the shape of the actual family to a satisfactory degree. The main issue is that asteroids that cross the $s - s_c$ secular resonance get to higher inclinations, which is what we mainly observe at the actual family, but they also go towards lower inclinations, along the track of the secular resonance. This second behavior is not observed in the real family to this extent. In order to resolve this issue we turn to the model including seven planets plus Ceres, as the influence of the inner planets could and should play a role; we didn't know a priori if they should play this role, but they should play a role. Surprisingly enough the inner planets eventually turned out to be the last missing piece of the puzzle. As seen in Figure 2.32 the model with the seven planets (blue points) has much fewer test particles that go toward lower inclinations compared to the one that has only the four giant planets (black points), and matches the distribution of the real family much better.

2.3.2 The (1128) Astrid asteroid family

The last asteroid family we studied with respect to the influence of the $s - s_c$ secular resonance upon the dynamical evolution of its members was that of (1128) Astrid¹³. This family is located at the middle part of the Main belt, at very low inclinations

¹³The presentation of this study will be kept as short as possible, as all the methods applied are identical as those mentioned above for the case of the Seinajoki asteroid family

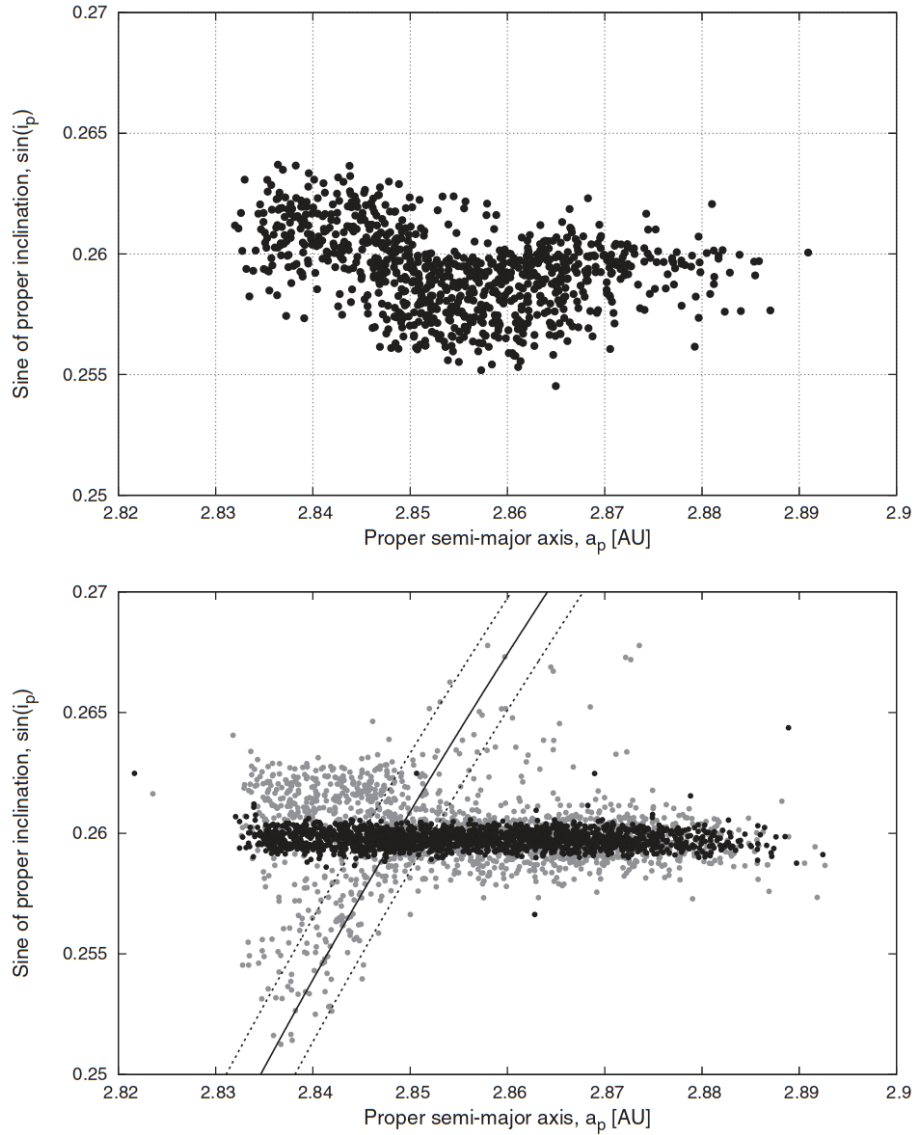


Fig. 2.31.: Top : The distribution of the nominal Seinajoki family members in the proper semi-major axis versus the proper inclination plane; Bottom : The distribution of the test particles after 150 Myr of the evolution. The black points represent particles integrated within the model without Ceres, while the gray points denote particles simulated using the dynamical model that also includes Ceres as a perturbing body. The solid and two dashed curves mark the center and the borders of the $s - s_c$ resonance, respectively.

and eccentricities. More specifically its members lie in the proper elements space within the ranges:

$$\begin{aligned}
 2.75 < a_p < 2.82 \text{ AU}, \\
 0.002 < \sin i_p < 0.022, \\
 0.045 < e_p < 0.053
 \end{aligned}
 \tag{2.15}$$

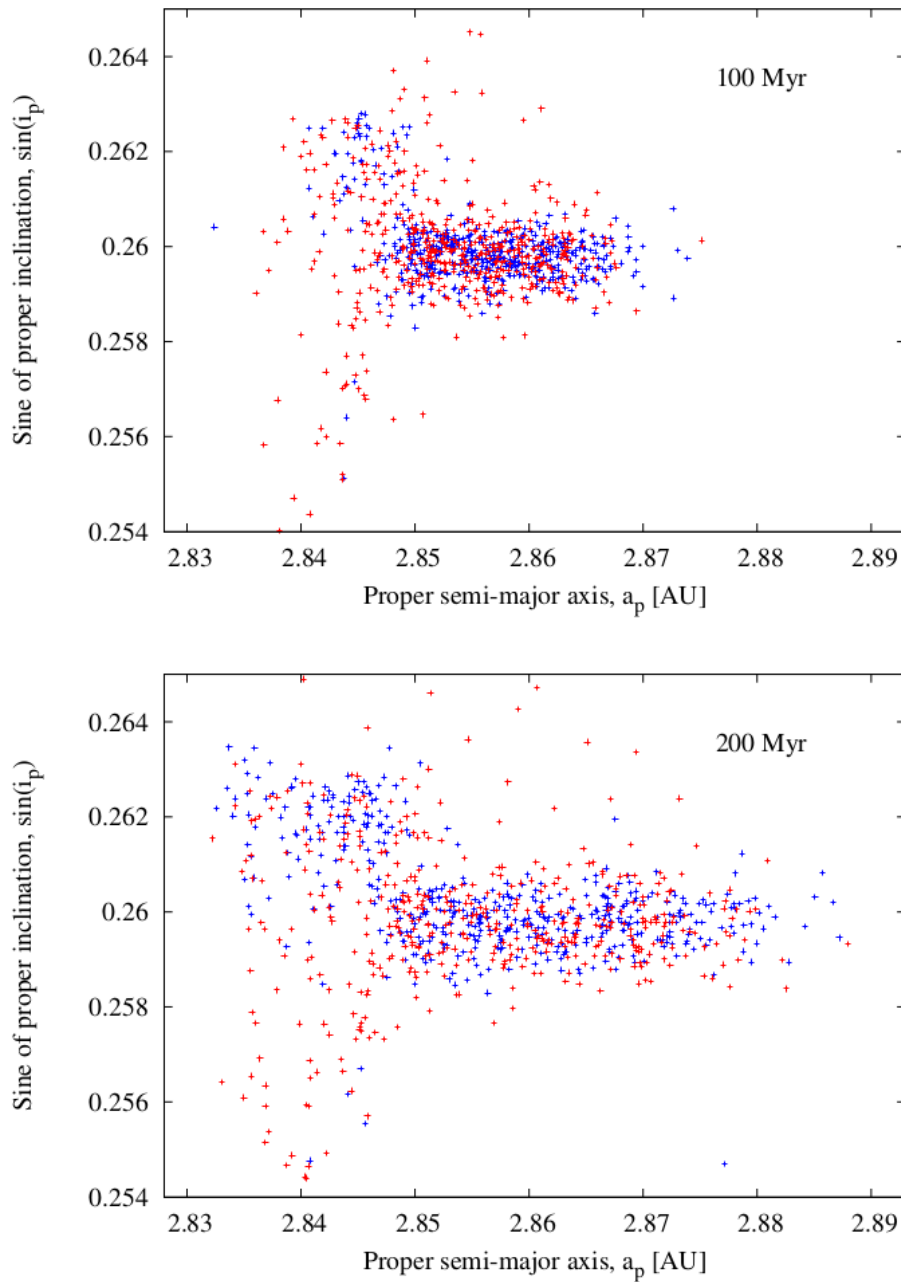


Fig. 2.32.: Snapshots of the distribution of test particles on the $(a_p, \sin i_p)$ at 100 Myr (Top) and 200 Myr (Bottom) for the two dynamical models: with four planets (Red) and with seven planets (Blue)

The family is well separated from any other group in the main belt, as well as from the local background population. An analysis of the region surrounding the family in the $(a_p, \sin i_p)$ plane reveals that the family is isolated as only a few background objects are present. The distribution of Astrid family members projected on the $(a_p, \sin i_p)$ plane (Top panel in Figure 2.33) shows a pattern similar to the case of the Hoffmeister family. For smaller values of semi-major axes, the spread in orbital

inclinations is notably larger than at larger values. Moreover, a similar lobe is also present in the right side of the family, even though it is not so prominent.

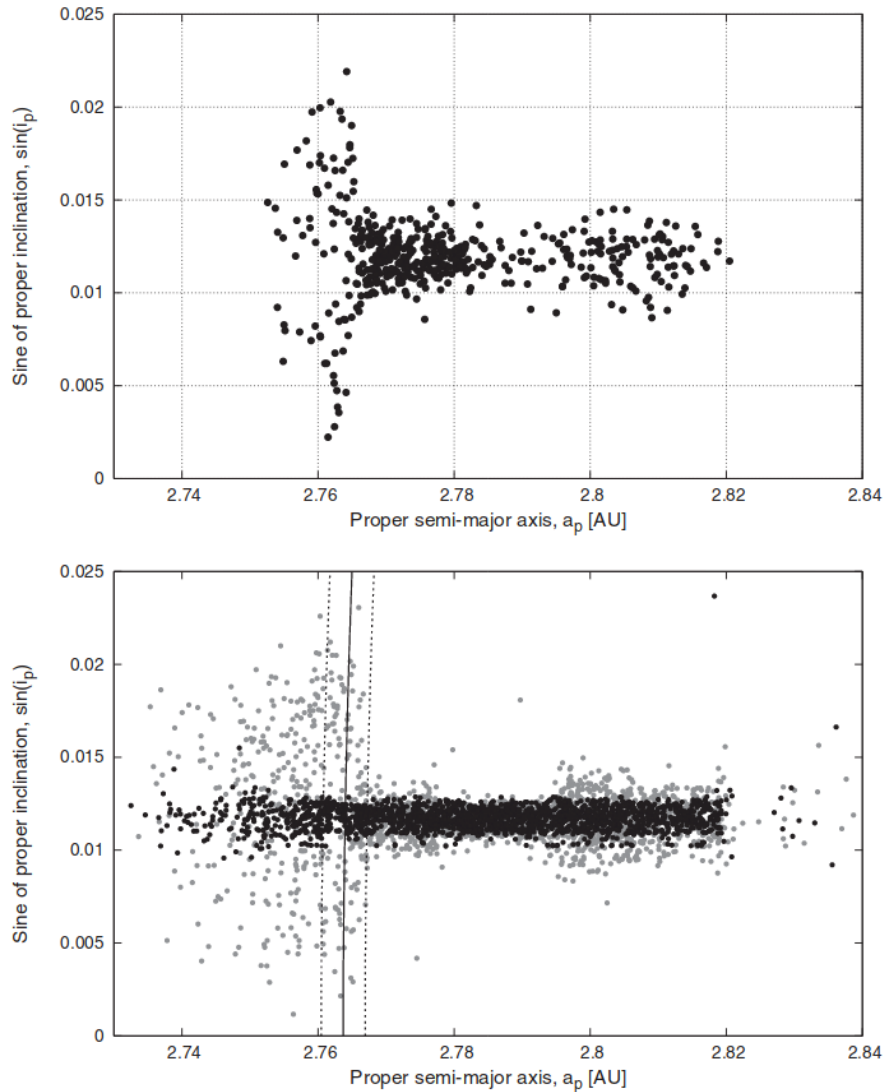


Fig. 2.33.: Same as Figure 2.31 but for the Astrid family.

Regarding the physical properties of the family members, WISE data, presented in Figure 2.34, suggest that Astrid is a dark C-type family, with a mean albedo of $p_v = 0.052$.

Once again, we utilized numerical integrations of the orbits of test particles to verify the importance of the $s - s_c$ secular resonance. The benchmark dynamical model we used consisted of only the four giant planets, and the second model that should reveal the influence of the secular resonance also included Ceres. As the Astrid family is characterized by very low eccentricities and inclinations, we argued that the inner planets should indeed be of negligible importance. The rest of the setup

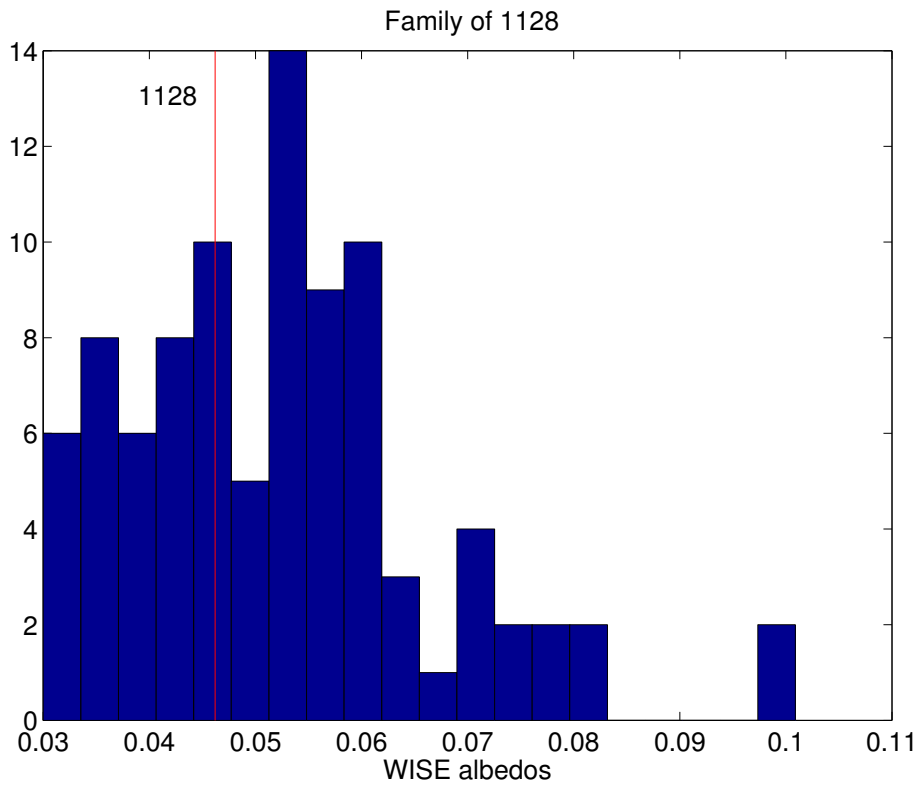


Fig. 2.34.: Histogram of the albedos of Astrid family members. The red line denotes the albedo of the parent body, asteroid (1128) Astrid.

of our simulations was methodologically identical to that of the Seinajoki family, i.e. same steps but with parameters derived from the specific physical and dynamical characteristics of the Astrid family. The output of the integrations was also handled in the same way, resulting in the time-series of the proper elements for each test particle.

As in the case of the Hoffmeister and Seinajoki families, if we include in our model only the giant planets and the Yarkovsky force, we do not see any modifications of the proper inclinations of the test particles as they spread in semi-major axis. Hence, it is clear that we cannot reproduce the shape of the family using only the four giant planets as perturbers and the Yarkovsky effect.

On the other hand, when Ceres is included in the dynamical model, the difference with respect to the previous case is evident, and the shape of the real family is well reproduced. This can be appreciated from the bottom panel shown in Figure 2.33, where gray points represent the state of the test particles after 150 Myr of evolution within the model with Ceres. Note that the spread in inclination occurs when a particle enters into the $s - s_c$ secular resonance, highlighted by the black lines.

The Yarkovsky effect continuing its action eventually pushes the test particles out of the resonance on the other side, but they have already suffered strong enough perturbations by it so that their inclinations have been excited significantly. Another interesting observation has to do with the smaller in absolute magnitude, but still clearly visible spreading in inclinations at the outer part of the family. This spreading is also visible in the distribution of the real family members, but was not reproduced by the model including only the four giant planets. This is a strong indication that the responsible mechanism for the formation of this small lobe is also a secular resonance with Ceres, although it has to be much weaker than the $s - s_c$. However, the identification of this weak resonance can be a tricky thing, because usually there may be more than one possible solutions. Our investigation suggests that this small effect in inclination of the outer part of the Astrid family members may be consequence of the $s - s_c + g_c - 2g_6 + g_5$ secular resonance, a harmonic so to say of the $s - s_c$.

2.4 Summary

We started from an odd shaped asteroid family in the proper elements space, that of Hoffmeister, and we ended up with the discovery of a dynamical mechanism which was hidden in plain sight, and plays a very important role in the dynamical evolution of the orbits of asteroids in the Main Belt. Although secular resonances and their effects have been known and excessively studied for many decades, only the planets of the Solar System, and mainly the giant ones have been considered as their originators.

Despite the much lower mass of even the largest asteroids, the fact that they are embedded inside the Main Belt themselves, reducing the mutual distances to small asteroids to minimal, is enough to drive secular resonances with noticeable, even dominant effects.

We have shown that for the case of the Hoffmeister asteroid family, no other logical assumption concerning the dynamical environment within which the orbits of its members evolve, can lead to the observed distribution in the proper elements space. Indeed we have shown beyond any doubt that the $s - s_c$ secular resonance with Ceres is the only solution to the problem regarding its strange, asymmetrical shape.

Following up on these results, we traced out the paths of the four presumably strongest secular resonances with asteroids, that is the two linear ones for each of the two largest asteroids by mass, (1) Ceres and (4) Vesta. We then carried out an extended study using numerical simulations in an effort to map the strength of the perturbations exerted by each of these resonances across the entire Main Belt. We have also highlighted which asteroid families are crossed by each resonance, and have a good chance to have been influenced by it throughout their lifetime.

Finally we selected two asteroid families that also had odd looking shapes in the proper elements space, those of (1521) Seinajoki and (1128) Astrid, and we have verified that the action of the $s - s_c$ secular resonance can indeed be the protagonist of their evolution through history.

New asteroid families: Discoveries and dynamical properties

In this chapter we will present our results concerning the discovery of two new asteroid families, each with its own characteristics. The first case, as we will detail in the following concerns an asteroid family hidden in plain sight. The second case concerns a small cluster of asteroids simply well hidden, a “needle in the haystack” case.

3.1 The (326)Tamara asteroid family

One of the most interesting regions of the Main Belt is its innermost part, referred to as the “inner belt”. It spans a range in semi-major axis from 2 to 2.5 AU i.e. from the ν_6 secular resonance to the 3/1 MMR with Jupiter. What makes this region particularly important is the complexity of the dynamical environment it resides in. First and foremost the resonances that bound it themselves are known to be important transport routes of asteroids from the main belt to the near-Earth region and are consequently linked to the delivery of meteorites on Earth (Bottke et al., 2015; Granvik et al., 2017). On top of that, the fact that this region is the closest to the terrestrial planets means that perturbations of the latter on the orbits of asteroids therein are substantial, adding even more complexity to their dynamical evolution.

The shape of the ν_6 secular resonance separates the high inclination asteroids of the inner belt, forming what is known as the Phocaea region. That region is also surrounded by various other resonances, effectively isolating it from the rest of the main belt (Knežević and Milani, 2003; Michtchenko et al., 2010). Most of the Phocaeas are classified as *S*-type asteroids (Carvano et al., 2001), typical for large objects that formed in the inner asteroid belt. But the fraction of *C*-type asteroids increases for smaller sized asteroids. Indeed, DeMeo and Carry (2014) showed that the relative mass contribution of each taxonomic class is a function of size in each

part of the asteroid belt. This increase of *C*-type objects at small sizes in the inner belt is the outcome of the collisional evolution and asteroid family formation taken place therein, which in turn is important to understanding the history and evolution of the belt, as well as the delivery of asteroids to the near-Earth region.

A large fraction of asteroids from the Phocaea region belong to the Phocaea collisional family (e.g. Milani et al., 2014), estimated to be about 1.2 Byr old (Milani et al., 2016). The possible existence of other families inside this region has been discussed by several authors (Carruba, 2009; Gil-Hutton, 2006; Masiero et al., 2013; Novaković et al., 2011) who proposed several candidate groups which might be collisional families. We have discovered yet another collisional family therein, with the difference that this one is the first to be the outcome of the breakup of a dark carbonaceous parent asteroid.

3.1.1 Dark Phocaea asteroids: identification and search for a family

There are currently more than 4000 asteroids in the Phocaea region¹. Using physical data obtained by the Wide-field Infrared Survey Explorer (WISE; Masiero et al., 2011), we found that $\sim 73\%$ of the asteroids there are bright ones with albedos higher than 0.1, as expected for a part of the inner belt.

However, the albedo distribution shows a clear separation between dark and bright asteroids (Figure 3.1). It is roughly the sum of two separated Gaussians, and the spreading of the low albedo part is narrower than what we usually observe across the asteroid belt. This suggests the possible existence of a dark asteroid family generating this part of the distribution.

The number density of the dark asteroids in the region is far lower than the total number density, making the possible dark family totally indistinguishable if one looks at the whole asteroid population. The only way to study this family is to consider solely dark asteroids.

¹Data obtained from the AstDyS service (hamilton.dm.unipi.it/astdys/).

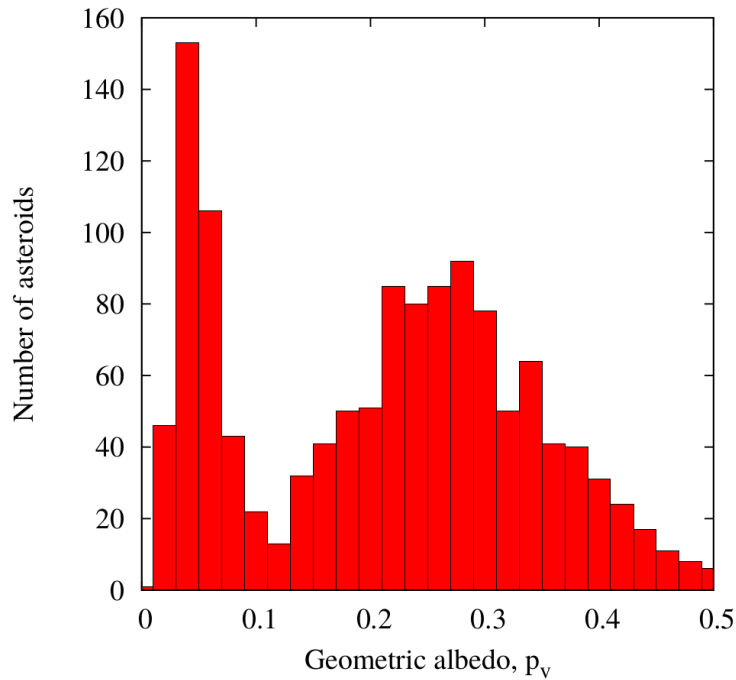


Fig. 3.1.: Geometric albedo distribution of asteroids in the Phocaea region.

The identification of dark asteroids

The next step in our study was to obtain a catalog of dark asteroids in the region. Following Walsh et al. (2013) we adopted to work with objects having geometric albedo p_v below 0.1. WISE data provide albedos for 1280 out of the 4072 asteroids in the region, and of those 1280 we found 348 dark ones. In an effort to expand this catalog we selected in a similar manner dark asteroids as identified by the AKARI (Usui et al., 2013), and the Infrared Astronomical Satellite (IRAS) (Tedesco et al., 2002) surveys, where we found 41 and 12 low-albedo asteroids respectively.

We also made use of the MOVIS catalog (Popescu et al., 2016), which uses VISTA colors in order to distinguish between C - and S -complex asteroids. According to Popescu et al. (2016) the $(Y-J)$ vs $(Y-K_s)$ color space provides the largest separation between the two complexes, the separatrix being the line $(Y - J) = 0.338^{\pm 0.027} \cdot (Y - K_s) + 0.075^{\pm 0.02}$. Therefore we considered as C -type those asteroids whose entire $1-\sigma$ error bar lies below this line. This way we obtained 8 dark asteroids.

Finally we extracted dark asteroids as characterized by Carvano et al. (2010) using the Sloan Digital Sky Survey data (Ivezić et al., 2001). There are 76 objects classified

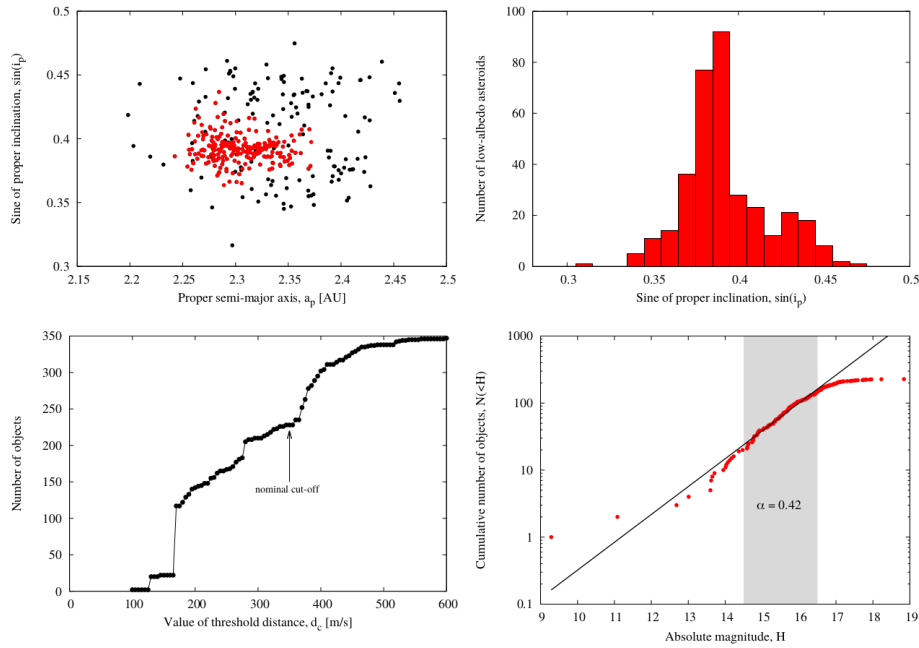


Fig. 3.2.: Properties of low-albedo asteroids in the Phocaea region. *Top-left panel:* Proper semi-major axis versus sine of proper inclination projection of the dark asteroids in the Phocaea region (black dots), and Tamara family members (red dots); *Top-right panel:* Histogram of orbital inclinations of dark Phocaeas; *Bottom-left panel:* Number of asteroids associated with the family as a function of distance threshold; *Bottom-right panel:* The cumulative magnitude distribution of the Tamara family (red dots), and its the best-fitting line (black solid line). The dashed area indicates the interval used for the fitting.

as either *C*- or *D*-type, but for the purpose of this work we used only 16 asteroids which have $> 50\%$ probability to belong to the specified taxonomic type.

In this way we identified 381 dark objects, and after removing 5 asteroids with contradictory albedos², we obtained the catalog of dark Phocaeas containing 376 objects.

The dark component of this population has a non-uniform number density in the proper elements space (Figure 3.2), suggesting the presence of an asteroid family.

²Some objects have albedo determined from two different surveys but the results are inconsistent. In our sample these are asteroids: 587, 2105, 4899, 8356, and 74749.

The search for a family

To the catalog of dark objects we used the Hierarchical Clustering Method, in order to obtain the membership of the new family. Being potentially the largest member of the family, we selected the asteroid (326) Tamara as the starting body, and increased the distance threshold from 100 to 600 m/s in steps of 5 m/s. The distance thresholds are overall higher than what we usually encounter in similar studies, but the fact that we use only dark asteroids whose number-density is low in this region justifies these values.³

The result is shown in the bottom-left panel of Figure 3.2. The family membership is defined at the distance threshold of 350 m/s, because this value belongs to the well defined *plateau* visible in Figure 3.2 (see e.g. Novaković et al., 2011, for details on this methodology). The nominal distance threshold corresponds to 226 members, that is about 60% of all dark asteroids found in the region. This membership includes asteroid (326) Tamara, as the largest family member, therefore we named this group the Tamara family.

3.1.2 Dynamical and physical properties

Size and escape velocity of the parent body

The size of the parent body of an asteroid family under study is an important property as it enables us, by calculating the escape velocity from it, to constrain the initial ejection velocity field (Sachse et al., 2015).

A simple way to estimate the size of the parent body is to sum up the diameters of the largest and the third largest family members Tanga et al. (1999). In this case these are the asteroids (326) Tamara and (1942) Jablunka, with diameters of 89.4 and 16.7 km, respectively. This gives a diameter for the parent body of 106.1 km. Consequently, the largest remnant contains about 60% of the total mass of the family, indicating that the Tamara family was formed in a typical catastrophic

³Nesvorný et al. (2015) used 150 m/s to determine the membership of the Phocaea family within the whole population of Phocaeas. As known dark asteroids account for about 9% of all Phocaeas (376/4072), but occupy almost the same volume in the orbital space, therefore a reasonable value to define the dark family should be about $\sqrt{9}$ times larger than the one used for the Phocaea family. This is why we select 350 m/s as the nominal threshold, rather than a value from the first plateau seen around 250 m/s.

collision. Assuming a density of 1300 km m^{-3} , typical for *C*-type asteroids (Carry, 2012), the escape velocity from the parent body was calculated to be 45 m/s.

The cumulative distribution of the absolute magnitudes

Another important characteristic of the family that we derived is the cumulative magnitude frequency distribution (CMFD), that should follow a power law in the form $N(< H) \approx 10^{\alpha H}$. The value of the slope parameter α can be estimated by numerically fitting the CMFD of the family members, in a specific range of absolute magnitudes.

Here we performed this fitting in the magnitude range 14.5 – 16.5, and we found the value of the exponent α to be 0.42 ± 0.02 , as illustrated in the bottom-right panel of Figure 3.2. The relatively shallow slope suggests that the Tamara family is probably not a young one, since young families are typically characterized by somewhat steeper slopes (Vokrouhlický et al., 2006b).

It is interesting to compare the slope of the family to that of the all Phocaeas, to estimate how large is the fraction of the Tamara family members among small Phocaeas. To this purpose, we derived the slope of the CMFD of all Phocaeas in the same magnitude range as for the Tamara family, i.e. 14.5 – 16.5, and we obtained a value of 0.28 ± 0.01 for the slope. This is significantly shallower than the one derived for the Tamara family. However, this does not seem to be unexpected, as the population of Phocaeas is dominated by the very old Phocaea collisional family.

Finally, assuming that the derived slopes of the CMFD are also valid for magnitudes larger than those used to compute them, from the corresponding slopes we computed the number of all Phocaeas and of Tamara family members in the 17 – 20 magnitude range, to be about 24,500 and 4200 objects respectively. Therefore, in the considered magnitude range about 17% of all Phocaeas should be members of the Tamara family. The fraction of family members is even larger for magnitudes $H > 20$, meaning that among the small Phocaeas there may be as many dark asteroids as bright ones.

Age of the family

In order to get an estimate of the age of the new family, we used the “V-shape” method, based on the size-dependent secular drift in semi-major axis, induced by the Yarkovsky effect. Moreover, the existence of such a structure, could be used to verify the collisional origin of the group (Walsh et al., 2013).

From the available physical data we computed the mean albedo for family members to be: $\bar{p}_v = 0.059 \pm 0.016$. Using this value we can convert absolute magnitudes to diameters⁴ and plot the semi-major axis versus the inverse of the diameter ($a_p, 1/D$), as shown in Figure 3.3. The V-shape structure is clearly visible, providing additional proof that this is a real collisional family.

In order to estimate the age of the Tamara family we employed a method very similar to the one proposed by Spoto et al. (2015). First we divided the family into left (inner) and right (outer) side with respect to the barycenter. Then we divided the $1/D$ -axis in intervals containing equal numbers of asteroids, and identified the objects with the minimum/maximum value of a_p for each interval on the left/right side.

This data was used to perform a two-step fitting procedure to determine the slopes of the distribution of the family members in the $(a_p, 1/D)$ plane. We fit the lines through these furthest objects on both sides in the $(a_p, 1/D)$ plane. Then the objects located more than 0.045 below the lines (in $1/D$) were removed from the calculation as outliers. Additionally, on the left (inner) side we also removed a single object with $a_p < 2.25$, because its semi-major axis may be affected by the 7/2 resonance with Jupiter. After removing these objects, we again fit the members with the minimum/maximum value of a_p for each interval and obtained the slopes of the V-shape (Figure 3.3).

The method of family age estimation based on V-shapes requires a Yarkovsky calibration, that is the maximum value of the Yarkovsky driven secular drift $(da/dt)_{max}$ for a hypothetical family member of diameter $D = 1$ km (Milani et al., 2014). The value of $(da/dt)_{max}$ is determined using a model of the Yarkovsky effect and assuming thermal parameters appropriate for regolith-covered C -type objects (Vokrouhlický

⁴Note that we estimated diameters in this way only for the members for which direct estimation is not available. This is because the infra-red surveys measure emitted flux, that is then used to derive the diameters. As a result, the obtained diameters are more reliable than the albedos (Mainzer et al., 2011).

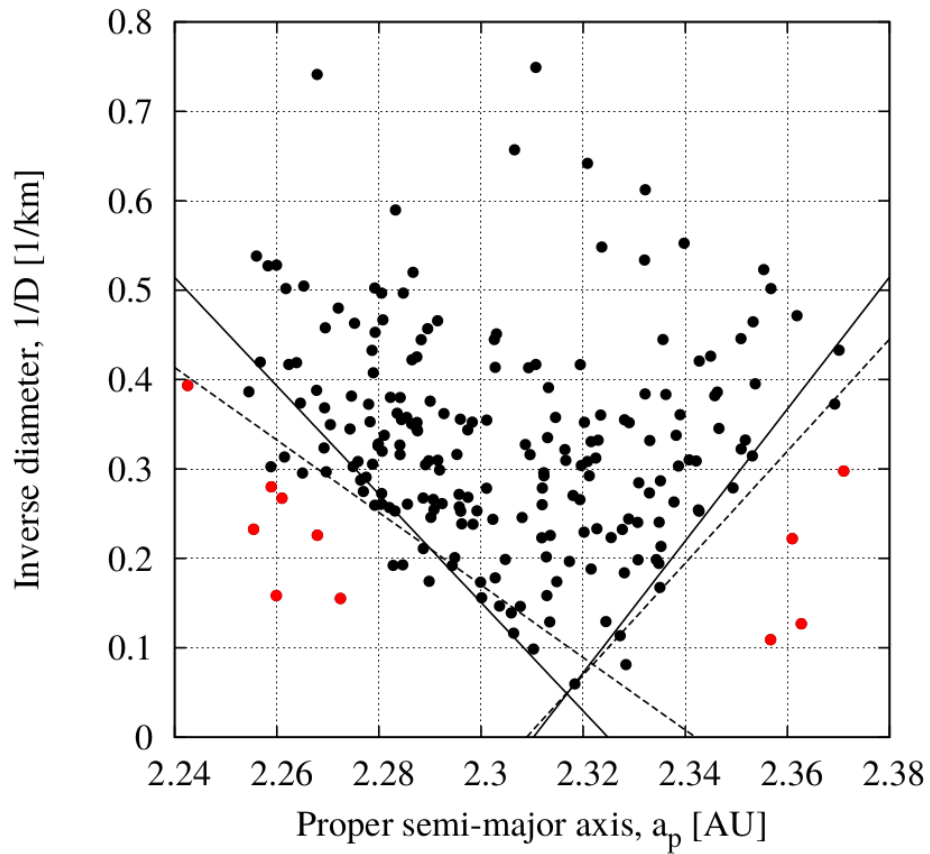


Fig. 3.3.: Proper semi-major axis versus the inverse diameter for the members of the family. The dashed and solid lines correspond to the initial and final V-shape fit, respectively. Red dots mark the outliers removed from the fit after the first iteration.

et al., 2015). We adopted values of $\rho_s = \rho_b = 1300 \text{ kg m}^{-3}$ for the surface and bulk densities (Carry, 2012), $\Gamma = 250 \text{ J m}^{-2} \text{ s}^{-1/2} \text{ K}^{-1}$ for the surface thermal inertia (Delbo' and Tanga, 2009), and $\epsilon = 0.95$ for the thermal emissivity parameter. With the above described parameters we estimated that for a body of $D = 1 \text{ km}$ the maximum drift speed $(da/dt)_{max}$ is about $5.3 \times 10^{-4} \text{ AU/Myr}$.

Finally, using the inverse slopes and the adopted Yarkovsky calibration we estimated the age of the family to be $264 \pm 43 \text{ Myr}$.

3.1.3 Dynamical evolution of the Tamara family

Asteroids undergo the effects of numerous gravitational and non-gravitational perturbations, leading to constant modifications of their orbits (e.g. Nesvorný et al., 2015). Thus asteroid families are also evolving in time, being gradually dispersed from their initial distribution by the action of mean motion or secular resonances (Carruba et al., 2016b; Novaković, 2010; Novaković et al., 2015), close encounters with planets or massive asteroids (Carruba et al., 2003; Novaković et al., 2010) and the Yarkovsky effect (Bottke et al., 2001; Vokrouhlický et al., 2015). Thus, it is of great importance to reconstruct the dynamical evolution of the family, as this may help for example to set additional constrains about its age, or to evaluate the possible leakage from the family towards the near-Earth region.

Dynamical model and initial conditions

To simulate the dynamical evolution of the Tamara family we performed a set of numerical integrations, using the *ORBIT9* integrator. The dynamical model used includes the gravitational effects of the Sun and seven major planets, from Venus to Neptune, and also accounts for the Yarkovsky effect, modeled as a pure along-track acceleration, inducing on average the same semi-major axis drift speed da/dt as predicted by the theory.

Since the Yarkovsky effect scales as $\propto 1/D$, the particle sizes are used to calculate the corresponding value of (da/dt) for each particle, by scaling from the reference value derived for a $D = 1 \text{ km}$ object (see Section 3.1.2). Assuming an isotropic distribution of spin axes in space, to each particle we randomly assign a value from the $\pm(da/dt)$ interval.

To obtain the sizes of the test particles, we first assign them absolute magnitude values which follow a CMFD with the same slope as that of the real family, found in Section 3.1.2, and then convert them to diameters.

Our simulations follow the long-term orbital evolution of test particles initially distributed randomly inside an ellipse determined by the Gauss equations. This ellipse corresponds to the dispersion of the Tamara family members immediately after the breakup event, assuming an isotropic ejection of the fragments from the parent body.

The dynamical evolution: outcome of numerical simulations

The dynamical evolution of the family in the proper elements space was simulated over 350 Myr, which is longer than the estimated age of the family. The results obtained after 250 – 300 Myr of evolution very nearly matched the current spreading of the family in the space of proper orbital elements, and only the low-inclination part of the family was not fully reproduced.

Being located at the inner edge of the main asteroid belt, the Tamara family could potentially be an important source of low-albedo near-Earth objects (NEOs). Since the current members of the family, being large enough, are still far from the resonances capable of transporting asteroids close to Earth, such as the ν_6 only smaller members which drift faster could have already contributed to the NEOs flux. Therefore, we focus here on objects with $17 < H < 19.35$ mag.

The flux towards the NEOs region

In order to estimate the number of NEOs originating from the family, we analyzed the outputs of the integrations, looking for those particles that at some point over the covered time span, reached perihelion distances below 1.3 AU. We determined the total number of objects reaching the near-Earth region as a function of time, as well as the number of members settled in the NEOs space at any specific point in time.

The results are shown in Fig. 3.5. In this figure the bold line shows the cumulative number of particles reaching perihelion distances $q < 1.3$ AU. It seems that the first

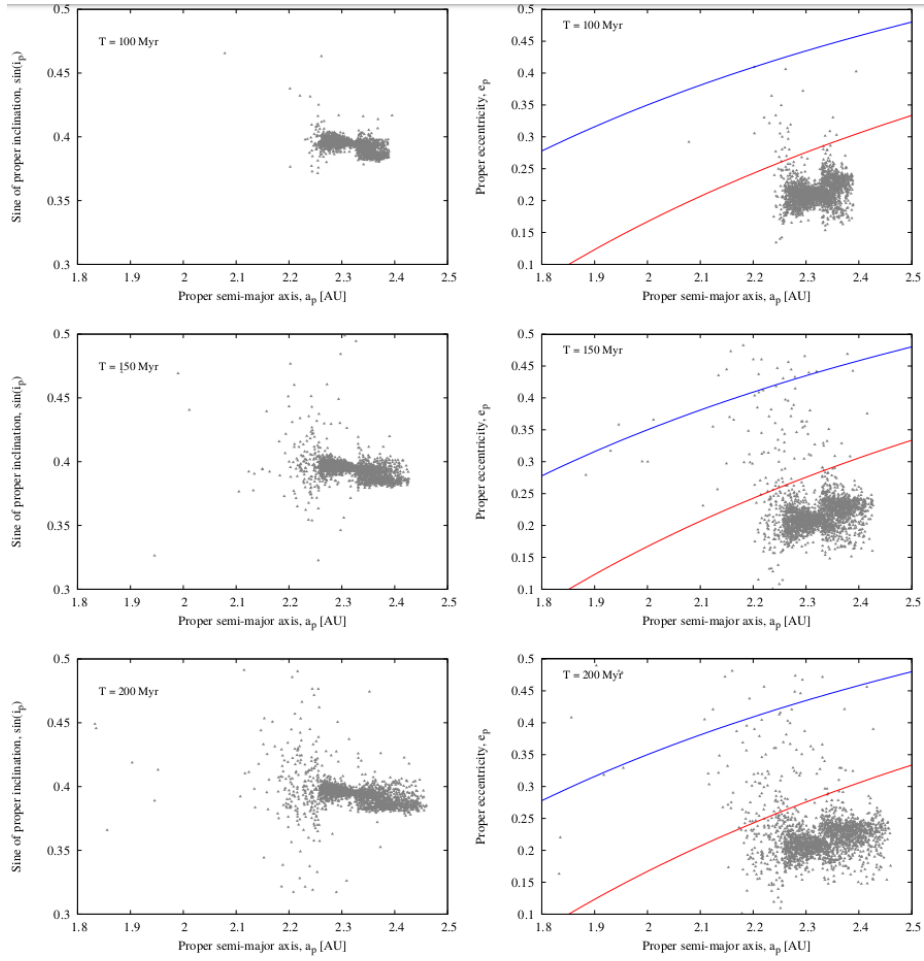


Fig. 3.4.: The evolution of the Tamara family in the space of proper orbital elements. The four panels in each column show the distribution of the test particles after 50, 100, 150 and 200 Myr (from top to bottom) of evolution. The red and blue lines mark perihelion distances q of 1.666, 1.3 AU, respectively.

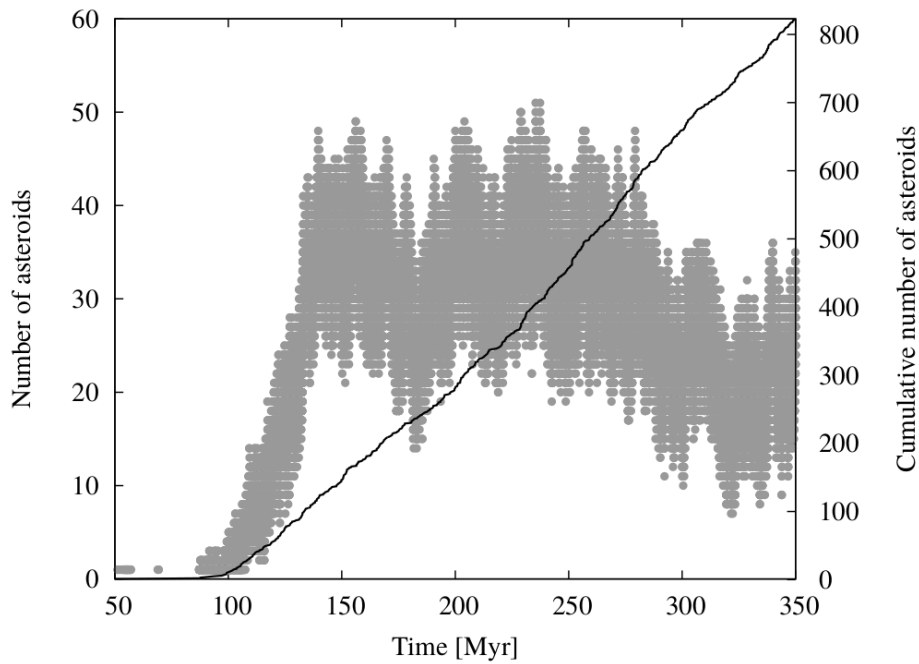


Fig. 3.5.: The Tamara asteroid family as a source of NEOs. The cumulative number of test particles entering the near-Earth region (bold curve), and the total number of members residing in the near-Earth region at any specific point in time (gray dots).

family members became NEOs about 100 Myr after the family formation event, with about 800 objects in total reaching this area during the subsequent 250 Myr of the simulation. Therefore, the cumulative number is increasing almost linearly with time, suggesting that the flux from the family is about 3 objects per Myr. Given the estimated age of the Tamara family of 264 Myr, about 500 of its members with $17 < H < 19.35$ should have reached NEOs space up to present time.

In Fig. 3.5 the gray points represent the number of the Tamara family members residing in the near-Earth region at any specific point in time. This result suggests that up to 50 objects from the family may be found in the region of terrestrial planets. Focusing on the time interval between 221 and 307 Myr of the evolution (lower and upper limit of the age of the family), we found that currently there should be 31 ± 6 family members in the NEOs space.

It is interesting to compare this number with the recent model of NEOs population by Granvik et al. (2016) where it was found that in the magnitude range we considered here, there should be about 250 Phocaeas residing in the NEOs space. Hence, about 12.5 to 20% of all NEOs coming from the Phocaea region should originate in the

newly discovered family and be dark ones. Having a somewhat steeper slope of the cumulative magnitude distribution than the rest of the Phocaeas, the contribution of the Tamara family is likely even a bit larger for smaller objects.

3.1.4 Summary

Analyzing the dark asteroid portion of the asteroids in the Phocaea region, we have discovered a new asteroid family, which is the outcome of the breakup of a ~ 100 km dark parent asteroid.

We have determined the slope of the cumulative magnitude distribution of the family, and compared it with the corresponding slope for all asteroids in the Phocaea region. This brought us to the conclusion that for sub-kilometer Phocaeas, the number of dark *C*-type asteroids is comparable to the number of bright *S*-type objects. This means that the well established view that this region's population is almost entirely composed of rocky asteroids, does not hold for small sized asteroids.

Furthermore, based on the standard V-shape method we estimated this family to be 264 ± 43 Myr old.

Finally, extensive numerical simulations were carried out allowing us to estimate that 31 ± 6 family members with $H \in [17, 19.35]$, should currently reside in the NEOs space.

3.2 The (633) Zelima cluster

3.2.1 Introduction

Asteroid families evolve over time due to various phenomena such as chaotic evolution of their orbits (Milani and Farinella, 1994; Nesvorný et al., 2002a), the semi-major drift induced by the Yarkovsky effect (Farinella and Vokrouhlický, 1999; Vokrouhlický et al., 2006b), further collisional evolution (Dell'Oro et al., 2002; Marzari et al., 1999), close encounters (Carruba et al., 2003; Novaković et al., 2010) and secular resonances with massive asteroids (Novaković et al., 2015; Tsirvoulis and Novaković, 2016b), the older a family is, the less likely it is for us to reconstruct its collisional birth. Therefore, young asteroid families which have not evolved

significantly allow us to extract information on the physical processes of colliding asteroids in a more direct manner.

Several such young asteroid families and small clusters have been identified over the past several years (Nesvorný and Vokrouhlický, 2006; Nesvorný et al., 2003, 2006; Novaković, 2010; Novaković et al., 2012b, 2014; Pravec and Vokrouhlický, 2009; Pravec et al., 2018; Vokrouhlický and Nesvorný, 2011). Of particular interest are the cases concerning young clusters that are sub-families of known large, old asteroid families, such as the (832) Karin cluster, a sub-family of (158) Koronis (Nesvorný et al., 2002b), and (656) Beagle, a sub-family of (24) Themis (Nesvorný et al., 2008). The existence of such young sub-families can help constrain the timescale of the evolution of the parent, large family due to collisional disruptions, and in consequence of the whole Main Belt. Another important aspect of young sub-families is the fact that their members have suffered less alterations of their surfaces due to space weathering effects (Vernazza et al., 2009) compared to the members of the original family (Fornasier et al., 2016). This can be of great importance in the study of both the physical processes of space weathering themselves, and of the physical properties of the parent family via the freshly exposed material.

We have discovered a new example of a very old large family having a sub-family of much younger age. The asteroid family of (221) Eos has been estimated to be about 1.5 *Gyrs* old (Brož and Morbidelli, 2013; Milani et al., 2017; Spoto et al., 2015; Vokrouhlický et al., 2006a), and among its family members we found a young cluster of asteroids only a few million years old. The parent body of the (221) Eos family is believed to have been partially differentiated (Mothé-Diniz and Carvano, 2005), so the discovery of this young cluster might be of great interest. The cluster members, which should be similar compositionally as they originate from a single fragment of the original disruption, could provide a fresh view of the interior of the Eos parent body.

3.2.2 Identification of the new family

Discovering intentionally a very small young family within one of the densest regions of the Main Belt, as is the region covered by the Eos family, is a very challenging undertaking, with few chances of success. One has to scrutinize every corner of the three dimensional region in question for any abnormalities in the distribution of asteroids, and then judge whether there is any statistically significant group that could be an actual asteroid family, originating from the disruption of a single

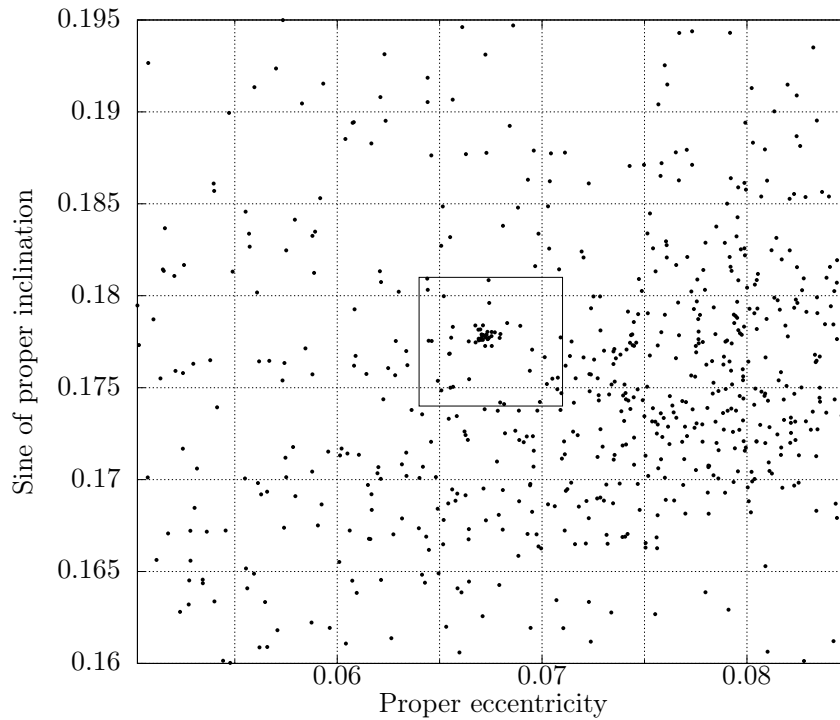


Fig. 3.6.: Distribution of asteroids in the $(e_p, \sin i_p)$ orbital planes, at a sub-region of the Eos family. There is an apparent over-density of asteroids (highlighted with the box), hinting the existence of a young cluster.

parent body. Much of this intense labor is eliminated though when the factor of luck manifests; certainly not a rare occasion in science, with the current work also being a beneficiary. As long as the statistical tests hold, nature does not care if we make discoveries by systematic search or by chance.

When looking at the distribution of asteroids in the proper elements space in a small region within the Eos asteroid family, a clustering of a small number of asteroids is apparent, especially in the proper eccentricity versus the sine of proper inclination projection $(e_p, \sin i_p)$, as seen in Figure 3.6.

In order to identify the members of this new family, the hierarchical clustering method (HCM) was used. From the catalog of synthetic proper elements (Knežević

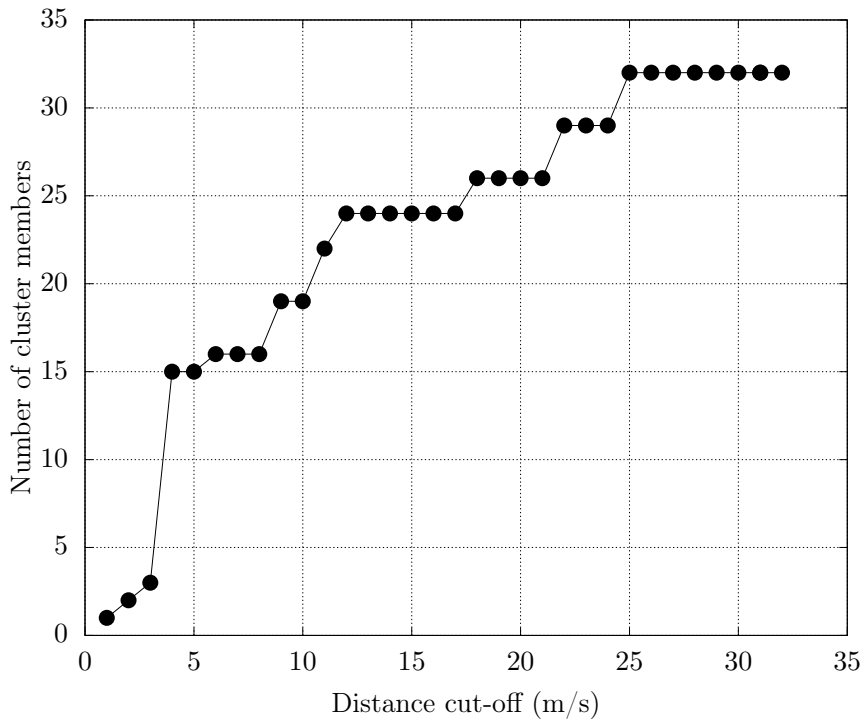


Fig. 3.7.: The number of asteroids associated to the (633) Zelima cluster as a function of the distance threshold.

and Milani, 2000, 2003) obtained from the AstDyS service⁵, all asteroids within the ranges:

$$2.96 < a_p < 3.15 \text{ AU},$$

$$0.02 < e_p < 0.13,$$

$$0.15 < \sin i_p < 0.21$$

i.e. in the region around the (221) Eos family, were extracted and used as the initial set. The choice of the starting body is not significant in this case, as long as an asteroid close to the center of the cluster is selected. Due to the apparently tight clustering of asteroids in the small family studied here, very small values of the starting distance threshold as well as the increasing step of 1 m s^{-1} was chosen. The result of this process is shown in Figure 3.7; for threshold greater than 4 m s^{-1} , a value where the core of the cluster is linked together, the number of asteroids associated increases steadily with increasing distance threshold, until a relatively constant number of asteroids is reached for values between $12 - 17 \text{ m s}^{-1}$, followed by another increase and a second plateau at $25 - 32 \text{ m s}^{-1}$, after which point the entirety of the population in our catalog is linked together.

⁵available at: <http://hamilton.dm.unipi.it/astdys/index.php>, accessed in June 2017

The correlation of the number of asteroids with the distance threshold needs to be evaluated together with the shape of the growing cluster in the proper elements space to make a choice for the nominal membership which should represent the statistical properties of the cluster despite small deviations. In this case the nominal membership was adopted as the one derived at to 20 m s^{-1} , as at this value the membership corresponds exactly to the isolated cluster as appearing in the $(e_p, \sin i_p)$ plane. This yields a family membership of 26 asteroids, with the lowest numbered one being (633) Zelima.

Finding a number of asteroids that can be linked by HCM to a single cluster does not necessarily mean that this cluster corresponds to a real asteroid family, even more so when that group of asteroids is so small. A simple test of the statistical significance of the cluster is necessary to address this question. As this is a subfamily within the Eos family population, the first step was to extract from the proper elements catalog the members of the latter. Then 1000 fictitious clones of the entire Eos family were created by randomly distributing the same number of asteroids within the same orbital volume occupied by the family members.⁶ Then the fictitious populations were searched by HCM for any clusterings of 26 or more asteroids at a distance threshold of 20 m s^{-1} , with negative outcome. This leads to the conclusion that a clustering of asteroids with this number of members at such a tight configuration can not be the outcome of chance, but it has to be the outcome of a real collisional breakup. It is important to note that we have only proven the statistical significance of the cluster as a whole. The statistical nature of the HCM does not allow for any conclusions on whether any individual asteroid identified as a member has indeed originated from the breakup event that formed the cluster, or it is an interloper. We will present in the next section a method of identifying interlopers among the identified family members.

3.2.3 Age of the cluster

As we have shown, the Zelima cluster is very compact in the proper elements space, and the threshold distance needed to identify its members is very small.

⁵Obtained from the Asteroid Families Portal (AFP) at: <http://asteroids.matf.bg.ac.rs/fam/index.php>

⁶As the actual family does not uniformly fill the cubic volume within which it resides, if we selected the actual borders of the family for the box, the mean number density would be smaller than it actually is. To avoid this the dimensions of the box were selected smaller than the size of the family, to the values where the bulk of the Eos family is enclosed, but with the total number of asteroids preserved. This may give an increased mean number density compared to the correct one, but it only means that the statistical significance test is more strict

These suggest that the cluster itself is a young one, with an age of the order of a few million years. The age determination method which is most suitable for young asteroid families and clusters is the Backward Integration Method (BIM). This method has been used frequently in the past to determine the ages of various young families and clusters, such as the Karin cluster (Nesvorný et al., 2002b), Veritas family (Nesvorný et al., 2003), the Datura cluster (Nesvorný et al., 2006), Theobalda family (Novaković, 2010), the Lorre cluster (Novaković et al., 2012b), the Gibbs cluster (Novaković et al., 2014) and the Schulhof family (Vokrouhlický et al., 2016).

Another important benefit of the BIM is the identification of potential interlopers among the family members as found by HCM (see e.g. Novaković et al. (2012a)). Any particular asteroid that is included in the membership but does not really belong to the collisional family should in principle have a different formation time. As such, its orbital elements (the secular angles more specifically) should not converge with those of the true family members at the time of the cluster formation, which is the essence of the method we used for interloper identification for the Zelima cluster.

Orbital evolution of the cluster members

For the BIM to be reliable, the cluster must be relatively young (up to about 10 Myrs) and dynamically stable. Both of these conditions are satisfied by the Zelima cluster, due to the tight packing of its members in the proper elements space and their long Lyapunov times. The first step was to integrate backwards in time the orbits of the nominal members of the cluster for 10 Myrs, using a dynamical model which includes the four outer planets, from Jupiter to Neptune, using the Orbit9 integrator. To account for the indirect effect of the inner planets, their masses are added to the mass of the Sun and a barycentric correction is applied to the initial conditions. After retrieving the evolution of each member's orbital elements, we calculate the mean differences in their two secular angles, the longitude of the ascending node (Ω), and argument of perihelion (ω), over time-steps of 500 years, as shown in Figure 3.8. The results show convergence of both angles⁷ at about 3.5 Myrs in the past, within 35° for $\langle \Delta\Omega \rangle$ and within 55° for $\langle \Delta\omega \rangle$. Even though both secular angles seem to converge at a single point in the past relatively well, one would expect to have even stronger convergence, i.e. deeper minima. Although in the ideal case one

⁷The convergence is worse for $\langle \Delta\omega \rangle$ because the corresponding secular frequency at the region of the cluster ($\dot{\omega} = \dot{\varpi} - \dot{\Omega} = g - s \approx 145.5''yr^{-1}$) is larger than that for $\langle \Delta\Omega \rangle$ ($\dot{\Omega} = s \approx -71.5''yr^{-1}$), leading to the faster dispersion of the arguments of perihelion

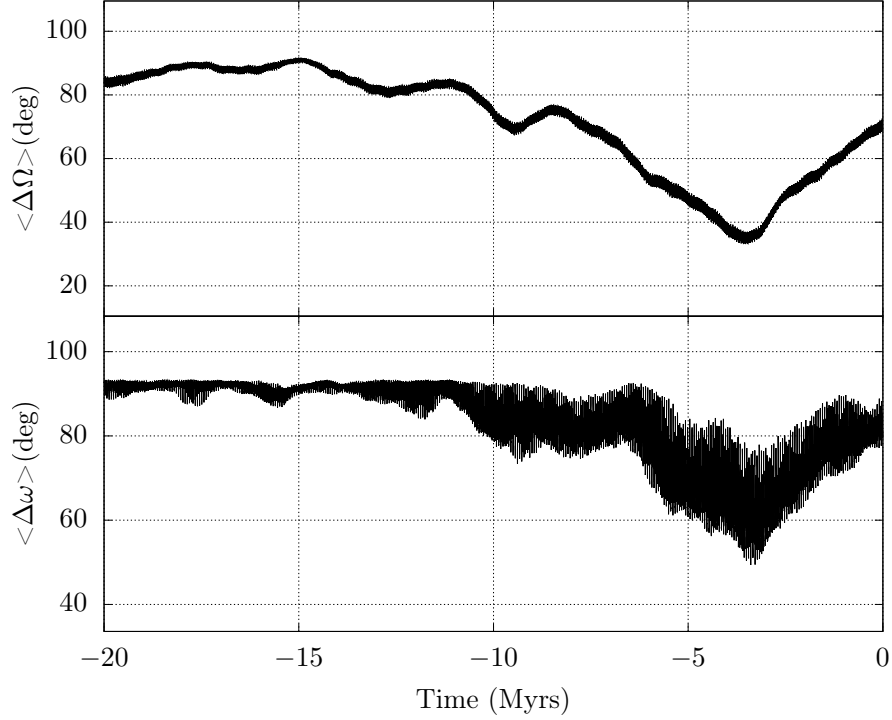


Fig. 3.8.: Evolution of the mean differences in the secular angles Ω (top) and ω (bottom) of the nominal Zelima cluster members.

might expect convergence to within one degree, assuming a typical initial dispersion of the fragments corresponding to an escape velocity of the order of 25 km s^{-1} , there are a number of reasons why this is not the case: i) Even though the orbits of most of the cluster members have long Lyapunov times, it is possible that they have spent a period in the past in more chaotic orbits, ii) the Yarkovsky effect, which is not included in the dynamical model, acting upon the members of the cluster, most of which are smaller than 5 km in diameter, can effectively change their semi-major axis even within such a short time, and consequently alter their secular frequencies as the gradients of the secular frequencies are relatively large in the region of the cluster ($ds/da \approx -70'' \text{ yr}^{-1} \text{ AU}^{-1}$, $d\omega/da = dg/da - ds/da \approx 200'' \text{ yr}^{-1} \text{ AU}^{-1}$). iii) The presence of potential interlopers worsens the convergence of the secular angles, as mentioned above, since any interloper essentially adds random terms to the sum of mutual differences in the secular angles when calculating the mean differences.

In order to identify potential interlopers and remove them from the family membership, we followed a simple yet effective method: Having the numerical integrations at hand we repeated 26 times the calculation of the mean differences in the secular angles at each time-step, each time excluding from the members list one asteroid, leaving only 25. We then compare the resulting plot to that of all 26 members

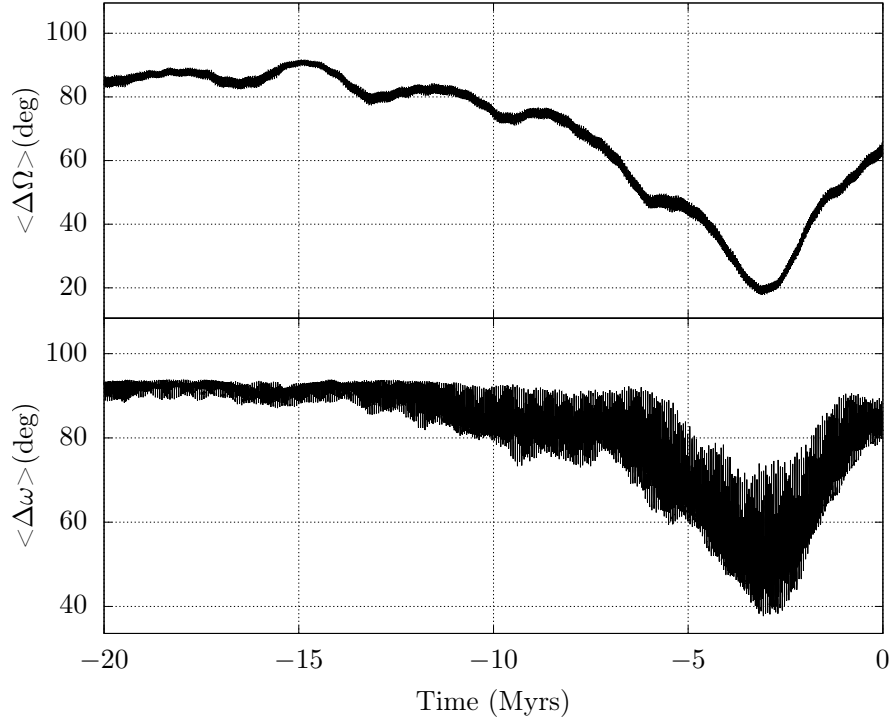


Fig. 3.9.: Evolution of the mean differences in the secular angles Ω (top) and ω (bottom) of the Zelima cluster members after the three identified interlopers have been removed.

(Figure 3.8), and we looked for any improvement in the convergence of the longitude of the ascending node (Ω), as it is much clearer to judge. In order to signify an asteroid as an interloper we demanded that both the mean difference and its standard deviation improve (decrease) by more than 5° at the time of convergence if that asteroid is excluded from the calculation. In this way we identified three interlopers, namely asteroids (1881), (25583) and (460267). The final result, that is the mean differences in the secular angles as a function of time of the 23 remaining family members, is shown in Figure 3.9 which features an improved convergence to within about 20° for $\langle \Delta\Omega \rangle$ and about 40° for $\langle \Delta\omega \rangle$, and at an earlier time, at about 3 Myrs in the past. Let us mention that for the 23 other asteroids there was no measurable improvement at all, of neither the mean difference nor the standard deviation, which means those are indeed real members, at least as far as this method suggests.

Orbital and Yarkovsky clones

The reliability of the BIM applied to the orbits of the nominal members of families or clusters suffers from two major sources of errors. The first one is the non-zero uncertainty in the orbital elements of their members, and the second is the secular evolution of their semi-major axis due to the Yarkovsky thermal force. To avoid the error in the estimated age introduced by those causes, we use a statistical implementation of the BIM, as originally proposed by Nesvorný and Vokrouhlický (2006). This method has also been used in the past to determine the ages of young clusters, such as the Schulhof family (Vokrouhlický and Nesvorný, 2011), the Lorre cluster (Novaković et al., 2012b) and the Gibbs cluster (Novaković et al., 2014).

This method uses a set of statistically equivalent orbital and Yarkovsky clones for each nominal member of the cluster. In detail, we generate 10 orbital clones for each member with orbital elements randomly chosen within the 3σ uncertainties of its nominal osculating orbital elements, assuming Gaussian distributions.

Next, in order to emulate the Yarkovsky thermal force (Vokrouhlický, 1998, 1999), for each orbital clone we calculate the maximum expected drift rate in semi-major axis according to its diameter, $(da/dt)_{max}(D)$: we first determine the maximum drift rate for a $D = 1km$ sized asteroid assuming the following physical parameters: bulk density $\rho = 2500kg\ m^{-3}$, surface density $\rho_s = 1500kg\ m^{-3}$, thermal conductivity $K = 0.001W\ m^{-1}K^{-1}$, specific thermal capacity $C = 680J\ kg^{-1}K^{-1}$, geometric albedo $p_v = 0.2$, infrared emissivity $\epsilon = 0.9$, i.e. all typical values for regolith covered basaltic asteroids (Brož and Morbidelli, 2013). The value obtained is: $(da/dt)_{max}(1km) = 3.4 \cdot 10^{-4}\ AU\ Myr^{-1}$. Then for an asteroid of diameter D we have $(da/dt)_{max}(D) = (da/dt)_{max}(1km)/D$, as the Yarkovsky effect scales inversely proportionally with the diameter. Finally for each orbital clone we generate 10 Yarkovsky clones, and to each we assign a drift rate randomly selected in the interval $\pm(da/dt)_{max}(D)$ to account for the possible orientations of the spin axis. In total, 100 statistically equivalent clones are generated for each of the 23 nominal members of the cluster, after the removal of interlopers. Next we integrate numerically the orbits of all clones backwards in time for 5 Myrs using the ORBIT9 integrator, using the same dynamical model as for the nominal members, i.e. containing only the four giant planets.

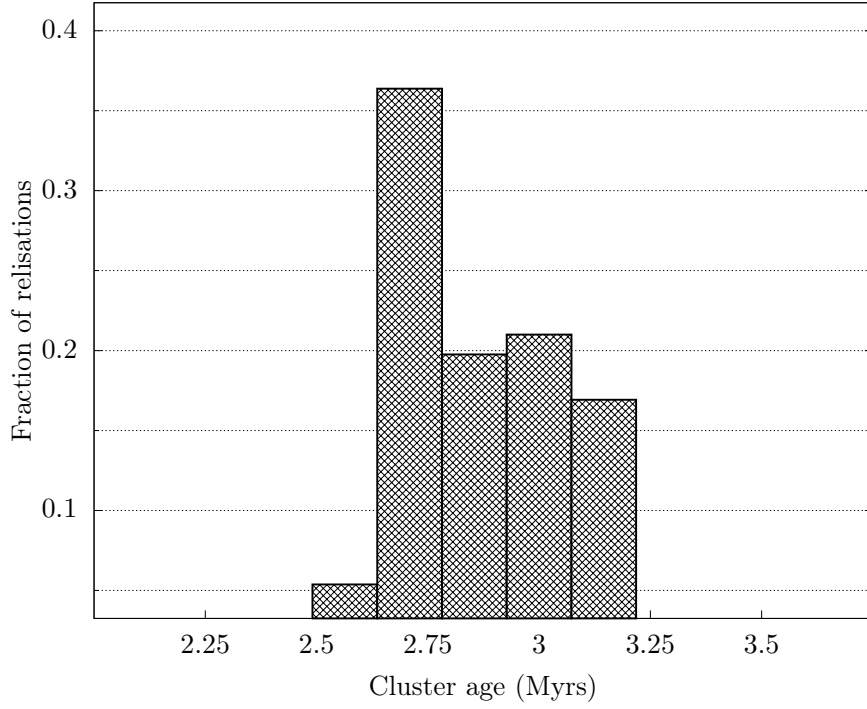


Fig. 3.10.: Histogram of the minima of the evaluated Equation 3.1, revealing the calculated age of the cluster.

Having obtained the evolution of each clone's orbital elements, we randomly select one clone for each member and determine the age as the minimum of the function:

$$\Delta V = na\sqrt{(\sin(i)\Delta\Omega)^2 + 0.5(e\Delta\omega)^2} \quad (3.1)$$

where $na = 17.14 \text{ km s}^{-1}$ is the mean orbital speed of the cluster members, $\Delta\Omega$ and $\Delta\omega$ are the dispersions in the longitude of the ascending node and argument of perihelion respectively, among the 23 clones (e.g.: $(\Delta\Omega)^2 = (\sum_{ij}(\delta\Omega)^2)/N_{pairs}$). We calculate the minimum of this function for $3 \cdot 10^6$ random combinations of clones, which is a sufficiently large statistical sample. In all cases the minimum of the function was less than 3 m s^{-1} with an average value of 2 m s^{-1} , which indicates good convergence for all the combinations, bearing in mind that the convergence criterion proposed by Vokrouhlický and Nesvorný (2011) is $\Delta V_{min} < 5 \text{ m s}^{-1}$. Figure 3.10 shows the distribution of the minima of this function, and the resulting age of the cluster was derived to be $2.9 \pm 0.2 \text{ Myrs}$.

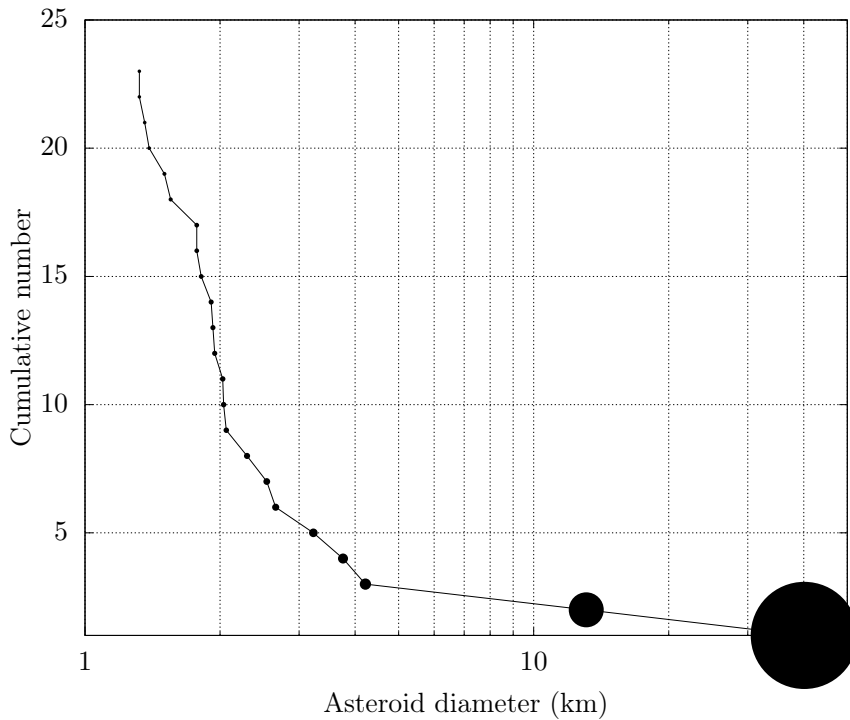


Fig. 3.11.: The cumulative size-frequency distribution of the (633) Zelima cluster members. The sizes of the points are proportional to the diameters of the corresponding asteroids.

3.2.4 Dynamical and physical properties

We will now present some important properties of the (633) Zelima cluster and its dynamical environment. In Table 3.1 we present the final list of the family members after the three interlopers have been removed. WISE (Masiero et al., 2011) provides diameters and albedos for the four largest cluster members. For the rest of the asteroids we calculated their diameter from their absolute magnitudes, assuming a geometric albedo of $p_v = 0.2$. Figure 3.11 shows the cumulative size-frequency distribution of the family members. We notice that apart from a single asteroid, namely (6733), the largest remnant of the collision is more than one order of magnitude larger than all of the other asteroids, and that the distribution of the latter is rather steep. This suggests that the collision that formed the cluster was a cratering event. We estimated the size of the parent body, assuming it had a spherical shape, by summing up the volumes of all known fragments into a single object. This yielded a diameter for the parent body of $D_{pb} \approx 40.66km$. The ratio of the sizes of the largest remnant, (633) Zelima, to that of the parent body turns out to be greater than 0.98.

In Figure 3.12 we show the distribution of family members in the three projections of the proper elements space, with the size of the points being proportional to the diameter of the corresponding asteroid. The patterned points are the three asteroids we excluded from the membership as interlopers and are shown only for reference.

The first thing we notice is the asymmetrical distribution of the small members with respect to the largest one, which also approximates the location of the barycenter of the family. Indeed as seen clearly in the bottom two panels, all the smaller asteroids have higher inclinations and than (633) Zelima, and almost all of them have lower eccentricities than it as well. The ellipses in these two panels are derived from the Gaussian equations and represent the outcome of an isotropic ejection resulting in a $\Delta v = 12 \text{ms}^{-1}$ velocity difference from the barycenter. This is not an unexpected outcome, since cratering collisions can in many cases produce a jet of fragments from the parent body (see e.g. Housen and Holsapple (2011)).

We also notice that four asteroids are separated from the rest of the cluster in semi-major axes, toward slightly lower values. It turns out that these asteroids have chaotic orbits as a result of their interaction with the 8-3-3 three-body mean motion resonance with Jupiter and Saturn, a fact that is also reflected by their higher Lyapunov exponents as shown in Table 3.1.

The region of the (221) Eos family, is also crossed by the z_1 secular resonance, which has been shown (Vokrouhlický et al., 2006a) to have a significant impact on the orbits of small asteroids, especially in conjunction with the Yarkovsky effect. Having propagated the orbits of the members of the Zelima cluster for the needs of the BIM as mentioned above, we were able to verify that the whole Zelima cluster was born inside this resonance. Constructing the critical argument of the resonance for each asteroid ($\sigma_{z_1} = \Omega + \varpi - \Omega_6 - \varpi_6$) as a function of time, we observed large amplitude librations with a period of about 4 Myr. The effect of the resonance on the orbits of family members is the induction of oscillations in their eccentricities and inclinations with amplitudes of the order of 0.005 and 0.12 degrees respectively. An illustrative example can be seen in Figure 3.13, where we show the evolution of the critical argument, the mean inclination and mean eccentricity of asteroid (633).

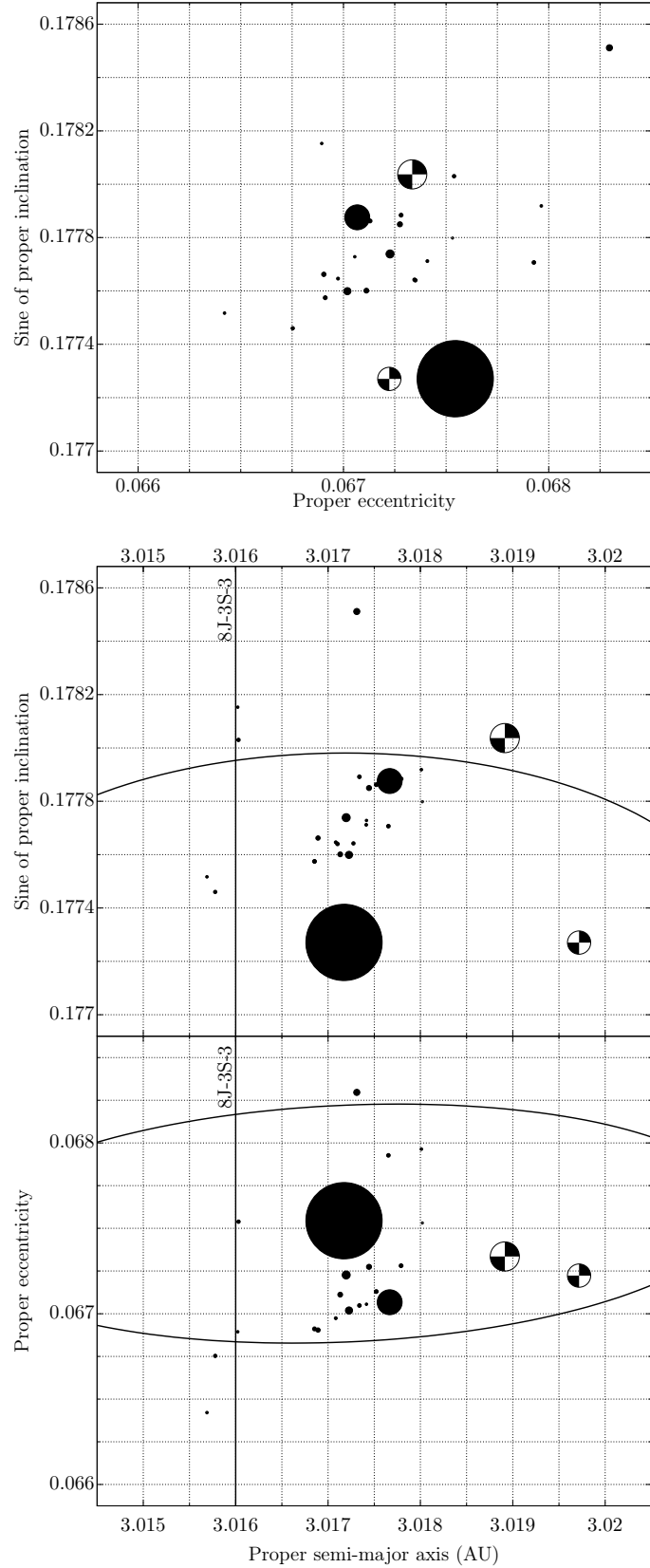


Fig. 3.12.: Distribution the Zelima cluster members in the $(e_p, \sin i_p)$ (top), $(a_p, \sin i_p)$ (middle) and (a_p, e_p) (bottom) orbital planes. The sizes of the points are proportional to the diameter of each asteroid. The patterned points indicate the identified interlopers. The ellipses in the bottom two panels represent equivelocity curves corresponding to a velocity change of $\Delta v = 12m s^{-1}$ from the barycenter of the cluster. The vertical lines show the approximate location of the 8J-3S-3 mean motion resonance (see e.g. Gallardo (2014)).

Tab. 3.1.: Members of the (633) Zelima cluster, and their physical properties⁸

<i>Asteroid</i> ^a	<i>H</i> ^b	<i>D</i> ^c	<i>LCE</i> ^d
633	9.79	40.15(w)	1.54
6733	11.81	13.05(w)	1.45
89714	14.22	4.22(w)	1.16
119786	14.76	3.76(w)	1.55
149046	14.82	3.22	0.40
230472	15.56	2.30	2.32
250011	15.34	2.54	0.87
292616	15.24	2.66	1.24
298735	15.82	2.04	1.46
299846	16.12	1.77	34.47
324175	15.92	1.95	1.27
364004	15.83	2.03	1.50
368472	15.79	2.07	1.98
372029	15.94	1.93	1.69
402372	15.96	1.91	1.49
411116	16.70	1.36	16.92
412371	16.12	1.77	1.76
421572	16.07	1.82	41.79
443574	16.65	1.39	1.03
449004	16.76	1.32	1.40
456020	16.48	1.50	1.49
475448	16.76	1.32	44.40
487314	16.41	1.55	1.12

^a Asteroid number

^b Absolute magnitude

^c Diameter in km (available WISE diameters (Masiero et al., 2011) are marked with (w), otherwise they are calculated from the absolute magnitude assuming a geometric albedo of $p_v = 0.2$)

^d Lyapunov characteristic exponent in $Myrs^{-1}$

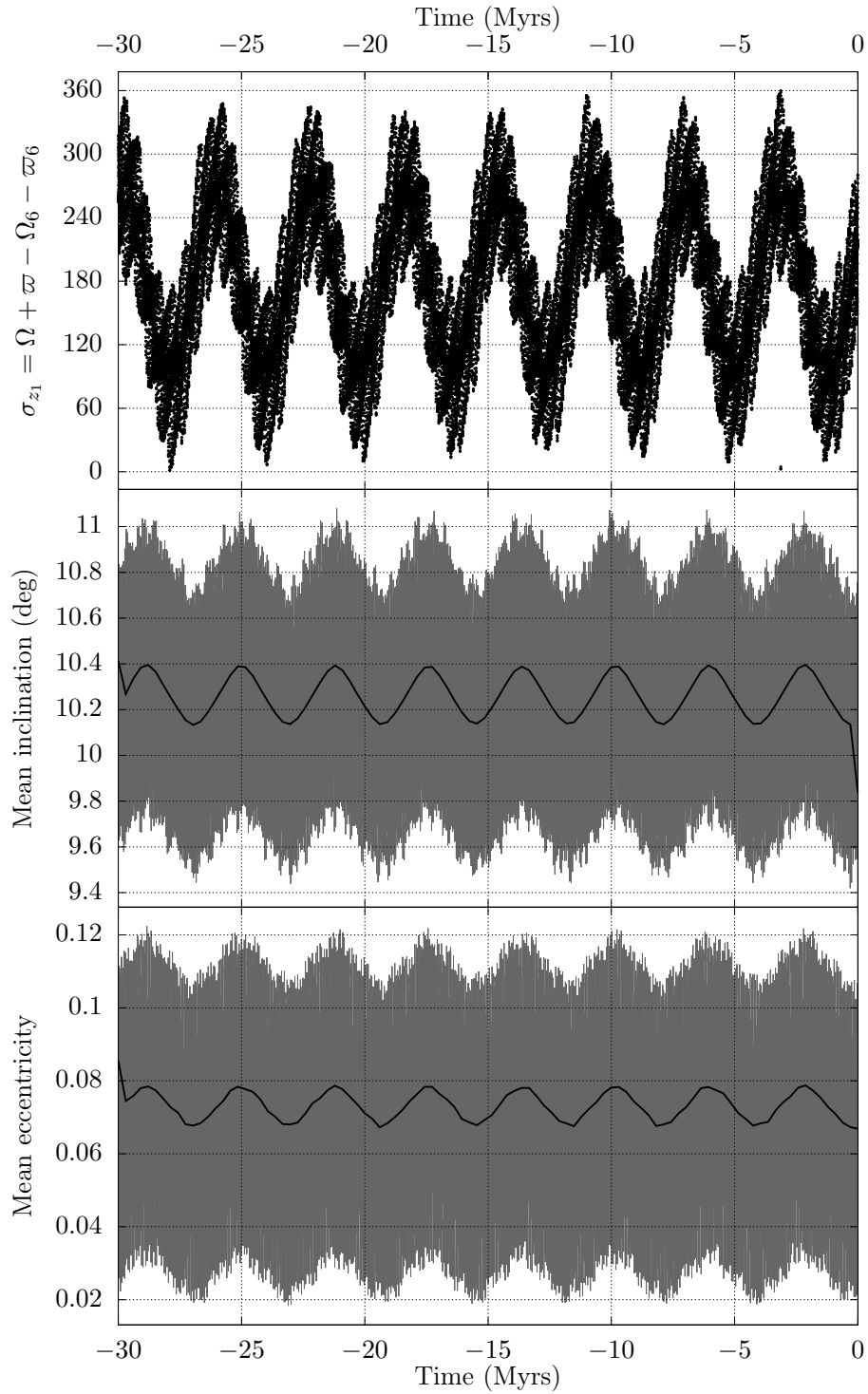


Fig. 3.13.: Evolution of the critical argument of z_1 ($\sigma_{z_1} = \Omega + \varpi - \Omega_6 - \varpi_6$) (top), mean inclination (middle) and mean eccentricity (bottom), of the asteroid (633). The solid black lines in the middle and bottom panels are the respective averaged mean elements, and are shown to better appreciate the effect of the resonance, i.e. the induced oscillations.

3.2.5 Summary

We have discovered a new sub-family of the very old and large asteroid family of (221) Eos. By applying the hierarchical clustering method to the catalog of proper elements and using a threshold distance of 20 m s^{-1} we have identified a group of 26 asteroids around the asteroid (633) Zelima, giving its name to the new cluster.

We then created 1000 clones of the Entire Eos family and searched within those for any clusterings of 26 or more asteroids within the same distance threshold, with no positive results, establishing that the cluster corresponds to the outcome of a real collisional disruption with $> 99\%$ statistical certainty.

Using the backward integration method we were able to identify and remove three interlopers from the family list, based on the fact that their orbits did not converge suitably well with those of the rest of the members.

In order to get a precise age estimation, and to eliminate possible errors in the initial conditions and the dynamical model, we run a statistical approach of the backward integration method. For each of the 23 member asteroids we created 100 clones, accounting for the variations in the initial conditions and the Yarkovsky effect parameters. After integrating their orbits we selected $3 \cdot 10^6$ random combinations of clones of each asteroid and evaluated a function depending on the mean differences in both secular angles, noting the time at which it features a global minimum. Thus we established a statistically accurate age of 2.9 ± 0.2 Myrs for the (633) Zelima cluster.

A short analysis of the physical and orbital characteristics of the family members led us to the conclusion that the cluster was formed in a cratering event, leaving the parent body with about 98% of the initial mass and producing a directional jet of fragments leading to the anisotropic distribution of orbital elements we observe today. The dynamical environment of the cluster is in principle stable with only the 8-3-3 three-body mean-motion resonance with Jupiter and Saturn leading four small members to chaotic orbits.

Conclusions

The major contribution of the present thesis is the discovery of the importance of secular resonances with massive asteroids to the orbits of small asteroids, and consequently on the evolution of asteroid families as distinct populations. Even though it could be argued that the already available analytical theories allow for any celestial object to be treated as a perturber, and therefore massive asteroids also, the major planets have been the only ones included in the studies for the motion of asteroids. The fact that the magnitude of the perturbation is proportional to the mass of the perturbing body, led to the belief that even the most massive asteroids could only affect the orbits of their smaller counterparts significantly only by close encounters, or 1/1 MMRs. Numerical studies have also systematically ignored massive asteroids as parts of the dynamical model, a decision justified on one part having in mind the computational cost, and on another part the complete absence of evidence suggesting otherwise.

The case of the (1726) Hoffmeister family, with its irregular shape in the proper elements space was the spark of our discovery. The realization that none of the known mechanisms implemented in our numerical simulations could reproduce the observed distribution, led us to pursue something new. Including (1) Ceres in the Dynamical model, solved the ambiguity, but the discovery of the exact mechanism by which Ceres affected the orbits of the test particles was the real fruit of our efforts. We found that the test particles, drifting in semi-major axis due to the Yarkovsky effect, were led to cross the linear nodal secular resonance with Ceres, which in turn caused them to experience alterations to their inclinations.

The discovery of this mechanism was the beginning of a thorough study of secular resonances with massive asteroids, focusing on (1) Ceres and (4) Vesta, the two most massive bodies in the Main Belt. We have then found the locations of the four linear secular resonances with Ceres and Vesta using a numerical approach that identifies asteroids which according to their proper frequencies appear to be in resonance. Due to the secular structure of the main belt, we found that the secular resonances with Ceres mostly cover the middle part of the main belt, with some extension to the high inclination part of the outer belt, whereas those with Vesta cover the inner belt and a moderate to high inclination part of the middle and outer belt.

We then performed a set of numerical simulations to study the magnitude of the effects of each resonance across the Main Belt. The results have shown that the perturbations on the orbits of test particles caused by these resonances are significant, especially when the former have semi-major axes close to the respective perturbing massive asteroid. Milani and Knežević (1992, 1994) have studied the effect of non-linear secular resonances with the giant planets, on the proper elements of main-belt asteroids. They found that resonant asteroids' proper elements undergo secular oscillations with amplitudes comparable to what we measured for the secular resonances with Ceres and Vesta. In the outer belt, which is considered far enough from both bodies, we could not clearly distinguish the impact of the secular resonances among the other dynamical mechanisms that act in the region. Although, as we have shown, the effect of the latter diminishes with increasing distance from the relevant massive asteroid in each case, it is important to note that in specific regions of the main belt, secular resonances with massive asteroids are equally, if not more important as the ones with the giant planets.

We have also identified all asteroid families that are crossed by each resonance and which could potentially have been affected by them over their past evolution. There are cases where the size of the families in the proper elements space is comparable to the amplitude of the oscillations induced by the secular resonance that crosses them, suggesting that the respective secular resonances should have the most evident effect.

Two of these cases were studied in more detail, namely (1521) Seinajoki and (1128) Astrid. We have verified that in these cases, as in the Hoffmeister one, the nodal secular resonance with Ceres is the mechanism with the most distinctive effects on the evolution of the distribution of their members, along with the Yarkovsky effect. In the case of Astrid we have also seen hints that a higher order harmonic of this resonance, although much weaker, can also have a clear impact on the orbits of test particles.

We believe we have not exhausted the cases of asteroid families where secular resonances with massive asteroids have had a significant impact. We do believe on the other hand that our work has revealed an important aspect of the dynamical behavior of asteroids in the Main Belt.

Regarding our discoveries of the new asteroid families we believe that each provides useful conclusions:

The dark family of (326) Tamara in the Phocaea region appears to be the origin of most of the dark asteroids therein. Our simulations suggest that despite their relatively small number in the near-Earth region, the impact rate from small, dark Phocaeas is non-negligible and may be an important source for dark meteorites whose parent bodies have absolute magnitudes $17 < H < 22$. We hypothesize that the Tamara family may partially be responsible for the peak in the distribution of meteor streams at about 35-40 degrees (see Fig. 14S in Granvik et al. (2016)).

The Zelima cluster on the other hand could be of great importance in the study of the Eos family, both dynamically and compositionally. However, the currently available physical data are limited to the diameters and albedos of the few largest members of the cluster (Table 3.1). New data concerning the spectral properties of the cluster members, either from targeted observations or from the next generation of surveys, will enable a deeper study of their physical properties, and in conjunction with the rest of the Eos family members, provide useful insights about the partially differentiated Eos parent body. Another interesting aspect is the association of recent asteroid disruptions to observed dust bands in the Main Belt (Nesvorný et al., 2003, 2008), and we believe it would be worth trying to find such a link for the Zelima cluster as well.

Bibliography

- Arnold, J. R. (Dec. 1969). „Asteroid Families and “jet Streams”“. In: *The Astronomical Journal* 74, p. 1235 (cit. on p. 14).
- Baer, J., S. R. Chesley, and R. D. Matson (May 2011). „Astrometric Masses of 26 Asteroids and Observations on Asteroid Porosity“. In: *The Astronomical Journal* 141, 143, p. 143 (cit. on p. 58).
- Bottke, W. F., M. C. Nolan, R. Greenberg, and R. A. Kolvoord (Feb. 1994). „Velocity distributions among colliding asteroids“. In: *Icarus* 107, pp. 255–268 (cit. on p. 146).
- Bottke, W. F., D. Vokrouhlický, M. Broz, D. Nesvorný, and A. Morbidelli (Nov. 2001). „Dynamical Spreading of Asteroid Families by the Yarkovsky Effect“. In: *Science* 294, pp. 1693–1696 (cit. on pp. 23, 92).
- Bottke, W. F., D. D. Durda, D. Nesvorný, et al. (Dec. 2005a). „Linking the collisional history of the main asteroid belt to its dynamical excitation and depletion“. In: *Icarus* 179, pp. 63–94 (cit. on p. 5).
- Bottke, W. F., D. D. Durda, D. Nesvorný, et al. (May 2005b). „The fossilized size distribution of the main asteroid belt“. In: *Icarus* 175, pp. 111–140 (cit. on pp. 128, 130, 146, 149, 150).
- Bottke, W. F., D. Vokrouhlický, K. J. Walsh, et al. (Feb. 2015). „In search of the source of asteroid (101955) Bennu: Applications of the stochastic YORP model“. In: *Icarus* 247, pp. 191–217 (cit. on p. 84).
- Bottke Jr., W. F., D. Vokrouhlický, D. P. Rubincam, and M. Broz (Mar. 2002). „The Effect of Yarkovsky Thermal Forces on the Dynamical Evolution of Asteroids and Meteoroids“. In: *Asteroids III*, W. F. Bottke Jr., A. Cellino, P. Paolicchi, and R. P. Binzel (eds), University of Arizona Press, Tucson, p.395-408. Ed. by W. F. Bottke Jr., A. Cellino, P. Paolicchi, and R. P. Binzel, pp. 395–408 (cit. on p. 129).
- Bottke Jr., W. F., D. Vokrouhlický, D. P. Rubincam, and D. Nesvorný (May 2006). „The Yarkovsky and Yorp Effects: Implications for Asteroid Dynamics“. In: *Annual Review of Earth and Planetary Sciences* 34, pp. 157–191 (cit. on p. 23).

- Bretagnon, P. (Jan. 1974). „Long-period terms in the solar system“. In: *A&A* 30, pp. 141–154 (cit. on p. 8).
- Brouwer, D. (Mar. 1951). „Secular variations of the orbital elements of minor planets“. In: *The Astronomical Journal* 56, p. 9 (cit. on pp. 8, 14).
- Brož, M. and A. Morbidelli (Apr. 2013). „The Eos family halo“. In: *Icarus* 223, pp. 844–849. arXiv: 1302.1447 [astro-ph.EP] (cit. on pp. 97, 104).
- Brož, M., A. Morbidelli, W. F. Bottke, et al. (Mar. 2013). „Constraining the cometary flux through the asteroid belt during the late heavy bombardment“. In: *Astronomy and Astrophysics* 551, A117, A117 (cit. on pp. 34, 129, 131, 132, 134).
- Carpino, M., A. Milani, and A. M. Nobili (July 1987). „Long-term numerical integrations and synthetic theories for the motion of the outer planets“. In: *A&A* 181, pp. 182–194 (cit. on p. 11).
- Carruba, V. (Sept. 2009). „An analysis of the region of the Phocaea dynamical family“. In: *MNRAS* 398, pp. 1512–1526 (cit. on p. 85).
- Carruba, V. and D. Nesvorný (Apr. 2016). „Constraints on the original ejection velocity fields of asteroid families“. In: *Monthly Notices of the Royal Astronomical Society* 457, pp. 1332–1338 (cit. on p. 34).
- Carruba, V., J. A. Burns, W. Bottke, and D. Nesvorný (Apr. 2003). „Orbital evolution of the Gefion and Adeona asteroid families: close encounters with massive asteroids and the Yarkovsky effect“. In: *Icarus* 162, pp. 308–327 (cit. on pp. 33, 40, 92, 96).
- Carruba, V., S. Aljbaae, and D. Souami (Sept. 2014). „Peculiar Euphrosyne“. In: *The Astrophysical Journal* 792, 46, p. 46 (cit. on p. 68).
- Carruba, V., D. Nesvorný, and S. Aljbaae (June 2016a). „Characterizing the original ejection velocity field of the Koronis family“. In: *Icarus* 271, pp. 57–66 (cit. on p. 35).
- Carruba, V., R. Domingos, S. Aljbaae, and M. Huaman (2016b). „On the highly inclined vW leptokurtic asteroid families“. In: *Monthly Notices of the Royal Astronomical Society*, pp. 00–00 (cit. on p. 92).
- Carry, B. (Dec. 2012). „Density of asteroids“. In: *Planet. Space Sci.* 73, pp. 98–118 (cit. on pp. 89, 92).
- Carusi, A. and E. Massaro (Oct. 1978). „Statistics and mapping of asteroid concentrations in the proper elements space“. In: *A&AS* 34, pp. 81–90 (cit. on p. 14).
- Carvano, J. M., D. Lazzaro, T. Mothé-Diniz, C. A. Angeli, and M. Florczak (Jan. 2001). „Spectroscopic Survey of the Hungaria and Phocaea Dynamical Groups“. In: *Icarus* 149, pp. 173–189 (cit. on p. 84).
- Carvano, J. M., P. H. Hasselmann, D. Lazzaro, and T. Mothé-Diniz (Feb. 2010). „SDSS-based taxonomic classification and orbital distribution of main belt asteroids“. In: *Astronomy and Astrophysics* 510, A43, A43 (cit. on pp. 74, 86).

- Cellino, A., V. Zappala, and P. Farinella (Dec. 1991). „The size distribution of main-belt asteroids from IRAS data“. In: *Monthly Notices of the Royal Astronomical Society* 253, pp. 561–574 (cit. on p. 130).
- Cellino, A., P. Michel, P. Tanga, et al. (Sept. 1999). „The Velocity-Size Relationship for Members of Asteroid Families and Implications for the Physics of Catastrophic Collisions“. In: *Icarus* 141, pp. 79–95 (cit. on p. 35).
- Charlier, C. V. L. (1900). „Mémoires et observations. Sur les points singuliers des inégalités séculaires des petites planètes“. In: *Bulletin Astronomique, Serie I* 17, pp. 209–219 (cit. on p. 21).
- (1902). *Die mechanik des himmels*. (Cit. on p. 21).
- Christou, A. A. and P. Wiegert (Jan. 2012). „A population of Main Belt Asteroids co-orbiting with Ceres and Vesta“. In: *Icarus* 217, pp. 27–42. arXiv: 1110.4810 [astro-ph.EP] (cit. on p. 40).
- Cuzzi, J. N., R. C. Hogan, and K. Shariff (Nov. 2008). „Toward Planetesimals: Dense Chondrule Clumps in the Protoplanetary Nebula“. In: *The Astrophysical Journal* 687, 1432–1447, pp. 1432–1447. arXiv: 0804.3526 (cit. on p. 128).
- Cuzzi, J. N., R. C. Hogan, and W. F. Bottke (Aug. 2010). „Towards initial mass functions for asteroids and Kuiper Belt Objects“. In: *Icarus* 208, pp. 518–538. arXiv: 1004.0270 [astro-ph.EP] (cit. on p. 129).
- Delbó, M. and P. Tanga (2009). „Thermal inertia of main belt asteroids smaller than 100 km from IRAS data“. In: *Planetary and Space Science* 57, p. 259 (cit. on p. 37).
- Delbo', M. and P. Tanga (Feb. 2009). „Thermal inertia of main belt asteroids smaller than 100 km from IRAS data“. In: *Planet. Space Sci.* 57, pp. 259–265. arXiv: 0808.0869 (cit. on p. 92).
- Dell'Oro, A., P. Paolicchi, A. Cellino, and V. Zappalà (Mar. 2002). „Collisional Rates within Newly Formed Asteroid Families“. In: *Icarus* 156, pp. 191–201 (cit. on p. 96).
- DeMeo, F. E. and B. Carry (Jan. 2014). „Solar System evolution from compositional mapping of the asteroid belt“. In: *Nature* 505, pp. 629–634. arXiv: 1408.2787 [astro-ph.EP] (cit. on p. 84).
- Doane, D.P. (Nov. 1976). „Aesthetic frequency classifications“. In: *American Statistician* 30, 181–183 (cit. on p. 46).
- Durda, D. D., W. F. Bottke, D. Nesvorný, et al. (Feb. 2007). „Size-frequency distributions of fragments from SPH/ N-body simulations of asteroid impacts: Comparison with observed asteroid families“. In: *Icarus* 186, pp. 498–516 (cit. on pp. 34, 141).
- Farinella, P. and D. Vokrouhlický (Mar. 1999). „Semimajor Axis Mobility of Asteroidal Fragments“. In: *Science* 283, p. 1507 (cit. on p. 96).

- Farinella, P., D. Vokrouhlický, and W. K. Hartmann (Apr. 1998). „Meteorite Delivery via Yarkovsky Orbital Drift“. In: *Icarus* 132, pp. 378–387 (cit. on p. 23).
- Fornasier, S., C. Lantz, D. Perna, et al. (May 2016). „Spectral variability on primitive asteroids of the Themis and Beagle families: Space weathering effects or parent body heterogeneity?“ In: *Icarus* 269, pp. 1–14. arXiv: 1601.05277 [astro-ph.EP] (cit. on p. 97).
- Fowler, J. W. and J. R. Chillemi (Dec. 1992). *IRAS asteroid data processing*. Tech. rep. (cit. on p. 146).
- Froeschle, C. and H. Scholl (Sept. 1989). „The three principal secular resonances $\nu(5)$, $\nu(6)$, and $\nu(16)$ in the asteroidal belt“. In: *Celestial Mechanics and Dynamical Astronomy* 46, pp. 231–251 (cit. on p. 21).
- Gallardo, Tabaré (2014). „Atlas of three body mean motion resonances in the Solar System“. In: *Icarus* 231, pp. 273–286 (cit. on p. 108).
- Gil-Hutton, R. (July 2006). „Identification of families among highly inclined asteroids“. In: *Icarus* 183, pp. 93–100 (cit. on p. 85).
- Granvik, M., A. Morbidelli, R. Jedicke, et al. (Feb. 2016). „Super-catastrophic disruption of asteroids at small perihelion distances“. In: *Nature* 530, pp. 303–306 (cit. on pp. 95, 114).
- Granvik, M., A. Morbidelli, D. Vokrouhlický, et al. (Feb. 2017). „Escape of asteroids from the main belt“. In: *Astronomy and Astrophysics* 598, A52, A52 (cit. on p. 84).
- Hanuš, J., M. Brož, J. Durech, et al. (Nov. 2013). „An anisotropic distribution of spin vectors in asteroid families“. In: *A&A* 559, A134, A134. arXiv: 1309.4296 [astro-ph.EP] (cit. on p. 25).
- Hirayama, K. (Oct. 1918). „Groups of asteroids probably of common origin“. In: *The Astronomical Journal* 31, pp. 185–188 (cit. on p. 6).
- (1922). „Families of Asteroids“. In: *Japanese Journal of Astronomy and Geophysics* 1, p. 55 (cit. on p. 6).
- (1927). „Families of Asteroids. Second Paper“. In: *Japanese Journal of Astronomy and Geophysics* 5, p. 137 (cit. on p. 6).
- Housen, K. R. and K. A. Holsapple (Jan. 2011). „Ejecta from impact craters“. In: *Icarus* 211, pp. 856–875 (cit. on p. 107).
- Ivezić, Ž., S. Tabachnik, R. Rafikov, et al. (Nov. 2001). „Solar System Objects Observed in the Sloan Digital Sky Survey Commissioning Data“. In: *The Astronomical Journal* 122, pp. 2749–2784 (cit. on pp. 31, 86).
- Ivezić, Ž., R. H. Lupton, M. Jurić, et al. (Nov. 2002). „Color Confirmation of Asteroid Families“. In: *The Astronomical Journal* 124, pp. 2943–2948. eprint: astro-ph/0208098 (cit. on p. 74).

- Johansen, A. and A. Youdin (June 2007). „Protoplanetary Disk Turbulence Driven by the Streaming Instability: Nonlinear Saturation and Particle Concentration“. In: *The Astrophysical Journal* 662, pp. 627–641. eprint: astro-ph/0702626 (cit. on p. 128).
- Johansen, A., J. S. Oishi, M.-M. Mac Low, et al. (Aug. 2007). „Rapid planetesimal formation in turbulent circumstellar disks“. In: *Nature* 448, pp. 1022–1025. arXiv: 0708.3890 (cit. on p. 128).
- Johansen, A., M.-M. Mac Low, P. Lacerda, and M. Bizzarro (Apr. 2015). „Growth of asteroids, planetary embryos, and Kuiper belt objects by chondrule accretion“. In: *Science Advances* 1, 1500109, p. 1500109. arXiv: 1503.07347 [astro-ph.EP] (cit. on pp. 128, 130).
- Klahr, H., A. Schreiber, and A. Johansen (2016). „All Planetesimals are born equal - Why Asteroids and Kuiper Belt objects have the same characteristic size“. In: *submitted* (cit. on pp. 129, 149).
- Knežević, Z. (1988). „Asteroid mean orbital elements.“ In: *Bulletin de l'Observatoire Astronomique de Belgrade* 139, pp. 1–6 (cit. on p. 8).
- (June 1989). „Asteroid long-periodic perturbations - The second order Hamiltonian“. In: *Celestial Mechanics and Dynamical Astronomy* 46, pp. 147–158 (cit. on pp. 8, 9).
 - (Apr. 1993). „Minor planet short periodic perturbations - The indirect part of the disturbing function“. In: *Celestial Mechanics and Dynamical Astronomy* 55, pp. 387–404 (cit. on p. 9).
- Knežević, Z. and A. Milani (2000). „Synthetic Proper Elements for Outer Main Belt Asteroids“. In: *Celestial Mechanics and Dynamical Astronomy* 78, pp. 17–46 (cit. on pp. 10, 11, 52, 98).
- (June 2003). „Proper element catalogs and asteroid families“. In: *Astronomy and Astrophysics* 403, pp. 1165–1173 (cit. on pp. 84, 99).
- Knežević, Z., A. Milani, P. Farinella, C. Froeschle, and C. Froeschle (Oct. 1991). „Secular resonances from 2 to 50 AU“. In: *Icarus* 93, pp. 316–330 (cit. on pp. 21, 52, 53).
- Knežević, Z., A. Lemaître, and A. Milani (Mar. 2002). „The Determination of Asteroid Proper Elements“. In: *Asteroids III*. Ed. by W. F. Bottke Jr., A. Cellino, P. Paolicchi, and R. P. Binzel, pp. 603–612 (cit. on p. 30).
- Kozai, Y. (1979). „The dynamical evolution of the Hirayama family“. In: *Asteroids*. Ed. by T. Gehrels and M. S. Matthews, pp. 334–358 (cit. on pp. 8, 14).
- Kuzmanoski, M., G. Apostolovska, and B. Novaković (Sept. 2010). „The Mass of (4) Vesta Derived from its Largest Gravitational Effects“. In: *The Astronomical Journal* 140, pp. 880–886 (cit. on p. 58).
- Lambrechts, M. and A. Johansen (Aug. 2012). „Rapid growth of gas-giant cores by pebble accretion“. In: *Astronomy & Astrophysics* 544, A32, A32. arXiv: 1205.3030 [astro-ph.EP] (cit. on p. 129).

- Le Verrier, U. J. (1856). „Recherches astronomiques : (suite)“. In: *Annales de l'Observatoire de Paris* 2 (cit. on p. 21).
- Lemaitre, A. (June 1993). „Proper elements - What are they?“. In: *Celestial Mechanics and Dynamical Astronomy* 56, pp. 103–119 (cit. on p. 10).
- Levison, H. F., A. Morbidelli, K. Tsiganis, D. Nesvorný, and R. Gomes (Nov. 2011). „Late Orbital Instabilities in the Outer Planets Induced by Interaction with a Self-gravitating Planetesimal Disk“. In: *The Astronomical Journal* 142, 152, p. 152 (cit. on p. 149).
- Lindblad, B. A. and R. B. Southworth (1971). „A Study of Asteroid Families and Streams by Computer Techniques“. In: *NASA Special Publication* 267, p. 337 (cit. on p. 14).
- Mainzer, A., J. Bauer, T. Grav, et al. (Apr. 2011). „Preliminary Results from NEOWISE: An Enhancement to the Wide-field Infrared Survey Explorer for Solar System Science“. In: *ApJ* 731, 53, p. 53. arXiv: 1102.1996 [astro-ph.EP] (cit. on p. 90).
- Marzari, F., P. Farinella, and D. R. Davis (Nov. 1999). „Origin, Aging, and Death of Asteroid Families“. In: *Icarus* 142, pp. 63–77 (cit. on p. 96).
- Masiero, J. R., A. K. Mainzer, T. Grav, et al. (2011). „Main Belt Asteroids with WISE/NEOWISE. I. Preliminary Albedos and Diameters“. In: *The Astrophysical Journal* 741, 68, p. 68. arXiv: 1109.4096 [astro-ph.EP] (cit. on pp. 31, 85, 106, 109).
- Masiero, J. R., A. K. Mainzer, J. M. Bauer, et al. (June 2013). „Asteroid Family Identification Using the Hierarchical Clustering Method and WISE/NEOWISE Physical Properties“. In: *ApJ* 770, 7, p. 7. arXiv: 1305.1607 [astro-ph.EP] (cit. on p. 85).
- Michel, P. (Oct. 1997). „Effects of Linear Secular Resonances in the Region of Semimajor Axes Smaller Than 2 AU“. In: *Icarus* 129, pp. 348–366 (cit. on p. 21).
- Michel, P., D. C. Richardson, D. D. Durda, M. Jutzi, and E. Asphaug (2015). „Collisional Formation and Modeling of Asteroid Families“. In: *Asteroids IV*. Ed. by P. Michel, F. E. DeMeo, and W. F. Bottke, pp. 341–354 (cit. on p. 35).
- Michtchenko, T. A., D. Lazzaro, J. M. Carvano, and S. Ferraz-Mello (Feb. 2010). „Dynamic picture of the inner asteroid belt: implications for the density, size and taxonomic distributions of real objects“. In: *MNRAS* 401, pp. 2499–2516 (cit. on p. 84).
- Migliorini, F., V. Zappalà, R. Vio, and A. Cellino (1995). „Interlopers within Asteroid Families“. In: *Icarus* 118, pp. 271–291 (cit. on p. 32).
- Migliorini, F., A. Manara, M. Di Martino, and P. Farinella (1996). „The Hoffmeister asteroid family - inferences from physical data“. In: *Astronomy and Astrophysics* 310, pp. 681–685 (cit. on pp. 31, 34).
- Milani, A. and P. Farinella (July 1994). „The age of the Veritas asteroid family deduced by chaotic chronology“. In: *Nature* 370, pp. 40–42 (cit. on p. 96).
- Milani, A. and Z. Knežević (Aug. 1992). „Asteroid proper elements and secular resonances“. In: *Icarus* 98, pp. 211–232 (cit. on pp. 21, 113).

- Milani, A. and Z. Knežević (Feb. 1994). „Asteroid proper elements and the dynamical structure of the asteroid main belt“. In: *Icarus* 107, pp. 219–254 (cit. on pp. 9, 113).
- Milani, A. and Z. Knežević (1990). „Secular perturbation theory and computation of asteroid proper elements“. In: *Celest. Mech. Dyn. Astr.* 49, pp. 347–411 (cit. on pp. 9, 22).
- Milani, A. and A. M. Nobili (1988). „Integration error over very long time spans“. In: *Celestial Mechanics* 43, pp. 1–34 (cit. on p. 11).
- Milani, A., A. Cellino, Z. Knežević, et al. (Sept. 2014). „Asteroid families classification: Exploiting very large datasets“. In: *Icarus* 239, pp. 46–73. arXiv: 1312.7702 [astro-ph.EP] (cit. on pp. 67, 85, 90, 129, 131–133, 135–137, 142).
- Milani, A., F. Spoto, Z. Knežević, B. Novaković, and G. Tsirvoulis (Jan. 2016). „Families classification including multiopposition asteroids“. In: *IAU Symposium*. Ed. by S. R. Chesley, A. Morbidelli, R. Jedicke, and D. Farnocchia. Vol. 318. IAU Symposium, pp. 28–45 (cit. on pp. 85, 129, 131, 132, 136, 142).
- Milani, A., Z. Knežević, F. Spoto, et al. (May 2017). „On the ages of resonant, eroded and fossil asteroid families“. In: *Icarus* 288, pp. 240–264. arXiv: 1607.01998 [astro-ph.EP] (cit. on p. 97).
- Milani, A, Zoran Knezevic, Federica Spoto, and P Paolicchi (Dec. 2018). „Asteroid cratering families: recognition and collisional interpretation“. In: *Astronomy Astrophysics* (cit. on p. 25).
- Milić Žitnik, I. and B. Novaković (Jan. 2016). „The Role of Mean-motion Resonances in Semimajor Axis Mobility of Asteroids“. In: *etters* 816, L31, p. L31 (cit. on p. 50).
- Monté-Diniz, T., F. Roig, and J. M. Carvano (2005). „Reanalysis of asteroid families structure through visible spectroscopy“. In: *Icarus* 174, pp. 54–80 (cit. on p. 31).
- Morbidelli, A. and J. Henrard (June 1991). „The main secular resonances ν_6 , ν_5 and ν_{16} in the asteroid belt“. In: *Celestial Mechanics and Dynamical Astronomy* 51, pp. 169–197 (cit. on p. 21).
- Morbidelli, A., V. Zappalà, M. Moons, A. Cellino, and R. Gonczi (1995). „Asteroid Families Close to Mean Motion Resonances: Dynamical Effects and Physical Implications“. In: *Icarus* 118, pp. 132–154 (cit. on p. 35).
- Morbidelli, A., W. F. Bottke, D. Nesvorný, and H. F. Levison (Dec. 2009). „Asteroids were born big“. In: *Icarus* 204, pp. 558–573. arXiv: 0907.2512 [astro-ph.EP] (cit. on p. 128).
- Morbidelli, A., K. J. Walsh, D. P. O’Brien, D. A. Minton, and W. F. Bottke (2015). „The Dynamical Evolution of the Asteroid Belt“. In: *Asteroids IV*. Ed. by P. Michel, F. E. DeMeo, and W. F. Bottke, pp. 493–507 (cit. on p. 150).
- Mothé-Diniz, T. and J. M. Carvano (Nov. 2005). „221 Eos: a remnant of a partially differentiated parent body?“ In: *Astronomy and Astrophysics* 442, pp. 727–729 (cit. on p. 97).

- Murray, C. D. and S. F. Dermott (1999). *Solar system dynamics* (cit. on p. 7).
- Nesvorný, D. and A. Morbidelli (Dec. 1998). „Three-Body Mean Motion Resonances and the Chaotic Structure of the Asteroid Belt“. In: *The Astronomical Journal* 116, pp. 3029–3037 (cit. on p. 68).
- Nesvorný, D. and D. Vokrouhlický (Nov. 2006). „New Candidates for Recent Asteroid Breakups“. In: *The Astronomical Journal* 132, pp. 1950–1958 (cit. on pp. 97, 104).
- Nesvorný, D., A. Morbidelli, D. Vokrouhlický, W. F. Bottke, and M. Brož (May 2002a). „The Flora Family: A Case of the Dynamically Dispersed Collisional Swarm?“ In: *Icarus* 157, pp. 155–172 (cit. on p. 96).
- Nesvorný, D., W. F. Bottke Jr., L. Dones, and H. F. Levison (June 2002b). „The recent breakup of an asteroid in the main-belt region“. In: *Nature* 417, pp. 720–771 (cit. on pp. 97, 101).
- Nesvorný, D., W. F. Bottke, H. F. Levison, and L. Dones (July 2003). „Recent Origin of the Solar System Dust Bands“. In: *The Astrophysical Journal* 591, pp. 486–497 (cit. on pp. 97, 101, 114).
- Nesvorný, D., R. Jedicke, R. J. Whiteley, and Ž. Ivezić (Jan. 2005). „Evidence for asteroid space weathering from the Sloan Digital Sky Survey“. In: *Icarus* 173, pp. 132–152 (cit. on pp. 30, 37).
- Nesvorný, D., D. Vokrouhlický, and W. F. Bottke (June 2006). „The Breakup of a Main-Belt Asteroid 450 Thousand Years Ago“. In: *Science* 312, p. 1490 (cit. on pp. 97, 101).
- Nesvorný, D., W. F. Bottke, D. Vokrouhlický, et al. (June 2008). „Origin of the Near-Ecliptic Circumsolar Dust Band“. In: *The Astrophysical Journal Letters* 679, p. L143 (cit. on pp. 97, 114).
- Nesvorný, D., M. Brož, and V. Carruba (2015). „Identification and Dynamical Properties of Asteroid Families“. In: *Asteroids IV*. Ed. by P. Michel, F. E. DeMeo, and W. F. Bottke, pp. 297–321 (cit. on pp. 88, 92).
- Novaković, B. (Sept. 2010). „Portrait of Theobalda as a young asteroid family“. In: *Monthly Notices of the Royal Astronomical Society* 407, pp. 1477–1486. arXiv: 1005.3574 [astro-ph.EP] (cit. on pp. 92, 97, 101).
- Novaković, B., K. Tsiganis, and Z. Knežević (June 2010). „Dynamical portrait of the Lixiaohua asteroid family“. In: *Celestial Mechanics and Dynamical Astronomy* 107, pp. 35–49 (cit. on pp. 92, 96).
- Novaković, B., A. Cellino, and Z. Knežević (2011). „Families among high-inclination asteroids“. In: *Icarus* 216, pp. 69–81 (cit. on pp. 30, 85, 88, 132).
- Novaković, B., H. H. Hsieh, and A. Cellino (Aug. 2012a). „P/2006 VW₁₃₉: a main-belt comet born in an asteroid collision?“ In: *Monthly Notices of the Royal Astronomical Society* 424, pp. 1432–1441. arXiv: 1205.4949 [astro-ph.EP] (cit. on p. 101).

- Novaković, B., A. Dell’Oro, A. Cellino, and Z. Knežević (Sept. 2012b). „Recent collisional jet from a primitive asteroid“. In: *Monthly Notices of the Royal Astronomical Society* 425, pp. 338–346. arXiv: 1206.1962 [astro-ph.EP] (cit. on pp. 35, 97, 101, 104).
- Novaković, B., H. H. Hsieh, A. Cellino, M. Micheli, and M. Pedani (Mar. 2014). „Discovery of a young asteroid cluster associated with P/2012 F5 (Gibbs)“. In: *Icarus* 231, pp. 300–309. arXiv: 1401.2966 [astro-ph.EP] (cit. on pp. 97, 101, 104).
- Novaković, B., C. Maurel, G. Tsirvoulis, and Z. Knežević (July 2015). „Asteroid Secular Dynamics: Ceres’ Fingerprint Identified“. In: *The Astrophysical Journal Letters* 807, L5, p. L5. arXiv: 1506.01586 [astro-ph.EP] (cit. on pp. 3, 51, 92, 96).
- Novaković, B., G. Tsirvoulis, S. Marò, V. ošović, and C. Maurel (Jan. 2016). „Secular evolution of asteroid families: the role of Ceres“. In: *Asteroids: New Observations, New Models*. Ed. by S. R. Chesley, A. Morbidelli, R. Jedicke, and D. Farnocchia. Vol. 318. IAU Symposium, pp. 46–54. arXiv: 1601.00905 [astro-ph.EP] (cit. on p. 3).
- Novaković, B., G. Tsirvoulis, M. Granvik, and A. Todović (June 2017). „A Dark Asteroid Family in the Phocaea Region“. In: *The Astronomical Journal* 153, 266, p. 266. arXiv: 1704.06088 [astro-ph.EP] (cit. on p. 4).
- Opik, E. J. (1951). „Collision probability with the planets and the distribution of planetary matter“. In: *Proc. R. Irish Acad. Sect. A, vol. 54, p. 165-199 (1951)*. 54, pp. 165–199 (cit. on p. 22).
- Paddack, S. J. (1969). „Rotational bursting of small celestial bodies: Effects of radiation pressure.“ In: *J. Geophys. Res.* 74, pp. 4379–4381 (cit. on p. 22).
- Parker, A., Ž. Ivezić, M. Jurić, et al. (Nov. 2008a). „The size distributions of asteroid families in the SDSS Moving Object Catalog 4“. In: *Icarus* 198, pp. 138–155. arXiv: 0807.3762 (cit. on p. 74).
- (Nov. 2008b). „The size distributions of asteroid families in the SDSS Moving Object Catalog 4“. In: *Icarus* 198, pp. 138–155. arXiv: 0807.3762 (cit. on p. 129).
- Popescu, M., J. Licandro, D. Morate, et al. (June 2016). „Near-infrared colors of minor planets recovered from VISTA-VHS survey (MOVIS)“. In: *A&A* 591, A115, A115. arXiv: 1605.05594 [astro-ph.EP] (cit. on p. 86).
- Pravec, P. and D. Vokrouhlický (Dec. 2009). „Significance analysis of asteroid pairs“. In: *Icarus* 204, pp. 580–588 (cit. on p. 97).
- Pravec, P., P. Fatka, D. Vokrouhlický, et al. (Apr. 2018). „Asteroid clusters similar to asteroid pairs“. In: *Icarus* 304, pp. 110–126 (cit. on p. 97).
- Radović, V., B. Novaković, V. Carruba, and D. Marčeta (Sept. 2017). „An automatic approach to exclude interlopers from asteroid families“. In: *MNRAS* 470, pp. 576–591. arXiv: 1705.09226 [astro-ph.EP] (cit. on p. 31).
- Radzievskii, V. V. (1952). „A mechanism for the disintegration of asteroids and meteorites“. In: *Azh* 29, pp. 162–170 (cit. on p. 22).

- Rubincam, D. P. (Jan. 1995). „Asteroid orbit evolution due to thermal drag“. In: *J. Geophys. Res.* 100, pp. 1585–1594 (cit. on pp. 23, 24).
- (Jan. 1998). „Yarkovsky thermal drag on small asteroids and Mars-Earth delivery“. In: *J. Geophys. Res.* 103, pp. 1725–1732 (cit. on p. 23).
- Sachse, M., J. Schmidt, S. Kempf, and F. Spahn (Nov. 2015). „Correlation between speed and size for ejecta from hypervelocity impacts“. In: *Journal of Geophysical Research (Planets)* 120, pp. 1847–1858 (cit. on p. 88).
- Spoto, F., A. Milani, and Z. Knežević (Sept. 2015). „Asteroid family ages“. In: *Icarus* 257, pp. 275–289. arXiv: 1504.05461 [astro-ph.EP] (cit. on pp. 26, 27, 38, 46, 49, 50, 90, 97).
- Tanga, P., A. Cellino, P. Michel, et al. (Sept. 1999). „On the Size Distribution of Asteroid Families: The Role of Geometry“. In: *Icarus* 141, pp. 65–78 (cit. on p. 88).
- Tedesco, E. F., P. V. Noah, M. Noah, and S. D. Price (Feb. 2002). „The Supplemental IRAS Minor Planet Survey“. In: *The Astronomical Journal* 123, pp. 1056–1085 (cit. on pp. 31, 86).
- Tisserand, F. (1882). „Memoire sur les mouvements seculaires des plans des orbites de trois planetes“. In: *Annales de l'Observatoire de Paris* 16, E.1–E.57 (cit. on p. 21).
- Tsiganis, K., R. Gomes, A. Morbidelli, and H. F. Levison (May 2005). „Origin of the orbital architecture of the giant planets of the Solar System“. In: *Nature* 435, pp. 459–461 (cit. on p. 149).
- Tsirvoulis, G. (Jan. 2019). „Discovery of a young subfamily of the (221) Eos asteroid family“. In: *MNRAS* 482, pp. 2612–2618. arXiv: 1810.10864 [astro-ph.EP] (cit. on p. 4).
- Tsirvoulis, G. and B. Novaković (Dec. 2016a). „Secular resonances with Ceres and Vesta“. In: *Icarus* 280, pp. 300–307. arXiv: 1607.02035 [astro-ph.EP] (cit. on p. 3).
- (Dec. 2016b). „Secular resonances with Ceres and Vesta“. In: *Icarus* 280, pp. 300–307. arXiv: 1607.02035 [astro-ph.EP] (cit. on p. 96).
- Tsirvoulis, G., A. Morbidelli, M. Delbo, and K. Tsiganis (Apr. 2018). „Reconstructing the size distribution of the primordial Main Belt“. In: *Icarus* 304, pp. 14–23. arXiv: 1706.02091 [astro-ph.EP] (cit. on p. 4).
- Usui, F., T. Kasuga, S. Hasegawa, et al. (Jan. 2013). „Albedo Properties of Main Belt Asteroids Based on the All-Sky Survey of the Infrared Astronomical Satellite AKARI“. In: *ApJ* 762, 56, p. 56. arXiv: 1211.2889 [astro-ph.EP] (cit. on p. 86).
- Vernazza, P., R. P. Binzel, A. Rossi, M. Fulchignoni, and M. Birlan (Apr. 2009). „Solar wind as the origin of rapid reddening of asteroid surfaces“. In: *Nature* 458, pp. 993–995 (cit. on p. 97).

- Vokrouhlický, D. (July 1998). „Diurnal Yarkovsky effect as a source of mobility of meter-sized asteroidal fragments. I. Linear theory“. In: *Astronomy and Astrophysics* 335, pp. 1093–1100 (cit. on pp. 24, 37, 104).
- (Apr. 1999). „A complete linear model for the Yarkovsky thermal force on spherical asteroid fragments“. In: *Astronomy and Astrophysics* 344, pp. 362–366 (cit. on pp. 37, 104).
- Vokrouhlický, D. and D. Nesvorný (July 2011). „Half-brothers in the Schulhof Family?“ In: *The Astronomical Journal* 142, 26, p. 26 (cit. on pp. 97, 104, 105).
- Vokrouhlický, D., A. Milani, and S. R. Chesley (Nov. 2000). „Yarkovsky Effect on Small Near-Earth Asteroids: Mathematical Formulation and Examples“. In: *Icarus* 148, pp. 118–138 (cit. on p. 23).
- Vokrouhlický, D., M. Brož, A. Morbidelli, et al. (May 2006a). „Yarkovsky footprints in the Eos family“. In: *Icarus* 182, pp. 92–117 (cit. on pp. 97, 107).
- Vokrouhlický, D., M. Brož, W. F. Bottke, D. Nesvorný, and A. Morbidelli (May 2006b). „Yarkovsky/YORP chronology of asteroid families“. In: *Icarus* 182, pp. 118–142 (cit. on pp. 23, 25, 89, 96).
- Vokrouhlický, D., W. F. Bottke, S. R. Chesley, D. J. Scheeres, and T. S. Statler (2015). „The Yarkovsky and YORP Effects“. In: *Asteroids IV*. Ed. by P. Michel, F. E. DeMeo, and W. F. Bottke, pp. 509–531 (cit. on pp. 58, 90, 92).
- Vokrouhlický, D., J. Ďurech, P. Pravec, et al. (Mar. 2016). „The Schulhof Family: Solving the Age Puzzle“. In: *The Astronomical Journal* 151, 56, p. 56 (cit. on p. 101).
- Walsh, K. J., A. Morbidelli, S. N. Raymond, D. P. O’Brien, and A. M. Mandell (July 2011). „A low mass for Mars from Jupiter’s early gas-driven migration“. In: *Nature* 475, pp. 206–209. arXiv: 1201.5177 [astro-ph.EP] (cit. on p. 149).
- Walsh, K. J., M. Delbó, W. F. Bottke, D. Vokrouhlický, and D. S. Lauretta (July 2013). „Introducing the Eulalia and new Polana asteroid families: Re-assessing primitive asteroid families in the inner Main Belt“. In: *Icarus* 225, pp. 283–297. arXiv: 1305.2821 [astro-ph.EP] (cit. on pp. 86, 90).
- Williams, J. G. (1979). „Proper elements and family memberships of the asteroids“. In: *Asteroids*. Ed. by T. Gehrels and M. S. Matthews, pp. 1040–1063 (cit. on p. 14).
- (1989). „Asteroid family identifications and proper elements“. In: *Asteroids II*. Ed. by R. P. Binzel, T. Gehrels, and M. S. Matthews, pp. 1034–1072 (cit. on p. 14).
- Yarkovsky, I. O. (1901). „The density of luminiferous ether and the resistance it offers to motion“. In: *published privately by the author* (cit. on p. 21).
- Youdin, A. and A. Johansen (June 2007). „Protoplanetary Disk Turbulence Driven by the Streaming Instability: Linear Evolution and Numerical Methods“. In: *The Astrophysical Journal* 662, pp. 613–626. eprint: astro-ph/0702625 (cit. on p. 128).

- Yuasa, M. (1973). „Theory of Secular Perturbations of Asteroids Including Terms of Higher Orders and Higher Degrees“. In: *PASJ* 25, p. 399 (cit. on pp. 8, 9).
- Zappala, V. and A. Cellino (1996). „Main Belt Asteroids: Present and Future Inventory“. In: *Completing the Inventory of the Solar System*. Ed. by T. Rettig and J. M. Hahn. Vol. 107. Astronomical Society of the Pacific Conference Series, pp. 29–44 (cit. on p. 137).
- Zappalà, V., A. Cellino, P. Farinella, and Z. Knežević (Dec. 1990). „Asteroid families. I - Identification by hierarchical clustering and reliability assessment“. In: *The Astronomical Journal* 100, pp. 2030–2046 (cit. on pp. 14, 129, 131).

Appendix

Reconstructing the size distribution of the primordial Main Belt

Georgios Tsirvoulis, Alessandro Morbidelli¹, Marco Delbo¹, Kleomenis Tsiganis²

1.Observatoire de la Côte d’Azur, Boulevard de l’Observatoire, 06304 Nice, France

2.Department of Physics, Aristotle University of Thessaloniki, 54124 Thessaloniki, Greece

Abstract

In this work we aim to constrain the slope of the size distribution of main-belt asteroids, at their primordial state. To do so we turn our attention to the part of the main asteroid belt between 2.82 and 2.96 AU, the so-called “pristine zone”, which has a low number density of asteroids and few, well separated asteroid families. Exploiting these unique characteristics, and using a modified version of the hierarchical clustering method we are able to remove the majority of asteroid family members from the region. The remaining, background asteroids should be of primordial origin, as the strong 5/2 and 7/3 mean-motion resonances with Jupiter inhibit transfer of asteroids to and from the neighboring regions. The size-frequency distribution of asteroids in the size range $17 < D(\text{km}) < 70$ has a slope $q \simeq -1$. Using Monte-Carlo methods, we are able to simulate, and compensate for the collisional and dynamical evolution of the asteroid population, and get an upper bound for its size distribution slope $q = -1.43$. In addition, applying the same ‘family extraction’ method to the neighboring regions, i.e. the middle and outer belts, and comparing the size distributions of the respective background populations, we find statistical evidence that no large asteroid families of primordial origin had formed in the middle or pristine zones.

A.1 Introduction

One of the reasons for which asteroids are subject of many studies is that they represent what is left over of the original population of planetesimals in the inner Solar System. Among the many properties of asteroids, their size-frequency distribution¹ (SFD) may be diagnostic of the processes by which planetesimals formed. The current cumulative SFD of asteroids is characterized by a quite steep slope in the size range $100\text{km} < D < 1,000\text{km}$ (with an exponent q of about -2.5), and a shallower slope for $D < 100\text{km}$ (with $q \sim -1.8$ down to $D \sim 10\text{km}$). The current SFD of the asteroids, however, is presumably not identical to the SFD that planetesimals had at the time of their formation, but has evolved over the age of the Solar System as a consequence of various phenomena: collisions between asteroids produce a plethora of small fragments from only two original bodies, directly altering the SFD of the total population. Moreover, dynamical depletion is constantly removing asteroids from the main belt: The interplay between the Yarkovsky thermal force and the strongest resonances (mean-motion and secular ones), is the most important depletion mechanism, and since the Yarkovsky effect is size-dependent the SFD is modified accordingly.

Using several observational constraints, Bottke et al. (2005b) concluded that the original SFD of planetesimals below $D = 100\text{km}$ had to be equal to or shallower than the current one. However, they could not constrain what the original slope had to be. Considering the possibility of a very shallow primordial slope, Morbidelli et al. (2009) suggested that asteroids formed big, with characteristic sizes in the 100 km-1,000 km range. The model emerging at the time about planetesimal formation from massive self-gravitating clumps of dust (Cuzzi et al., 2008) and pebbles (Johansen et al., 2007) seemed to support, at least qualitatively, that claim.

More recently, Johansen et al. (2015) studied in details the formation of planetesimals by streaming instability (Johansen and Youdin, 2007; Youdin and Johansen, 2007), using hydrodynamical simulations with multiple resolutions. They found that the planetesimals formed by this process have a characteristic cumulative SFD with exponent $q = -1.8$. Because this slope is very close to that currently observed for asteroids with $D < 100\text{km}$, Johansen et al. (2015) proposed that 100 km is the maximal size of the planetesimals formed by the streaming instability. The asteroids currently larger than 100 km would have grown from primordial sizes smaller than

¹The size-frequency distribution of asteroids is usually approximated by a power law, with a characteristic exponent q : $N(D) \sim D^q$

this upper limit in a subsequent process named "pebble accretion" (Lambrechts and Johansen, 2012). Klahr et al. (2016) instead, found that the characteristic size of the planetesimals formed by the streaming instability is $D \sim 100km$, but with the wings of the size probability function extending to smaller and larger bodies. Cuzzi et al. (2010) had obtained a similar result, but for the turbulent concentration of clumps of small particles, rather than the streaming instability.

It is clear that the papers quoted above about planetesimal accretion, present quite different views on the characteristic sizes of the first planetesimals. In order to discriminate among them, it would be important to have an observational assessment of the primordial planetesimal SFD below 100 km in size. But, as said above, the asteroid SFD has evolved through collisions and dynamical depletion.

In principle, asteroids (tens of km in diameter) produced in collisions should be identifiable as members of asteroid families. Thus, if one removes the asteroid families from asteroid catalogs, one should be left with the population of these bodies which have not been produced by collisions through the lifetime of the Solar System: namely the primordial population. However, this procedure is not so easy to implement. The Hierarchical Clustering Method (Zappalà et al., 1990) the most used procedure for the identification of asteroid family members usually succeeds in linking only the compact core of the family. This has been shown by Parker et al. (2008b), who demonstrated that each nominal family identified by HCM is surrounded by a halo sharing the same spectral properties. Recent upgrades of the HCM (Milani et al., 2014, 2016)) attempt to identify the family halos through a multi-step approach. However, it is unlikely that the entire family population can be identified with confidence even with this more sophisticated approach. The situation may be better for relatively large asteroids that we are interested here, but this is not certain.

Here, we assess the fraction of the background asteroid population (i.e. the population not belonging to any family) that is made of rogue family members and the characteristic size at which this contamination starts to be relevant. To do so, we focus in a zone of the asteroid belt, with semi-major axis $2.82 < a < 2.96$ AU, which contains much fewer asteroids than any other zone. The explanation for this deficit of asteroids, according to Brož et al. (2013), is due to the bordering of the 5/2 and the 7/3 mean motion resonances with Jupiter, which prevent the influx of asteroids migrating due to the Yarkovsky effect (Bottke et al., 2002) from the neighboring regions. Also, because the region is quite narrow, only few asteroid families formed in it. For these reasons, Brož et al. (2013) dubbed this region as

the "pristine zone", as it is probably the one that reflects the best the primordial distribution of asteroids.

In this region it is fairly easy to subtract the family members, given the small number of families and the low orbital density of the overall population. We can also try to subtract all family members from the two regions that border the pristine zone, which contain a larger number of asteroids. This procedure is explained in section 5.2. In principle, there is no reason that the primordial orbital densities of asteroids were different in neighboring regions. Thus, in Section 5.3, by comparing the nominal background population in the pristine zone with those in neighboring regions with the same semi major axis width, we can get statistical information on which fraction of these neighboring background populations should be in reality made of rogue family members that we cannot identify as such.

We then go further in our analysis in Section 5.4. To gain confidence that the background population in the pristine zone really represents the primordial SFD of asteroids and to determine up to which absolute magnitude this is true, we compare it with those in the neighboring regions. We require that at least in one of the neighboring zones the SFD of the background population is the same as in the pristine zone (e.g. same shape, same slopes, number of asteroids within a factor of ~ 2). We find that this is the case in the inner neighboring region up to absolute magnitude $H \sim 12$, while we explain why the outer neighboring zone is different. Moreover we verify that the background SFD for $H < 12$ in the pristine zone is different from those of the families in these two regions, as suggested by Cellino et al. (1991).

Based on these results, in Sect. 5.5 we measure the slope of the SFD of the background population in the pristine zone between $9 < H < 12$. However, this is not yet the slope of the SFD of the primordial planetesimals below 100 km in size, because some original asteroids in this magnitude range might have been destroyed by collisions, even if, in principle, none of the current background asteroids was produced by collisions (by definition of background, if selected correctly). Thus, we correct the SFD slope by the size-dependent probability to have been catastrophically disrupted over the age of the Solar System, given in Bottke et al. (2005b). Finally, we compare this slope with that expected by the streaming instability in the Johansen et al. (2015) simulations.

The conclusions of this work are summarized and discussed in Sect. 5.6.

A.2 Identification of family members

The first step of our study is to obtain the background population of the pristine zone. To do so we simply remove from the catalog of proper elements of numbered and multi-opposition asteroids ² those asteroids that have been identified as family members following the classification of Milani et al. (2014, 2016). However due to the fact that the focus of their study was to obtain a good classification of families, the authors of these works adopted a conservative approach in the selection of their Quasi Random Level (QRL)³ for the hierarchical clustering analysis Zappalà et al. (1990), in order to avoid background objects from being incorrectly identified as family members and maintain good separation in orbital elements between families. Moreover they used the same QRL parameter for the pristine zone as for the rest of the outer belt. This resulted in a statistically significant family identification, which however left as background a lot of asteroids that should belong to the halos of asteroid families. This can be appreciated by looking at Figure A.1 panel b, where we see that even after removing all family members according to the Milani et al. classification, most of the very same families are still recognizable by the density contrast in the proper element space. For our purpose, which is to obtain as clear of a background as possible this is not the optimal solution. Therefore we decided to proceed with a modified application of the hierarchical clustering method, trying to get rid of as many family members as possible. We perform the hierarchical clustering method to the catalog of proper elements of the pristine zone, starting with the parent bodies identified by Milani et al. (2014). Moreover we also consider the parent bodies of asteroid families identified in Brož et al. (2013) which are not present in the Milani et al. (2014) classification, to make sure we remove as many family members as possible. We obtain for each asteroid family the number of associated members as a function of the cut-off velocity. We vary the latter, in increments of 2 m/s, from very small values where no close neighbor is found, up to the point where the family includes an abnormally large portion of the total population of asteroids. Then we select for each asteroid family the optimal cut-off velocity in the following way: We select the highest possible value at which each family is still identifiable as a single cluster of asteroids, before merging with the background. If two families are merged together at some value of the cut-off velocity,

²Obtained from: <http://hamilton.dm.unipi.it/astdys/index.php?pc=5>

³The Quasi Random Level is a measure of the statistical significance when identifying asteroid families. It sets a threshold on the cut-off velocity, the maximum distance in the proper elements space between asteroids belonging to the same group, above which there is no statistical difference between an actual family and a statistical fluke of a random distribution of asteroids. For more see: Zappalà et al. (1990)

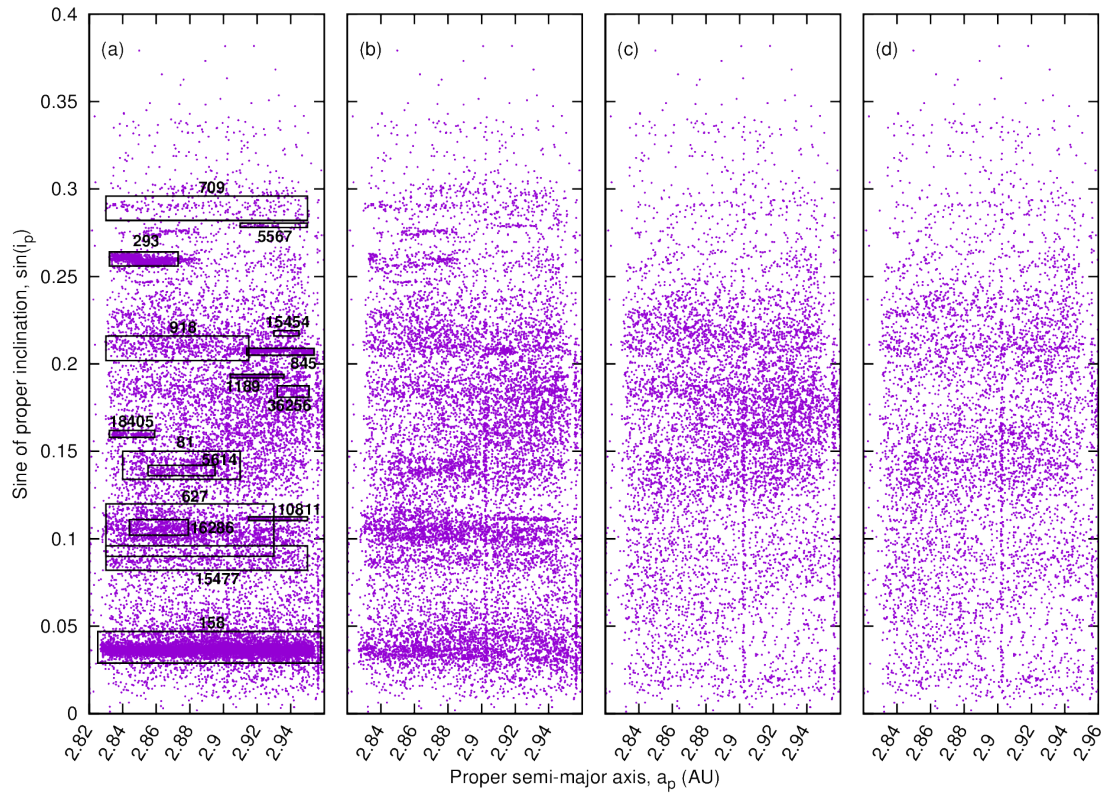


Fig. A.1.: Asteroids in the pristine zone of the main belt in the proper semi-major axis versus sine of proper inclination plane. Panel a: all numbered and multi-opposition asteroids. The boxes highlight the asteroid families in the region. Panel b: The remaining asteroids after removing the family members according to the classifications of Brož et al. (2013) and Milani et al. (2014, 2016). Panel c: The remaining asteroids after removing family members with our method as discussed in the text. Panel d: Same as panel c, with the asteroids originating from the family of Eos also removed.

we consider them as a group and go on until the background is included, assigning to the group the cut-off velocity value of the previous step before merging with the background happens.

As an example, the family of (16286) was found by Milani et al. (2014) to have 83 family members at a cutoff velocity of 40 m/s. Our method gives the result seen in Figure A.2. The family membership starts growing linearly with increasing cut-off velocity from 34 m/s up to 60 m/s. Then between 60 m/s and 112 m/s it grows at a much smaller rate, giving the distinctive “plateau”, the midpoint of which is often used as the nominal cut-off when aiming for a reliable family membership (see e.g. Novaković et al. (2011)). At 114 m/s it merges with the family of (15447) (identified by Brož et al. (2013)), and they both merge with the background at 118 m/s. The family of (15477) was found by Brož et al. (2013) to have 144 members at

110 m/s. In this case since the two families do not grow as a group after they merge together until they extend to the background, we select the value of 112 m/s for both families resulting in 1296 members for (16286) and 542 members for (15477). Note that these membership numbers are considerably larger than the respective ones given by the aforementioned authors. In the case of (16286) although we use the same catalog of proper elements both the identification method and the selection of cut-off velocity are different. We use a straightforward application of the HCM compared to the multi-step procedure of Milani et al. (2014), and we select on purpose a very high cut-off velocity compared to the QRL approach of the latter. In the case of (15477) although the methods and the cut-off velocity are the same, the catalog of proper elements used is different, since we use a more updated version which also contains multi-opposition asteroids.

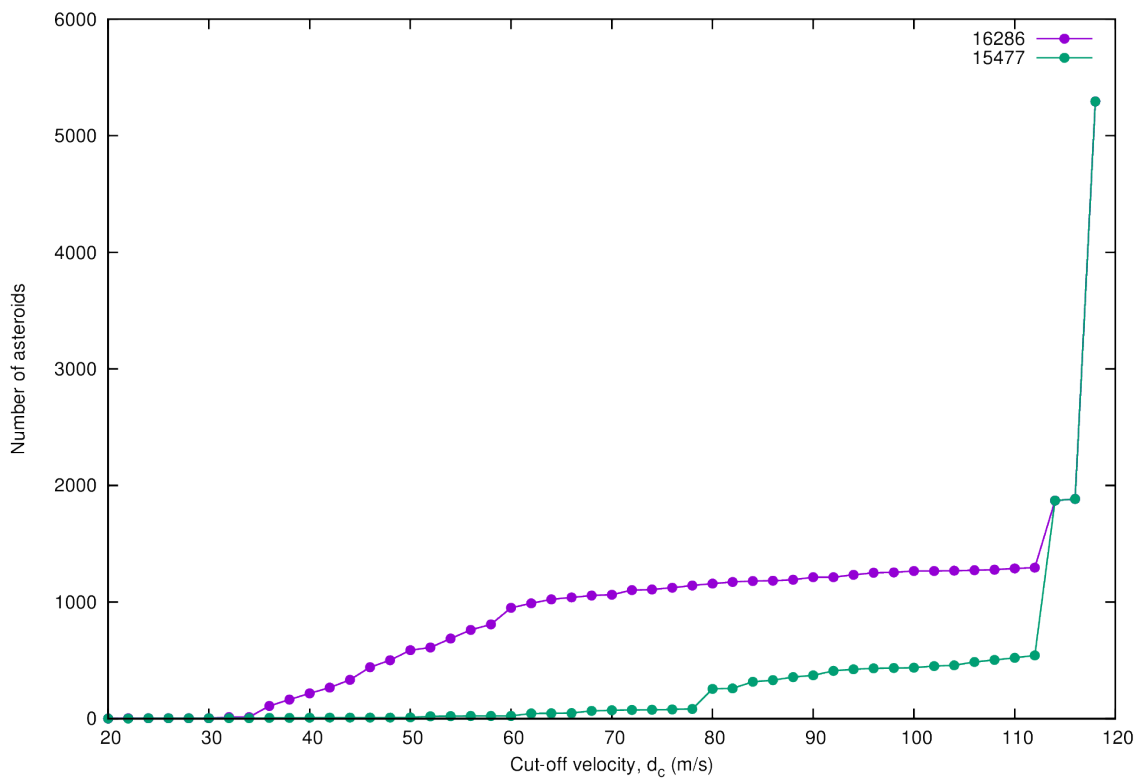


Fig. A.2.: The number of asteroids associated to asteroids (16286) and (15477) as a function of cut-off velocity.

In all cases we end up with more family members than in the works of other authors. We know that many of these asteroids which we identify as family members are in reality interlopers, and thus we do not claim to have produced another family classification. Our aim was to obtain a background population contaminated as little as possible by family members. In doing so we lose a lot of background asteroids into

the families, but we expect that the number of background objects lost in this way is too small to have a significant effect on the resulting size distribution. The final result is seen in Figure A.1 (c), where we see that we have removed substantially more family members compared to (b). The background we obtain is much more uniform.

Still, in Figure A.1 (c), there is one extended concentration of asteroids in the range $0.12 < \sin i_p < 0.25$ which needs to be further investigated. For the asteroid families of (1189), (16286) and (36256), this population of asteroids is included in their membership list at a cut-off velocity one step higher than the one selected. This means that the maximal cut-off velocity we used for these three small families was in fact chosen in order to avoid merging them together with this large concentration of asteroids. However, visual inspection of Figure A.1 (c) suggests that this concentration is not the halo of either of the mentioned families but instead it is an independent family, previously unidentified. If this is true, this concentration should have some properties distinctive of families. One such property is the so-called “V-shape”, that is the shape of the distribution in the (a_p, H) plane that a family has to acquire due to the size-dependent action of the so-called Yarkovsky effect. We selected all background asteroids from the previous step in the volume containing this concentration, i.e. $2.82 < a_p < 2.96$, $0.03 < e_p < 0.1$ and $0.12 < \sin i_p < 0.2$, and plotted them in the (a_p, H) plane as seen in Figure A.3. The result is striking. The left half of a V-shape is clearly visible, meaning that the other half must exist at larger semi-major axes. But this range in eccentricities and inclinations matches almost perfectly the range covered by the family of (221) Eos in the outer belt. Indeed plotting the family members of (221) Eos in the same plane shows that it extends into the pristine zone, creating this mysterious high concentration of asteroids. This is proving that this region is not so pristine as previously believed (Brož et al., 2013), and it can indeed be contaminated by asteroids drifting from the adjacent regions. To remove those asteroids within this orbital volume originating from Eos, we took a step back, and used a higher cut-off value for the neighboring family of (1189). In this way we remove the families of (1189), (16286) and (36256), together with asteroids coming from Eos in one step.

The final result is shown in Figure A.1 (d). Table 2.1 shows a summary of the numbers of family members and background asteroids at each step, and Figure A.4 presents the corresponding size distributions.

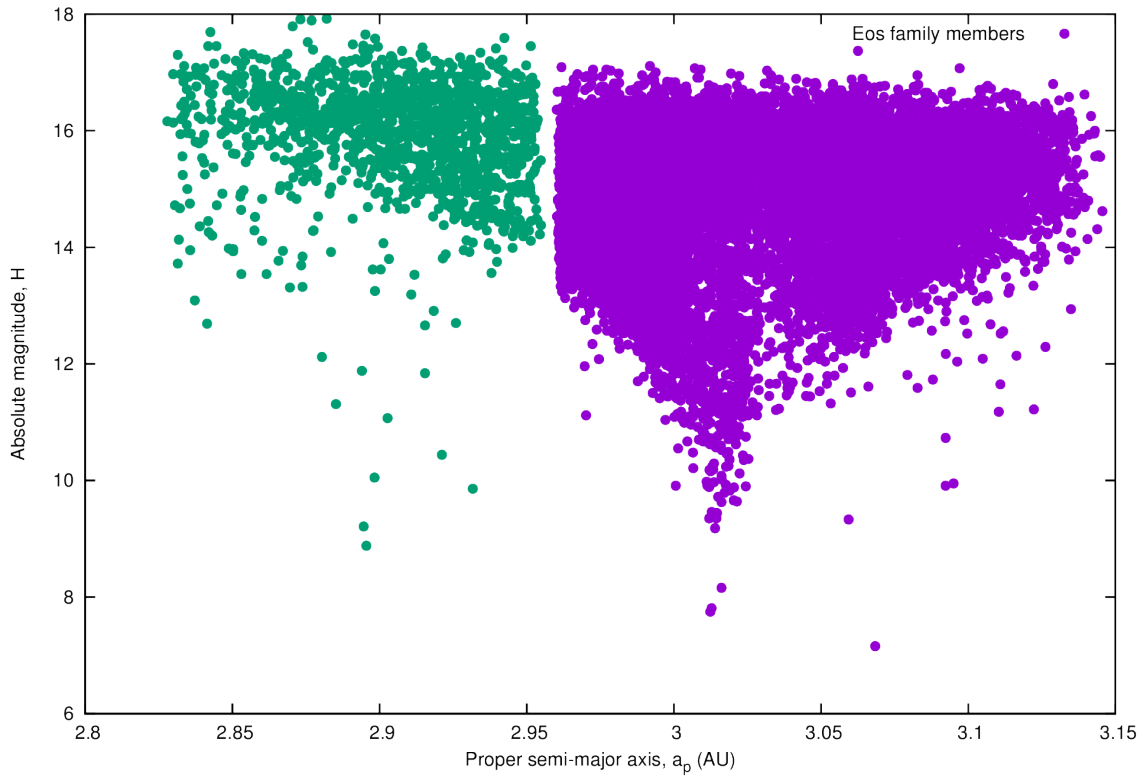


Fig. A.3.: The asteroid family of (221) Eos in the proper semi-major axis versus absolute magnitude plane. In purple are the asteroids belonging to the classical family, as identified by Milani et al. (2014), while in green are asteroids in the pristine zone with $2.82 < a_p < 2.96$, $0.03 < e_p < 0.1$ and $0.12 < \sin i_p < 0.2$. Notice that the V-shape of Eos extends into this population.

We then performed the same procedure of removing family members from the middle and outer belts⁴. For the middle belt we chose to analyze the region with $2.65 < a_p < 2.82$, excluding its innermost part. This choice was made because that part contains the asteroid family of (5) Astraea, which is very disperse and has a large halo, and is crossed by several secular resonances. This makes our identification method useless given that almost all asteroids form a large clump with a small increase of the cut-off velocity. As the middle and outer belts have a much higher number density of asteroids and many more asteroid families than the pristine zone, the application of our method of extending the family membership was more challenging. More families had to be treated together as groups due to their proximity, and the choice of cut-off velocity for each case was not so straightforward. For example, in order to remove asteroids belonging to the family

⁴In some works the outer belt is considered to extend from the 5/2 out to the 2/1 MMRs with Jupiter ($2.82 < a_p < 3.26$ AU). Since in this work we treat the pristine zone separately, we use as the limits of the outer belt the 7/3 and 2/1 MMRs with Jupiter ($2.96 < a_p < 3.26$ AU)

Tab. A.1.: Number of asteroids classified as family members and background objects according to Milani et al. (2016) and our method.

	Milani et al. 2016	Extended families	Extended families + Eos members
Family members	8430	13839	15533
Background	13122	7713	6019
Total		21552	

of (221) Eos, as we increase the cut-off velocity the families of (179), (283), (507), (8737) and (21885) were merged with (221) resulting in a big cluster of ~ 35000 asteroids. Also in the outer belt, in the range $0.35 < \sin i_p < 0.42$, Milani et al. (2014) identified four small families, namely (1101), (3025), (6355) and (10654), whereas by increasing the cut-off velocity we find that almost the whole region merges into one large family. We argue that this new big family is real, based on the apparent half “V-shape” of its members on the (a_p, H) plane (see Figure A.5), a characteristic of asteroid families and not of random samples of asteroids. The size distributions of the family members and background asteroids for the middle and outer belts are shown in Figure A.6 and Figure A.7 respectively.

A.3 Background asteroids vs. rogue family members

The first piece of statistical information we can extract from the size distributions obtained, is which fraction of the background population is made of primordial asteroids and which of collisionally generated ones. To do this we turn our attention to the size distributions of background objects in the three regions as shown in Figure A.8. To compare the three regions we study here, we normalized the populations of asteroids in the three regions in terms of the orbital volume they contain, essentially dividing the number of asteroids in each region with its corresponding semi-major axis range. In the bottom panel of Figure A.8 we show the absolute magnitude distributions of background asteroids per AU for the middle belt, the pristine zone and the outer belt. The first thing we notice is that the total number of asteroids in the middle and outer belts is substantially larger than that in the pristine zone. This result was expected, as in the more populous regions of the main belt we can’t remove all family members by applying the HCM, but the consequence is rather surprising: More than 80% of what we would consider as the “background” population of the middle and outer belts is in fact rogue family members, as the

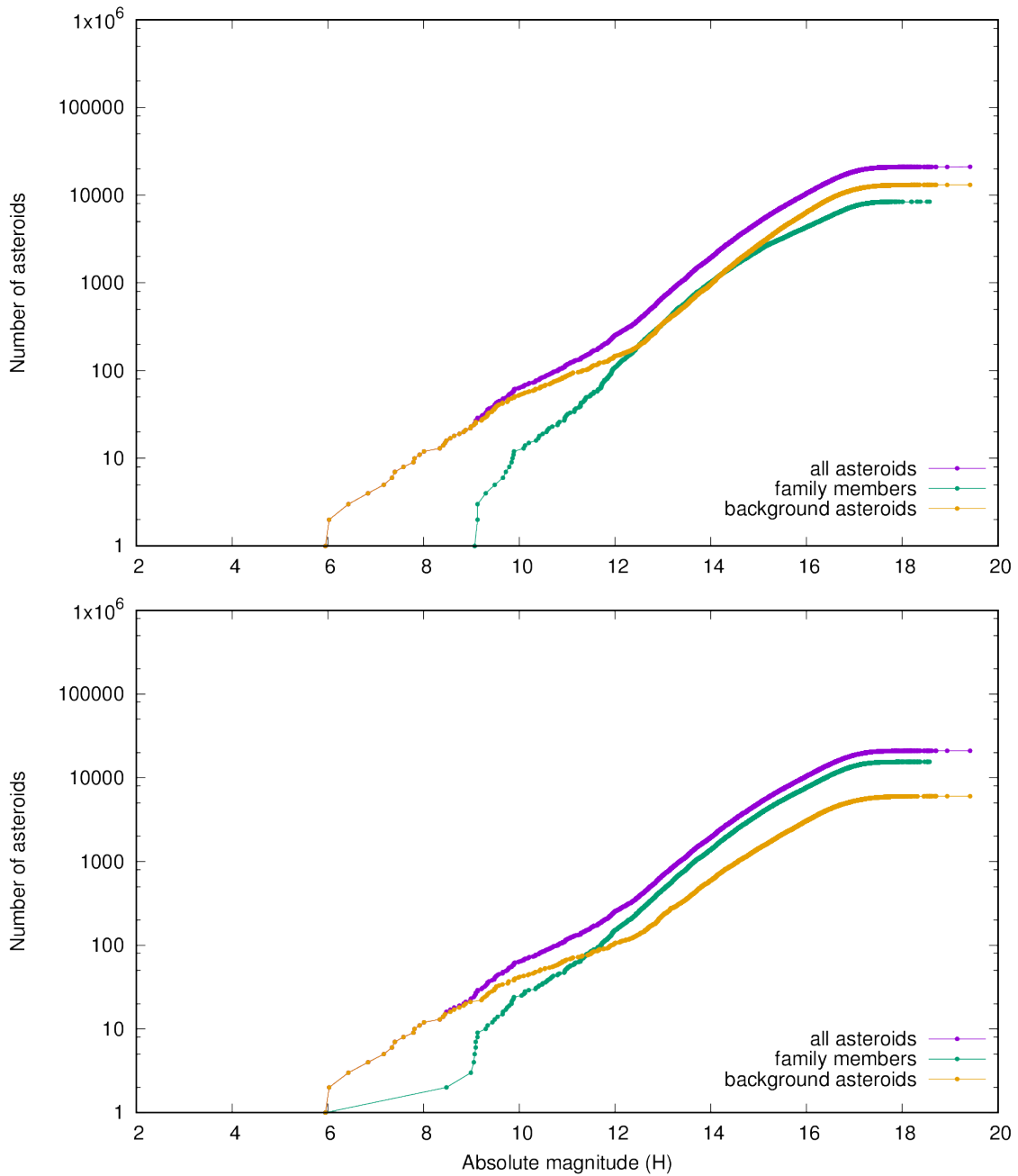


Fig. A.4.: Cumulative size distribution of asteroids in the pristine zone according to the classification of Milani et al. (2014) (top) and the one in this work (bottom). The colors represent: all asteroids (purple), asteroid family members (green) and background objects (orange).

number of asteroids per astronomical unit in these regions is about seven times larger than in the pristine zone. Zappala and Cellino (1996) predicted, based on the difference in the slopes of the SFDs of family members and background asteroids, that more than 90% of discovered small asteroids should belong to asteroid families. Our result not only verifies, but also reinforces their prediction, as we find that

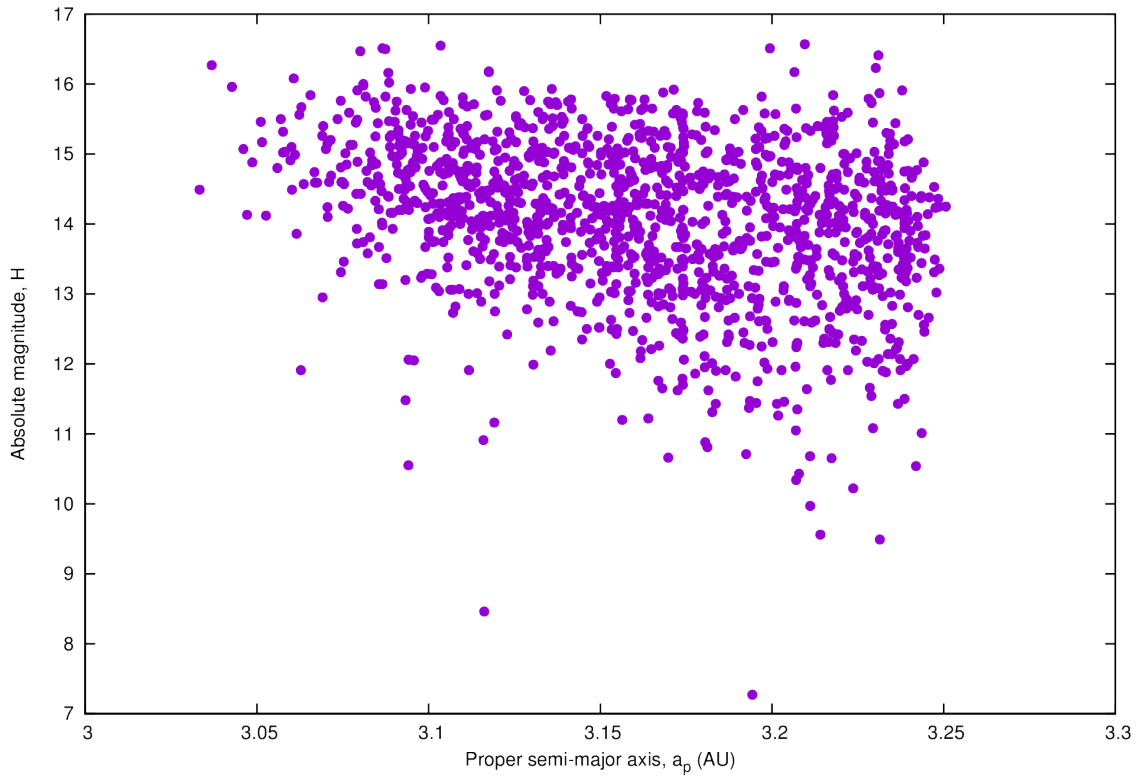


Fig. A.5.: The distribution of asteroids of the family around (892) Seeligeria on the (a_p, H) plane. Note the apparent left half of a V-shape.

even our aggressively obtained background consists in fact mainly of collisionally generated asteroids. This means that the vast majority of the asteroids we currently observe in the main belt, even when they are not identified as family members, are products of collisional evolution, rather than primitive bodies.

A.4 The collisional history of the main-belt

Figure A.8 reveals two key aspects regarding our study of the primordial distribution of main-belt asteroids: The first is that the magnitude distributions of the background population in the middle and pristine zones share the same qualitative characteristics, especially in the range $9 < H < 12$ of absolute magnitudes, as their slopes in this range are $q_{mid} \simeq 4.8$ for the middle belt and $q_{pri} \simeq 5.2$ for the pristine zone. The second, obviously but equally important aspect, is that they differ from the size distribution of the outer belt, as the latter has a slope of $q_{out} \simeq 7$ in the same range of absolute magnitudes.

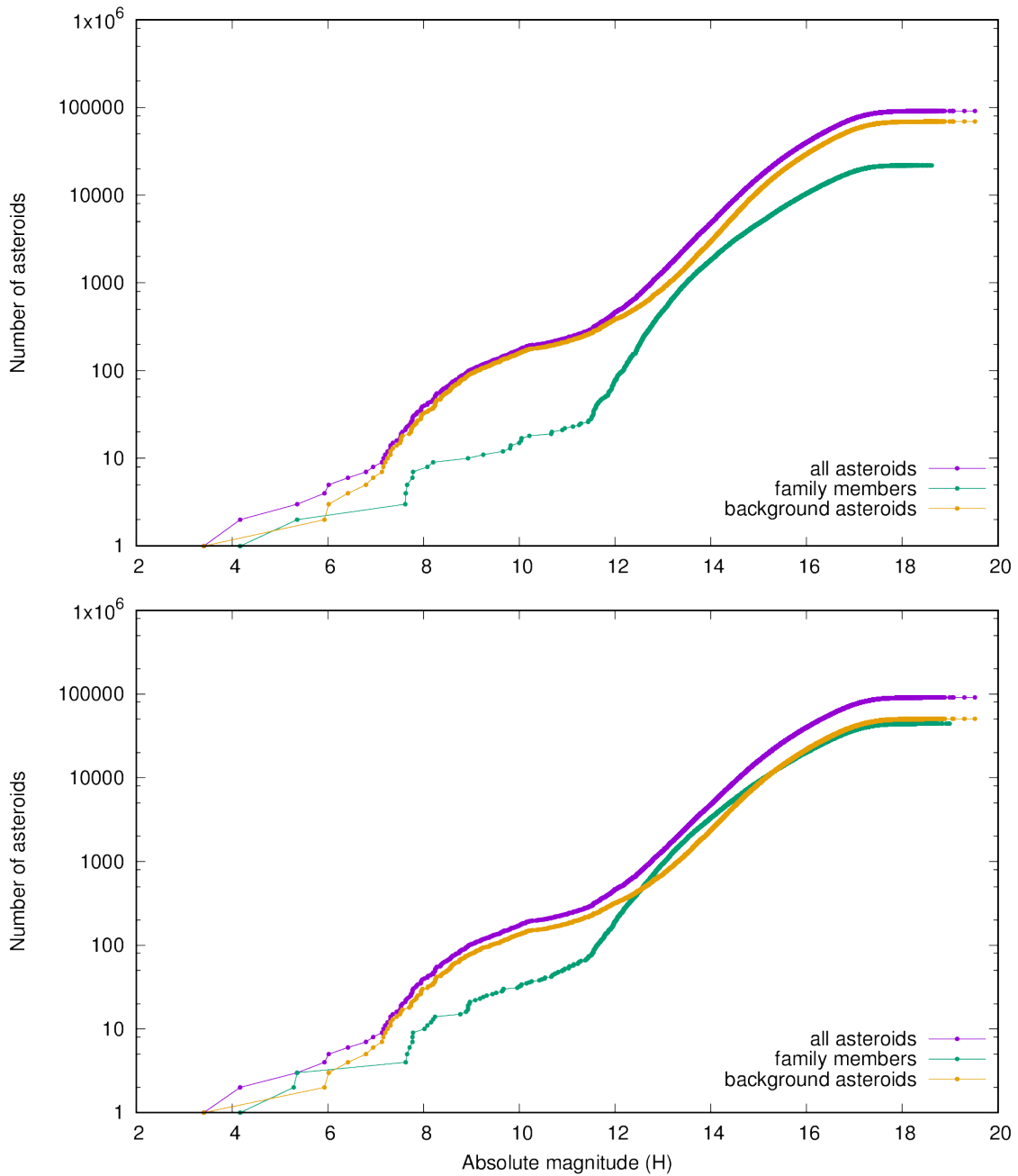


Fig. A.6.: Same as Figure A.4 for the middle belt

The first aspect is a strong suggestion that the background population of the pristine zone we have obtained should reflect the size distribution of primordial asteroids with $H < 12$. This claim is also supported by the fact that the composite magnitude distribution of family members in the pristine zone differs drastically from the one of the background (Figure A.4). This confirms that the families in the pristine zone have been adequately removed, and do not contaminate the background significantly.

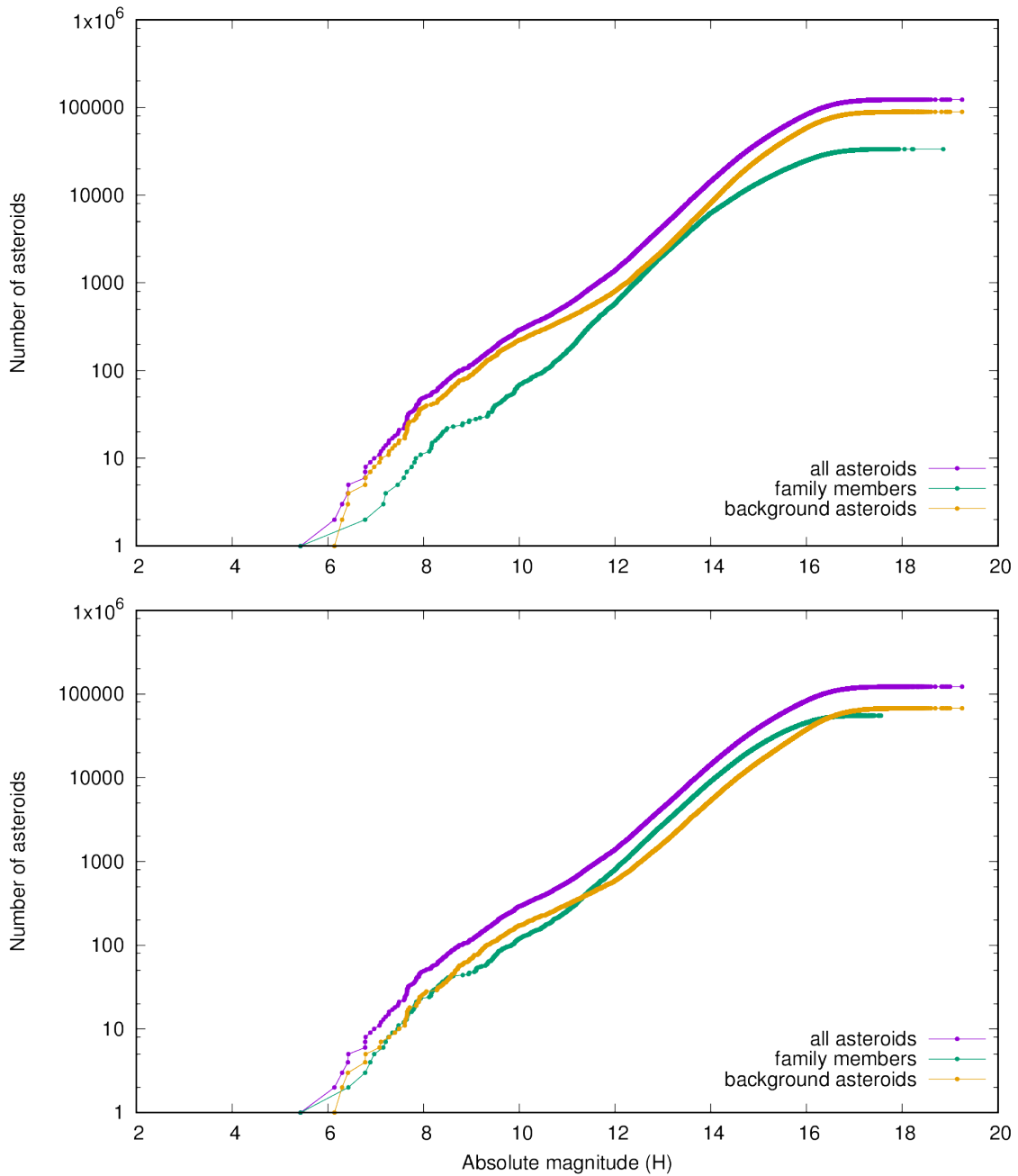


Fig. A.7.: Same as Figure A.4 for the outer belt

The second aspect actually concerns not only the background populations, but also the SFD of all families together, as evident when comparing Figure A.6 and Figure A.7, where we see that not only the backgrounds but also the composite populations of family members in the three regions have different magnitude distributions. As we explained above, the asteroids originating from family creating events dominate the populations in the middle and outer belts, and as a consequence the background size distributions in each region. This means that the difference

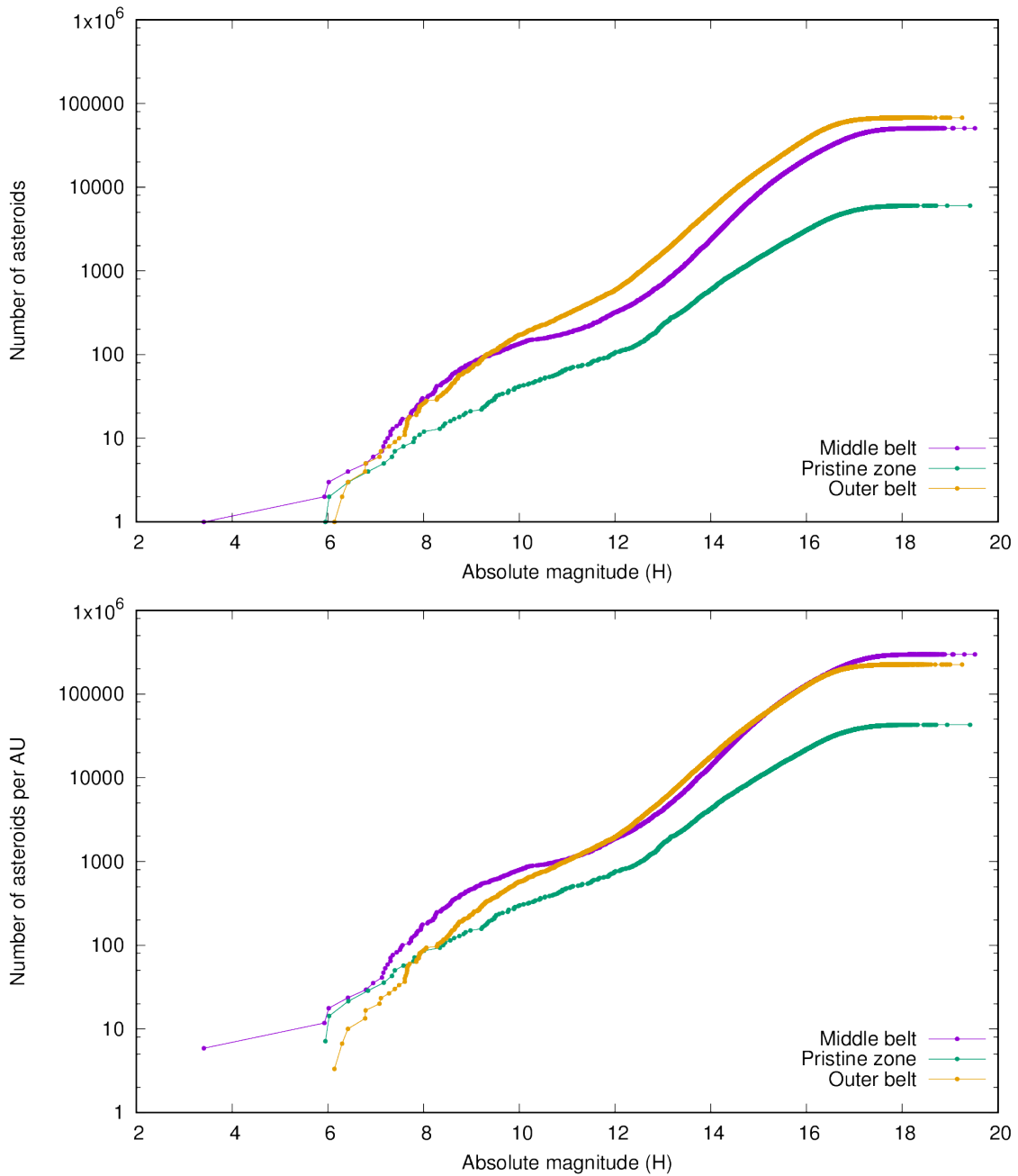


Fig. A.8.: The cumulative absolute magnitude distribution of background asteroids in the three regions. In the bottom panel the population of each region is normalized in terms of semi-major axis.

in the shape of the size distributions of the middle and outer belts should reflect different collisional records. Thus, we seek the cause of the difference in the distributions of the populations of the middle and outer belts by looking into the individual families therein. According to Durda et al. (2007) the conditions and

scale of the family forming event (e.g. cratering vs. catastrophic event⁵, impactor velocity and incident angle, size ratio etc.) are reflected on the SFD of family members.

Using the asteroid family classification of Milani et al. (2014, 2016) we produced the absolute magnitude distributions for each family in the middle (Figure A.9) and outer belts (Figure A.10). There is a key difference in the size distributions of asteroid families in the two regions: In the middle belt, all the families with large parent bodies are cratering events, whereas all catastrophic families have parent bodies with $H > 10$. On the contrary, in the outer belt there are two families with large parent bodies, those of (221) Eos and (24) Themis, which are of the catastrophic type. What this means is that in the middle belt there was no collisional event capable of producing a significant number of asteroids larger than magnitude $H=12$, as can be seen in Figure A.9. Only the families of (10) Eunomia and (170) Maria have some small contribution of larger asteroids, as even these asteroids are smaller than magnitude $H=10$. On the other hand, the two aforementioned fragmentation families in the outer belt, have a substantial number of members in the ($9 < H < 12$) range of absolute magnitudes, as shown in Figure A.10, dominating in this way the composite size distributions of family members and consequently the contaminated “background” population.

By removing from the composite population of family members the ones originating from these two large catastrophic families, we can verify that they are the sole reason for the observed difference in the magnitude distributions between the middle and outer belt. Indeed, as shown in Figure A.11, the removal of the families of Eos and Themis gives a size distribution of family members with much shallower slope in the ($9 < H < 12$) range, resembling that of the middle belt.

Based on the above we can reach two important conclusions: The magnitude distribution of background asteroids in the pristine zone reflects qualitatively that of the primordial population of main-belt asteroids in the range $9 < H < 12$. This is based on the facts that in this range the asteroid families in the pristine zone have a completely different distribution from the background; Moreover it is similar to

⁵Asteroid families are usually classified as being of the cratering type, if the volume of the largest remnant is much larger than the sum of the volumes of the rest of the family members ($> 90\%$), suggesting that the family was formed from material excavated from a relatively small crater on the parent body. If, on the other hand, the volume of the largest remnant is comparable to the sum of the volumes of the other family members ($< 90\%$), the asteroid family is classified as being of the catastrophic or fragmentation type. In this case the family-forming impact was severe enough to completely fragment the parent body. The value of 90% used for the ratio of the volumes to distinguish between the two types is used conventionally.

the magnitude distribution of the background population in the middle zone in the same H-range and the difference with that of the outer zone is fully understood by the contamination from the catastrophic large-parent body families of Eos and

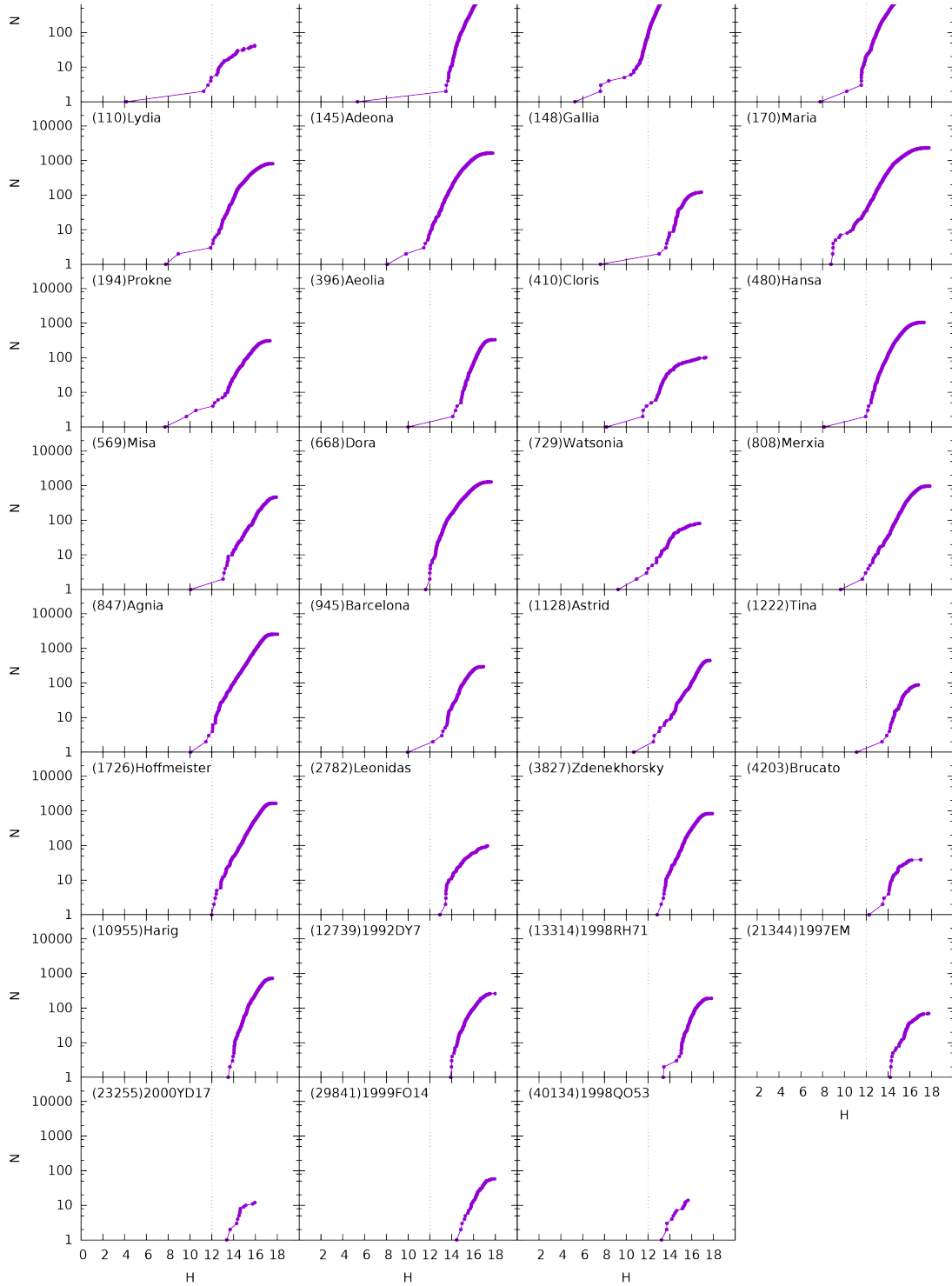


Fig. A.9.: Absolute magnitude distributions of the asteroid families in the middle belt.

Themis. As a consequence of this, we can draw the second conclusion, that is: There are no large ancient families of the catastrophic type which are not yet identified in the middle or pristine zone. We cannot claim the same for the outer belt; The

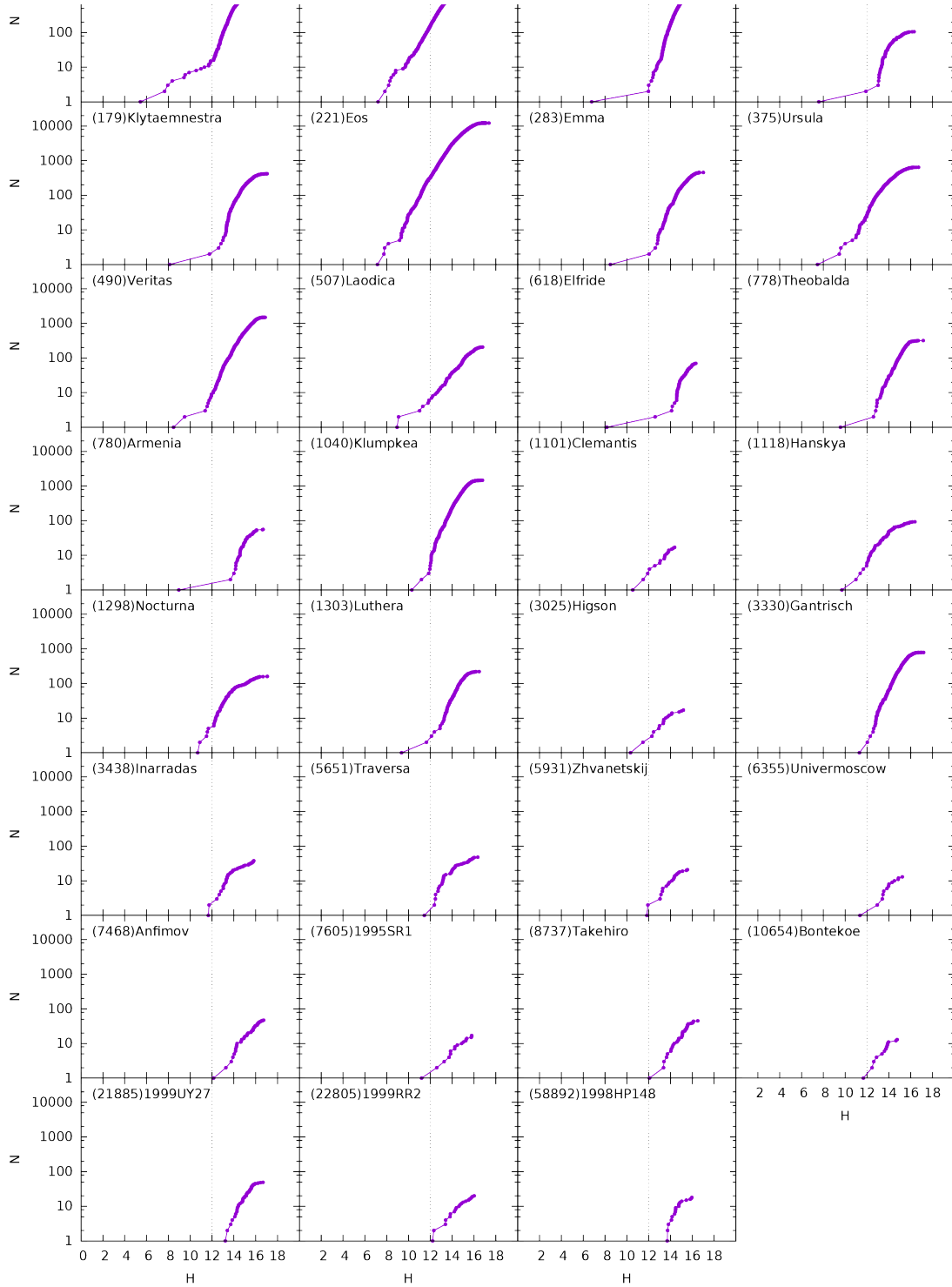


Fig. A.10.: Absolute magnitude distributions of the asteroid families in the outer belt.

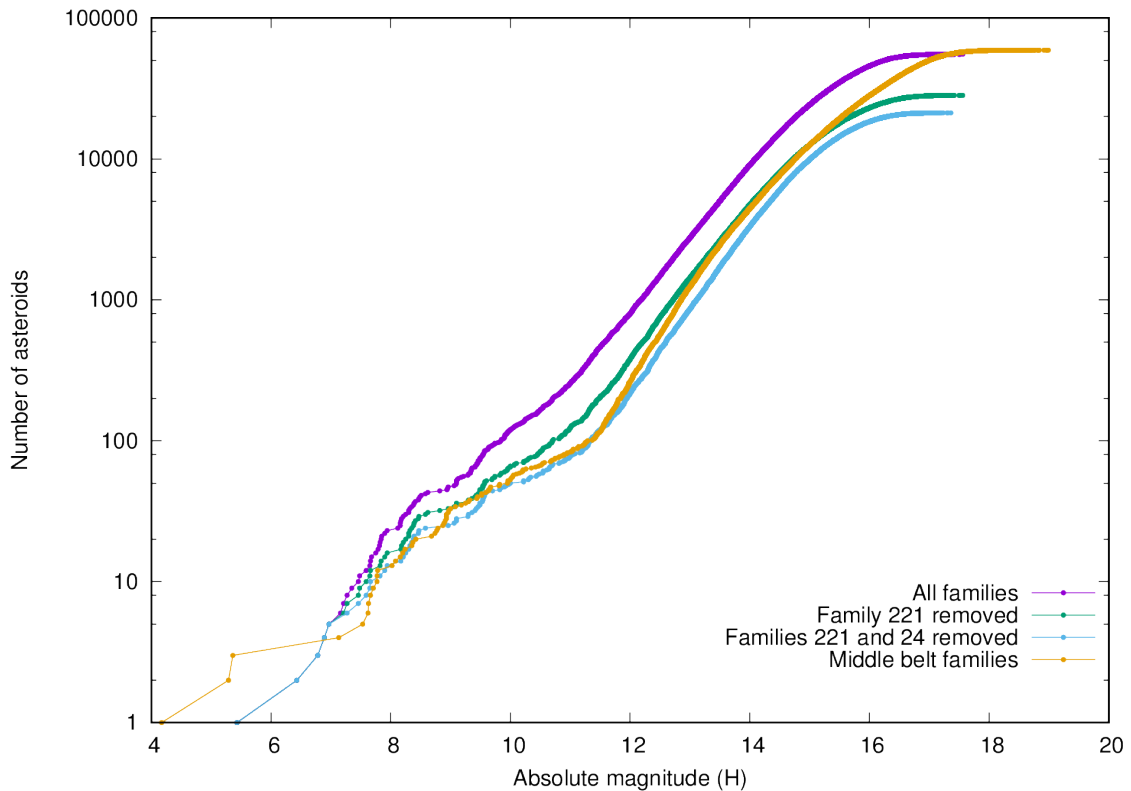


Fig. A.11.: Composite size distribution of the outer belt asteroid family members after removing the two big catastrophic type families Eos and Themis

catastrophic families of Eos and Themis, as we have shown, are responsible for the contamination of the background population with $H < 12$, but they might not be solely responsible. We cannot exclude the potential existence of another large unidentifiable family whose signature in the SFD has been overwritten by Eos and Themis.

A.5 The size distribution of the primordial asteroid population

Even though we are confident that the background population of the pristine zone is not contaminated significantly by rogue family members in the range $9 < H < 12$, we know that it still does not represent exactly the primordial population of asteroids. The reason for this is that the background population we observe today has undergone both collisional and dynamical evolution over the age of the Solar System, causing a number of asteroids to be removed from the region. As a

consequence, the slope of the primordial population of asteroids must have been steeper than the current one. In order to constrain the primordial slope, we need to quantify the effects of the collisional and the dynamical evolution, and compensate for them.

We start by computing the cumulative size distribution from the magnitude distribution, making use of the formula $D(km) = \frac{1329}{\sqrt{p_v}} 10^{-0.2H}$ (Fowler and Chillemi, 1992) and adopting a mean albedo of ($p_v = 0.092$), as used in Bottke et al. (2005b). Doing this we obtain Figure A.12, where the cumulative size distribution of the background is shown in purple. The range $9 < H < 12$ corresponds to approximately $17.5 < D(km) < 70$, and can be fit with a power law function with a slope $q \simeq -1$. Then, to compensate for the collisional erosion, we take into account the probability for an asteroid of a given size to have been catastrophically disrupted over the age of the Solar system. For this we need to use the collisional probabilities of asteroids in the pristine zone. Since the pristine zone appears to be a special region of the Main-Belt, it is not straightforward how to obtain these. One approach is to use the mean collisional probabilities of different diameter main-belt asteroids taken from Bottke et al. (1994) (with updated collision frequencies kindly provided to us by the author). However, due to the fact that the number density of asteroids in the pristine zone is lower than the average of the main-belt, we expect the collisional probabilities therein to be different. Therefore, we need to calculate a new set of collisional probabilities for the pristine zone specifically. Indeed, we calculated the collisional probabilities for target asteroids residing in the pristine zone, with the same sizes as those in Bottke et al. (1994), and found them to be almost half as high. The two different sets of collisional probabilities will give different corrections to the slope of the size frequency distribution, as we will discuss later on.

We are now able to correct the slope of the cumulative size distribution, to better reflect the actual primordial size-distribution of planetesimals smaller than 70 km. To do so we use the following idea: The difference in lifetime of asteroid populations with different diameters leads to a difference in the rate at which these populations decay collisionally over time, and consequently the size distribution should be corrected accordingly.

For each diameter bin of Table A.2 we set up a simple Monte Carlo run of 100,000 test particles, that simulates the collisional decay over the age of the Solar system based on the respective lifetime. The result is a factor $f_c(D)$ by which the observed population at each bin should be multiplied to compensate for the collisional grinding that has taken place.

Tab. A.2.: Sample absolute magnitudes and computed diameters and lifetimes.

Absolute magnitude (H)	Diameter (Km)	Lifetime (My)
13.25	9.8092	4725.3
12.75	12.349	4995.9
12.25	15.547	5235.3
11.75	19.572	5693.0
11.25	24.64	6572.1
10.75	31.019	8266.1
10.25	39.051	10916.0
9.75	49.162	14984.9
9.25	61.892	20797.9
8.75	77.917	27593.9
8.25	98.092	33703.9
7.75	123.49	34905.0

Another effect that has to be taken into account for the correction of the primordial size distribution of asteroids is the dynamical depletion. Over time, asteroids in the pristine zone drift secularly in semi-major axis due to the Yarkovsky effect, until they reach the powerful MMRs bounding the region, at which point they are ejected ⁶. This means that the initial population of asteroids in the pristine zone must have been larger than the current one. To compensate for this effect we devised another Monte Carlo scheme: For each diameter bin we create 10,000 fictitious asteroids with random initial conditions (a, e, i) and random spin-axis obliquities (γ) in the pristine zone. Then assuming a typical maximum drift speed of $(da/dt)_{max} = 3 \cdot 10^{-4} AU/Myr$ for an asteroid with $D=1$ km, each asteroid will drift over 4 billion years a distance: $4 \cdot 10^3 \times 3 \cdot 10^{-4} \times \cos(\gamma) \times D^{-1} AU$. We thus obtain the fraction of asteroids that have escaped the pristine zone and we can compute the corresponding correction due to the dynamical depletion $f_d(D)$.

Having obtained the corrections for both the collisional and the dynamical depletion of the primordial asteroid population in the pristine zone, we can compute the corrected size distribution. From the cumulative SFD of the pristine zone's background population we build the incremental size distribution, using the bins in diameter from Table A.2. Then we multiply the population in each bin by the corresponding factor $f(D) = 1 + f_c + f_d$, and compute the new corrected cumulative distribution as shown in Figure A.12 (upper ends of error bars). These points give a slope: $q_{high} \simeq -1.50$. Using the collisional probabilities for target asteroids in the

⁶We ignore here other dynamical effects, given that in the pristine zone there are no important resonances, capable of contributing significantly in the depletion of asteroids.

pristine zone, which are only half as high as those given in Table A.2, the collisional lifetimes will be twice as long. Following the same procedure as before we find the second corrected SFD (lower ends of error bars) which has a slope: $q_{low} \simeq -1.38$. The true collisional probabilities for each target diameter should be between these two values, and we select the arithmetic mean as the nominal ones, from which we obtain our final corrected slope of the primordial SFD: $q_c = -1.43^{+0.07}_{-0.05}$, as shown in green in Figure A.12.

Our computation, despite our efforts has some shortcomings that may affect the value of the slope we obtain for the primordial SFD. One shortcoming is that the removal of asteroid family members can never be perfect. Even in the pristine zone, where the families are few and well separated, there should be a small number of asteroids originating from collisions that are unidentifiable as family members by HCM. Still the value we obtained can be considered an upper bound to the slope of the primordial SFD.

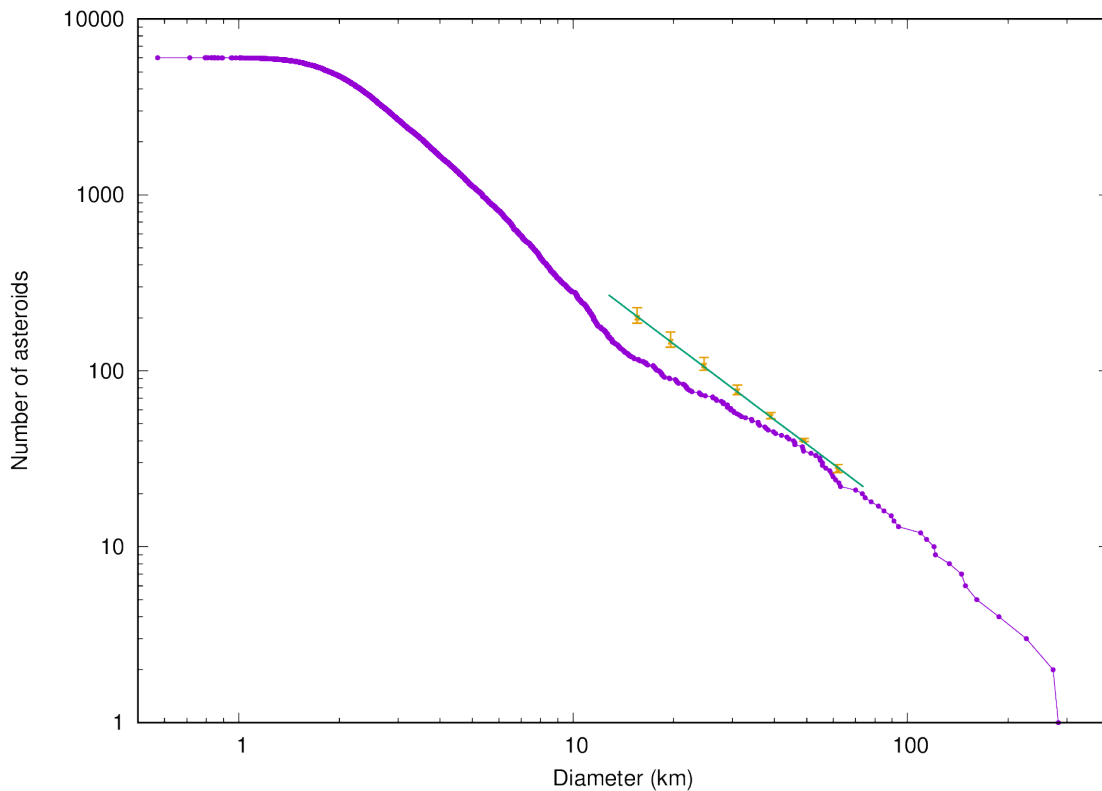


Fig. A.12.: Purple: The size distribution of the background population of the pristine zone, Orange: The values at each bin after applying the corrections described in the text, and Green: The power law function fitting the corrected SFD in the range $17.5 < D(km) < 70$, with a slope of $q_c = -1.43^{+0.07}_{-0.05}$

A.6 Conclusions

In this work, we believe to have found evidence, by removing asteroid family members, that the primordial slope of the asteroids' SFD with $D < 70km$ was much shallower than the current one. This is in agreement with the predictions of Bottke et al. (2005b). We give, for the first time, an estimate of what that slope should have been, i.e. $q_c = -1.43^{+0.07}_{-0.05}$. This is significantly shallower than the current slope of -1.8, which is also the slope predicted by streaming instability simulations. However, it is not clear to which size range the slope found in those simulations applies to. The fact that the slope we measured below 70 km is shallower, suggests that the streaming instability slope (-1.8 for the cumulative distribution) applies for bodies larger than this threshold size, and that below 70 km the streaming instability process may be less efficient (Klahr et al., 2016). Moreover, by comparing the SFD in the outer belt to those of the two other zones, we see exactly what Bottke et al. (2005b) predicted: namely, that the SFD below the primordial “knee” (here at $D = 70km$) grew through catastrophic break-ups of the primordial asteroids with $D > 70km$. Here, we identified Eos and Themis to be the responsible for the increase of the SFD exponent in the outer zone. The fact that families contaminate substantially the background, steepens the asteroid SFD as a whole.

An interesting point arises in view of these results, that is which specific epoch in the evolution of the Main Belt, as part of the Solar System, corresponds to the designation “primordial” in the context of our work. Essentially the evolution of the population of large asteroids ($9 < H < 12$ as discussed) should be size independent, given that the Yarkovsky effect is practically zero for these asteroids, and all other processes (depletion, implantation, excitation) are indeed size independent. Therefore the remaining question regarding the exact definition of the primordial SFD in terms of which era we are talking about, has to do with the last possible mixing of asteroids in semi-major axis, as this defines our zones. The Grand Tack (Walsh et al., 2011) is indeed the last large-scale process the Solar system suffered that resulted in a mixing of asteroids with respect to their semi-major axis. The giant planet instability (Levison et al., 2011; Tsiganis et al., 2005) that happened after that is known to cause mixing only in the eccentricities and inclinations of asteroids, but this does not change the population within each of the three zones as we use them. Therefore by primordial we refer to the post Grand Tack state of the Solar System which coincides with the time of the depletion of the gas nebula.

Secondly, we found evidence that no catastrophic disruption of large ($D > 70km$) asteroids ever occurred in the middle and pristine zone. In fact, if this had happened in the primordial times, even if the corresponding family would have been dispersed in eccentricity and inclination, the imprint in the global SFD of the region would still be visible. This gives very important information on the asteroid belt collisional grinding in the old times. Let's assume here that the asteroid belt was substantially reshuffled in eccentricity and inclination about 4 Gyr ago, when the giant planets underwent a dynamical instability. Then, for large families like Eos and Themis, we can say that those that formed less than 4 Gyr ago are identifiable today and those that formed before are not, at least in the middle and pristine zones. We have 2 families formed in the last 4 Gyr in 3 out of 3 zones (Eos and Themis) and no comparable families formed before 4 Gyr ago in 2 out of 2 zones (for the outer belt we cannot exclude that there are no additional families). Thus, the cumulative collisional evolution in the first 0.5 Gyr had to be less than that of the last 4 Gyr (for an equal cumulative collisional evolution we would expect $\frac{2}{3} \cdot 2$ families and we see none). This, again, is in perfect agreement with Bottke et al. (2005b) and strongly suggests that the asteroid belt either was never massive or it was dynamically depleted very quickly (Morbidelli et al., 2015). Of course, if the giant planet instability happened early (i.e. just after the removal of the gas from the disk, ~ 4.5 Gyr ago), this constraint becomes much less significant.

Finally we have shown that the designation “pristine zone” for the region of the main-belt with $2.82 < a_p < 2.96$ is at least inaccurate. If fragments originating from the neighboring asteroid family of Eos can cross the 7/3 MMR with Jupiter and contaminate the region, it is safe to deduce that the “barrier” formed by this resonance is not completely impenetrable, but rather acts as an attenuator. Thus, not only the identified Eos members, but also background asteroids of the two regions can migrate due to the Yarkovsky effect across the resonance. If this is the case, the question why the “pristine zone” has a much lower number density of asteroids compared to the neighboring regions, remains open.

List of Figures

1.1	The geometrical relationship among the osculating, free and forced eccentricities and longitudes of pericenter (From Murray and Dermott (1999))	7
1.2	The frequency response of the digital filter used in the 2 Myrs integrations.	12
1.3	Comparison of osculating versus proper elements of the population of asteroids with $H < 15$ in the Main Belt.	13
1.4	The number of clustered asteroids as a function of the distance threshold for an example case.	17
1.5	The locations of secular resonances of degree 2 and 4 for eccentricity $e = 0.1$ in the Main Belt, from Milani and Knežević (1990)	22
1.6	Distribution of the members of the (434) Hungaria asteroid family in the $(a_p, 1/D)$ plane, from Spoto et al. (2015).	26
2.1	Distribution of the Hoffmeister family members in the proper semi-major axis versus sine of proper inclination plane $(a_p, \sin i_p)$. The shaded part highlights the excited in inclination inner part of the family.	29
2.2	Number of associated asteroids versus distance threshold(d_c) for the Hoffmeister asteroid family.	30
2.3	Initial equivelocity ellipse (dark red line) plotted in the (a_p, e_p) and $(a_p, \sin(i_p))$ planes. Background grey dots represent the family identified using the HCM for a distance threshold of 35 m/s. The ellipse is obtained assuming an initial ejection velocity of 40 m/s, a mean anomaly of 90° , and an argument of pericenter of 330°	36
2.4	Comparison between the distribution of the real family members (red), and the test particles after 150 Myrs of the simulation (green).	39
2.5	Comparison between the distribution of the real family members (red), and the test particles after 150 Myrs of the simulation (green), with Ceres included in the model.	40

2.6	In the left panels a comparison between the distributions of the test particles in the two models (red points correspond to the model containing Ceres while gray points to the one without it) is shown for two times, 15 Myrs (top) and 145 Myrs (bottom). In the right panels the test particles of the simulation that includes Ceres are compared to the real family members at the same times.	41
2.7	Example of a test particle crossing the 1/1 MMR with Ceres. The black line mapped on the left y-axis shows its semi-major axis drifting due to the Yarkovsky effect, whereas the red points mapped on the right y-axis show its mean inclination.	42
2.8	Example of a test particle suffering a close encounter with Ceres. The black line mapped on the left y-axis shows its semi-major axis drifting due to the Yarkovsky effect, whereas the red points mapped on the right y-axis show its mean inclination. The highlighted region and the sudden increase of the semi-major axis therein correspond to a close encounter with Ceres.	43
2.9	The proper frequencies of the test particles representing the Hoffmeister family. The lines denote the solutions for which alignment of the test particles implies interaction with the z_1 and $s - s_c$	44
2.10	Example of a test particle crossing the $s - s_c$ secular resonance. In the top panel we show the evolution of the critical angle $\sigma = \Omega - \Omega_c$. In the bottom panel we show the evolution of the mean inclination in red dots. The black line shows an average of the mean inclination for clarity. The shaded regions correspond to the time of libration of the critical angle.	45
2.11	Evolution of the orbital elements of three example particles on the $(a_p, \sin i_p)$ plane on the left, and on the (a_p, e_p) plane on the right. Yellow points denote evolution under the influence of the Yarkovsky effect only, red points denote interaction with the $s - s_c$ secular resonance (red lines), blue points denote interaction with the z_1 secular resonance (blue lines), while gray points show the final snapshot of the evolution of the entire population. Black dashed lines show the locations of MMRs.	47
2.12	The division of the $(a_p, \sin(i_p))$ into bins for the estimation of the family age.	48

2.13	Estimation of the age of the Hoffmeister asteroid family. The black crosses show the calculated values of ψ as a function of time and the solid black line the fitted 10 th degree polynomial. The vertical dashed line denotes the location of the global minimum of the polynomial at $\sim 156 Myrs$ and the gray shaded region the standard deviation of $\pm 20 Myrs$	49
2.14	The location of the v_{1c} secular resonance on the $(a_p, \sin i_p)$ plane. Solid lines represent the analytical solution for different values of the eccentricity (see legend). The colored dots show the resonant asteroids within $0.2''/yr$, while the different colors correspond to values of eccentricity centered to those of the analytical solutions and spanning 0.05 in each direction	54
2.15	The location of the v_{1c} secular resonance on the (a_p, e_p) plane (top), and on the $(a_p, \sin i_p)$ plane (bottom). The gray dots represent all main belt asteroids, and the colored points the resonant ones for different inclinations (top panel) and eccentricities (bottom panel) according to the respective color codes given in the legend.	55
2.16	The location of the v_c secular resonance on the (a_p, e_p) plane (top), and on the $(a_p, \sin i_p)$ plane (bottom). The gray dots represent all main belt asteroids, and the colored points the resonant ones for different inclinations (top panel) and eccentricities (bottom panel) according to the respective color codes given in the legend.	56
2.17	The location of the v_{1v} secular resonance on the (a_p, e_p) plane (top) and on the $(a_p, \sin i_p)$ plane (bottom). The gray dots represent all main belt asteroids, and the colored points the resonant ones for different inclinations (top panel) and eccentricities (bottom panel) according to the respective color codes given in the legend.	57
2.18	The location of the v_v secular resonance on the (a_p, e_p) plane (top), and on the $(a_p, \sin i_p)$ plane (bottom). The gray dots represent all main belt asteroids, and the colored points the resonant ones for different inclinations (top panel) and eccentricities (bottom panel) according to the respective color codes given in the legend.	59
2.19	The location of the groups of initial conditions for the simulations about the v_{1c} secular resonance on the (a_p, e_p) plane. The gray dots represent all main belt asteroids, and the colored points the resonant ones for different inclinations according to the color code. Black circles denote the location and black arrows the Yarkovsky drift direction of each group of initial conditions.	61

- 2.20 Orbital evolution due to the secular resonance ν_{1c} for the three representative regions. Top: low inclination middle belt, Mid: high inclination middle belt, Bottom: high inclination outer belt. Left panels: In black the evolution of the critical angle $\sigma = \Omega - \Omega_c$ of a test particle. The red line shows the evolution of the sine of proper inclination of the same test particle with Ceres included in the model. The blue line shows the evolution of the proper inclination of the same test particle without Ceres in the model. Right panels: The evolution of the 20 test particles of the whole group in the two dynamical models, red with Ceres and blue without. 62
- 2.21 Orbital evolution due to the secular resonance ν_c for the three representative regions. Top: low eccentricity middle belt, Mid: high eccentricity middle belt, Bottom: outer belt. Left panels: In black the evolution of the critical angle $\sigma = \varpi - \varpi_c$ of a test particle. The red lines show the evolution of the proper eccentricity of the same test particle with Ceres included in the model. The blue lines show the evolution of the proper eccentricity of the same test particle without Ceres in the model. Right panels: The evolution of the 20 test particles of the whole group in the two dynamical models, red with Ceres and blue without. 64
- 2.22 Orbital evolution due to the secular resonance ν_{1v} for the three representative regions. Top: low inclination inner belt, Mid: high inclination inner belt, Bottom: high inclination middle belt. Left panels: In black the evolution of the critical angle $\sigma = \Omega - \Omega_v$ of a test particle. The red line shows the evolution of the sine of proper inclination of the same test particle with Vesta included in the model. The blue line shows the evolution of the proper inclination of the same test particle without Vesta in the model. Right panels: The evolution of the 20 test particles of the whole group in the two dynamical models, red with Vesta and blue without. 65
- 2.23 Orbital evolution due to the secular resonance ν_v for the inner belt. Left panel: In black the evolution of the critical angle $\sigma = \Omega - \Omega_v$ of a test particle. The red line shows the evolution of the proper eccentricity of the same test particle with Vesta included in the model. The blue line shows the evolution of the proper eccentricity of the same test particle without Vesta in the model. Right panel: The evolution of the 20 test particles of the whole group in the two dynamical models, red with Vesta and blue without. 66

2.24	Asteroid families crossed by the secular resonance ν_{1c} with Ceres. Gray dots represent all main belt asteroids, and blue dots those who belong to asteroid families. The red points represent resonant asteroids belonging to asteroid families (highlighted in black boxes).	68
2.25	Asteroid families crossed by the secular resonance ν_c with Ceres. Gray dots represent all main belt asteroids, and blue dots those who belong to asteroid families. The red points represent resonant asteroids belonging to asteroid families (highlighted in black boxes).	69
2.26	Asteroid families crossed by the secular resonance ν_{1v} with Vesta. Gray dots represent all main belt asteroids, and blue dots those who belong to asteroid families. The red points represent resonant asteroids belonging to asteroid families (highlighted in black boxes).	70
2.27	Asteroid families crossed by the secular resonance ν_v with Vesta. Gray dots represent all main belt asteroids, and blue dots those who belong to asteroid families. The red points represent resonant asteroids belonging to asteroid families (highlighted in black boxes).	71
2.28	Number of associated asteroids versus distance threshold(d_c) for the Seinajoki asteroid family.	73
2.29	Distribution of geometric albedos of the members of the Seinajoki asteroid family.	74
2.30	Distribution of the members of the Seinajoki asteroid family with available SDSS color data, in the proper elements space. Each asteroid is represented by its taxonomic type letter.	75
2.31	Top : The distribution of the nominal Seinajoki family members in the proper semi-major axis versus the proper inclination plane; Bottom : The distribution of the test particles after 150 Myr of the evolution. The black points represent particles integrated within the model without Ceres, while the gray points denote particles simulated using the dynamical model that also includes Ceres as a perturbing body. The solid and two dashed curves mark the center and the borders of the $s - s_c$ resonance, respectively.	78
2.32	Snapshots of the distribution of test particles on the $(a_p, \sin i_p)$ at 100 Myr (Top) and 200Myr (Bottom)for the two dynamical models: with four planets (Red) and with seven planets (Blue)	79
2.33	Same as Figure 2.31 but for the Astrid family.	80
2.34	Histogram of the albedos of Astrid family members. The red line denotes the albedo of the parent body, asteroid (1128) Astrid.	81
3.1	Geometric albedo distribution of asteroids in the Phocaea region.	86

3.2	Properties of low-albedo asteroids in the Phocaea region. <i>Top-left panel:</i> Proper semi-major axis versus sine of proper inclination projection of the dark asteroids in the Phocaea region (black dots), and Tamara family members (red dots); <i>Top-right panel:</i> Histogram of orbital inclinations of dark Phocaeas; <i>Bottom-left panel:</i> Number of asteroids associated with the family as a function of distance threshold; <i>Bottom-right panel:</i> The cumulative magnitude distribution of the Tamara family (red dots), and its the best-fitting line (black solid line). The dashed area indicates the interval used for the fitting.	87
3.3	Proper semi-major axis versus the inverse diameter for the members of the family. The dashed and solid lines correspond to the initial and final V-shape fit, respectively. Red dots mark the outliers removed from the fit after the first iteration.	91
3.4	The evolution of the Tamara family in the space of proper orbital elements. The four panels in each column show the distribution of the test particles after 50, 100, 150 and 200 Myr (from top to bottom) of evolution. The red and blue lines mark perihelion distances q of 1.666, 1.3 AU, respectively.	94
3.5	The Tamara asteroid family as a source of NEOs. The cumulative number of test particles entering the near-Earth region (bold curve), and the total number of members residing in the near-Earth region at any specific point in time (gray dots).	95
3.6	Distribution of asteroids in the $(e_p, \sin i_p)$ orbital planes, at a sub-region of the Eos family. There is an apparent over-density of asteroids (highlighted with the box), hinting the existence of a young cluster.	98
3.7	The number of asteroids associated to the (633) Zelima cluster as a function of the distance threshold.	99
3.8	Evolution of the mean differences in the secular angles Ω (top) and ω (bottom) of the nominal Zelima cluster members.	102
3.9	Evolution of the mean differences in the secular angles Ω (top) and ω (bottom) of the Zelima cluster members after the three identified interlopers have been removed.	103
3.10	Histogram of the minima of the evaluated Equation 3.1, revealing the calculated age of the cluster.	105
3.11	The cumulative size-frequency distribution of the (633) Zelima cluster members. The sizes of the points are proportional to the diameters of the corresponding asteroids.	106

3.12	Distribution the Zelima cluster members in the $(e_p, \sin i_p)$ (top), $(a_p, \sin i_p)$ (middle) and (a_p, e_p) (bottom) orbital planes. The sizes of the points are proportional to the diameter of each asteroid. The patterned points indicate the identified interlopers. The ellipses in the bottom two panels represent equivelocity curves corresponding to a velocity change of $\Delta v = 12m.s^{-1}$ from the barycenter of the cluster. The vertical lines show the approximate location of the 8J-3S-3 mean motion resonance (see e.g. Gallardo (2014)).	108
3.13	Evolution of the critical argument of z_1 ($\sigma_{z_1} = \Omega + \varpi - \Omega_6 - \varpi_6$) (top), mean inclination (middle) and mean eccentricity (bottom), of the asteroid (633). The solid black lines in the middle and bottom panels are the respective averaged mean elements, and are shown to better appreciate the effect of the resonance , i.e. the induced oscillations.	110
A.1	Asteroids in the pristine zone of the main belt in the proper semi-major axis versus sine of proper inclination plane. Panel a: all numbered and multi-opposition asteroids. The boxes highlight the asteroid families in the region. Panel b: The remaining asteroids after removing the family members according to the classifications of Brož et al. (2013) and Milani et al. (2014, 2016). Panel c: The remaining asteroids after removing family members with our method as discussed in the text. Panel d: Same as panel c, with the asteroids originating from the family of Eos also removed.	132
A.2	The number of asteroids associated to asteroids (16286) and (15477) as a function of cut-off velocity.	133
A.3	The asteroid family of (221) Eos in the proper semi-major axis versus absolute magnitude plane. In purple are the asteroids belonging to the classical family, as identified by Milani et al. (2014), while in green are asteroids in the pristine zone with $2.82 < a_p < 2.96$, $0.03 < e_p < 0.1$ and $0.12 < \sin i_p < 0.2$. Notice that the V-shape of Eos extends into this population.	135
A.4	Cumulative size distribution of asteroids in the pristine zone according to the classification of Milani et al. (2014) (top) and the one in this work (bottom). The colors represent: all asteroids (purple), asteroid family members (green) and background objects (orange).	137
A.5	The distribution of asteroids of the family around (892) Seeligeria on the (a_p, H) plane. Note the apparent left half of a V-shape.	138
A.6	Same as Figure A.4 for the middle belt	139
A.7	Same as Figure A.4 for the outer belt	140

A.8	The cumulative absolute magnitude distribution of background asteroids in the three regions. In the bottom panel the population of each region is normalized in terms of semi-major axis.	141
A.9	Absolute magnitude distributions of the asteroid families in the middle belt.	143
A.10	Absolute magnitude distributions of the asteroid families in the outer belt.	144
A.11	Composite size distribution of the outer belt asteroid family members after removing the two big catastrophic type families Eos and Themis .	145
A.12	Purple: The size distribution of the background population of the pristine zone, Orange: The values at each bin after applying the corrections described in the text, and Green: The power law function fitting the corrected SFD in the range $17.5 < D(km) < 70$, with a slope of $q_c = -1.43_{-0.05}^{+0.07}$	148

List of Tables

2.1	Summary table of the maximal changes in the proper elements of the main belt asteroids caused by the secular resonances with Ceres and Vesta.	66
3.1	Members of the (633) Zelima cluster, and their physical properties ⁷ . .	109
A.1	Number of asteroids classified as family members and background objects according to Milani et al. (2016) and our method.	136
A.2	Sample absolute magnitudes and computed diameters and lifetimes. .	147

A.7 Biography of the author

Georgios Tsirvoulis was born in Katerini, Greece in 1987. After high school he enrolled at the Physics Department of the Aristotle University of Thessaloniki, where he got his degree in physics in 2011, with a major in Astronomy. For his undergraduate thesis, titled "Chaotic diffusion of asteroid orbits", he worked under the supervision of Dr. Kleomenis Tsiganis, leading to the publication of the main results. He then continued his studies at the Department of Physics of the Uppsala University in Sweden, following a master program in Astronomy and Space Physics, under a scholarship from the State Scholarships Foundation of Greece. For his master thesis he worked, in collaboration with Athanasia Toliou, on "The delayed formation of the Oort cloud" under the supervision of Professor Hans Rickman. He received his master degree in 2013, after which he was awarded an FP-7 Marie Curie fellowship, to pursue his PhD studies under the supervision of Dr. Bojan Novaković at the Department of Astronomy, University of Belgrade, while working as an early stage researcher for the "Stardust" Initial Training Network at the Astronomical Observatory of Belgrade, under the supervision of Dr. Zoran Knežević. In the framework of Stardust, he also completed two three-month internships, the first in Pisa, Italy working with Professor Andrea Milani, and the second in Nice, France, working with Alessandro Morbidelli and Marco Delbo. During his doctoral studies he worked on the dynamical evolution of asteroid populations and he co-authored nine scientific articles, two review chapters, and presented the main results of his research in six international conferences and four workshops.

Изјава о ауторству

Име и презиме аутора Георгиос Тсирвоулис

Број индекса 2036/2014

Изјављујем

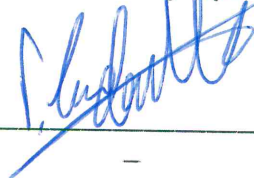
да је докторска дисертација под насловом

Секуларна динамика изабраних фамилија астероида

- резултат сопственог истраживачког рада;
- да дисертација у целини ни у деловима није била предложена за стицање друге дипломе према студијским програмима других високошколских установа;
- да су резултати коректно наведени и
- да нисам кршио/ла ауторска права и користио/ла интелектуалну својину других лица.

У Београду, 18.01.2019. године

Потпис аутора



Изјава о истоветности штампане и електронске верзије докторског рада

Име и презиме аутора Георгиос Тсирвоулис

Број индекса 2036/2014

Студијски програм Астрономија и астрофизика

Наслов рада Секуларна динамика изабраних фамилија астероида

Ментор доцент др Бојан Новаковић

Изјављујем да је штампана верзија мог докторског рада истоветна електронској верзији коју сам предао/ла ради похрањена у **Дигиталном репозиторијуму Универзитета у Београду**.

Дозвољавам да се објаве моји лични подаци везани за добијање академског назива доктора наука, као што су име и презиме, година и место рођења и датум одбране рада.

Ови лични подаци могу се објавити на мрежним страницама дигиталне библиотеке, у електронском каталогу и у публикацијама Универзитета у Београду.

У Београду, 18.01.2019. године

Потпис аутора



Изјава о коришћењу

Овлашћујем Универзитетску библиотеку „Светозар Марковић“ да у Дигитални репозиторијум Универзитета у Београду унесе моју докторску дисертацију под насловом:

Секуларна динамика изабраних фамилија астероида

која је моје ауторско дело.

Дисертацију са свим прилозима предао/ла сам у електронском формату погодном за трајно архивирање.

Моју докторску дисертацију похрањену у Дигиталном репозиторијуму Универзитета у Београду и доступну у отвореном приступу могу да користе сви који поштују одредбе садржане у одабраном типу лиценце Креативне заједнице (Creative Commons) за коју сам се одлучио/ла.

1. Ауторство (CC BY)
2. Ауторство – некомерцијално (CC BY-NC)
3. Ауторство – некомерцијално – без прерада (CC BY-NC-ND)
4. Ауторство – некомерцијално – делити под истим условима (CC BY-NC-SA)
5. Ауторство – без прерада (CC BY-ND)
6. Ауторство – делити под истим условима (CC BY-SA)

(Молимо да заокружите само једну од шест понуђених лиценци.
Кратак опис лиценци је саставни део ове изјаве).

У Београду, 18.01.2019. године

Потпис аутора



1. **Ауторство.** Дозвољаваате умножавање, дистрибуцију и јавно саопштавање дела, и прераде, ако се наведе име аутора на начин одређен од стране аутора или даваоца лиценце, чак и у комерцијалне сврхе. Ово је најслободнија од свих лиценци.

2. **Ауторство – некомерцијално.** Дозвољаваате умножавање, дистрибуцију и јавно саопштавање дела, и прераде, ако се наведе име аутора на начин одређен од стране аутора или даваоца лиценце. Ова лиценца не дозвољава комерцијалну употребу дела.

3. **Ауторство – некомерцијално – без прерада.** Дозвољаваате умножавање, дистрибуцију и јавно саопштавање дела, без промена, преобликовања или употребе дела у свом делу, ако се наведе име аутора на начин одређен од стране аутора или даваоца лиценце. Ова лиценца не дозвољава комерцијалну употребу дела. У односу на све остале лиценце, овом лиценцом се ограничава највећи обим права коришћења дела.

4. **Ауторство – некомерцијално – делити под истим условима.** Дозвољаваате умножавање, дистрибуцију и јавно саопштавање дела, и прераде, ако се наведе име аутора на начин одређен од стране аутора или даваоца лиценце и ако се прерада дистрибуира под истом или сличном лиценцом. Ова лиценца не дозвољава комерцијалну употребу дела и прерада.

5. **Ауторство – без прерада.** Дозвољаваате умножавање, дистрибуцију и јавно саопштавање дела, без промена, преобликовања или употребе дела у свом делу, ако се наведе име аутора на начин одређен од стране аутора или даваоца лиценце. Ова лиценца дозвољава комерцијалну употребу дела.

6. **Ауторство – делити под истим условима.** Дозвољаваате умножавање, дистрибуцију и јавно саопштавање дела, и прераде, ако се наведе име аутора на начин одређен од стране аутора или даваоца лиценце и ако се прерада дистрибуира под истом или сличном лиценцом. Ова лиценца дозвољава комерцијалну употребу дела и прерада. Слична је софтверским лиценцама, односно лиценцама отвореног кода.